



Department of Energy

Washington, DC 20585

AUG 31 1992

Mr. Joseph J. Holonich, Director
Repository Licensing and Quality Assurance
Project Directorate
Division of High-Level Waste Management
Office of Nuclear Material Safety
and Safeguards
U.S. Nuclear Regulatory Commission
Washington, DC 20555

Dear Mr. Holonich:

Enclosed for your information and comment is a copy of the report
"TSPA 1991: An Initial Total-System Performance Assessment for
Yucca Mountain", SAND91-2795. If you have any questions about
this document, please contact Priscilla Bunton of my staff at
(202) 586-8365.

Sincerely,

Linda J. Powell

for

John P. Roberts
Acting Associate Director for
Systems and Compliance
Office of Civilian Radioactive
Waste Management

Enclosure: As Stated

on the shelf

030044

9209080179 920831
PDR WASTE
WM-11 PDR

Part 1

*102.8
WM-11
N403*

cc: w/o enclosure

R. Loux, State of Nevada
M. Baughman, Lincoln County, NV
J. Bingham, Clark County, NV
B. Raper, Nye County, NV
P. Niedzielski-Eichner, Nye County, NV
G. Derby, Lander County, NV
P. Goicoechea, Eureka, NV
C. Schank, Churchill County, NV
F. Mariani, White Pine County, NV
V. Poe, Mineral County, NV
E. Wright, Lincoln County, NV
J. Pitts, Lincoln County, NV
R. Williams, Lander County, NV
J. Hayes, Esmeralda County, NV
M. Hayes, Esmeralda County, NV
B. Mettam, Inyo County, NV

SANDIA REPORT

AND91-2795 • UC-814

Unlimited Release

Printed July 1992

Yucca Mountain Site Characterization Project

TSPA 1991:

An Initial Total-System Performance Assessment for Yucca Mountain

R. W. Barnard, M. L. Wilson, H. A. Dockery, J. H. Gauthier,
P. G. Kaplan, R. R. Eaton, F. W. Bingham, T. H. Robey

Prepared by
Sandia National Laboratories
Albuquerque, New Mexico 87185 and Livermore, California 94550
for the United States Department of Energy
under Contract DE-AC04-76DP00789



SF29000(8-81)

~~9208280127~~

102.8

"Prepared by Yucca Mountain Site Characterization Project (YMSCP) participants as part of the Civilian Radioactive Waste Management Program (CRWM). The YMSCP is managed by the Yucca Mountain Project Office of the U.S. Department of Energy, DOE Field Office, Nevada (DOE/NV). YMSCP work is sponsored by the Office of Geologic Repositories (OGR) of the DOE Office of Civilian Radioactive Waste Management (OCRWM)."

Issued by Sandia National Laboratories, operated for the United States Department of Energy by Sandia Corporation.

NOTICE: This report was prepared as an account of work sponsored by an agency of the United States Government. Neither the United States Government nor any agency thereof, nor any of their employees, nor any of their contractors, subcontractors, or their employees, makes any warranty, express or implied, or assumes any legal liability or responsibility for the accuracy, completeness, or usefulness of any information, apparatus, product, or process disclosed, or represents that its use would not infringe privately owned rights. Reference herein to any specific commercial product, process, or service by trade name, trademark, manufacturer, or otherwise, does not necessarily constitute or imply its endorsement, recommendation, or favoring by the United States Government, any agency thereof or any of their contractors or subcontractors. The views and opinions expressed herein do not necessarily state or reflect those of the United States Government, any agency thereof or any of their contractors.

Printed in the United States of America. This report has been reproduced directly from the best available copy.

Available to DOE and DOE contractors from
Office of Scientific and Technical Information
PO Box 62
Oak Ridge, TN 37831

Prices available from (615) 576-8401, FTS 626-8401

Available to the public from
National Technical Information Service
US Department of Commerce
5285 Port Royal Rd
Springfield, VA 22161

NTIS price codes
Printed copy: A17
Microfiche copy: A01

*rec'd with file
add 8/31/92*
Distribution
Category UC-814

SAND91-2795
Unlimited Release
Printed July 1992

TSPA 1991: An Initial Total-System Performance Assessment for Yucca Mountain

R. W. Barnard*, M. L. Wilson*, H. A. Dockery*,
J. H. Gauthier†, P. G. Kaplan*, R. R. Eaton†,
F. W. Bingham*, T. H. Robey†

*System Performance Assessment Department

†Thermal and Fluid Engineering Department
Sandia National Laboratories
Albuquerque, NM 87185

‡Spectra Research Institute
Albuquerque, NM 87102

Abstract

This report describes an assessment of the long-term performance of a repository system that contains deeply buried highly radioactive waste; the system is assumed to be located at the potential site at Yucca Mountain, Nevada. The study includes an identification of features, events, and processes that might affect the potential repository, a construction of scenarios based on this identification, a selection of models describing these scenarios (including abstraction of appropriate models from detailed models), a selection of probability distributions for the parameters in the models, a stochastic calculation of radionuclide releases for the scenarios, and a derivation of complementary cumulative distribution functions (CCDFs) for the releases. Releases and CCDFs are calculated for four categories of scenarios: aqueous flow (modeling primarily the existing conditions at the site, with allowances for climate change), gaseous flow, basaltic igneous activity, and human intrusion. The study shows that models of complex processes can be abstracted into more simplified representations that preserve the understanding of the processes and produce results consistent with those of more complex models.

The study uses the currently available data from the site. Because the site data are not complete, the study incorporates two different conceptual models for aqueous flow. An update and extension of earlier total-system assessments, the study is intended to guide site characterization and future assessments. Because it relies on incomplete data and does not model all the phenomena that may eventually be considered significant, the study is not a definitive assessment of the suitability of the site.

102:8

The work described in this report was performed for the
Yucca Mountain Site Characterization Project
under WBS 1.2.1.4.1.

Contents

	<u>Page</u>
Executive Summary	ES-1
Chapter 1 Introduction	1-1
1.1 Description and participants	1-1
1.2 Purposes of the SNL TSPA	1-2
1.3 Differences from previous calculations	1-4
1.4 Caveats.....	1-5
1.5 Summary of report contents	1-6
Chapter 2 The Process That Produced This Performance Assessment	2-1
2.1 The process described in the Site-Characterization Plan	2-1
2.2 The hierarchy of models.....	2-3
2.3 The process used in interim exercises	2-6
2.4 Steps in this total-system performance assessment	2-8
Chapter 3 Problem Setup	3-1
3.1 Construction of relational-diagrams and scenarios	3-1
3.1.1 Conceptual models	3-5
3.2 Geohydrologic data.....	3-5
3.2.1 Problem domain	3-6
3.2.2 Stratigraphy	3-6
3.2.2.1 Stratigraphic cross-section	3-9
3.2.3 Initial and boundary conditions	3-10
3.2.4 Parameters.....	3-11
3.3 Development of parameter distributions	3-11
3.3.1 PDF construction methods.....	3-12
3.3.2 Elicitations	3-16
3.3.3 PDFs of hydrogeologic parameters	3-20
3.3.3.1 Matrix saturated hydraulic conductivity, K_s	3-22
3.3.3.2 Matrix saturated volumetric water content, θ_s	3-23
3.3.3.3 Matrix porosity, n	3-23
3.3.3.4 Water-retention parameters.....	3-23
3.3.3.5 Fracture parameters	3-25
3.3.4 Transformation of data for TSA input	3-27
3.3.4.1 Approximating the PDF for LHS input	3-28
3.3.4.2 Approximating the PDFs of fracture parameters for the TSA.....	3-32
Degree of saturation (residual) S_r	3-33
Fracture porosity n_f	3-35
3.4 Geochemistry data	3-38
3.4.1 Sorption coefficients for tuff	3-40
3.4.2 Sorption coefficients for the carbonate aquifer	3-48

Chapter 4 Groundwater Flow and Transport	4-1
4.1 Problem development and scenario screening	4-2
4.2 Method	4-7
4.3 Radionuclide source term for aqueous releases	4-10
4.3.1 Radionuclide inventory	4-13
4.3.2 Container environments and types of releases	4-14
4.3.3 Container wetting and failure	4-17
4.3.4 Modes of waste mobilization	4-18
4.3.5 Radionuclide transport out of the waste container	4-19
4.3.6 Convolution of the processes	4-22
4.3.7 Generic shape functions	4-24
4.3.8 Combining the release components	4-25
4.3.9 Parameter values for the source model	4-28
4.4 Unsaturated-zone flow models	4-31
4.4.1 Composite-porosity model of unsaturated flow	4-32
4.4.2 Parameters for the composite-porosity flow model	4-37
4.4.3 Weeps model of unsaturated flow	4-41
4.4.4 Adaptation of the source model for weeps	4-51
4.4.5 Parameters for the weeps model	4-52
4.5 Saturated-zone flow models	4-54
4.5.1 Saturated flow using Czarnecki's model	4-54
4.5.2 TSA model of saturated flow	4-61
4.5.3 Parameters for the saturated-zone flow model	4-64
4.6 Transport model	4-65
4.6.1 The TOSPAC transport model	4-65
4.6.2 Parameters for the transport model	4-70
4.7 Results	4-72
4.7.1 Comparison of results using the composite-porosity model with performance measures	4-73
4.7.2 Comparison of results using the weeps model with performance measures	4-80
4.7.3 Conditional CCDFs for aqueous releases	4-83
4.8 Analysis of the average case	4-85
4.8.1 Average composite-porosity-flow case	4-86
4.8.2 Average weeps-flow case	4-90
 Chapter 5 Gas Flow and Transport	 5-1
5.1 Problem development and scenario screening	5-2
5.2 Radionuclide source term for gaseous releases	5-6
5.3 The gas-flow model	5-9
5.4 Adaptation of gas flow and transport for the TSA	5-17
5.5 Results	5-22
5.6 Analysis of the average case	5-27

Chapter 6 Human Intrusion	6-1
6.1 Introduction	6-1
6.2 Problem definition	6-1
6.3 Estimation of probability of occurrence.....	6-4
6.3.1 Natural resources	6-4
6.3.2 Geometric probability.....	6-7
6.4 Modeling assumptions	6-9
6.4.1 Source term for surface releases.....	6-9
6.4.2 Source term for saturated-zone releases	6-12
6.4.3 Parameters.....	6-13
6.5 Description of TSPA calculation	6-17
6.5.1 Surface-release calculations	6-18
6.5.2 Saturated-zone calculations	6-19
6.5.3 Sensitivity studies for surface-release calculations	6-20
6.6 Results.....	6-21
6.6.1 Surface-release calculations	6-21
6.6.2 Surface-release sensitivity studies	6-26
6.6.3 Saturated-zone calculations	6-32
6.7 Summary	6-39
 Chapter 7 Basaltic Igneous Activity	 7-1
7.1 Introduction	7-1
7.2 Problem definition	7-1
7.3 Estimation of probability of occurrence.....	7-5
7.3.1 Frequency of an eruption in the region.....	7-6
7.3.2 Probability of an eruption in the repository	7-6
7.3.3 Conditional probability of releases $P[E_3 E_1E_2]$	7-7
7.4 Consequence of release from the repository	7-7
7.4.1 Consequence model	7-7
7.4.2 Estimates of parameter values	7-8
7.4.3 Geologic features	7-9
7.4.4 Description of computations	7-14
7.5 Results.....	7-16
7.5.1 Sensitivity studies	7-20
7.5.2 Normalized CCDF for basaltic igneous activity	7-24
7.6 Discussion	7-26
 Chapter 8 Combination of Conditional CCDFs.....	 8-1
8.1 Methods of generating an overall CCDF	8-2
8.2 Combination of CCDFs for this study.....	8-5
 Chapter 9 Comments and Comparisons.....	 9-1
9.1 Comments on abstraction	9-1
9.2 Comparisons with detailed calculations.....	9-2
9.2.1 Comparisons for unsaturated flow.....	9-3
9.2.1.1 Results and comparisons.....	9-3

9.2.2 Other comparisons	9-9
9.2.2.1 Saturated-zone calculations	9-9
9.2.2.2 Human intrusion and basaltic igneous activity	9-9
9.2.2.3 Gas transport.....	9-9
9.3 Success of abstraction	9-10
9.4 Comments on performance measures.....	9-11
Chapter 10 Conclusions and Summary	10-1
10.1 General conclusions	10-1
10.2 Technical conclusions and summaries of components.....	10-2
10.2.1 Overall	10-2
10.2.2 Data set	10-4
10.2.3 Nominal processes	10-5
10.2.3.1 Groundwater flow and transport	10-5
10.2.3.1.1 Composite-porosity model	10-6
10.2.3.1.2 Weeps model.....	10-6
10.2.3.2 Gas flow and transport.....	10-7
10.2.4 Disturbed conditions	10-7
10.2.4.1 Human intrusion	10-8
10.2.4.2 Basaltic igneous activity	10-9
Chapter 11 Areas for Future Work	11-1
11.1 General Areas	11-1
11.2 Parameters	11-2
11.2.1 Data set	11-2
11.2.2 Source-term	11-4
11.2.3 Geochemistry	11-5
11.3 Aqueous flow and transport.....	11-5
11.3.1 Unsaturated flow and transport	11-5
11.3.2 Saturated flow and transport	11-6
11.4 Gaseous flow and transport.....	11-7
11.5 Human intrusion	11-8
11.6 Basaltic igneous activity	11-8
11.7 Conclusions	11-9
References.....	12-1
Bibliography.....	13-1
Appendix I Calculation of Probabilities for Intersecting Waste Packages	I-1
Appendix II Setup for 2-D Groundwater-Flow Analyses	II-1
II.1 Geometry and numerical grid	II-1
II.2 Boundary and initial conditions.....	II-4
Appendix III RIB/SEPDB Data	III-1

Figures

	<u>Page</u>
2-1. The hierarchy of models	2-4
3-1. TSPA analysis transect through Yucca Mountain.....	3-7
3-2. Schematic cross-section of unsaturated-zone stratigraphy	3-8
3-3. Various shapes taken by the beta distribution	3-16
3-4. PDF for groundwater percolation rate	3-20
3-5. PDF for matrix porosity in Layer 1	3-30
3-6. Truncated PDF for matrix porosity in Layer 1	3-30
3-7. Comparison of exact and approximated PDFs for Layer-1 porosity	3-31
3-8. Beta probability density for residual saturation.....	3-34
3-9. Approximated beta probability density for residual saturation.....	3-35
3-10. Exponential PDF for fracture porosity, Layer 2, in fault zone	3-39
3-11. PDF for K_d , uranium or selenium on devitrified tuff.....	3-43
3-12. Beta PDF for K_d , uranium or selenium on zeolitic tuff	3-43
3-13. PDF for K_d , uranium or selenium on vitric tuff	3-43
3-14. Beta PDF for K_d , neptunium on devitrified tuff.....	3-43
3-15. Beta PDF for K_d , neptunium on zeolitic tuff.....	3-44
3-16. Beta PDF for K_d , neptunium on vitric tuff.....	3-44
3-17. Beta PDF for K_d , cesium on devitrified tuff.....	3-44
3-18. Beta PDF for K_d , cesium on zeolitic tuff.....	3-44
3-19. Uranium K_d as a function of pH.....	3-46
3-20. Neptunium K_d as a function of pH.....	3-47
3-21. Exponential probability density function (Np on devitrified tuff).....	3-48
3-22. Stepwise-uniform probability density function (U on carbonates).....	3-49
4-1. Upper section of the Nominal-Flow FEP diagram.....	4-3
4-2. Lower part of the Nominal-Flow FEP diagram, for unsaturated conditions..	4-5
4-3. Lower part of the Nominal-Flow FEP diagram, for locally saturated conditions	4-6
4-4. Top-level flow chart for the Total-System Analyzer (TSA)	4-8
4-5. Diagram showing how the two alternative conceptual models of flow are implemented in the TSA	4-9
4-6. Important factors included in the model of the radionuclide source term	4-11
4-7. One concept for a vertically emplaced waste container	4-12
4-8. Two release mechanisms included in the source-term model	4-15
4-9. The generic shape function for alteration-limited releases	4-25
4-10. The generic shape function for solubility-limited releases	4-26
4-11. Important factors included in the two groundwater-flow models	4-31
4-12. A conceptual model of composite-porosity flow at Yucca Mountain.....	4-33
4-13. How the strength of the matrix/fracture coupling influences flow.....	4-34
4-14. Saturation versus elevation, given an influx of 1 mm/yr (0.001 m/yr)	4-36

4-15. Groundwater velocity given an influx of 1 mm/yr (0.001 m/yr)	4-38
4-16. Transect of Yucca Mountain showing the locations of the six vertical columns.....	4-39
4-17. Division of the repository into six equal-area subregions	4-41
4-18. Stratigraphies of the six vertical columns	4-42
4-19. A conceptual model of significant fracture flow (weeps) at Yucca Mountain	4-43
4-20. Estimates of some weeps-model parameters for three different sizes of fractures	4-46
4-21. Geometric considerations in calculating the number of containers contacted by flowing fractures	4-47
4-22. Relationship between flow aperture and number of waste containers contacted.....	4-49
4-23. Relationship between flow aperture and releases from the potential repository	4-50
4-24. Map of potential repository showing the accessible environment.....	4-55
4-25. Location of hydraulic-head measurement sites	4-57
4-26. Layout of SZ hydraulic properties and boundary conditions.....	4-58
4-27. Simulated SZ hydraulic heads	4-59
4-28. Saturated-zone travel times	4-61
4-29. Geometry of the horizontal flow tube used to model the saturated zone.....	4-62
4-30. Coupling of six vertical columns with the horizontal flow tube	4-63
4-31. Coupling of the weeps model with the horizontal flow tube	4-64
4-32. Effective water velocities used to model the saturated zone	4-65
4-33. Concentration surface of ⁷⁹ Se in the unsaturated zone.....	4-68
4-34. Concentration surface of ⁷⁹ Se in the saturated zone.....	4-69
4-35. Concentration surface of ⁷⁹ Se in the saturated zone (weeps model)	4-70
4-36. Conditional CCDFs for aqueous releases (composite-porosity model).....	4-74
4-37. Conditional CCDFs for aqueous releases of individual nuclides (composite-porosity model).....	4-76
4-38. Contribution of individual nuclides to mean partial EPA sum (composite-porosity model)	4-76
4-39. Probability distributions of the NRC ratio	4-77
4-40. Distributions of travel times through the unsaturated zone and the saturated zone.....	4-79
4-41. Conditional CCDFs for aqueous releases (weeps model).....	4-80
4-42. Conditional CCDFs for aqueous releases of individual nuclides (weeps model)	4-82
4-43. Contribution of individual nuclides to mean partial EPA sum (weeps model)	4-82
4-44. Conditional CCDFs for aqueous releases.....	4-84
4-45. Release rates to the accessible environment (composite-porosity model)	4-87
4-46. Cumulative releases to the accessible environment (composite-porosity model)	4-88
4-47. Release rates from the EBS (composite-porosity model)	4-89

4-48. Distributions of travel times for the composite-porosity model and the weeps model	4-89
4-49. Release rates to the accessible environment (weeps model)	4-91
4-50. Cumulative releases to the accessible environment (weeps model)	4-92
4-51. Release rates from the EBS (weeps model)	4-93
5-1. Factors included in the gas-flow problem.....	5-1
5-2. Flow diagram for the two TSA gaseous-transport simulations	5-3
5-3. FEP diagram for nominal gas flow.....	5-4
5-4. Map of the repository	5-11
5-5. Geometry of cross-section N760000	5-12
5-6. Geometry of cross-section N762500	5-12
5-7. Geometry of cross-section N765000	5-13
5-8. Geometry of cross-section N767500	5-13
5-9. Path lines with ambient temperature, cross-section N762500.....	5-14
5-10. Path lines with the repository heated to 330 K, cross-section N762500	5-14
5-11. Retardation factor as a function of temperature	5-17
5-12. The four ¹⁴ C travel-time distributions.....	5-18
5-13. Temperature vs. time at the center of the repository.....	5-20
5-14. Conditional CCDFs for gaseous releases (composite-porosity and weeps models)	5-23
5-15. Probability distributions of the NRC ratio	5-25
5-16. Conditional CCDFs for gaseous releases (composite-porosity model)	5-25
5-17. Conditional CCDFs for gaseous releases (weeps model)	5-26
5-18. Release rate to the accessible environment for ¹⁴ C (composite-porosity model)	5-27
5-19. Release rate to the accessible environment for ¹⁴ C (weeps model).....	5-28
5-20. ¹⁴ C EPA ratio as a function of time (composite-porosity model)	5-28
5-21. ¹⁴ C EPA ratio as a function of time (weeps model).....	5-29
5-22. ¹⁴ C NRC ratio as a function of time (composite-porosity model)	5-29
5-23. ¹⁴ C NRC ratio as a function of time (weeps model).....	5-30
6-1. FEP diagram for human intrusion scenarios	6-2
6-2. Schematic of mobilization process for surface-release scenario	6-4
6-3. Schematic of mobilization process for saturated-zone-release scenario.....	6-5
6-4. Resource-exploration areas near Yucca Mountain	6-6
6-5. Diffusion profiles vs time	6-11
6-6. Geometric layout for drilling scenarios	6-12
6-7. Distribution of surface releases from drilling (base case).....	6-22
6-8. Conditional CCDF for surface releases due to drilling	6-22
6-9. Conditional CCDF showing contributions of near misses	6-23
6-10. Conditional CCDF showing effect of releasing entire waste package	6-23
6-11. Distribution of hits on waste packages for base-case drilling density.....	6-24
6-12. Distribution of releases for mean drilling density of 3 holes/km ²	6-25
6-13. Comparison of conditional CCDFs for different assumptions for drilling density	6-25

6-14. Distribution of hits on waste packages for mean drilling density of 3 boreholes/km ²	6-26
6-15. Comparison of lumped-inventory and multiple-inventory source terms	6-27
6-16. Conditional CCDF showing increases in surface releases due to increasing the number of holes drilled over 10,000 years	6-28
6-17. Distribution of hits on waste packages for drilling density of 30 boreholes/km ²	6-28
6-18. Distributions of hits on waste packages for drilling density of 60 boreholes/km ²	6-29
6-19. Conditional CCDF showing increases in surface releases due to increasing the near-miss inventory.....	6-30
6-20. Comparison of distributions of releases for base case and 100-fold increase in diffusion coefficient	6-30
6-21. Conditional CCDF showing change in surface releases due to biasing drilling events to later in performance period	6-31
6-22. Conditional CCDF for releases to accessible environment through saturated-tuff zone due to human intrusion	6-32
6-23. Cumulative releases to accessible environment through saturated-tuff zone	6-33
6-24. Average percentages of radionuclides released through saturated-tuff zone	6-34
6-25. Conditional CCDF for releases to accessible environment through carbonate aquifer due to human intrusion.....	6-35
6-26. Average percentages of radionuclides released through carbonate aquifer...	6-36
6-27. Cumulative releases to accessible environment through carbonate aquifer...	6-37
6-28. Distributions of tracer travel times.....	6-37
6-29. Comparison of CCDFs for releases for three drilling scenarios.....	6-38
6-30. Combined conditional CCDF for three drilling scenarios	6-39
7-1. FEP diagram for basaltic igneous activity	7-2
7-2. Interaction of dike with waste package	7-3
7-3. Distribution mechanism for waste at surface	7-4
7-4. Probability density function for dike width	7-9
7-5. Probability density function for dike orientation.....	7-10
7-6. Probability density function for erosion depth	7-11
7-7. Probability density function for eruption volume	7-12
7-8. Probability density function for wall-rock fraction entrained	7-13
7-9. Modified repository shape with randomly placed dikes.....	7-15
7-10. Distribution of surface releases due to igneous activity (method 1)	7-16
7-11. Conditional probability distribution for releases due to igneous activity (method 1)	7-17
7-12. Distribution of surface releases due to igneous activity (method 2)	7-18
7-13. Conditional probability distribution for releases due to igneous activity (method 2)	7-19
7-14. Distribution of volume of lithic fragments at surface originating in the repository	7-19

7-15. Average percentages of radionuclides released due to igneous activity.....	7-20
7-16. PDFs for parameters used in sensitivity studies	7-22
7-17. Comparison of releases for base-case and modified parameter PDFs (method 2)	7-23
7-18. Comparison of base-case releases with releases for greater dike width (method 1)	7-23
7-19. Comparison of base-case releases with releases for uniform parameter distributions	7-24
7-20. Effect of specifying that maximum dike length be in repository (method 2) .	7-25
7-21. Conditional CCDF for surface releases from igneous activity, including probability of occurrence (method 1)	7-25
7-22. Conditional CCDF for surface releases from igneous activity, including probability of occurrence (method 2)	7-26
8-1. Schematic for combining 14 conditional CCDFs into 1	8-6
8-2. Schematic for combining the conditional CCDFs keeping the “alternative conceptual models” separate.....	8-7
8-3. Combination of the aqueous and gaseous conditional CCDFs for the composite-porosity model	8-10
8-4. Combination of the aqueous and gaseous conditional CCDFs for the weeps model	8-10
8-5. Conditional CCDFs for aqueous releases from the six columns.....	8-11
8-6. Overall conditional CCDF (composite-porosity model)	8-12
8-7. Overall conditional CCDF (weeps model)	8-13
8-8. Overall conditional CCDF, with three weightings of composite-porosity and weeps models.....	8-14
8-9. Same as Figure 8-8, but with linear probability axis.....	8-14
9-1. Darcy velocity vectors calculated by NORIA-SP	9-4
9-2. Darcy velocity vectors for three fluxes calculated by LLUVIA-II	9-5
9-3. Particle pathlines for 0.01 and 1.0 mm/yr fluxes calculated by LLUVIA-II ...	9-6
9-4. Vertical groundwater velocities at the water table	9-8
9-5. Horizontal groundwater velocity at x = 250 m	9-8
10-1. Overall CCDF for releases assuming the composite model for aqueous transport	10-3
10-2. Overall CCDF for releases assuming the weeps model for aqueous transport	10-4
II-1. Problem domain for 2-D NORIA-SP analysis.....	II-2
II-2. NORIA-SP computational mesh	II-2
II-3. LLUVIA-II computational mesh	II-3

Tables

	<u>Page</u>
3-1. Hydrostratigraphy used for unsaturated-zone aqueous problems.....	3-9
3-2. Elevations of layers at selected locations in geohydrologic problem domain.	3-10
3-3. Stochastic hydrogeologic data base.....	3-12
3-4. Relation between amount of information and maximum-entropy PDF	3-14
3-5. Effects of beta-distribution exponents on PDF shape.....	3-15
3-6. Summary of expert elicitations	3-19
3-7. Probability density distributions from expert elicitations	3-21
3-8. Matrix saturated hydraulic conductivity	3-22
3-9. Matrix saturated volumetric water content, θ_s	3-23
3-10. Matrix porosity	3-24
3-11. Matrix air-entry parameter, α_{vG}	3-24
3-12. Matrix desaturation parameter, β_{vG}	3-25
3-13. Matrix residual degree of saturation, S_r	3-25
3-14. Hydrologic properties for fractures (based on sand)	3-26
3-15. Fracture density	3-26
3-16. Fracture density in fault zone	3-27
3-17. Distributions for approximated matrix porosity.....	3-31
3-18. Distributions for approximated matrix air-entry parameter, α_{vG}	3-32
3-19. Distributions for approximated matrix degree of residual saturation, S_r	3-32
3-20. Distributions for approximated air-entry parameter for fractures, α_{vG} (based on sand).....	3-33
3-21. Approximated residual degree of saturation, S_r (based on sand).....	3-35
3-22. Values used in the calculation of fracture porosity	3-37
3-23. Fracture porosity, n_f	3-38
3-24. Geohydrologic units for geochemistry	3-41
3-25. Probability distributions for K_{ds}	3-42
3-26. Bulk density used for retardation-factor calculation.....	3-49
3-27. Probability distributions for K_d in carbonate aquifer.....	3-50
4-1. Radionuclides included in the aqueous-release calculations	4-13
4-2. Values for source-model parameters	4-29
4-3. Elevations used for the composite-porosity model of the UZ	4-40
4-4. Parameters used by the composite-porosity model	4-40
4-5. Parameters used by the weeps model	4-53
4-6. Parameters used to model the saturated zone.....	4-64
4-7. Parameters used to model transport.....	4-71
4-8. Comparison of deterministic and probabilistic calculations (EPA Sums).....	4-86
5-1. Some ^{14}C data.....	5-6

5-2. Probability distributions assumed for ^{14}C inventory	5-8
5-3. Probability distributions assumed for ^{14}C transport.....	5-22
6-1. Probabilities of hits for binomial distribution	6-8
6-2. Probabilities of hits for Poisson distribution	6-8
6-3. Parameters for surface-release scenario	6-14
6-4. Radioisotopes used in source term	6-15
6-5. Parameters for saturated-zone release problems	6-17
6-6. Multiple-source inventory parameters	6-18
7-1. Parameters varied for basaltic igneous activity sensitivity studies.....	7-21
9-1. Resources for abstractions used in TSPA models	9-2
9-2. Relative lateral flow	9-7
9-3. Gas-phase releases of ^{14}C	9-10
II-1. Material properties for 2-D problems	II-1

Acknowledgments

We would like to acknowledge other technical contributors to this document. Arend Meijer (LANL) supplied information on the geochemical-retardation factors used in both unsaturated and saturated zone calculations. Greg Valentine (LANL) helped with the formulation of both the problem and the parameter set for the study of basaltic igneous activity. William O'Connell (LLNL) developed the source term and associated parameter distributions for the aqueous-release calculations. Ben Ross (DSI) provided additional gas-flow information for temperatures not specified in his published reports. Franz Lauffer was part of the group that formulated the weeps model. David Gallegos wrote the memo on the geometric probability of drilling into a waste container that constitutes Appendix I. Lee Skinner (Spectra Research Institute) provided programming support in the development of the codes used for the human-intrusion, volcanism, and nominal-case analyses.

The entire document benefited from extensive technical reviews performed by Franz Lauffer, Mert Fewell, Larry Costin, and Tom Blejwas. Other persons that provided reviews of specific chapters are Chapter 3, Chris Rautman and Arend Meijer; Chapter 5, Ben Ross; Chapters 4, 5, and 9, Ron Dykhuizen; Chapter 6, David Gallegos, and Chapter 7, Greg Valentine.

Kassandra Sanchez assisted in all stages of document preparation, including drawing and preparing figures and providing typing support. Mary Heerdt also provided support in preparation of the document. Several drawings were supplied by David Eley for Chapter 3 and by Leo Gabaldon (Tech Reps), for Chapter 7.

Glossary of Acronyms

BWR	boiling-water reactor
CCDF	complementary cumulative distribution function
DOE	U. S. Department of Energy
EA	Environmental Assessment
EBS	Engineered Barrier System
EPA	Environmental Protection Agency
EPRI	Electric Power Research Institute
ESSE	Early Site Suitability Evaluation
FEPs	features, events, and processes
GWTT	ground water travel time
LANL	Los Alamos National Laboratory
LBL	Lawrence Berkeley Laboratory
LHS	Latin Hypercube Sampler
LLNL	Lawrence Livermore National Laboratory
MTHM	metric tons heavy metal
NRC	Nuclear Regulatory Commission
PA	performance assessment
PACE-90	Performance Assessment Computational Exercises, 1990
PDF	probability distribution function
PNL	Battelle Pacific Northwest Laboratory
PWR	pressurized-water reactor
RIB	Yucca Mountain Reference Information Base
SCP—CDR	Site Characterization Plan—Conceptual Design Report
SEPDB	Yucca Mountain Site and Engineering Properties Data Base
SNL	Sandia National Laboratories
SZ	Saturated zone
TSA	Total System Analyzer
TSPA	Total-system performance assessment
UNLV	University of Nevada, Las Vegas
UZ	Unsaturated zone
WIPP	Waste Isolation Pilot Project
YMP	Yucca Mountain Site Characterization Project

Executive Summary

Introduction

In 1991, the U. S. Department of Energy, Yucca Mountain Site Characterization Project Office requested a preliminary total-system performance assessment (TSPA) of the potential high-level radioactive waste repository system at Yucca Mountain, Nevada. The TSPA was to take into account the features, events, and processes thought to be important in estimating the behavior of such a system during the 10,000-year period after it has been closed. As discussed in this report, this TSPA represents an initial attempt to estimate the releases of radionuclides that might occur because of processes in four categories: human intrusion, basaltic igneous activity, and aqueous and gaseous flow and transport.

This TSPA differed from prior work in several respects. For example, it made stochastic simulations (instead of deterministic) on an expanded number of phenomena; it modeled radionuclide transport through the unsaturated and saturated rock to the accessible environment (5 km distant from the repository for aqueous-based releases, and to the surface above the repository for other releases); it used two conceptual models for flow through the unsaturated zone; and it included a limited number of sensitivity studies. All the analyses systematically addressed the total-system requirements by describing sequences of events and processes to be modeled, estimating probabilities, stating assumptions, explicitly treating parameter uncertainties, and interpreting the results with due regard for the input data that produced them.

Several organizations contributed to the TSPA. The problem definition was coordinated by Sandia National Laboratories (SNL). SNL and Battelle Pacific Northwest Laboratory (PNL) performed the TSPA calculations, although only SNL's work is reported here. Lawrence Livermore National Laboratory (LLNL) and Lawrence Berkeley Laboratory (LBL) both contributed to the specification of the radionuclide source term by defining the waste-package failure modes and associated parameters. Los Alamos National Laboratory (LANL) provided information on geologic events and features and the associated parameter distributions for the igneous-activity analysis. LANL also provided information and parameter-value distributions for the geochemical retardation modeled in the aqueous-flow analyses.

The primary purpose of the SNL TSPA effort was to attempt to develop an ability to derive "abstracted" representations of the complex processes that contribute to the behavior of a repository system. Such abstractions are essential to the probabilistic modeling required for examining compliance with repository regulations. This TSPA is therefore an attempt to perform that abstraction and to use its results in an estimate of the behavior of a total repository system. The abstraction process, as applied to the TSPA analyses, identified the essential aspects of the four categories listed above; the TSPA then used models that embodied those essential aspects. As part of the evaluation of the worth of this abstraction, some of the TSPA results have been compared with analyses done with more complex process-oriented models.

A secondary purpose of the TSPA analysis was to demonstrate that complex combinations of distributions of data could be assembled to provide a reasonable overall estimate of system performance. The measure of total-system performance was chosen to be the cumulative release of radionuclides to the accessible environment, expressed in terms of the limits given by the EPA in 40 CFR Part 191. This measure was expressed as a probability distribution (called a CCDF—complementary cumulative distribution function) of radionuclide releases due to the four categories of processes listed previously.

Because of the limited number of components included, it was not intended that this performance estimate would constitute a definitive evaluation of Yucca Mountain as a site for a potential radioactive-waste repository. Because many data are yet to be obtained for Yucca Mountain and several important choices among conceptual models are yet to be made, a more appropriate use of these results is as guidance for site characterization and for the next iterations of total-system performance assessment. Furthermore, although mean values of releases have been calculated from this study, they should not be considered "best estimates" of the behavior of Yucca Mountain as a potential site for a repository. Very broad ranges were chosen for many parameters to ensure that they would encompass most possibilities. Consequently, the results presented here may be substantially modified in future analyses.

Description of Analyses

The formulation of the four categories of analyses were based on prior work, as listed below. The radionuclide source term is an abstraction of the source terms developed previously for PA analyses. Twelve radionuclides were used in the

source term for the aqueous-flow analyses: ^{234}U , ^{243}Am , ^{241}Am , ^{240}Pu , ^{239}Pu , ^{237}Np , ^{135}Cs , ^{129}I , ^{126}Sn , ^{99}Tc , ^{79}Se , and ^{14}C . These radionuclides were chosen because they include those with large inventories in the spent fuel, those thought to have low geochemical retardation, and those with large contributions to dose effects. For the direct-surface-release components of the TSPA (human-intrusion drilling and igneous intrusion), the source term included 41 radionuclides that have significant inventories.

The aqueous flow and transport analysis modeled radionuclide movement through a two-dimensional cross-section through Yucca Mountain at the site of the potential repository. This cross-section was a modification of that used in prior unsaturated-zone PA analyses. Distributions of hydrologic-property values were derived from site data, analog data, and elicitation of expert opinion. Distributions were chosen that attempted to reflect both the variability of the materials and the uncertainty in our knowledge of them.

Two alternative conceptual models of groundwater flow through the unsaturated zone were used—the composite-porosity model (embodied in the computer code TOSPAC) and the weeps model. The former assumes pressure equilibrium between groundwater flow through the rock matrix and the fractures; the latter model assumes that flow is exclusively in the fractures. The two models were intended to represent the end points of the range of models for groundwater-flow processes. TOSPAC modeled aqueous flow and transport through six one-dimensional columns that represented the analysis cross-section. The weeps model represented fracture flow with a non-dimensional model. TOSPAC also modeled saturated-zone transport for both conceptual models. By sampling from the parameter-value distributions and using the sampled values as input to the flow models, stochastic estimates of the aqueous-transport performance of Yucca Mountain were made.

Gas flow was modeled by abstracting a currently available model of flow of $^{14}\text{CO}_2$ through Yucca Mountain as a function of temperature. Other available analyses provided the time-dependent temperature profiles necessary to calculate travel times for the gas over 10,000 years. The travel times, combined with a source-term model, produced an estimate of releases of ^{14}C to the surface.

Human intrusion was modeled as drilling. One sequence modeled direct release of waste to the surface; another assumed that waste could fall down a borehole to the saturated zone, where it would be carried to the accessible environment.

The models made several simplifying assumptions about the processes by which drilling might mobilize the waste from the waste packages.

The model of releases from basaltic igneous activity assumed that a dike intrudes the repository and carries waste to the surface. The entrainment process and the probabilities of occurrence were abstracted from work done by Crowe and Valentine (LANL). Two models that describe the interaction of the dike and the waste packages in different ways were used.

Results

CCDFs for radionuclide releases to the accessible environment were produced for the four categories. Most of them show that releases from the potential repository do not exceed the probabilistic standard set by the EPA in 40 CFR Part 191. Some analyses do estimate releases that exceed the EPA limit.

The CCDFs for aqueous releases are shown in Figure 4-44 (page 4-84), where the two curves are the results of calculations made with the composite-porosity model and the weeps model. Neither curve exceeds the EPA limit. For the aqueous flow and transport analyses, the weeps model predicts greater releases, because in that model the unsaturated zone is a less effective barrier to radionuclide transport. This condition is a consequence of the assumption that water flowing in the fractures would move almost instantaneously through the unsaturated zone. Releases calculated with the composite model are lower because of the many thousands of years necessary for groundwater to move through the unsaturated zone to the saturated zone. For both aqueous-flow models, the non-retarded isotopes ^{99}Tc and ^{129}I are the greatest contributors to releases (Figures 4-38 and 4-43; pp. 4-76 and 4-82).

The estimate of gaseous releases of ^{14}C exceeds the EPA limit when the composite-porosity model is used to compute the rate at which radionuclides are mobilized from the waste packages (see Figure 5-14; p. 5-23). In comparison with the weeps model, this model describes a more pervasive contact between groundwater and the waste packages, resulting in a higher rate of waste-package failure and a greater availability of ^{14}C . A more realistic source model (i.e., taking more credit for the engineered barriers against releases) would probably reduce releases to below the EPA limits.

Estimates of direct surface releases caused by drilling do not exceed the EPA limit, nor do the estimates for waste placed directly in the saturated zone (see Figures 6-8, 6-22 and 6-25; pp. 6-22, 6-32, 6-35). These results are based on an assumption that the probability of future drilling activities at the site is 1, and on

guidance from the EPA regarding the number of holes drilled into the repository over 10,000 years. Several sensitivity studies were performed for this analysis; the greatest effect occurred by increasing the number of boreholes drilled to ten or twenty times the EPA guidance. Even under these assumptions, however, the estimates of surface releases did not exceed the EPA limit (Figure 6-16; p. 6-28). An evaluation of the potential for exploitable resources at the site could reduce this probability of drilling, and thus reduce still further the probability of having releases exceed the EPA limit.

Estimates of releases at the surface due to intrusion by an igneous dike also do not exceed the EPA limits. Furthermore, when the probability of occurrence of an igneous intrusion ($\sim 2 \times 10^{-4}$ over 10,000 years) is included, the contribution to the overall CCDF becomes inconsequential (Figures 7-21 and 7-22; pp. 7-25 and 7-26).

The total-system CCDF combined CCDFs from the four component analyses. Several techniques were used to combine the components in ways that reflect assumptions about the correlations among the models and the independence of the processes. The preliminary total-system CCDF calculated using the composite-porosity model for unsaturated-zone water flow exceeds the EPA limit because of the high gas-phase releases of ^{14}C mentioned above (Figure 8-6; p. 8-12). The CCDF using the weeps model for unsaturated-zone water flow was below the EPA limit (Figure 8-7; p. 8-13).

Conclusions

This TSPA analysis demonstrated an ability to abstract complex models for use in a broader application. The CCDFs generated produced results that are sensitive to our understanding of the processes at Yucca Mountain and are consistent with work done using other models and techniques. The results of this TSPA analysis reflect considerable uncertainty and many conservative assumptions. They should not be used as the sole basis for any recommendation of higher-level suitability of the Yucca Mountain site, nor should they serve as a baseline for licensing documents, except as an example analysis to illustrate aspects of later performance assessments. However, the results can aid in assigning priorities to the collection of site-characterization data and can provide an incentive for further field work and research. For this reason, the report includes recommendations for future work; for example, additional data on the gas permeability of Yucca Mountain rock are suggested as useful for removing the possibly unnecessary conservatism behind the TSPA modeling of gas flow.

This TSPA analysis is expected to be the first of a sequence of analyses, each of which will build on prior efforts. In future analyses the sensitivities of the aqueous and gaseous releases to the input parameters will be investigated. The systematic methodology for identifying sequences of processes and events and for selecting conceptual models will be expanded.

Chapter 1

Introduction

(Dockery, Barnard)

1.1 Description and participants

The development of a repository for highly radioactive waste requires technical analyses of many kinds. One of the most important analyses is total-system performance assessment (TSPA), which estimates the behavior of the repository system for thousands of years after it has received waste and been closed.

It is important to make total-system performance assessments even in the early stages of repository development. The ultimate use for such assessments is in determining whether the system meets the regulatory standards set by the U. S. Environmental Protection Agency (EPA). Preliminary assessments, however, are useful in repository design, in the characterization of a repository site, for early determinations of the suitability of a site, and in the development of the methods that will be used to make the ultimate assessment of compliance with the EPA standards. For these reasons, TSPAs are important to the work of the Yucca Mountain Site Characterization Project (YMP), an activity of the U. S. Department of Energy (DOE) that is examining the suitability of a potential repository site at Yucca Mountain, Nevada.

In June 1991, the YMP requested that a preliminary total-system performance assessment be completed by the end of that year. The TSPA was to estimate the behavior of an entire high-level radioactive waste repository system at the potential site. The YMP participants completed the requested TSPA and presented their results in November 1991.

To estimate the future behavior of the repository system, the TSPA uses mathematical and conceptual models of the natural and engineered components that make up the total system. The calculations estimate the performance of these components under two different basic assumptions: that the site remains undisturbed for 10,000 years and that the site is disturbed by unlikely but possible natural phenomena and human activities. Because the YMP has just begun acquiring data to characterize the site and because the time available for these calculations was only about 3 months, the TSPA is not as comprehensive as the calculations that YMP expects to perform in the next few years. This TSPA is the first step in a series of iterative performance assessments. Nevertheless, it is more extensive than previous

calculations, and it enlarges significantly upon previous overall performance-assessment (PA) efforts for Yucca Mountain.

Although the regulatory standards set forth in 40 CFR Part 191 (EPA, 1985) have been remanded by a court decision and are currently being reevaluated by the EPA, this TSPA assumes that the revised standard will be similar in nature, if not in detail, to the 1985 version of the standard. Therefore, the TSPA uses the remanded EPA standard as a measure against which to compare the results of the assessment.

Several organizations contributed to the TSPA. The initial stages were coordinated by Sandia National Laboratories (SNL). SNL and Battelle Pacific Northwest Laboratory (PNL) performed the TSPA calculations. Analyses of the effects of human intrusion, basaltic igneous activity, and aqueous and gaseous flow on the repository system were performed by both SNL and PNL. In addition, PNL performed a tectonic analysis. Los Alamos National Laboratory (LANL) helped define the igneous-activity analysis by providing information on relevant geologic events and features and the associated parameter distributions. They also provided information and parameter value distributions for the geochemical processes (retardation) modeled in the aqueous-flow analyses. Lawrence Livermore National Laboratory (LLNL) and Lawrence Berkeley Laboratory (LBL) both contributed to the specification of the radionuclide source term by defining the waste-package failure modes and associated parameters. They also provided information on the interactions between the waste packages and the immediately adjacent environment.

This report documents the work by SNL, as supported by LANL, LLNL, and LBL. The work done by PNL is to be reported separately.

1.2 Purposes of the SNL TSPA

The primary purpose of the SNL TSPA effort was to contribute to the development of a particular process that will be a necessary part of future total-system performance assessments. This process, described in Chapter 2, is the derivation of "abstracted" representations of the complex processes that contribute to the behavior of a repository system. Our use of the word abstracted is intended to imply that the *essence* of the model or process has been captured. As explained in Chapter 2, such abstracted representations are needed to produce useful estimates of the principal measure of compliance with the EPA standard. This TSPA contains an early attempt to use the results of abstraction in a stochastic estimate of the behavior of a total repository system. The abstraction cannot be said to be complete; like the

total-system analysis itself, the abstraction will have to be greatly expanded before it will be rigorous and complete enough to satisfy the needs of the repository-licensing process. Nevertheless, an important objective of the TSPA was not only to use abstraction in producing values of performance measures, but also to begin learning how to perform abstraction defensibly.

The abstracted models were not necessarily simple to develop. As the chapters describing each TSPA component will illustrate, SNL expended considerable effort in trying to capture the essential features of the processes with models that were less computationally complex than the models used for detailed calculations. In contrast, PNL used detailed models as the basis for its total-system analysis.

To facilitate comparison between the abstracted SNL calculations and the more detailed PNL calculations, a common basic information set was established. The common information agreed upon was the definition of the stratigraphic cross-section, the geohydrologic parameters and distributions, the radionuclide inventory, and the initial and boundary conditions.

A secondary purpose of the SNL TSPA analysis was to demonstrate that complex combinations of probabilistic data can be assembled to provide a reasonable overall estimate of system performance. Some questions have been raised by the technical community about the feasibility of this process. To address these questions, the performance measure was chosen to be the release of radionuclides to the accessible environment. This measure was expressed as a complementary cumulative probability distribution (CCDF) of radionuclide releases from four components described in detail in later chapters: nominal aqueous flow, gas flow, human intrusion, and volcanic activity.

Because of the limited number of components included, it was not intended that this performance estimate would constitute an evaluation of Yucca Mountain as a site for a potential radioactive-waste repository. However, the study may be regarded as an update of certain aspects of previous studies of total-system performance because the performance measures produced in this study were derived from the data available as of the summer of 1991. It is important to remember, however, that many data are yet to be obtained for Yucca Mountain, several important choices among conceptual models are yet to be made, and formal methods for using abstraction and expert judgment are yet to be developed. Because so much work remains to be completed, the results of this study are not direct measures of the higher-level suitability of the Yucca Mountain site under the system criteria of 10 CFR 960 (DOE 1984), as described in Younker et al. (1992). A more appropriate

use of these results is as guidance for site characterization and for the next iterations of total-system performance assessment.

1.3 Differences from previous calculations

The technical bases for these performance-assessment analyses were developed primarily from prior HYDROCOIN (Prindle and Hopkins, 1990), COVE-2A (Dykhuizen and Barnard, 1992), and PACE-90 (Barnard and Dockery, 1991) work. The human-intrusion analyses drew upon prior calculations performed for the YMP Early Site-Suitability Evaluation (ESSE) (Younker et al., 1992). The TSPA differed from previous analyses in a number of ways. Following is a list of elements not included in prior calculational exercises, such as PACE-90.

- A six-step formalism, described in Chapter 2, was used to perform the analysis systematically and to aid in the interpretation of results. Thus, the analysis of each component includes a description of the scenario modeled, an estimation of probabilities, statements of assumptions, treatment of parameter uncertainties, and interpretations consistent with the inputs.
- The simulations were stochastic. Probability density functions (PDFs) were developed for a number of parameters. These distributions were randomly sampled in the analyses to obtain ranges of outcomes.
- The set of modeled phenomena was expanded. Multiple conceptual models were used in the aqueous-flow calculations. Releases from scenarios that included volcanism, gas flow, and human intrusion were calculated for the first time.
- Releases were calculated at the accessible environment. Most of the earlier PA calculational exercises calculated releases only at the water table, whereas all of the calculations in this study were run either to the surface or to the 5-km radius (in the saturated zone) defined by the EPA (1985).
- The saturated-zone flow and transport were included explicitly for both the tuff and carbonate aquifers beneath Yucca Mountain. Geochemical retardation was also included in the saturated-zone transport calculations.
- A larger number of radionuclides was included. For surface-release analyses, essentially all radionuclides of concern were included. For aqueous-flow

analyses, the list of four radionuclides used in PACE-90 (^{237}Np , ^{99}Tc , ^{129}I , and ^{135}Cs) was augmented by Pu, U, and Am isotopes (for their large contribution to the radionuclide inventory) and by ^{79}Se and ^{126}Sn (for their importance in dose calculations). Another additional isotope, ^{14}C , was included for the gas-release component.

- An abstracted source term was used for the aqueous-flow components. Additional work done by LLNL since the PACE-90 analyses has resulted in the development of abstracted models for mobilization mechanisms for radionuclides. As a result of this work, the source terms used in the TSPA include near-field interactions (those involving the engineered-barrier system and the immediately surrounding rock).
- Sensitivity studies were included for the human-intrusion and volcanism analyses. For example, the effects of varying the assumptions about drilling rate recommended by the EPA were studied for human intrusion.
- Results obtained by both SNL and PNL were used by PNL for dose calculations. PNL used the SUMO (Eslinger et al.*) and GENII (Napier et al., 1988) codes to calculate doses for several of the scenarios. The dose information is reported in Eslinger et al.

Other simplifying treatments of the total-system analysis problem have been undertaken by the Electric Power Research Institute (EPRI) (Shaw et al., 1992) and Golder and Associates (Miller et al., 1992). The approach taken by these other researchers differs from that of SNL, which is derived from the scheme outlined in the Site Characterization Plan (SCP) (DOE, 1988), as discussed in Chapter 2.

1.4 Caveats

The data and processes modeled in the TSPA analyses reflect our current ability to model the phenomena that may occur at a potential radioactive-waste repository at Yucca Mountain. The calculations have been performed using abstracted representations of the processes. Similar but more refined future calculations are expected to contribute ultimately to estimates of the site's ability to comply with total-system regulations. However, this first set of analyses is not comprehensive, and it is based on models that are limited by the current understanding of the site

* Information on documents not cited may be found in the bibliography.

and the current preliminary designs for the engineered parts of the repository system. Before those models can be said to be complete and valid, the site-characterization process will have to supply much additional data and interpretation; the repository-design process will have to make important decisions about the construction of the underground workings and the waste packages. Thus, this TSPA cannot be said to be a definitive representation of the total repository system.

Furthermore, although mean values of releases may be calculated from this study, they should not be considered "best estimates" of the behavior of Yucca Mountain as a potential site for a repository. Very broad ranges were established for many parameters. These ranges were chosen to ensure that they would encompass most possibilities, even to the point of incorporating unreasonably high or low values. This was particularly true of the values for the percolation flux within the mountain: the range included exceptionally high values in order to force the system, as modeled, to undergo fracture flow. The most widely accepted estimates of values for present-day flux and for increased flux due to climate change are smaller than the values used here. Another example of the use of broad ranges is the treatment of the source term for releases from the waste packages. The use of values from these ranges has resulted in what are probably very conservative assumptions about the source-term releases. (Chapter 3 discusses the philosophy and techniques for the development of distribution functions for the geohydrologic data; Section 4.3 discusses the assumptions about the source term.) Because the "answers" generated by this TSPA are preliminary, they should not be used as baseline values for licensing documents. As explained in Section 1.2, the results may, however, be useful in guiding near-term site-characterization activities.

The analyses may be the first in a periodic series of total-system evaluations. We would expect subsequent TSPA analyses to expand upon and add new components to this total-system performance assessment. A discussion of the directions for future work suggested by the results of this exercise is included in Chapter 11.

1.5 Summary of report contents

Chapter 2 gives the principles behind the formulation of the SNL TSPA, and the relation of the TSPA to the PA analyses outlined in the SCP. Chapter 3 details the problem setup, the development of input-data PDFs, and the conceptual-model assumptions. Chapters 4 through 7 discuss the components of the TSPA: aqueous flow (including the development of a source-term model), gaseous flow, human intrusion, and basaltic volcanism. Chapter 8 covers the methods used in this study to

combine the conditional CCDFs for each component into a total-system CCDF. Chapter 9 discusses the rationale and justifications for the abstractions developed for the TSPA, and includes some comparisons between abstracted and complex models. Chapter 10 is a summary of the results of the SNL TSPA effort, and Chapter 11 includes suggestions for future TSPA-style analyses.

This report contains only the problem definitions and results of the SNL analyses, as supported by LANL, LLNL, and LBL. Results of the PNL analyses are contained in Eslinger et al. (1992b). A complete description of the formulation of the geohydrologic parameter data set and distributions is contained in Gainer et al. (1992).

Chapter 2

The Process That Produced This Performance Assessment

(Bingham)

For reasons explained in the first section of this chapter, the activity described in this document contributes to an evaluation process described in the SCP (DOE, 1988). The first section summarizes that process. The second section explains the concept of a hierarchy of models. This concept is useful in understanding how the DOE expects to carry out the process; it underlies much of the work reported in this document. The third section describes the interim process that has been adopted for preliminary exercises of the SCP evaluation process, and the fourth section explains the specific steps followed by the total-system assessment described in this document. Readers who are familiar with the SCP and the model hierarchy may wish to skip the first and second sections and go directly to the third and fourth sections, which are more directly useful in understanding the rest of this document.

2.1 The process described in the Site-Characterization Plan

If studies of the Yucca Mountain site show it to be a suitable location for a radioactive-waste repository, the DOE expects to apply to the Nuclear Regulatory Commission (NRC) for authorization to construct the repository and for a license to operate it. The application will have to contain an examination of the ability of the repository system to comply with the regulations that govern it. One of the most fundamental of these regulations is the performance objective for the total system, established by the NRC in 10 CFR 60.112. This regulation requires that the system meet the standard set by the EPA in the current version of 40 CFR Part 191. To examine compliance with that standard, the DOE will conduct a performance assessment of the total system.

In Section 8.3.5.13 of the SCP, the DOE has described a process by which it expects to produce this performance assessment for the license application. Although the full description is complex enough to fill several pages of the SCP, it may be summarized simply as six steps:

1. List the potentially significant events and processes that may take place at the site.

2. List the "scenario classes" that may be modeled as part of the examination of total-system performance—i.e., list the sequences of events and processes that may release radioactive material from the repository.
3. Develop mathematical models of these scenario classes.
4. Screen the scenario classes on the basis of the releases they might produce, eliminating the classes that do not contribute significantly to releases of radionuclides from the system. To estimate the releases, use the mathematical models developed in Step 3.
5. Develop simplified, efficient mathematical models of the classes that remain after the screening.
6. Make probabilistic estimates of the releases, using the simplified models. Because these estimates will be expressed in a CCDF, this step will require the construction of a "total-system simulator", a computer routine for making the estimates.

The description in the SCP emphasizes that these steps are to be performed iteratively and not necessarily in strict order. The DOE recognizes that the knowledge gained from any of the steps, as well as from newly acquired data, may require revisions of previous steps. For example, the list of scenario classes prepared early in the process, before the site-characterization program acquires new data, will be preliminary; the process specifically requires revision of the list as new data are obtained and before all the remaining steps have been carried out.

Although the description in the SCP states that Step 6 will be performed last, there are significant benefits to be gained from performing it in a preliminary fashion before all the steps that precede it have been finished. The total-system performance assessment described in this document is an effort to perform step 6 in such a preliminary fashion. As Chapter 1 points out, the DOE expects to produce preliminary total-system assessments throughout the period of site characterization. The activity described in this document may be considered one assessment in that series.

2.2 The hierarchy of models

The mathematical models that describe phenomena at Yucca Mountain are indispensable in assessing the performance of a potential repository there. Because the repository would have to isolate waste for thousands of years, there can be no definitive set of tests to show once and for all that a repository system will perform as required. Instead, the DOE expects to estimate the system's future performance by using mathematical models that are based on test data describing the site. If the data are thorough enough and if there is enough confidence in the models, the estimates will give the NRC and the DOE reasonable assurance that the system will or will not perform as required.

For these reasons, the SCP process for producing the total-system assessment (Section 2.1) relies explicitly on mathematical models. To be useful in that process, the models will have to describe all the phenomena that may cause significant releases from the repository. Many models of such phenomena have been developed. For example, some of them describe in detail the geochemical processes that may occur if radionuclides move away from the repository; others describe the movement of fluids that may carry radionuclides; others describe the seismic events that may occur. Many of these models are highly complex. Embodied in large computer codes, they may require many hours of time on modern supercomputers to estimate the effects they describe. Such codes are indispensable in achieving the detailed understanding needed for the NRC and the DOE to feel reasonably assured that the repository will behave as predicted.

The production of probabilistic estimates (step 6 of the SCP process), however, may not be possible with models that are as detailed as these complex models. As Section 8.3.5.13 of the SCP explains, the probabilistic estimates will be made using the Monte Carlo method, i.e., by repeated random sampling from distributions of the variables that appear in the mathematical models. To achieve the statistical significance necessary to provide reasonable assurance, the sampling must be repeated perhaps tens or hundreds of thousands of times. Models that require hours of computer time for each sampling will not be able to produce the probabilistic estimates of releases. Instead, the estimates must use simplified models that run quickly on computers and that nevertheless reproduce all the essential phenomena. This reasoning, explained more fully in the SCP, lies behind step 5 (the development of simplified, efficient models) in the SCP process. These simplified models, used directly in performance assessment—i.e., in the modeling of the total repository system and of its major sub-

systems—can be described as lying toward the top of a hierarchy of models. Generally speaking, these models are more suited for probabilistic studies and are less detailed than the lower models in the hierarchy.

Figure 2-1 shows a pyramid that represents, in simple form, the hierarchy of models that has arisen from the need for detailed models of phenomena and for simpler system-assessment models. At the bottom of the pyramid are the models that try to express as many details as possible of the phenomena at Yucca Mountain. For example, the detailed models of nonisothermal effects contained in the computer code TOUGH (Pruess, 1987) would belong near the bottom of the pyramid. As the figure suggests, models of this kind are useful in further development of models and in mechanistic modeling of phenomena.

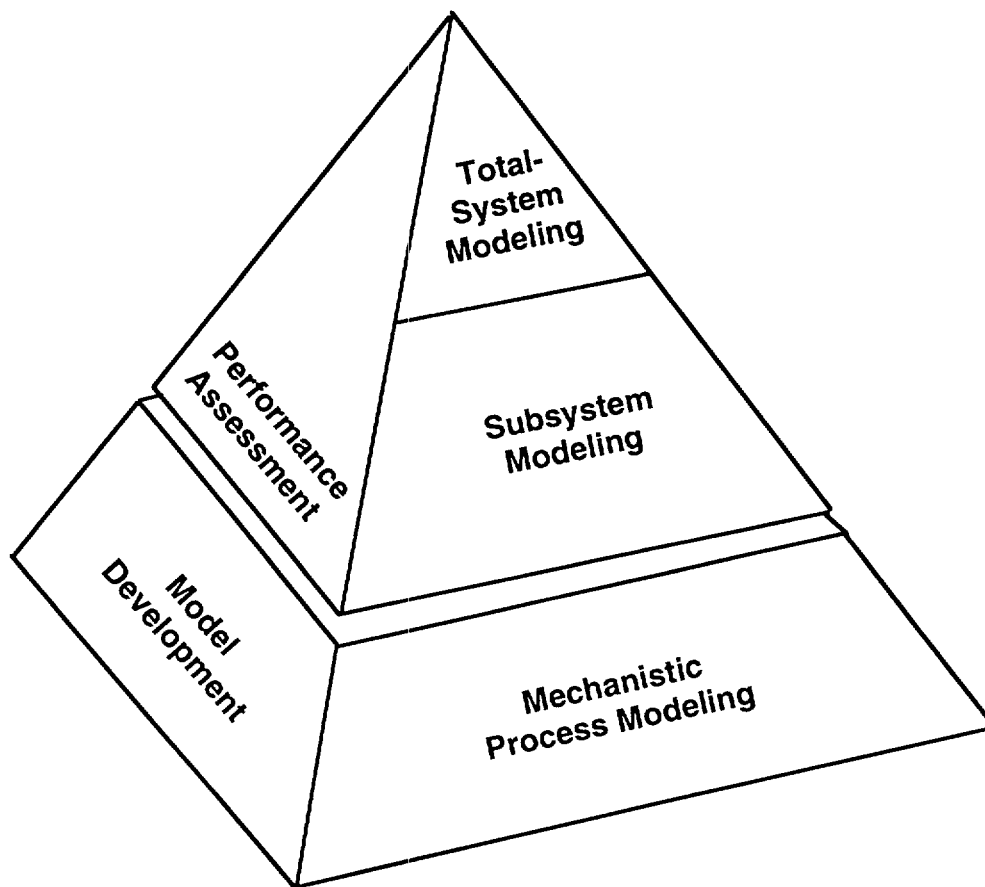


Figure 2-1. The hierarchy of models

Models that appear higher in the pyramid tend to be less detailed. They may adopt simpler mathematical expressions for the phenomena they describe; they may omit phenomena that have been demonstrated to be of little significance for releases of radionuclides; instead of calculating all the effects they describe, they may use tables produced by calculations done with models lower in the pyramid. An example of such a model is the one-dimensional flow model in the computer code TOSPAC (Dudley et al., 1988), which is useful under conditions that produce predominantly vertical water movement.

The models at the very top of the pyramid would include total-system models that do few calculations of their own but prepare CCDFs from distributions prepared by other models. Examples of such total-system models might include the models used to produce recent assessments by the Electric Power Research Institute (McGuire et al., 1990) and by Golder Associates (Miller et al., 1992).

To contribute defensibly to the SCP process for total-system assessment, the models higher in the pyramid must be firmly grounded on the lower models because they must successfully reproduce all the phenomena that are significant to the performance of the total repository system. Constructing these simplified models will not be a simple task. Although Section 8.3.5.13 of the SCP describes in general terms how the simplification can be done, the actual construction of the upper models has to proceed by a series of iterations. Calculations using the lower models will explore the effects of the phenomena and allow the upper models to incorporate the effects that prove significant. Moreover, the understanding gained from this work will allow the upper models to handle quantitatively the uncertainties associated with the results of the explorations. Calculations with the upper models will help the analysts identify phenomena and uncertainties to which estimates of total-system performance are most sensitive; this information will guide the next iteration of studies with the lower models. Developing the models near the top of the pyramid will thus involve calculations with both upper-level and lower-level codes.

One of the major purposes of the TSPA described in this document is the exercise and enhancement of an ability to develop the models near the top of the pyramid. In this TSPA the development of the upper models is called "abstraction" rather than "simplification". This usage is intended to emphasize two important aspects of the development:

- The development proceeds by pulling out the essential features from the detailed calculations done with the lower models—i.e., by abstracting those calculations.
- The main distinction between the upper models and the lower models is not that the upper models are generally less complex. In fact, the upper models may describe, though in simplified ways, so many phenomena that their implementation will require large computer codes and state-of-the-art computation methods. The main distinction is the thought process—the abstraction described in the item above—by which the upper models are developed from the lower. This abstraction may itself be a complex process, and “simplification” would be an inexact name for it.

The results that this TSPA has achieved in furthering the abstraction process are described later in this document, particularly in Chapter 9.

2.3 The process used in interim exercises

Since the SCP was published, the DOE has carried out interim exercises (e.g., Barnard and Dockery, 1991, and Fewell et al., 1992) of its ability to assess the performance of a repository system. These exercises have had several different purposes: for example, to help guide the planning for site characterization, to help with the design of the exploratory-studies facility, and to develop the capability for making assessments. It has not been possible to carry out, in any of these exercises, the full set of six steps in the SCP process for total-system assessment: the site-characterization program has not yet yielded many data, and much of the work necessary for the six steps is in the future. Because they could not follow the SCP process, the exercises have generally followed a simpler, interim process (Barnard, 1992) that uses the data and understanding available at the time the exercise is carried out. The exercises have attempted, however, to advance the SCP process while meeting their other purposes, and for that reason the interim process they have followed is derived from the six steps in the SCP. By coincidence, the interim process also has six steps. The TSPA reported in this document is itself an interim exercise, and the specific activities carried out in each of its components are derived from the six steps of the interim process. Those six steps are explained in the following list.

1. Screen scenarios to determine which phenomena are to be modeled in the exercise. A full listing of scenarios will not be possible until after site characterization has produced further understanding of the site. Nevertheless, an important part of each exercise is to decide systematically what the exercise should model in order to meet its purposes; ideally, the choice should reflect the current understanding of the events and processes that may be important. In the absence of definitive lists of scenarios, the exercises have been able to draw on preliminary lists of events and processes that the Yucca Mountain Project has already developed. This preliminary work and some earlier modeling have produced some indications of the sequences of events and processes that would be most likely to affect waste isolation at Yucca Mountain. This kind of screening is appropriate for choosing the modeling to be done in an interim exercise.
2. Estimate the probabilities of occurrence of those scenarios. In the absence of site-characterization data, most of the current estimates of these probabilities are uncertain. Preliminary estimates can, however, usually be made by drawing on expert opinion and on the few published documents that deal with the probabilities.
3. Choose the conceptual models to be assumed in the modeling of releases. The scientific community has not yet reached consensus on the conceptual models that properly describe the major features of the Yucca Mountain site—for example, a model identifying the general features that control the flow of moisture through the unsaturated rock there and describing the relative importance of flow in fractures and in the rock matrix. The mathematical models used in any exercise must incorporate one or more of the conceptual models that have been suggested as appropriate for Yucca Mountain.
4. Estimate parameter values and the uncertainties in them. Once the conceptual models have been chosen and have been applied to the scenarios whose consequences are to be estimated, an analyst must choose values for the parameters in those models. For probabilistic studies, the natural variabilities in these values are often expressed as probability distributions. An important part of the analyst's choice is the estimate

of the uncertainties in the chosen values, which also contribute to the probability distribution. This estimate contributes to the estimates of uncertainty in the final calculations of radionuclide releases.

5. Calculate releases. This task generally requires that the analyst use computer codes containing the models that estimate releases. The boundary and initial conditions used in the calculations should also be stated here.
6. Interpret results. This step is largely a matter of deciding what conclusions can be drawn from the calculations of releases and how the lessons learned from the exercise should guide future work. The interpretation focuses on meeting the particular purposes of the exercise; none of the exercises done so far has been simply for the purpose of producing numerical results.

2.4 Steps in this total-system performance assessment

This TSPA consists of several components, described in Chapters 4 through 7, that lead to the construction of conditional CCDFs for radionuclide releases from the repository system (Chapter 8). The steps carried out in each of the components follow the interim process described in Section 2.3; moreover, many of the steps used to produce the data base common to the components (Chapter 3) also followed the interim process. To avoid repeating information in each of Chapters 3 through 7, this section describes some specific features of the way the interim process has been adapted for the TSPA.

To choose the features of the system to be modeled for any component of this analysis, a screening of scenarios is the first step in the interim process outlined in Section 2.3. In this TSPA that screening was generally done by examining the preliminary trees that the Project has prepared to link features, events and processes (FEPs), and by consulting the experts who prepared them. At least one path through an appropriate "FEP tree" was selected for the modeling of each component. The selection was usually intended to capture a sequence of events that would be representative of the group of similar scenarios in which it appears; for example, a sequence might be considered representative because its consequences seem likely to bound the consequences of that group. The descriptions in Chapters 4 through 7 explain how each selection was made. The choice of components for the analysis was itself a screening of scenarios on a large

scale: ground-water flow, gas flow, human intrusion, and basaltic volcanism have been suggested by the preliminary development of scenarios as the primary sequences that total-system analysis should examine. (A fifth scenario category, tectonic activity, will be discussed in a report from PNL).

After choosing the scenarios, the TSPA carried out steps 2 through 4 of the interim process: estimating probabilities of occurrence, choosing conceptual models, and estimating parameter values and uncertainties. To do these tasks, the TSPA relied on review of available data and on elicitation, formal and informal, of expert opinion. Although many of the parameters were to be used deterministically in the analyses, with single assigned values, the need to treat others probabilistically required the construction of numerous probability distributions of parameter values. Separate discussions in Chapters 3 through 7 describe how each set of data was chosen.

Step 5 of the interim process, the calculation of releases, was done separately for each component of this TSPA by first choosing the simulation tools to be used and then using them to make multiple computer estimations of consequences. The tools were usually chosen from available computer codes, although some simulations were simply adoptions of results generated by models near the bottom of the model hierarchy. To produce probabilistic estimations for some components, the codes were run in a sampling mode that produced the multiple estimates of consequences; i.e., the Monte Carlo method was used.

Because the TSPA was intended to produce CCDFs, step 5 of the interim process was augmented by incorporating the probabilities of the modeled sequences. These probabilities had been obtained as part of the reviews and elicitations. With the calculated releases and these probabilities, one or more "conditional" CCDFs were produced for each component. They were then combined to produce CCDFs that display the behavior of the repository system. This final construction of an overall conditional CCDF is described separately from the descriptions of components, in Chapter 8.

The final step in the interim process calls for the interpretation of results. To meet the purposes of this TSPA, the interpretation, which appears in Chapters 4 through 7 and particularly in Chapters 9 through 11, is aimed at the lessons learned from the abstraction process (Section 2.2) and at suggestions for future analyses. A secondary aim of the interpretation is to derive insights into the ability of the site to isolate waste. Because site characterization is still in

early stages, the data available to the TSPA are not definitive enough to allow many firm conclusions about that ability.

Chapter 3

Problem Setup

(Kaplan, Dockery, Wilson, Barnard)

As is discussed in Chapter 2, a TSPA requires definition of processes and events that could influence the isolation of waste at a potential repository at Yucca Mountain. In this chapter, we first discuss how processes and events were chosen for study in this TSPA. Then we discuss the abstraction of the models of these processes. Finally, we define the model parameters—measures of features and conditions that make the models specific to Yucca Mountain.

In theory, both the list of important processes and events being modeled and the values of model parameters could be derived directly from site-characterization data. In practice, site-characterization data can probably never be complete (and are presently quite sparse) for the following reasons:

- the possibility of changing conditions at Yucca Mountain,
- the possibility of effects that cannot be directly measured and are difficult to define through inference (e.g., igneous activity), and
- the low probability of discovering extreme behavior (e.g., the fastest groundwater flow path).

Thus, our judgment and the opinion of experts working on the YMP form an undercurrent throughout the discussions in this chapter. An effort has been made to place this subjectivity into a well-defined framework that emphasizes objective, quantitative data and reasoning as much as possible.

3.1 Construction of relational diagrams and scenarios

To ensure that all the TSPA analyses have been performed in a systematic fashion and to permit these analyses to be more readily compared with other (past and future) calculational exercises, a six-step process (Barnard, 1992) has been adopted. As explained in Chapter 2, this process is a derivative of the procedures outlined in the SCP for performance-assessment analyses used in the repository-licensing activities.

An important characteristic of PA analyses that follow the six-step method is that each calculation of repository behavior is stated explicitly in terms of the physical phenomena occurring in the repository system. This is done by expressing the

calculation in terms of a scenario. Here we use the word "scenario" (which also has other meanings in some performance-assessment documents) as a well-defined connected sequence of features, events, or processes. *Features* are the geologic or hydrologic properties of the site or system, which are expected to be durable. *Processes* are phenomena that have gradual, continuous interactions with the system. *Events* are occurrences that have a specific starting time (and usually a duration shorter than the time being simulated). There are many ways that logical and physical relationships among features, events, and processes (FEPs) can be depicted. SNL has chosen, for convenience, to display them in relational diagrams called "FEP diagrams". This use of the term "FEP diagram" is a departure from SNL's prior work in which the logic trees were called "event trees" (Barr et al., 1991). The change has been made because the structures include not only events, but also geologic and hydrologic features and various thermal, geochemical, volcanic, and other processes. Additionally, there is unnecessary confusion with other popular usage. In other usage, the term "event tree" has been confined to describing system behavior as a series of events leading to failure (OECD, 1992). At the beginning of each chapter dealing with a specific component of the TSPA, the scenarios used for that component and the FEP diagram from which those scenarios were derived are discussed in detail.

Because the site-characterization process at Yucca Mountain is immature, the features, events, and processes occurring at the site are not well understood. Indeed, there may be many important FEPs which have not yet been identified. In particular, the FEPs cannot yet be categorized definitively (e.g., into expected processes and unexpected conditions or events). The initial FEP diagrams do not limit themselves to descriptions of events only (i.e., phenomena with an identifiable time of occurrence). Furthermore, branches in the diagrams can represent either mutually exclusive FEPs (such as waste being carried to the surface by drilling or the same waste being carried to the water table) or FEPs whose parameters simply take on different values. Additionally, we are using branches of the diagram to represent FEPs that may occur at different times in the history of the system.

The FEP diagrams connect sequences of FEPs which lead from initiation of the sequence to release of radionuclides to the accessible environment. The diagram is used to systematically organize the analysts' knowledge and understanding of the hydrogeologic system, repository interactions, and associated phenomena. A "scenario", under the definition made earlier, can be thought of as a possible future history of the repository system. Because scenarios are defined by specifying the

features, events and processes that occur, a scenario can be represented by one or more paths through the FEP diagram. Because the branches of the FEP diagram are not mutually exclusive, more than one path may be active at the same time during the future history of the system; also, different paths may be active at different times or at different spatial locations. An example of the former situation would be nominal flow and human intrusion. They are described in separate diagrams, but the complete specification of a scenario involving human intrusion would require specification of paths through both FEP diagrams, since nominal flow takes place before, during, and after the human intrusion. An example of the latter situation would be the "Hot Repository" and "Cold Repository" branches of the Nominal Flow FEP diagram (see Figures 4-2 and 4-3 in Chapter 4). The repository will be hot at early times and cold at late times, so complete specification of a nominal-flow scenario would require specification of paths through both branches of the diagram. Also, repository cooling will not be uniform, so some parts of the repository may effectively be cold while other parts are still hot.

Converting paths through the FEP diagrams from simple sequences of FEPs to a scenario that can be modeled requires adding sufficient detail to capture and state mathematically all of the essential features necessary to make the calculations. Note that a sophisticated computer model may simulate many paths through a FEP diagram at the same time. For example, the Nominal Flow FEP diagram (see Figure 4-1) contains branches describing several variations on matrix and fracture flow through Yucca Mountain. A sufficiently general flow code could model all those branches at once.

Each FEP diagram contains a large number of through-going paths. A complete analysis of any scenario category (such as the scenarios initiated by igneous activity) would require that the analysis of the FEP diagram defining that category include all scenarios in the category. If every scenario were analyzed, some would result in insignificant releases relative to others. Some scenarios would have relatively low probabilities of occurrence. Because a CCDF relates releases and their probabilities of occurrence, those scenarios with both low consequence and low probability should not contribute significantly to the total-system CCDF. After the paths that contribute little to the overall performance measure have been identified, either through analyses or expert judgment, these branches may be pruned from the FEP diagram. Conversely, those scenarios that contribute significantly to the CCDF can be identified for more rigorous investigation. This process for pruning

scenarios has not formally begun; for the preliminary TSPA, scenario selection was based on informal judgments of the participants.

SNL has constructed FEP diagrams for the four scenario categories investigated in the TSPA—nominal-flow aqueous and gas transport, human intrusion, and igneous intrusion. The nominal-flow diagram includes present-day groundwater and gas flow, as well as changes in the flow patterns induced by climate change and the transient thermal effects of a repository. Disturbed conditions, such as those initiated by volcanism and human intrusion, are displayed in separate diagrams. Our approach for this TSPA is to model different scenario categories separately rather than modeling scenarios that are part of an exhaustively specified class. This approach and the assumptions behind it are described in Chapter 8.

From the FEP diagrams, specific scenarios were selected for modeling. The scenarios selected for the TSPA from the nominal-flow diagram describe processes currently considered to be important potential contributors to releases. From the FEP diagrams for disturbed conditions, scenarios were chosen that appear to have the highest likelihood of occurrence or the greatest releases. The volcanism scenario was added because it is perceived to be of greater public concern than most other scenarios.

Full, detailed modeling of each scenario requires that the conceptual models and parameters describing the component features, events, and processes be specified. In any natural system, there will be considerable variability in the parameters of the models being used. At a site as incompletely characterized as Yucca Mountain, there are additional uncertainties associated with our lack of information. The TSPA analyses address these variabilities and uncertainties by using stochastic simulation techniques. The development of data sets for stochastic analyses is discussed in this chapter.

This preliminary TSPA investigates only a limited number of scenarios; there still remain a large number of FEPs that must be considered for inclusion in the final total-system analyses. The parameter and model uncertainties and variabilities associated with each FEP mean that there can be many possible combinations of parameter values, each leading to a possible value of release. As explained in later chapters, this study used thousands of combinations in producing the CCDFs. To characterize the behavior of the site adequately for the final evaluation of its suitability may require many more thousands of simulations, each with a selected realization of parameter values. It is not feasible to perform such a large number of simulations using complex calculations, given current computing resources and

time available. Primarily for this reason, this TSPA analysis attempts to use abstracted models.

3.1.1 Conceptual models

There are many conceptual models which could be used to represent the processes associated with each of the TSPA components. Some of the conceptual models were chosen because they represent reasonable bounds on alternative models. For example, the weeps model, which is an abstraction of a more complex non-equilibrium model of fracture and matrix flow, is a reasonable bound to the current alternative conceptual models for groundwater flow. Other conceptual models were chosen as simplified representations of processes for which no detailed models yet exist (e.g., interactions of an igneous intrusion with a repository). The abstraction of the models was as important an enhancement of the ability to perform TSPA analyses as the abstraction of the data was. The details of each model used for a TSPA component are described in the respective chapters.

3.2 Geohydrologic data

In order to apply the conceptual models for simulating aqueous transport (Chapter 4), the parameter values and boundary conditions for those models have been defined. This section describes how the input data sets were developed. The authors' interpretation of both site-specific and analog geohydrologic data, along with our current understanding of basic physical processes operating at Yucca Mountain, have been used. However, the data set was built to be general enough to be used in exercises other than the TSPA. For this reason, it will be considered for inclusion in the YMP Reference Information Base.

The parameters given in this section for each rock unit in the stratigraphic interpretation include saturated hydraulic conductivity; porosity; saturated volumetric water content; and the van Genuchten air-entry parameter (α_{vG}), desaturation parameter (β_{vG}), and degree of residual saturation (S_r). Also provided are the same parameters representing the fracture hydrogeologic properties for each unit. For each of the parameter values in each unit, a probability density distribution was generated. The development of this geohydrologic data set is described in detail in Gainer et al. (1992). The geohydrologic parameters have been used only in the composite-porosity aqueous flow calculations. The data used for the weeps aqueous flow and the gaseous flow calculations are discussed in later chapters.

3.2.1 Problem domain

All the TSPA analyses considered the transport of radionuclides from the repository to the accessible environment. The aqueous-transport problem domain sampled the volume directly beneath the repository to the water table and, in the saturated zone, out to the accessible environment.

A 2-D transect in the northern part of the repository block was chosen to represent unsaturated-zone hydrologic conditions throughout the repository block. The location of this transect through the repository was chosen because unsaturated-zone geohydrologic data were available from a number of drillholes in that area. The transect extends from east to west, starting approximately 500 m east of drillhole UE-25 a#1 (in Drill Hole Wash) through USW G-4, to USW H-5 at the crest of Yucca Mountain (Figure 3-1). The surface trace of the Ghost Dance Fault is crossed by the transect. The fault was modeled using a 14-m offset and increased fracture permeability (Eley, 1990). The increased permeability was modeled by using increased fracture densities and apertures.

The saturated-zone calculations included the area from beneath the repository to a boundary 5 km downstream. The saturated zone was represented by a flow field taken from Czarnecki and Waddell (1984) and Czarnecki (1985) (Section 4.4). In the Czarnecki and Waddell model, the regional flow originates to the northwest of the repository block and flows to the southeast.

The vertical domain for aqueous-transport problems extended from the potential repository horizon to the water table. The stratigraphy was represented as heterogeneous and layered, as described in Section 3.2.2. The gas-flow problem domain went from the repository to the surface directly above. It used different 2-D cross-sections than were used for the aqueous calculations (see Chapter 5). One of the human-intrusion analyses extends through the section of saturated tuffs, into the underlying aquifer in the Paleozoic carbonate rocks. The projected position of the potential repository, with respect to the vertical and horizontal problem domains, is shown in Figure 3-2. Note that the distances in Figure 3-2 are given along the path line of the transect. Therefore, from G-4 to UE-25 a#1 the distances differ from the gridded-terrain model coordinates for those drillholes.

3.2.2 Stratigraphy

The stratigraphic scheme used for the composite-porosity unsaturated zone aqueous flow calculations in this TSPA was simplified from the PACE-90 hydrostratigraphy (Barnard and Dockery, 1991). One of the conclusions of PACE was

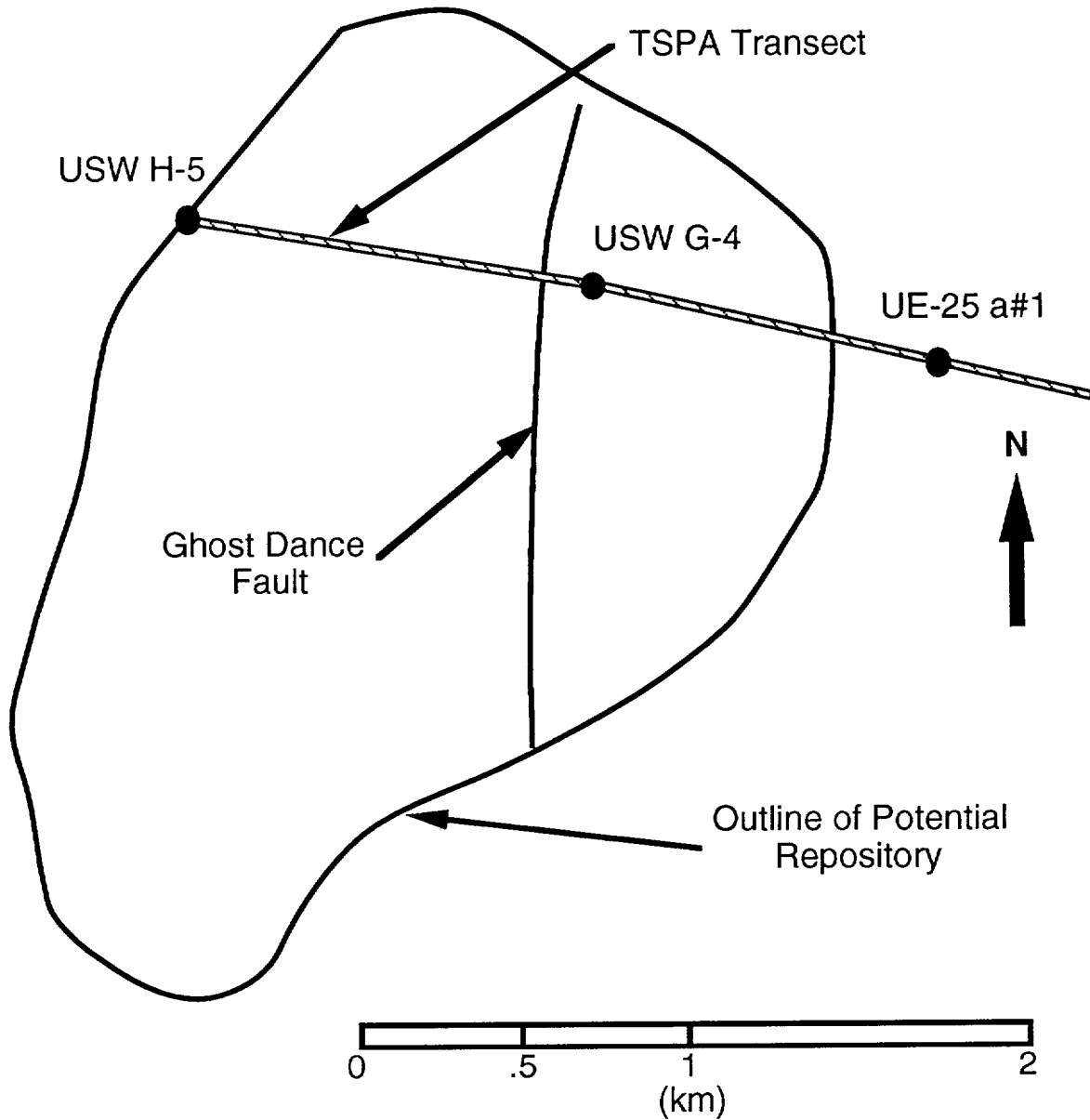


Figure 3-1. TSPA analysis transect through Yucca Mountain

that the final calculational results (which were one-dimensional) were not sensitive to the high degree of detail incorporated into the stratigraphy (for the boundary and initial conditions used). In general, there was very little contrast in the physical properties between successive layers in the PACE stratigraphy. The one layer that caused lateral diversion in PACE (the Tpt-TNV) had been purposely specified with extremely high contrast as a test of the numerical simulations. Because there are no

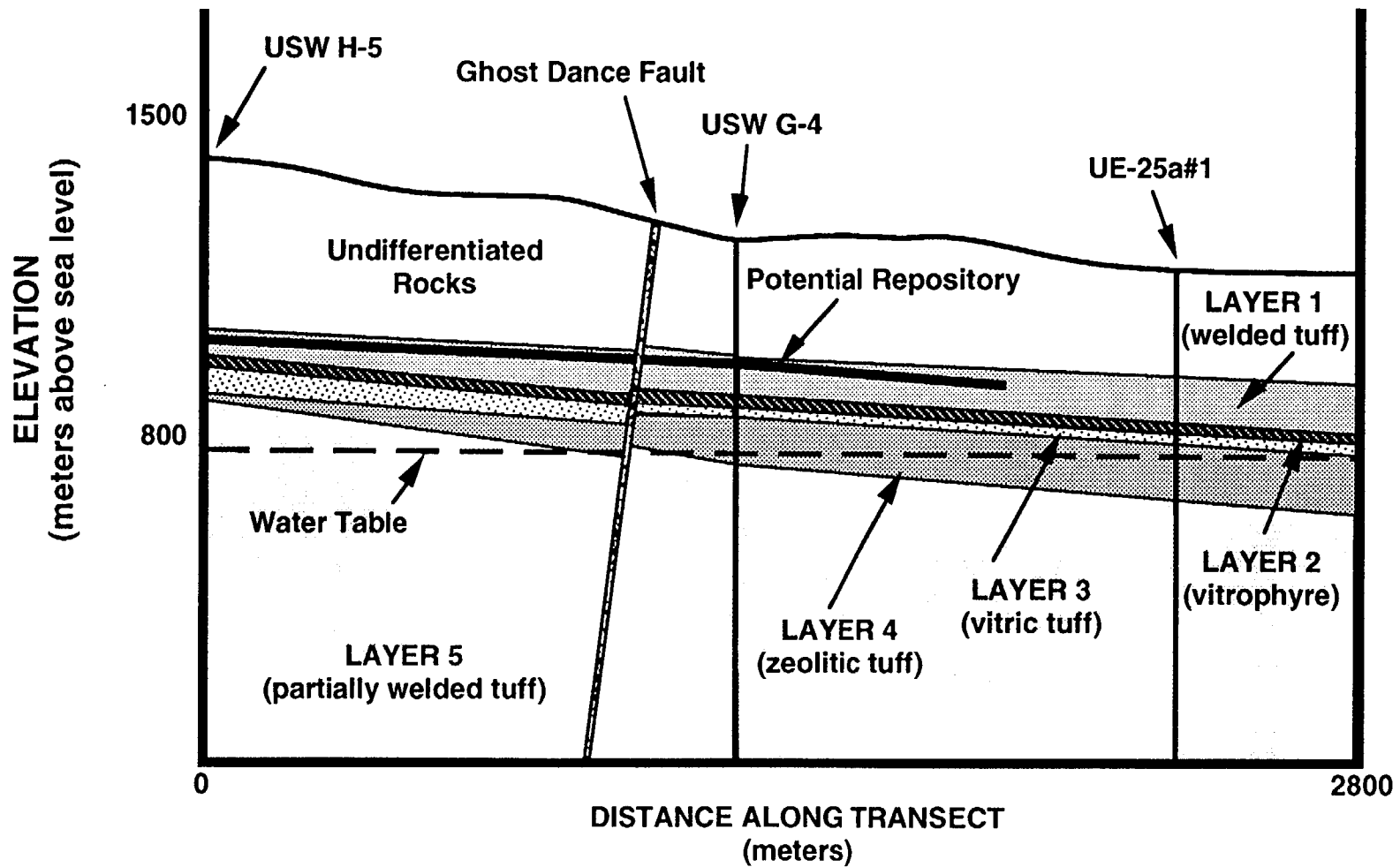


Figure 3-2. Schematic cross-section of unsaturated-zone stratigraphy

naturally occurring analogs for the values used in the PACE problem, more realistic values have been chosen for the hydrologic properties of the Tpt-TNV layer.

3.2.2.1 Stratigraphic cross-section

Five layers were used in the cross-section for the problem to describe the unsaturated zone. The layers are a very simplified representation of different types of ash-flow tuff observed at Yucca Mountain. A number of layers that have been identified in the field have been lumped into single layers. The resulting layers were designated by the dominant rock type within that interval. The details of the stratigraphy were determined by reviewing the USGS lithologic logs for drillholes USW H-5 (Bentley et al., 1983), USW G-4 (Bentley, 1984), and UE-25 a#1 (Spengler et al., 1979) and the PACE-90 nominal-case hydrostratigraphy (Barnard and Dockery, 1991). Actual "picks" for the layer boundaries were taken from the IGIS database (Eley, 1990). Depending on the horizontal location along the transect, up to five layers, representing five different tuff types, have been included. From the top of the domain to the bottom, the layers are given in Table 3-1.

Table 3-1
Hydrostratigraphy used for unsaturated-zone aqueous problems

Layer	PACE-90 Designation for Hydrostratigraphy	Dominant Lithology
1	Tpt-TM	moderately welded
2	Tpt-TV	vitrophyre
3	Tpt-TNV	vitric, non- to partially welded
4	Tcb-TN	zeolitic, non- to partially welded
5	Tcpp-TP	partially to moderately welded

A more detailed description of the PACE-90 hydrostratigraphic zones can be found in Barnard and Dockery (1991) (Table 3-2). Development of the stratigraphy and the hydrogeologic parameters for this problem is described in Gainer et al. (1992).

The saturated zone was divided into two layers, although the exact elevations of the layer boundaries were not used in the TSPA analyses. The upper layer of the

saturated zone occurs within Cenozoic tuff. This section of saturated tuff is called the "tuff aquifer" in this exercise, even though most of the rocks in this interval are nonwelded tuffs, which, in most locations, are not sufficiently permeable to be classified as an aquifer (SCP, Chapter 3). The tuff aquifer extends from the water table to the interface with the Paleozoic basement rocks. The lower saturated layer is called the "carbonate aquifer". It occurs within the Paleozoic carbonate rocks and extends from the contact with the tuff aquifer to depth. Location of the relevant features and layers is shown in Table 3-2.

Information for fracture density and orientation in the unsaturated-zone layers was derived from Spengler and Chornack (1984). Fracture-property information was derived from Zimmerman and Vollendorf (1982), and Carsel and Parrish (1988).

Table 3-2
Elevations of layers at selected locations in
geohydrologic problem domain

Layer # or Feature	Lithology	USW H-5 (m)*	West Boundary of Ghost Dance Fault (m)*	USW G-4 (m)*	UE-25 a#1 (m)*	500 m East of UE-25 a#1 (m)*
Surface		1478	1309	1270	1199	1175
Repository		1030	966	956	(870)	(831)
1	welded tuff	996	875	869	811	781
2	vitrophyre	974	863	860	798	771
3	vitric tuff	905	832	836	784	759
4	zeolitic tuff	885	734	723	637	596
5	partially welded tuff/water table boundary	770	731	731	729	730

* Elevation above sea level of the feature, or in the case of an individual layer, to the base of that layer.

(Values in parentheses are projections)

3.2.3 Initial and boundary conditions

Both the eastern and western vertical boundaries of the two-dimensional unsaturated-zone domain were assumed to be no-flow. For the western boundary at

drillhole USW H-5, (which is on the up-dip side of the flow field), this boundary condition is unlikely to influence the results. To prevent the no-flow condition at the eastern vertical boundary from influencing the flow field between drillholes USW G-4 and UE-25 a#1, the problem boundary was extended 500 m east of UE-25 a#1. This extension was intended to prevent the no-flow condition from introducing modeling artifacts, such as ponding, into the interpretation of flow processes near UE-25 a#1.

The simulations were started from specified initial saturation and flux conditions and were run to the steady-state conditions consistent with the imposed percolation rate. Percolation values ranged from 0.0 to 39 mm/yr. This range was chosen to include all possible increases in infiltration due to climate changes. At the higher percolation values the calculations simulate fracture-dominated flow.

3.2.4 Parameters

The model domain for the unsaturated zone described in Section 3.2.1 is defined as a variably layered sequence of volcanic tuffs. Each layer is believed to be fractured, with the degree of fracturing varying from layer to layer. The fracturing is assumed to be more extensive in the fault zone than in the surrounding rock. The rock matrix is assumed to be porous and capable of transmitting fluid independently of the fractures. To model the process of fluid flow through the domain, hydrologic parameters characterizing both the fractures and the porous matrix need to be specified for each individual hydrostratigraphic unit. The data set used for the TSPA analysis (Gainer et al., 1992) attempted to capture all these factors. It is one of many possible interpretations of what has been observed at the site. The models for unsaturated-zone flow used the parameters from the data set with different degrees of detail. The composite-porosity model used most of the parameters, while the weeps model used only one.

It should be noted that the data set described here was intentionally made quite general. Data were included that were not used by every analysis. This has been done to make this data set more universally applicable, and to avoid biasing any analysis.

3.3 Development of parameter distributions

One of the specific criteria that this data base was intended to meet was the ability to support stochastic performance assessments. This means that the numerical descriptions of the hydrologic parameters are not necessarily single-valued.

Instead, the parameter is described by a probability density function (PDF) that defines the likelihood of various outcomes when the function is randomly sampled. The methods by which these distributions were generated are described in detail in this section. Table 3-3 lists the hydrogeologic parameters.

To summarize the development of the stochastic data base to be described in this section, probability density functions have been generated for almost 60 parameters for the hydrogeologic, geochemical, and volcanic components of the TSPA analysis. These PDFs have been developed from both site and analog data and from expert elicitation. A rigorous formalism has been applied to ensure that the PDFs chosen are consistent with the amount of information available. As a result, the parameter-value distributions are minimally biased throughout their ranges.

Table 3-3
Stochastic hydrogeologic data base

Matrix Parameters	Fracture Parameters
Saturated Hydraulic Conductivity, K_s	Saturated Hydraulic Conductivity, K_s
Saturated Volumetric Water Content, θ_s	Saturated Volumetric Water Content, θ_s
Porosity, n	Fracture Density, ρ_f
Air-Entry Parameter, α_{vG}	Air-Entry Parameter, α_{vG}
Desaturation Parameter, β_{vG}	Desaturation Parameter, β_{vG}
Residual Degree of Saturation, S_r	Residual Volumetric Water Content, θ_r

3.3.1 PDF construction methods

Monte Carlo, or other stochastic simulations have been used for the TSPA analyses. These types of analyses require the definition of probability density functions for the simulation parameters. At this time, only sparse data are available to support a model of the PDFs for most parameters. For some of the simulation parameters there are no data at all. Sparse or nonexistent data lead to uncertainty in the choice of an appropriate distribution for a performance-assessment input parameter. This section discusses the formalism that was used to generate the PDFs for the hydrogeologic parameters specified in Table 3-3.

The density functions generated by applying the formalism described below are models of the analyst's uncertainty as to the appropriate value of the parameters to use in a performance-assessment simulation. The density functions are not models of the frequency distribution of the parameter that would be obtained either

from a site-specific sampling program or from expert judgment. Details are discussed in Kaplan (1991), and specifically in regard to this data set in Gainer et al. (1992).

The formalism starts by defining the parameter of interest as a random variable; this point may seem trivial but it is necessary for the next definition. The next step defines the uncertainty in the parameter as Shannon's informational entropy (Shannon, 1948). There are two important points here to remember. First, Shannon's informational entropy is a quantity that can be thought of as a measure of our confidence in a proposition. Second, it is a function of the probability density of the parameter but not of the value of the parameter. There are a number of qualitative interpretations of Shannon's informational entropy: information, state of knowledge, ignorance, and confidence. The functional form of Shannon's informational entropy simply states that *if* the probability density function of the random variable is known, the uncertainty in the stochastic process is the dependent variable of the entropy function—a number.

As is often the case, the probability density of the random variable is not known. In this case, the assumption is made that of all the possible distributions one could choose, the distribution that maximizes Shannon's informational entropy, subject to the known or plausible constraints on the random variable, is the most appropriate. This last assumption is known as the Maximum Entropy Formalism (Jaynes, 1957).

The next step follows a recommendation by Harr (1987). He proposed to define the possible elements of the set of constraints for the random variable as: 1) the minimum value of the variable, 2) the maximum value, 3) the mean, and 4) the coefficient of variation. The term "mean value" is interpreted here to be an estimate of central tendency. When there are either sparse data, or no data, the mean is unlikely to represent the expected value of observations. For these distributions, the mean should be thought of primarily as a fitting parameter.

The elements of the set of constraints can be thought of as pieces of information. Depending on how many pieces of information are available—one, two, three, or four—there is a PDF that maximizes Shannon's informational entropy consistent with the number of pieces of information available. The relationship between information and the choice of distribution under the formalism is given in Table 3-4.

Using the truncated normal PDF can be difficult, since it involves the solution of transcendental equations. In its place, Harr has suggested using the beta distribution (Harr, 1987), which also defines a PDF using the range, mean and variance.

Furthermore, the other distributions listed in the table can also be produced from (or closely approximated by) the beta distribution. Therefore, the beta distribution has been used to represent the probability density functions for many parameters defined in this TSPA. Tables in the rest of Chapter 3 list choices of distribution function.

The objective of the formalism is to generate distributions that describe the likelihood of an outcome that is constrained or consistent with the analyst's beliefs and yet allows the analyst to remain maximally noncommitted beyond the available knowledge. In other words, a probability statement about an input parameter should reflect the analyst's state of knowledge about that parameter, including the analyst's uncertainties.

Having briefly defined the conceptual basis for the formalism that will be followed in generating the PDFs of the hydrogeologic parameters, next we will discuss the practical application of the formalism.

Table 3-4
Relation between amount of information
and maximum-entropy PDF

Available Information	Distribution
Range, ([a,b])	Uniform
Mean, (E[x])	Exponential
Mean and Variance, (E[x] and $\sigma[x]$)	Normal
Range, Mean, and Variance	Truncated Normal

The beta distribution is given by the expression

$$p(x) = C (x - a)^{\alpha} (b - x)^{\beta}, \quad (3.1)$$

where α and β are > -1 and C is the normalizing constant. To avoid confusion with the α and β used as parameters of the van Genuchten formula for moisture retention, the van Genuchten α and β parameters will always be labeled α_{vG} and β_{vG} . Parameters without the subscripts will refer to the beta distribution.

A solution of Equation 3.1 requires four pieces of information: the minimum and maximum values that define the range of the random variable (a and b , respectively) and the two exponents α and β . The exponents can be calculated if the mean value $E[x]$ and the coefficient of variation $CV[x]$ are known (Harr 1977, 1987;

Kaplan and Yarrington, 1989). The coefficient of variation is defined as the standard deviation divided by the mean, i.e.,

$$CV[x] = \sigma[x] / E[x], \quad (3.2)$$

where $\sigma[x]$ is the standard deviation. The exponents α and β determine the shape of the probability density function. Table 3-5 summarizes the conditions on the exponents under which certain shapes occur. Plots of some of the various shapes used in the TSPA analyses are illustrated in Figure 3-3.

The flexibility of the beta distribution greatly simplifies the process of preparing input for a performance-assessment problem. Input tables for a simulation can be standardized and pre-formatted. The same distributional information is provided by the analyst for each random variable, which simplifies the problem conceptually. The next link in the software chain is the Latin Hypercube Sampler (Iman and Shortencarrier, 1984), which will accept a beta distribution as input.

Table 3-5
Effects of beta-distribution exponents
on PDF shape

Shape of Beta Distribution	α	β
Uniform	0.0	0.0
Left Triangle	0.0	1.0
Right Triangle	1.0	0.0
Symmetrical	$\alpha = \beta$	$\beta = \alpha$
Skewed Right	$\alpha < \beta$	$\beta > \alpha$
Skewed Left	$\alpha > \beta$	$\beta < \alpha$
U-Shape	$\alpha < 0.0$	$\beta < 0.0$
J-Shape	$\alpha \geq 0.0$	$\beta < 0.0$
Reverse J-Shape	$\alpha \leq 0.0$	$\beta > 0.0$

No attempt was made in the current exercise to include correlation structures in the simulation. Cross correlation is suggested by Carsel and Parrish (1988). This cross-correlation could be particularly useful for the fracture parameters developed in Section 3.3.4. The sand data reported in Carsel and Parrish were used as a direct analog for the fracture properties of the composite-porosity model. The issue of cross correlation is discussed in greater detail by Wang and Narasimhan. Preliminary sensitivity analyses of the output to the type of cross-correlation struc-

ture given by Carsel and Parrish suggests that this information can substantially alter the results only in the case of a column of uniform material. As the layered structure becomes more complex, the sensitivity to cross correlation appears to decrease dramatically. Two simple cross-correlation structures, among several of the hydrologic parameters for total-system performance-assessment calculations, were tried by Wilson et al. (1991), but no significant effect was found. Autocorrelation structures specific to Yucca Mountain are discussed by Rautman and Flint (1992). The sensitivity of the output to this information has yet to be investigated.

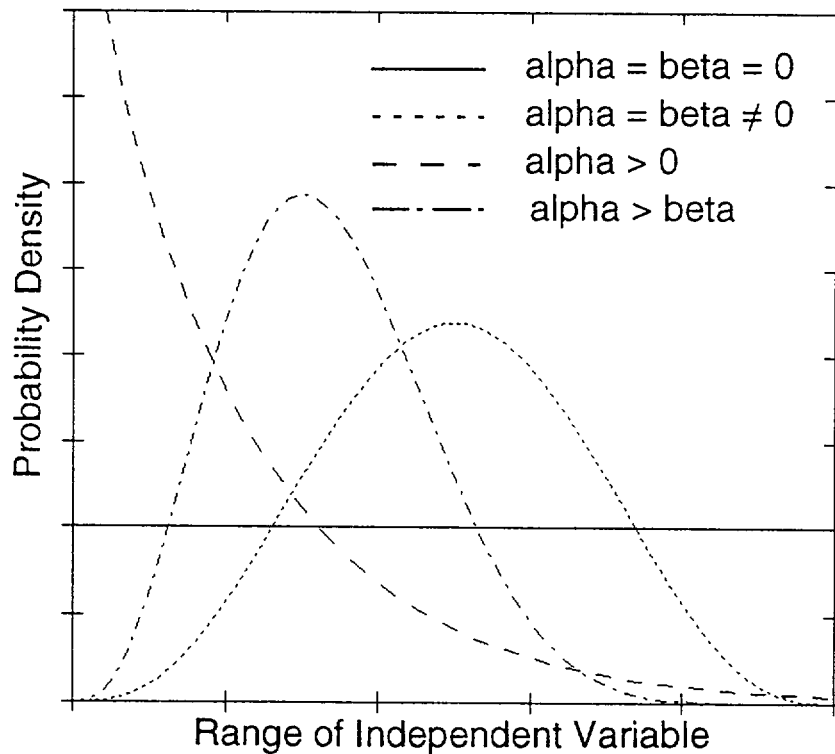


Figure 3-3. Various shapes taken by the beta distribution

3.3.2 Elicitations

In the previous section, a formalism for generating probability distributions was defined. The purpose of the formalism is to provide a consistent methodology to follow when confronted by the uncertainties inherent in a sparse data set. The formalism was followed in the construction of the hydrogeologic parameter distributions for the unsaturated zone (Sections 3.3.3 and 3.3.4).

The application of the formalism, although not excessively time-consuming, does require a review of the following:

- existing site-specific data,
- any analog data that may be available,
- the physical meaning and definition of the variable, and
- the behavior of the function that defines the variable (such as the air-entry parameter in the van Genuchten formula).

This effort implied a time commitment that, for this exercise, precluded applying it to each parameter in the simulation. As an experiment, it was decided to elicit expert opinion in support of selected geochemical and geological parameters required for the total-system simulation, using some of the same logic, along with the interactive software discussed in Section 3.3.1.

To do an elicitation, the expert is asked for information about range, mean, and variability of the parameter. In addition, the expert is asked what data exist to support the assertions. To arrive at his opinion, the expert questions the end user (i.e., the requester of the data), about assumptions in the model, scale of the problem domain, implicit and explicit processes in the model, and any other information that may be relevant.

By the use of interactive graphics, PDFs consistent with the expert's judgment can be displayed. The expert has not been asked any questions as to what shape the distribution may take or to comment explicitly on the parameters of the distribution. When the distribution is displayed graphically, the meaning of the distribution and the distribution of probability density are discussed with the expert. If the expert believes that the probability model is not representative of his or her belief, then the basic assumptions that were used to generate the model are reviewed. This process of assumption, display, and review is repeated until the expert is satisfied.

This method of elicitation was tried for the first time during this exercise, for a limited number of parameters. The results were generally quite satisfying to all involved. First, the experts themselves seemed genuinely pleased with the resulting model, since it fairly and accurately represented their degrees of belief. Second, the amount of time spent in the elicitation process was minimal. Some of the probability distributions were produced in only a few minutes, from start to finish of the elicitation process. Third, the resulting model was of the same form as all the other probability distributions and therefore immediately available for input to the simu-

lation. Fourth, with both the expert and the modeler present at the elicitation process, assumptions that cannot be modeled explicitly can be accounted for in the model by having the PDF reflect the expert's conception of the consequences if they had been included.

Despite the success of the elicitation, a few caveats are in order. The process just described for elicitation of expert opinion as the basis of a probability model was tried for the first time in this exercise and with only a limited number of experts. It is not known how well the process would have worked had a group of experts been brought together for a consensus. It is not known to what degree the person actually generating the distributions needs to be trained as a facilitator. And, it is not known if the process generally would go as smoothly and quickly as it did in these few cases. Additionally, the experts were not conditioned using any of the accepted techniques (to avoid biased results) during the elicitations.

Before presenting the elicited distributions, the reader should be aware of an important conceptual difference between these distributions and the distributions of the hydrogeologic parameters to be developed in Section 3.3.3. The distributions of hydrologic parameters have been generated following the formalism in Section 3.3.1. This formalism is intended to provide the analyst with a probability-density model that is maximally noncommittal as to the likelihood of obtaining a particular value of a parameter, except for the constraints of known data or referenceable and documentable assumptions. The distributions given in this section are models of the experts' degree of belief in the likelihood of an outcome. Two experts, having the same information available to them, might generate very different probability models during the elicitation process. Two modelers, having the same information available to them and following the formalism in Section 3.3.1, would generate exactly the same probability models as input for a simulation.

Table 3-6 gives the names of the experts elicited, the parameters being elicited, and the forms of the resulting probability models. Table 3-7 gives the coefficients of the probability models in the form of Equation 3.1, the beta distribution.

Illustrations of the density functions for the volcanic parameters created during the elicitation process are shown in Chapter 7, Figures 7-4, 7-5, 7-7, and 7-8. The PDFs for the geochemical parameters are discussed in Section 3.4.

Note that the models use several parameters for which no data exist. These parameters have been described either with uniform or log-uniform distributions, to minimize the biases in the distributions. Both distributions imply that the analysts have no indications that any value in the range is more likely than any other.

When the range of data extends over several orders of magnitude, it is the logarithms of the values which we assumed to follow the uniform distribution.

Table 3-6
Summary of expert elicitations

Expert	Parameter	Distribution
G. Valentine	Volume of Erupted Material	Beta
G. Valentine	Dike Width	Beta
G. Valentine	Fraction Wall Rock Entrained	Beta
G. Valentine	Dike Length	Beta
H. Dockery, C. Rautman	Dike Orientation	Beta
(many)	Uniform percolation rate	Exponential
A. Meijer	K _d , C _s , Devitrified Tuff	Beta
A. Meijer	K _d , C _s , Zeolitic Tuff	Beta
A. Meijer	K _d , N _p , Devitrified Tuff	Exponential
A. Meijer	K _d , N _p , Vitric Tuff	Exponential
A. Meijer	K _d , N _p , Zeolitic Tuff	Exponential
A. Meijer	K _d , U, Devitrified Tuff	Uniform
A. Meijer	K _d , U, Vitric Tuff	Uniform
A. Meijer	K _d , U, Zeolitic Tuff	Beta

The PDF for groundwater percolation rates was chosen to reflect both current and future conditions. We assume that climate change can be modeled by an increase in percolation rate. It should be noted that for the TSPA analyses, we are specifying not the infiltration rate at the earth's surface, but the percolation rate at depth. The two rates can be quite different. The SCP specifies that climate change is not an unexpected condition, so high percolation rates representative of this change are not unreasonable to include in the base-case PDF. A wide range for the percolation rate can be developed from many prior analyses. The PACE-90 analysis showed that a percolation rate of 0.01 mm/yr, or less, was consistent with the stratigraphy used for those unsaturated conditions. The SCP (DOE, 1988) and prior PA analyses (e.g., Sinnock et al., 1984) have used percolation values of about 4.5 to 6.0 mm/yr. The PDF chosen for the TSPA analyses sought to include this range. An exponential PDF was chosen to weight the lower values of percolation more heavily, since those were considered to be much more likely than high values. The mean and coefficient of variation listed in Table 3-7 resulted in a suitable range of values for the analyses. Figure 3-4 shows the distribution used.

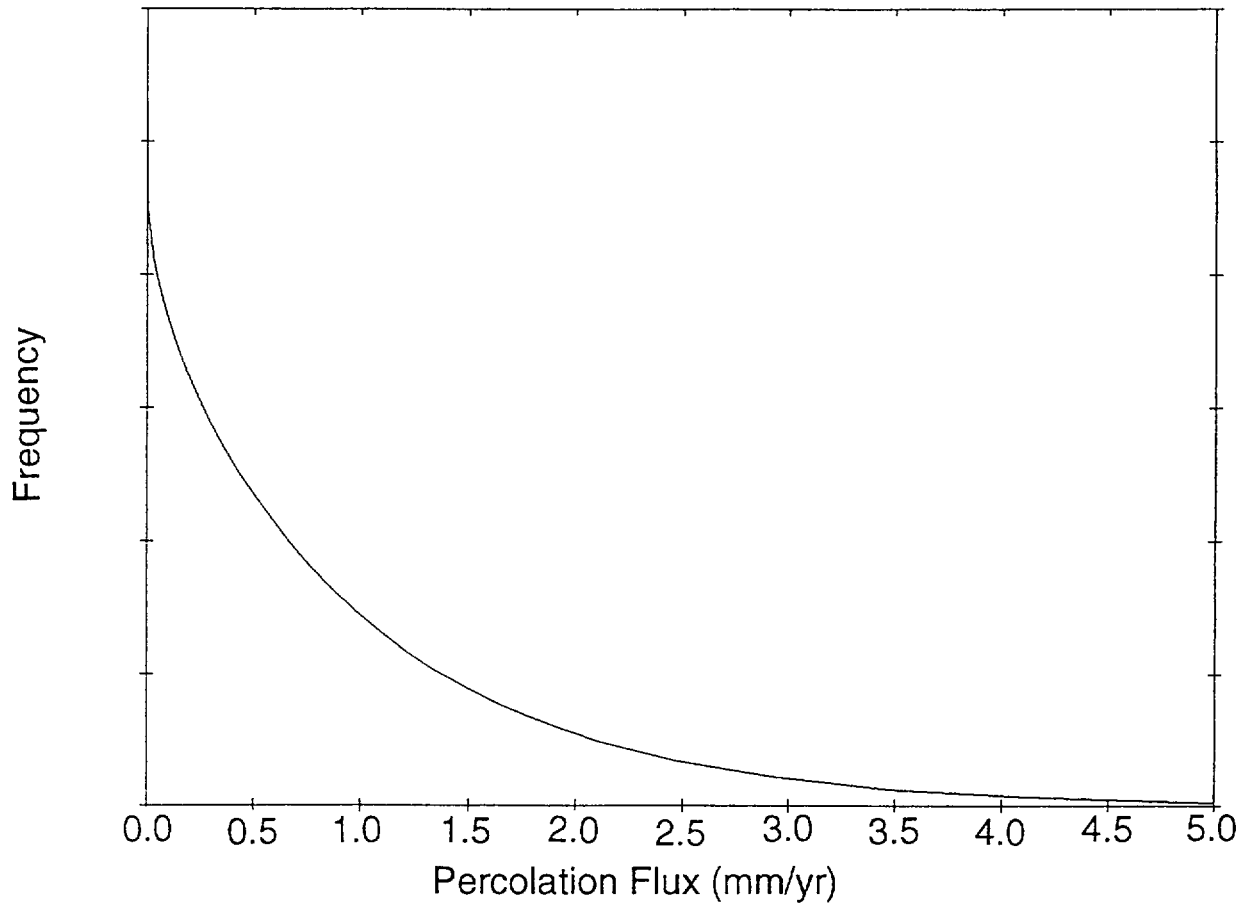


Figure 3-4. PDF for groundwater percolation rate

3.3.3 PDFs of hydrogeologic parameters

This section briefly discusses the assumptions used to generate the probability density functions of the hydrogeologic parameters. For each parameter, a table with the following information is provided:

- The hydrostratigraphic units,
- The mean value of the parameter,
- The coefficient of variation, the minimum and maximum values of the parameter, and
- The exponents of the beta distribution as given in Equation 3.1.

For each of the parameters described in this section, the formalism described in Section 3.3.1 was followed to generate the probability distributions. In a number

Table 3-7
Probability density distributions from expert elicitations

Parameter	E[x]	CV[x]	Min[x]	Max[x]	α	β
Beta Distributions						
Erupted Volume of Igneous Dike	2.7×10^7 (m ³)	0.60	3.4×10^5	1.0×10^8	0.71627	3.69945
Fraction of Wall Rock Entrained	3.0×10^{-4}	0.30	9.0×10^{-5}	6.0×10^{-4}	1.79085	2.98693
Dike Width	1.5 (m)	0.50	0	4.5	1.33333	3.66667
Dike Orientation	15 (deg)	1.00	-10	90	0.83333	4.5
Percolation Rate	1.0 (mm/yr)	1.00	0	39	-0.0513	35.0513
K _d [*] , Cs Devitrified, or Vitric Tuff	50 (ml/g)	0.20	20	100	4.25	7.75
K _d , Cs Zeolitic Tuff	2000	0.25	0	6000	9.33	19.67
K _d , Np Devitrified Tuff	2	1.00	0	50	-0.08	21.08
K _d , Np Vitric Tuff	0.5	1.00	0	12.5	-0.08	21.08
K _d , Np Zeolitic Tuff	4	1.00	0	100	-0.08	21.08
K _d , U (or Se) Devitrified Tuff	2.5	0.57735	0	5	0.0	0.0
K _d , U (or Se) Vitric Tuff	2	0.57735	0	4	0.0	0.0
K _d , U (or Se) Zeolitic Tuff	10	0.30	5	21	0.59722	2.51389
Constant Values						
K _d , C (all rocks)	0					
K _d , Tc (all rocks)	0					
K _d , Sn (all rocks)	100					
K _d , I (all rocks)	0					
K _d , Pu (all rocks)	100					
K _d , Am (all rocks)	100					

* K_d's for all entries in table are in ml/g.

of instances, one or more of the constraints on the parameter distributions (Section 3.3.1) had to be estimated because of a lack of data. Matrix and fracture properties are discussed separately. The data base provided here is intended to be general; Section 3.3.4 contains a discussion of the specific transformation of the data

discussed in this section for the TSPA. This data base was prepared to support the TSPA exercise, and should be used judiciously for other applications.

The hydrostratigraphic units modeled are simplifications of what is believed to be a more complex stratigraphy. The parameters that describe those units are derived from models of processes that are not used by all modelers. The data are intended to challenge the current capabilities of performance assessment to execute and run total-system simulations.

Preparation of a data base for a performance-assessment simulation is considered to be an iterative process. What is presented here are the results of only a few iterations (i.e., HYDROCOIN, COVE-2A, PACE-90, ESSE). Each iteration has built upon the prior ones. In some analyses, a greater level of detail was included. However, the level of detail must be consistent with both the technical and administrative constraints on the analysis. We feel that this data base is adequate for this exercise, and can be used as a basis for future sensitivity and uncertainty studies. We caution that this data base should be used with discretion by modelers for other applications.

3.3.3.1 Matrix saturated hydraulic conductivity, K_S

Saturated hydraulic conductivity values for the matrix of the hydrostratigraphic units were adapted from Peters et al. (1984), Table A.2 and Table A.4. For all units it was felt that the most reliable information available in support of a probability model was the estimate of the mean, $E[x]$. As a consequence, by the formalism in Section 3.3.1, the distribution of hydraulic conductivity in each of the units was taken to be exponential. The data in Table 3-8 correspond to a beta-distribution approximation of the exponential.

Table 3-8
Matrix saturated hydraulic conductivity

Layer	$E[x]$ (m/s)	CV[x]	Min[x] (m/s)	Max[x] (m/s)	α	β
1	2.00E-11	1.0	0.0	7.93E-10	-0.0526	34.078
2	3.01E-12	1.0	0.0	1.27E-10	-0.0473	38.298
3	7.99E-11	1.0	0.0	3.11E-09	-0.0515	34.894
4	3.01E-12	1.0	0.0	1.27E-10	-0.0473	38.298
5	1.40E-08	1.0	0.0	5.43E-07	-0.0515	34.869

3.3.3.2 Matrix saturated volumetric water content, θ_s

Saturated volumetric water contents for the matrix were taken from Peters et al. (1984), Table A.1. Minimum and maximum values are, by definition, 0.0 and 1.0, respectively. (The theoretical values for minimum and maximum have been chosen to minimize biases due to inadequate sample data. As will be discussed in Section 3.3.4, the range can be truncated with little loss of accuracy.) An estimate of the coefficient of variation was taken from the analog-site porosity data obtained from the Apache Leap Tuff (Rasmussen et al., 1990, Table 8). Based on the information available, saturated volumetric water content was modeled as a beta distribution in each of the hydrostratigraphic layers. Data are given in Table 3-9.

Table 3-9
Matrix saturated volumetric water content, θ_s

Layer	E[x]	CV[x]	Min[x]	Max[x]	α	β
1	0.093	0.20	0.0	1.0	21.582	219.2352
2	0.011	0.20	0.0	1.0	23.714	2221.0133
3	0.180	0.20	0.0	1.0	19.320	91.5689
4	0.343	0.20	0.0	1.0	15.082	29.8043
5	0.230	0.20	0.0	1.0	18.020	62.6757

3.3.3.3 Matrix porosity, n

Porosity values for the matrix of the hydrostratigraphic units were taken from Peters et al. (1984), Table A.2. Minimum and maximum values are, by definition, 0.0 and 1.0, respectively. An estimate of the coefficient of variation was taken from the porosity data obtained from the Apache Leap Tuff Site (Rasmussen et al., 1990, Table 8). Based on the information available, porosity was modeled as a beta distribution in each of the hydrostratigraphic layers. Data are given in Table 3-10.

3.3.3.4 Water-retention parameters

Water-retention parameter values for the matrix of the hydrostratigraphic units were adapted from Peters et al. (1984), Table A.2. There are several empirical relationships that describe the ability of a medium to retain or imbibe water. These formulas also provide relationships between the conductivity and the saturation state of the medium. In this exercise, we use the van Genuchten model (van

Genuchten, 1980) for the saturation state of the system as a function of pressure head (or suction potential) ψ . $S(\psi)$ is defined in terms of degree of saturation as

Table 3-10
Matrix porosity

Layer	E[x]	CV[x]	Min[x]	Max[x]	α	β
1	0.11	0.20	0.0	1.0	21.14	178.13
2	0.04	0.20	0.0	1.0	21.66	228.12
3	0.21	0.20	0.0	1.0	18.54	72.51
4	0.41	0.20	0.0	1.0	13.34	19.64
5	0.24	0.20	0.0	1.0	17.76	58.41

$$S(\psi) = (S_S - S_r) [1 / (1 + \alpha_{vG} / \psi) \beta_{vG}]^{(1 - 1/\beta_{vG})} + S_r, \quad (3.3)$$

where S_S is the maximum degree of saturation, S_r is the residual degree of saturation, α_{vG} is sometimes referred to as the air-entry parameter and has units of 1/m, and β_{vG} describes the rate at which the medium saturates or desaturates. No consideration is given in this exercise to hysteresis. The maximum degree of saturation S_S is taken to be 1.0. Parameter values are given in Tables 3-11 through 3-13.

Table 3-11
Matrix air-entry parameter, α_{vG}

Layer	E[x] (1/m)	CV[x]	Min[x] (1/m)	Max[x] (1/m)	α	β
1	0.0057	0.37	0.0004	137.0	5.310	164029.4
2	0.0017	0.37	0.0004	137.0	4.631	267879.3
3	0.0265	0.37	0.0004	137.0	6.084	37177.12
4	0.0220	0.37	0.0004	137.0	6.040	44644.5
5	0.0140	0.37	0.0004	137.0	5.892	69422.45

Table 3-12
Matrix desaturation parameter, β_{vG}

Layer	E[x]	CV[x]	Min[x]	Max[x]	α	β
1	1.798	0.20	1.05	10.0	2.881	41.56
2	1.708	0.20	1.05	10.0	2.364	41.39
3	2.223	0.20	1.05	10.0	4.917	38.23
4	1.236	0.20	1.05	10.0	-0.466	24.14
5	2.640	0.20	1.05	10.0	6.279	32.70

Table 3-13
Matrix residual degree of saturation, S_r

Layer	E[x]	CV[x]	Min[x]	Max[x]	α	β
1	0.080	0.20	0.0	1.0	21.92	262.2
2	0.052	0.20	0.0	1.0	22.66	432.9
3	0.164	0.20	0.0	1.0	19.74	104.9
4	0.010	0.20	0.0	1.0	23.74	2448.3
5	0.066	0.20	0.0	1.0	22.28	328.5

3.3.3.5 Fracture parameters

Data are presented to support a number of alternative conceptual models for the fracture domain. For the composite-porosity model (also called the equivalent-porous-medium model), the fracture is assumed to have the hydrologic properties of sand. Data for sand properties are taken from Carsel and Parrish (1988). The choice of sand as a porous-medium equivalent is arbitrary. Data in support of discrete-fracture models are taken from Zimmerman and Vollendorf (1982). For both conceptual models, fracture hydrologic properties are assumed to be the same in each hydrostratigraphic unit. This assumption is an arbitrary one, with no data to support or refute it. The fracture characteristics of the units vary because of variations in fracture densities, which were derived from Spengler and Chornack (1984). Table 3-14 presents the hydrologic properties for fractures.

Fracture density is assumed to vary among units. Estimates of the mean fracture density are from Spengler and Chornack (1984). Table 3-15 gives the beta distribution coefficients for each unit in the unfaulted sections of the problem domain.

Table 3-16 gives the beta distribution coefficients for the fault zone, where it is arbitrarily assumed that fracture densities are 10 times greater. The distributions are approximations of the exponential distribution.

Table 3-14
Hydrologic properties for fractures
(based on sand)

Layer	E[x]	CV[x]	Min[x]	Max[x]	α	β
Saturated Hydraulic Conductivity (m/s)						
All	8.25×10^{-5}	0.524	9.34×10^{-6}	2.35×10^{-4}	1.723	10.03
Air-Entry Parameter, α_{vG} (1/m)						
All	14.5	0.203	0.0004	137.0	20.59	181.41
Desaturation Parameter, β_{vG}						
All	2.68	0.203	1.05	10.0	6.16	31.15
Residual Volumetric Water Content, θ_r						
All	0.045	0.223	0.0	1.0	18.16	405.6
Saturated Volumetric Water Content, θ_s						
All	0.43	0.151	0.0	1.0	23.57	31.57

Table 3-15
Fracture density

Layer	E[x] (m^{-3})	CV[x]	Min[x] (m^{-3})	Max[x] (m^{-3})	α	β
1	28.3	1.0	0.0	1099	-0.0515	34.8854
2	35.6	1.0	0.0	1382	-0.0515	34.8717
3	2.0	1.0	0.0	78	-0.0513	35.0513
4	1.6	1.0	0.0	63	-0.0508	35.4258
5	4.4	1.0	0.0	171	-0.0515	34.9151

Table 3-16
Fracture density in fault zone

Layer	E[x] (m ⁻³)	CV[x]	Min[x] (m ⁻³)	Max[x] (m ⁻³)	α	β
1	283	1.0	0.0	10985	-0.0515	34.8678
2	356	1.0	0.0	13819	-0.0515	34.8689
3	20	1.0	0.0	777	-0.0515	34.9015
4	16	1.0	0.0	622	-0.0514	34.9264
5	44	1.0	0.0	1708	-0.0515	34.8697

In the composite model, the fracture aperture b is related to the air-entry parameter α_{vG} of the water retention model. The relationship is given as

$$b = (2\sigma/\rho g)\alpha_{vG}, \quad (3.4)$$

where σ is surface tension, ρ is fluid density, and g is gravitational acceleration. The PDFs for fracture aperture are discussed in Section 3.3.4. For the discrete-fracture models, an estimate of the fracture aperture of 99 μm was taken from Zimmerman and Vollendorf (1982). The estimate is based on tests conducted in G-Tunnel in a welded section of the Grouse Canyon Member of the Belted Range Tuff.

3.3.4 Transformation of data for TSA input

This section describes the methods taken to prepare the data presented in previous sections for input to the total-system simulations conducted at SNL. As discussed previously, the hydrogeologic parameters and the probability density functions for those parameters represent a generalized data base for performance-assessment applications. For a specific application, some transformations may be required.

In the previous section, the mean, coefficient of variation, and range of each of the hydrogeologic parameters were given along with the exponents of the beta probability-density function

$$f(x) = C(x-a)\alpha(b-x)\beta. \quad (3.5)$$

The range, $[a,b]$, for the density function given by equation 3.5 is constrained by one of three arguments: definition, functional, or theoretical. The advantage of using

one of the three arguments to determine the range of equation 3.5 is that the least amount of inference in excess of the available information is demanded of the analyst. If the parameter has a defined range, the range over which the parameter is defined determines a and b . An example would be porosity,

$$n = V_v/V_t, \quad (3.6)$$

given by the ratio of the volume of void space V_v in a porous medium to the total volume V_t of the medium. By definition, porosity has a range of 0.0 to 1.0.

The disadvantage of a minimally biased approach is a practical one. The exponents of equation 3.5, α and β , are calculated using the range, mean, and coefficient of variation. The value of one or both of the exponential terms can be particularly sensitive to values chosen for a and b . Problems may arise if very high values of the exponents occur. The Latin Hypercube Sampler (LHS) is used to generate input parameters for the TSA. However, if the specified distribution has an exponential term in excess of about 80, limitations within the LHS cause problems. As a result, some of the distributions in Section 3.3.3 have been approximated for use with the TSA. For example, in Table 3-14, the β parameter of the van Genuchten air-entry factor has a value of more than 180. A number of ways of approximating the distributions with exponents greater than 80 are possible. The approximation that was followed in this exercise meets the following criteria:

- it is consistent with the software available to us for this exercise,
- it is fast,
- it is very simple conceptually,
- it can be applied consistently to all the distributions that require an approximation, and
- most importantly, it preserves to a great degree the probability density of the original distribution.

3.3.4.1 Approximating the PDF for LHS input

The high values of the exponents in Equation 3.5 are often a direct consequence of a broad range $[a,b]$. The approximation will assume that the range can be narrowed without any loss in the important features of the distribution. The new

range $[a', b']$ will be defined so that with respect to $f(x)$ given in equation 3.5, a' is the value of the random variable x such that

$$P[x < a'] = 0.0001, \quad (3.7)$$

and b' is the value of the random variable x such that

$$P[x < b'] = 0.9999. \quad (3.8)$$

As an illustration, Figure 3-5 shows the probability density function given in Section 3.3.3 for the porosity of Layer 1. The range of the distribution is 0.0 to 1.0. One of the exponential terms in this distribution has a value greater than 80 ($\beta=178.1327$). We wish to approximate this distribution with one of the same functional form but with exponents consistent with the limitations of the software. However, we must preserve the essential features of the distribution—the shape of the probability-density curve. The total probability is always 1.0, and is given by the area under the curve of the density function. As Figure 3-5 illustrates, although the function may exist between 0.0 and 1.0, the area under the curve is nonnegligible over a much smaller range. Definitions 3.7 and 3.8 take advantage of this fact. The definition for the minimum value, a' , states that we will choose the value of a' from the distribution of the parameter x within range $[a, b]$ such that the probability of x being less than a' is only one in ten thousand. Similarly, the definition for a maximum value b' states that we will choose the value of b' from the distribution of the parameter x within range $[a, b]$ such that the probability of x being greater than b' is only one in ten thousand.

The values for a' and b' , the minimum and maximum of the approximated distribution, can be derived from the distribution shown in Figure 3-5. A program called Q_BETA has been written to do this. The software, working from the cumulative probability distribution, returns values of the random variable consistent with the definitions in 3.7 and 3.8. For our example we obtain a new range of $[0.044, 0.197]$. This new range, along with the mean and coefficient of variation used in the original distribution, is used to generate a new probability density function.

Figure 3-6 shows the probability density function of porosity using a minimum value of 0.044, a maximum value of 0.197, an expectation of 0.11, and a coefficient of variation of 0.2. The exponential terms of this new distribution, α and β , are 3.6863 and 5.1774, respectively—well within the range of the LHS.

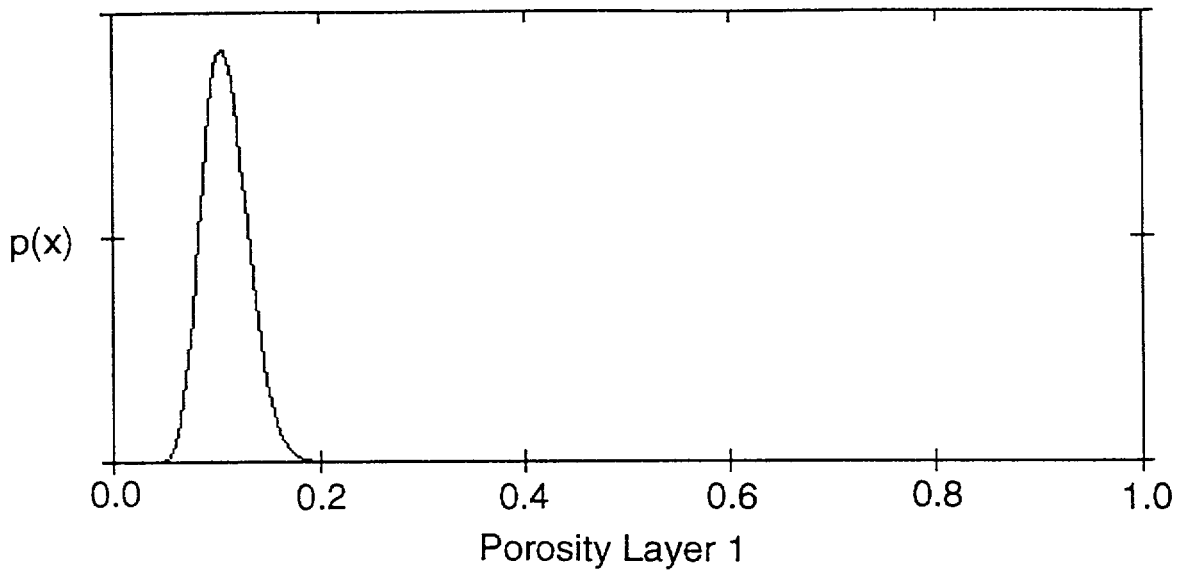


Figure 3-5. PDF for matrix porosity in Layer 1

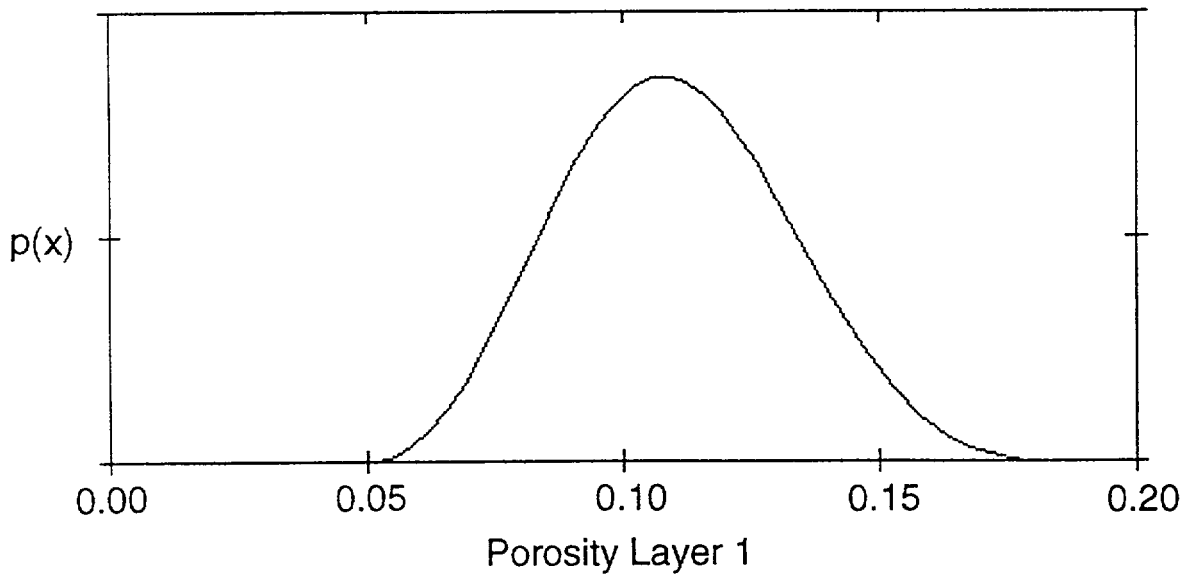


Figure 3-6. Truncated PDF for matrix porosity in Layer 1

The similarities and differences between the two distributions are shown in Figure 3-7, where the two distributions are superimposed. The dashed curve is the original distribution, with the range $[0,1]$. The dotted line is the approximation. A slightly better match might be obtained with more work, but the approximation has preserved the essence of the original distribution.

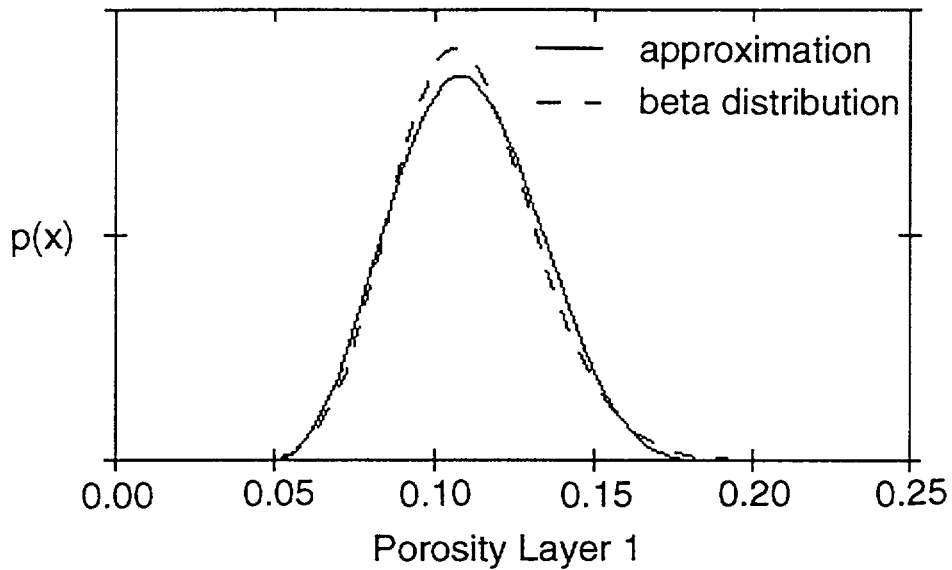


Figure 3-7. Comparison of exact and approximated PDFs for Layer-1 porosity

The paradigm just followed—calculate a new range using definitions 3.7 and 3.8, and use the same expectation and coefficient of variation—has been used as necessary for the current application. New distributions were prepared only for those distributions in Section 3.3.3 that the LHS was unable to accept as input. This included the PDFs for matrix porosity for layers 1 and 2, the PDFs for the van Genuchten matrix air-entry parameter for all five layers, and the distributions of the matrix residual saturation parameter for all five layers. New values of the range and exponents are given in Tables 3-17, 3-18, and 3-19. The saturated volumetric water content defined in Section 3.3.4 has been used as a surrogate for porosity in the approximation of the residual degree of saturation.

Table 3-17
Distributions for approximated matrix porosity

Layer	$E[x]$ (m^{-3})	$CV[x]$	$Min[x]$ (m^{-3})	$Max[x]$ (m^{-3})	α	β
1	0.11	0.20	0.044	0.197	3.6863	5.1774
2	0.09	0.20	0.037	0.161	3.5367	5.0775

Table 3-18
Distributions for approximated matrix air-entry parameter, α_{vG}

Layer	E[x] (1/m)	CV[x]	Min[x] (1/m)	Max[x] (1/m)	α	β
1	0.0057	0.37	0.001066	0.014068	1.7508	3.9674
2	0.0033	0.37	0.000699	0.008146	1.6037	3.8509
3	0.0265	0.37	0.004122	0.065385	1.9409	4.1103
4	0.0220	0.37	0.003458	0.054283	1.9310	4.1031
5	0.0140	0.37	0.002281	0.034545	1.8960	4.0770

Table 3-19
Distributions for approximated matrix degree of residual saturation, S_r

Layer	E[x]	CV[x]	Min[x]	Max[x]	α	β
1	0.080	0.20	0.03249	0.14296	3.5951	5.0894
2	0.052	0.20	0.02130	0.09295	3.5517	5.0715
3	0.164	0.20	0.06503	0.29275	3.7130	5.1311
4	0.010	0.20	0.00415	0.01788	3.4842	5.0403
5	0.066	0.20	0.02691	0.11796	3.5753	5.0817

3.3.4.2 Approximating the PDFs of fracture parameters for the TSA

This section assumes that the continuum model of Klavetter and Peters (1986) will be used in the simulation. The input data for the flow model described in this section is not necessarily appropriate as input to other flow models. As was the case with the matrix, the distribution of the van Genuchten air-entry parameter for the fractures requires an approximation because of the constraints of the LHS. For fractures, the same procedure was followed as for the matrix. The input data for the LHS are given in Table 3-20. The calculations to obtain PDFs for residual degree of saturation for the fracture and the fracture porosity require some detailed explanation.

Table 3-20
Distributions for approximated air-entry parameter for fractures, α_{vG}
(based on sand)

Layer	E[x] (1/m)	CV[x]	Min[x] (1/m)	Max[x] (1/m)	α	β
All	14.5	0.203	5.75	26.08	3.603	5.0917

Degree of saturation (residual) S_r

The water content of a porous medium is usually given in terms of volumetric water content θ or degree of saturation S . The data obtained for the fracture hydro-logic properties reported water content in terms of residual volumetric water content. Input for the TSA requires the degree of residual saturation. As a starting point, definitions of the two are offered. The definitions follow Campbell (1985). Define the volumetric water content θ as

$$\theta = V_l/V_t \quad (3.9)$$

and the degree of saturation S as

$$S = V_l/V_f \quad (3.10)$$

where V_l is volume of liquid, V_t is total volume, and V_f is fluid volume (both liquid and gas phase). To relate θ and S , define porosity n as

$$n = V_f/V_t \quad (3.11)$$

so that

$$\theta = nS, \quad (3.12)$$

or, given that we know θ ,

$$S = \theta/n. \quad (3.13)$$

We can infer from Equation 3.13 that the residual degree of saturation S_r can be calculated by dividing the residual volumetric water content θ_r by the porosity n . For the data given in Section 3.3.3 an estimate of the mean of S_r is

$$E[S_r] = E[\theta_r]/E[n] = 0.045/0.43 = 0.105, \quad (3.14)$$

assuming θ_r and n are independent. An estimate of the coefficient of variation CV for S_r can be approximated by

$$CV^2[S_r] = CV^2[\theta_r] + CV^2[n]. \quad (3.15)$$

The calculation is not intuitively obvious, but details are given on page 202 of Harr (1987). The coefficient of variation for θ_r is given in Table 3-17 as 0.223. The coefficient of variation for n is obtained from Carsel and Parrish (1988). In this exercise we assume that $n = \theta_s$. The coefficient of variation of θ_s is given as 0.151. Using equation 3.15 above,

$$CV^2[S_r] = (0.223)^2 + (0.151)^2 = 0.0725,$$

the square root of which gives us a coefficient of variation of about 0.269 for S_r . The range of degree of saturation is 0.0 to 1.0.

Illustrated in Figure 3-8 is the distribution of S_r obtained by using the formalism discussed in Section 3.3.1. Since this distribution has an exponential greater than the limit for the LHS software, the distribution is approximated in the same way as the others. The new distribution is illustrated in Figure 3-9, and data for this distribution are given in Table 3-21.

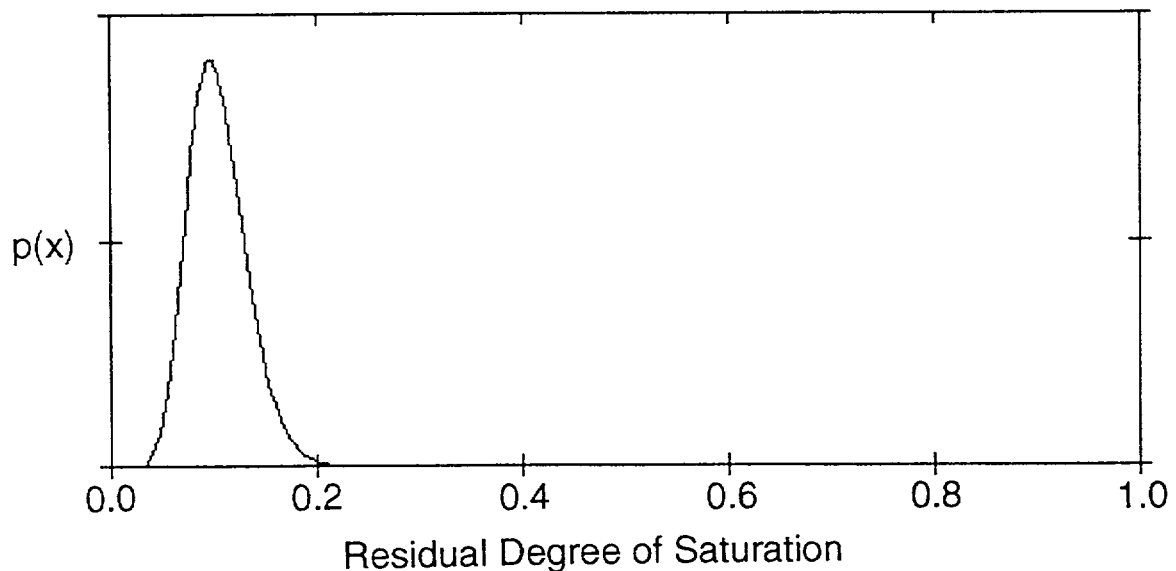


Figure 3-8. Beta probability density for residual saturation

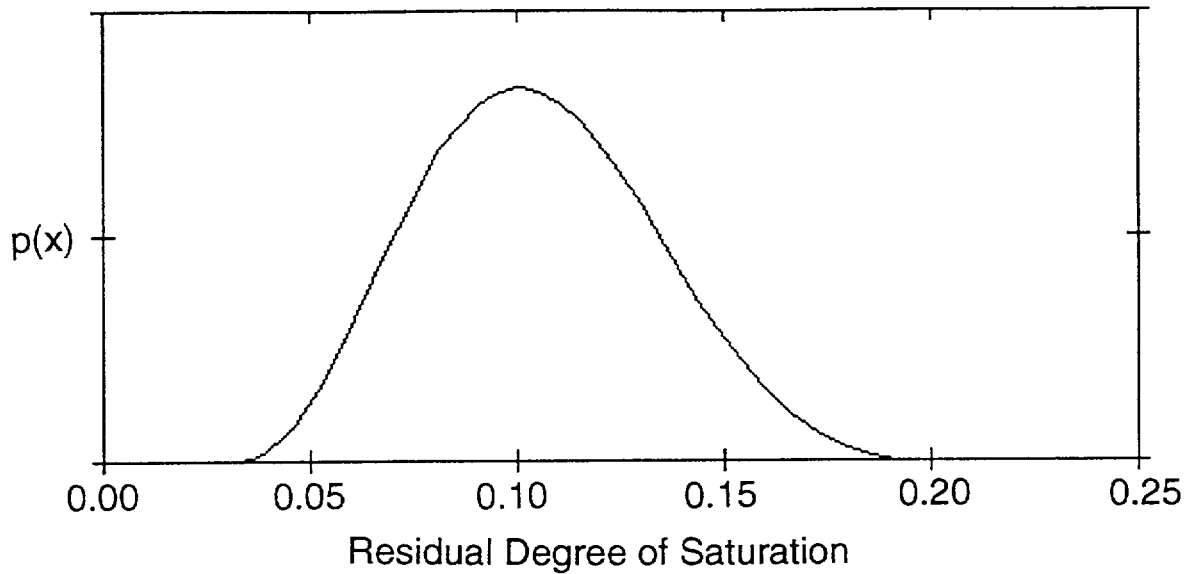


Figure 3-9. Approximated beta probability density for residual saturation

Table 3-21
Approximated residual degree of saturation, S_r
(based on sand)

Layer	E[x]	CV[x]	Min[x]	Max[x]	α	β
All	0.105	0.269	0.02767	0.21649	3.0163	4.7905

Fracture porosity n_f

Fracture porosity n_f is the product of three terms: fracture density ρ_f , an effective aperture term b , and a unit area:

$$n_f = (\rho_f)(b)(\text{unit area}). \quad (3.16)$$

The density term ρ_f is an estimate of the number of fractures per cubic meter of rock. The density estimate is a function of linear frequency and dip orientation. The aperture term b is treated as a function of the van Genuchten alpha parameter.

$$b = f(\alpha_{vG}). \quad (3.17)$$

The relationship is given by equation 3.4 (Section 3.3.3.5). The underlying assumption in the calculation of the aperture is that the composite model sacrifices the explicit geometry of the fractures for an effective porous medium.

The model for the distribution of n_f that follows is assumed to be a function of the distributions of two independent random variables, ρ_f and b . The distribution of ρ_f is given as exponential in Section 3.3. The distribution of b is assumed to be the same as α_{vG} except for a scalar transformation of the random variable by

$$2\sigma/\rho g, \quad (3.18)$$

where σ is surface tension, ρ is fluid density, and g is gravitational acceleration. For the purpose of this exercise, σ , ρ , and g are assumed to be constants.

The mean value of n_f is approximated by

$$E[n_f] = E[\rho_f] E[b] \text{ (unit area)}, \quad (3.19)$$

and the coefficient of variation CV is approximated by

$$CV^2[n_f] = 1 + CV^2[b], \quad (3.20)$$

where the CV for an exponentially distributed variable (ρ_f) is 1. Using the value of 0.203 as the coefficient of variation for b , the value of the coefficient of variation for α_{vG} from Table 3-20, yields

$$CV^2[n_f] = 1 + (0.203)^2 = 1.0412,$$

for a coefficient of variation of 1.02. The minimum value of n_f is taken as 0.0. To calculate a maximum

$$MAX[n_f] = MAX[\rho_f] MAX[b] \text{ (unit area)} \quad (3.21)$$

requires a calculation for the maximum value of b and ρ_f .

$$MAX [b] = (2\sigma/\rho g)\alpha_{max}. \quad (3.22)$$

Using the value of 26.08 from Table 3-20 as α_{max} and the values for σ , ρ , and g from Section 3.3 yields

$$MAX[b] = [2(0.07183)/(1000)(9.80665)]26.08 = 3.821 \times 10^{-4} \text{ m.}$$

These values are summarized in Table 3-21 and used in Table 3-22.

The estimate of $\rho_f(max)$ for each of the five layers was obtained from the RS/1 program EXPONENT. The routine generates an exponential distribution from the

expectation of the random variable. The exponential distribution can also be approximated by a beta distribution. There are three reasons why the beta distribution may be preferable to the exponential. First, the exponential has no upper bound and the beta is constrained to a finite range. Using the beta function therefore provides an approximation for the maximum value of the random variable. Second, preparing the input for the LHS is simpler if the distributions for the random variables are all beta distributions. Third, the LHS does not accept the exponential distribution as input. The values used to generate the distributional models for n_f are given in Table 3-22 and the PDF parameters are given in Table 3-23. Note the values for $n_f(max)$ in Table 3-22 for Layers 1 and 2 in the fault zone. They are calculated to be larger than 1. Since the proportion of the domain that is occupied by the fractures cannot exceed 100%, the maximum value for the distributional model in Table 3-23 is set at 1.0 for those two units.

Table 3-22
Values used in the calculation of fracture porosity

Layer	ρ_f (m ⁻³)	b (m)	n_f	$\rho_f(min)$ (m ⁻³)	$\rho_f(max)$ (m ⁻³)	b_{max} (m)	b_{min} (m)	$n_f(max)$
1	28.3	2.1x10 ⁻⁴	5.94x10 ⁻³	0.0	1099	3.82x10 ⁻⁴	0.0	0.41993
2	35.6	2.1x10 ⁻⁴	7.48x10 ⁻³	0.0	1382	3.82x10 ⁻⁴	0.0	0.52806
3	2.0	2.1x10 ⁻⁴	4.20x10 ⁻⁴	0.0	78	3.82x10 ⁻⁴	0.0	0.02980
4	1.6	2.1x10 ⁻⁴	3.36x10 ⁻⁴	0.0	63	3.82x10 ⁻⁴	0.0	0.02407
5	4.4	2.1x10 ⁻⁴	9.24x10 ⁻⁴	0.0	171	3.82x10 ⁻⁴	0.0	0.06534
Fault Zone								
1	283	2.1x10 ⁻⁴	5.94x10 ⁻²	0.0	10985	3.82x10 ⁻⁴	0.0	4.19627
2	356	2.1x10 ⁻⁴	7.48x10 ⁻²	0.0	13819	3.82x10 ⁻⁴	0.0	5.27886
3	20	2.1x10 ⁻⁴	4.20x10 ⁻³	0.0	777	3.82x10 ⁻⁴	0.0	0.29681
4	16	2.1x10 ⁻⁴	3.36x10 ⁻³	0.0	622	3.82x10 ⁻⁴	0.0	0.23760
5	44	2.1x10 ⁻⁴	9.24x10 ⁻³	0.0	1708	3.82x10 ⁻⁴	0.0	0.65246

Table 3-23
Fracture porosity, n_f

Layer	E[x]	CV[x]	Min[x]	Max[x]	α	β
1	5.94×10^{-3}	1.02	0.0	0.4199	-0.0664	64.5111
2	7.48×10^{-3}	1.02	0.0	0.5281	-0.0666	64.0018
3	4.20×10^{-4}	1.02	0.0	0.0298	-0.0665	64.3025
4	3.36×10^{-4}	1.02	0.0	0.0241	-0.0662	65.0460
5	9.24×10^{-4}	1.02	0.0	0.0653	-0.0666	64.0322
Fault Zone						
1	5.94×10^{-2}	1.02	0.0	1.0	-0.1554	12.3673
2	7.48×10^{-2}	1.02	0.0	1.0	-0.1855	9.0810
3	4.20×10^{-3}	1.02	0.0	0.2968	-0.0666	64.0280
4	3.36×10^{-3}	1.02	0.0	0.2376	-0.0666	64.0738
5	9.24×10^{-3}	1.02	0.0	0.6525	-0.0666	63.9802

One might be tempted to assume that the distribution of fracture porosity is similar to that of the matrix porosity. As can be seen from Figure 3-6, an assumption of normality for matrix porosity would not be unreasonable. Figure 3-10 shows the distribution of fracture porosity for Layer 2 in the fault zone. For this PDF, an exponential model would obviously be more appropriate than a normal distribution function. Although both parameters are called porosities, they represent different physical phenomena.

3.4 Geochemistry data

This section concerns the calculation of radionuclide retardation factors. First, we need to provide a brief explanation of the terminology and assumptions. Radionuclide transport is retarded by adsorption on the rock. The sorption is assumed to take place only in the pores of the rock matrix; sorption in the fractures is assumed to be negligible because there is much less surface area available for sorption than in the porous matrix (see Sinnock et al., 1984, for example). The latter assumption unrealistically implies that there is no retardation during transport in the weeps model. (Retardation is simulated in the weeps model by a random variable—the weeps and composite-porosity models of radionuclide flow and transport are described in Chapter 4.) The composite-porosity calculations were made using

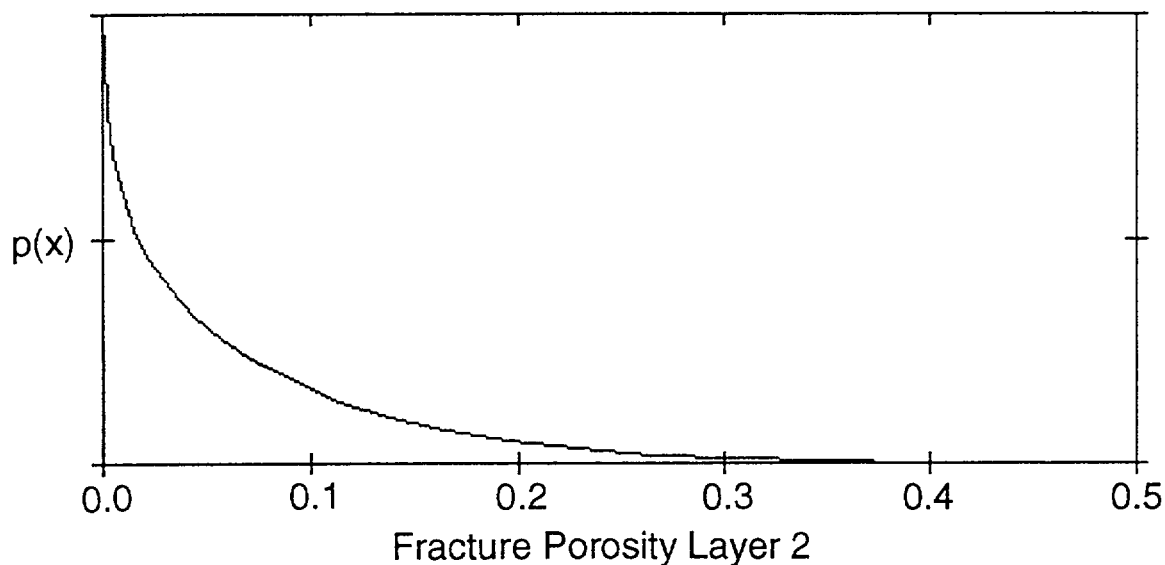


Figure 3-10. Exponential PDF for fracture porosity, Layer 2, in fault zone

the flow and transport computer code TOSPAC, which was described by Dudley et al. (1988). Dudley et al. give the following formulas for retardation factors:

$$R_m^i = 1 + \rho_b K_d^i / \theta_m, \quad (3.23)$$

$$R_f^i = 1 + \sigma_f K_a^i / \theta_f, \quad (3.24)$$

where R_m^i is the retardation factor for transport in the porous matrix for nuclide i , R_f^i is the retardation factor for fracture transport of nuclide i , ρ_b is the bulk density of the rock, σ_f is the fracture surface area per unit volume, θ_m is the moisture content in the porous matrix, and θ_f is the moisture content of the fractures. K_d^i and K_a^i are distribution coefficients, or sorption coefficients, and are density-based and area-based, respectively. As mentioned above, no credit was taken for any possible sorption in the fractures in this study; K_a^i was set to zero for all calculations. Few data are available at present regarding possible values for K_a^i . Because K_a^i is assumed to be zero, it is not necessary to determine values for σ_f . The moisture contents, θ_m and θ_f are calculated by TOSPAC as part of the groundwater-flow calculation. Thus, the only terms in Equations 3.23 and 3.24 that need to be discussed are the distribution coefficients K_d^i and the bulk density ρ_b .

3.4.1 Sorption coefficients for tuff

The primary sources of sorption data for Yucca Mountain tuffs are DOE (1988, Section 4.1.3), Thomas (1987), and Meijer (1990). Other sources may be found referenced in those three. The task of determining appropriate sorption coefficients for the Yucca Mountain site is being undertaken by investigators at Los Alamos National Laboratory. The approach preferred at LANL is termed the "minimum K_d " approach (Meijer, 1991). In this approach, rather than expending a great deal of effort to determine the K_d 's for all nuclides under all possible conditions (which could then be used to define probability distributions for the K_d 's for various scenarios), the effort is put into determining the "worst case" for the strongly sorbing nuclides, leading to the smallest credible value of K_d for each element. This minimum K_d would correspond to the lower bound of the probability distribution, and use of it rather than the distribution of higher values would be conservative. It is recognized that this approach cannot be followed for all elements of interest because the minimum K_d for several elements would be zero, or very close to zero. Roughly speaking, the important elements in spent fuel can be put into three categories:

- 1) those elements with very little or no sorption on Yucca Mountain tuffs, including carbon, chlorine, technetium, and iodine;
- 2) those elements with small K_d values, including selenium, uranium, and neptunium; and
- 3) elements which have high to very high K_d values, including plutonium, americium, and most other elements in spent fuel.

The minimum- K_d approach is really aimed at the third category, the strongly sorbing elements. For most transport calculations that have been made so far, once the K_d is above about 10 or 20 ml/g, the actual value is not important because no significant amount of the radionuclide can reach the accessible environment within the calculation time. There are two potential problems with this approach. First, in future calculations, for other scenarios, the exact value of K_d for the highly sorptive nuclides could possibly be more important. Second, the approach is dependent on the time of interest; it takes little retardation to prevent nuclides from reaching the accessible environment in 10,000 years, but if calculations are continued to 100,000 years or longer and the peak rate at which radioactivity reaches the accessible envi-

ronment is the quantity of interest (as with a dose-based standard), then the actual value of K_d may be important. However, for the purposes of the present TSPA study, the minimum- K_d approach is acceptable for the strongly sorbed elements and for the nonsorbed elements. For the elements with intermediate sorption strength, probability distributions of K_d were defined, on the basis of the data available. The Yucca Mountain tuffs were represented by three rock types for purposes of defining the sorption-coefficient distributions: devitrified, zeolitic, and vitric. The correspondence between those rock types and the stratigraphy defined earlier is shown in Table 3-24.

Table 3-25 lists the types of K_d PDFs that were adopted for this preliminary TSPA, and lists the figures illustrating the distributions. The values used were provided by A. Meijer of Los Alamos National Laboratory. Only ten elements are listed in the table, because only those ten elements were included in the groundwater transport calculations. Mean values for the distributions, and the constant values, are listed in Table 3-25. The complete parameter sets for the distributions are listed in Table 3-7 (Section 3.3). Figures 3-11 through 3-18 shows the shapes of the distributions.

Carbon, Iodine. These elements are known to have little or no sorption on Yucca Mountain tuffs. It would probably not be worth a large effort to characterize a very small amount of sorption.

Technetium. Technetium shows slightly greater sorption than carbon and iodine. Including a small amount of sorption for technetium would reduce the calculated releases somewhat, especially since technetium is the dominant contributor to the normalized aqueous release (EPA sum), as discussed in Chapter 4. However,

Table 3-24
Geohydrologic units for geochemistry

Geohydrologic Unit	Rock Type For K_d Definition
Welded	devitrified
Vitrophyre	vitric
Vitric	vitric
Zeolitic	zeolitic
Partially welded	devitrified
Tuff saturated zone	devitrified

Table 3-25
Probability distributions for K_d s

Element (rock type)	Distribution Type*	Mean value (ml/g)	Illustrated in Figure Number
Carbon, Iodine, Technetium	constant	0	—
Tin, Plutonium, Americium	constant	100	—
Uranium, Selenium (devitrified)	uniform	2.5	3-11
Uranium, Selenium (zeolitic)	beta	10	3-12
Uranium, Selenium (vitric)	uniform	2	3-13
Neptunium (devitrified)	beta	2	3-14
Neptunium (zeolitic)	beta	4	3-15
Neptunium (vitric)	beta	0.5	3-16
Cesium (devitrified)	beta	50	3-17
Cesium (zeolitic)	beta	2000	3-18
Cesium (vitric)	beta	50	3-17

* See Table 3-7 for distribution parameters.

technetium's normalized inventory is low enough that including its sorption is not of great importance. Thus, in keeping with the minimum- K_d approach, $K_d = 0$ was used for technetium.

Tin, plutonium, americium. These elements have very high sorption on many minerals that are common in the Yucca Mountain tuffs. It is felt that their K_d 's would be at least 100 ml/g with any combination of the rock types and groundwaters in the area and under any circumstances likely to occur at Yucca Mountain (Meijer, 1991). This designation is, of course, preliminary and subject to change as more data accrue. Since a K_d of 100 ml/g is already enough sorption to prevent any releases to the accessible environment within 10,000 years under the assumptions made for the present TSPA calculations, there is no reason to define a probability distribution with higher values. This is not to say that some combination of circumstances does not exist that would lead to large releases of these elements, so the question of what K_d values to use must be revisited each time a new set of circumstances is modeled.

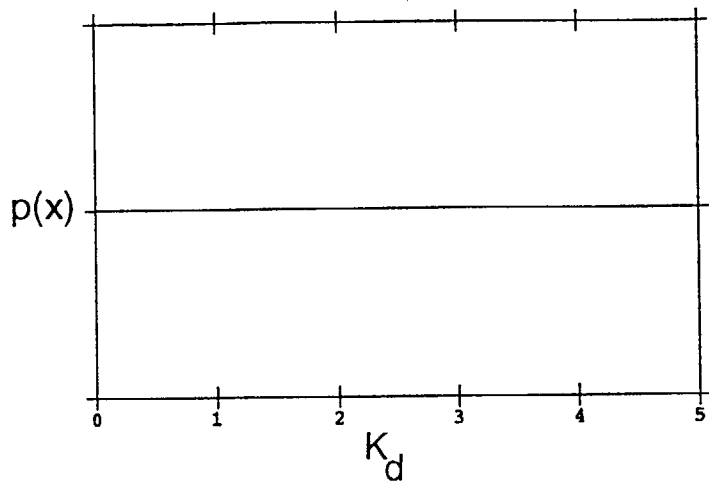


Figure 3-11. PDF for K_d , uranium or selenium on devitrified tuff

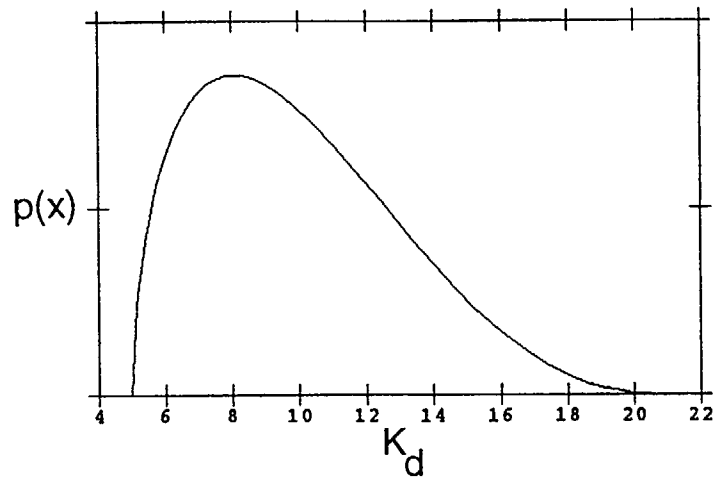


Figure 3-12. Beta PDF for K_d , uranium or selenium on zeolitic tuff

3-43

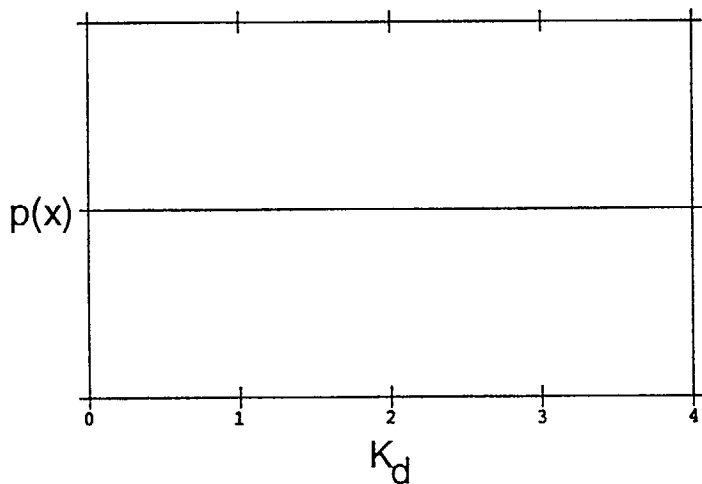


Figure 3-13. PDF for K_d , uranium or selenium on vitric tuff

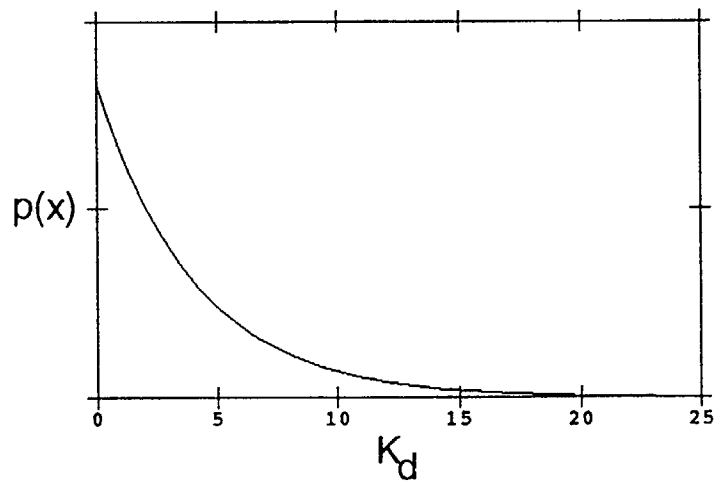


Figure 3-14. Beta PDF for K_d , neptunium on devitrified tuff

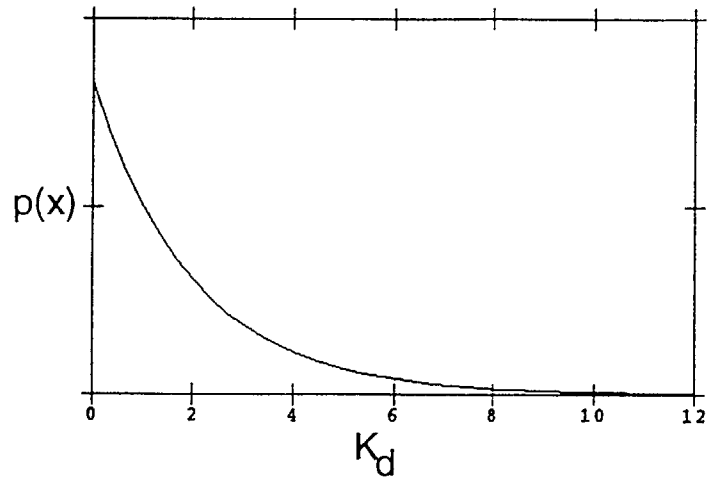


Figure 3-15. Beta PDF for K_d , neptunium on zeolitic tuff

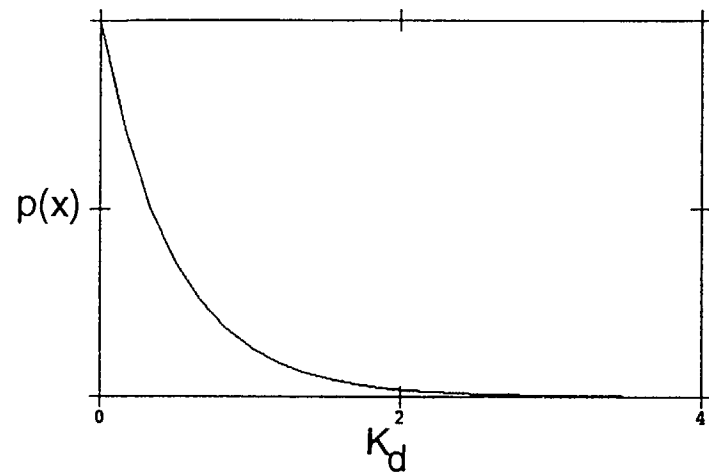


Figure 3-16. Beta PDF for K_d , neptunium on vitric tuff

3-44

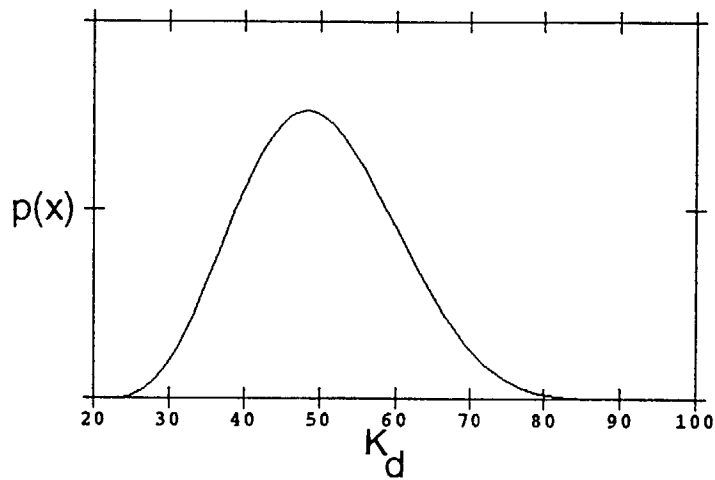


Figure 3-17. Beta PDF for K_d , cesium on devitrified or vitric tuff

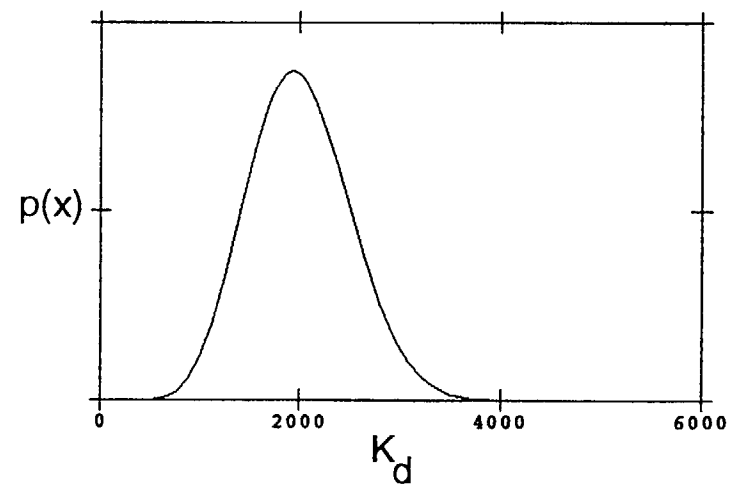


Figure 3-18. Beta PDF for K_d , cesium on zeolitic tuff

Uranium, selenium. Figure 3-19 shows some of the data available for sorption of uranium on Yucca Mountain tuffs. It can be seen that sorption is greatest on the zeolitic rock type and that sorption is greater for lower pH values. The pH at Yucca Mountain is most likely to be about 7.0 to 7.5, but there is some chance of pH's being higher or lower. The available data suggest that a uniform probability distribution is the best representation of the uncertainty for the devitrified and vitric rock types. Figures 3-11 and 3-13 show the uniform distributions. The range for the zeolitic rock type is greater, and values from the middle of the range were thought to be most likely. Figure 3-12 shows the shape chosen for the zeolitic distribution.

The choices of probability distributions in Table 3-25 are subjective, but represent reasonably well the LANL researchers' current expectations. There are far fewer data available for sorption of selenium, but its sorption behavior appears to be similar to that of uranium. For this study, the same K_d distributions were used for selenium as for uranium; i.e., uranium is assumed to be an analog for selenium. This assumption may be modified when additional data become available.

Neptunium. Figure 3-20 shows some of the data available for sorption of neptunium on Yucca Mountain tuffs in J-13 water. The higher values shown in the figure are for K_d 's derived from desorption experiments. For experimental reasons, these values are less reliable. Since many of the measured K_d values are small, a probability distribution (the exponential distribution) was chosen that is strongly skewed to low values but that does include higher values. Figures 3-14 through 3-16 show the distributions. Once again, the choices are subjective but reflect what is currently known about sorption of neptunium. The LHS program that was used for sampling from the probability distributions (Iman and Shortencarrier, 1984) does not have the exponential distribution built in, so the exponential distributions were approximated by beta distributions. The exponential distribution is a degenerate case of the beta distribution, so it is theoretically possible to approximate the exponential distribution arbitrarily closely with a beta distribution. Because of the limitations in the LHS computer program discussed previously, only close approximations are achievable. The beta-distribution parameters are listed in Table 3-7; if exponential distributions were used, they would be characterized by the means shown in the table. Figure 3-21 shows one of the exponential distributions and the beta distribution that approximates it. It can be seen that, compared to the exponential, the beta has slightly increased weighting of very small K_d 's and slightly decreased weighting of intermediate K_d 's.

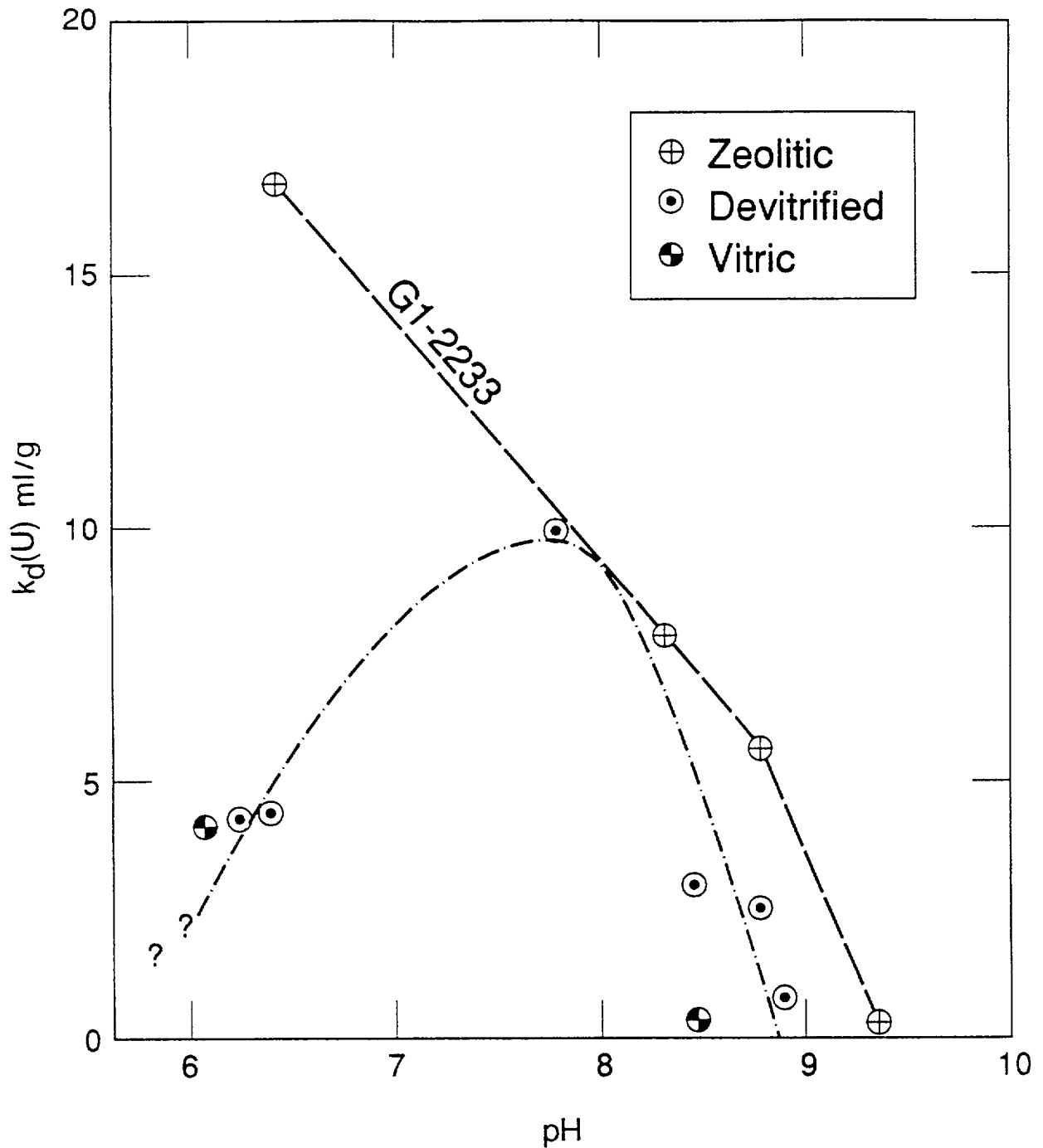


Figure 3-19. Uranium K_d as a function of pH; (taken from Meijer, 1991).

Cesium. Cesium is strongly sorbed to most rock types at Yucca Mountain, but especially to the zeolitic rocks. The minimum-K_d approach could have been used for cesium, with a value of about 20 ml/g, but it was decided to use distributions for the different rock types so that the extremely high sorption on zeolitic rocks

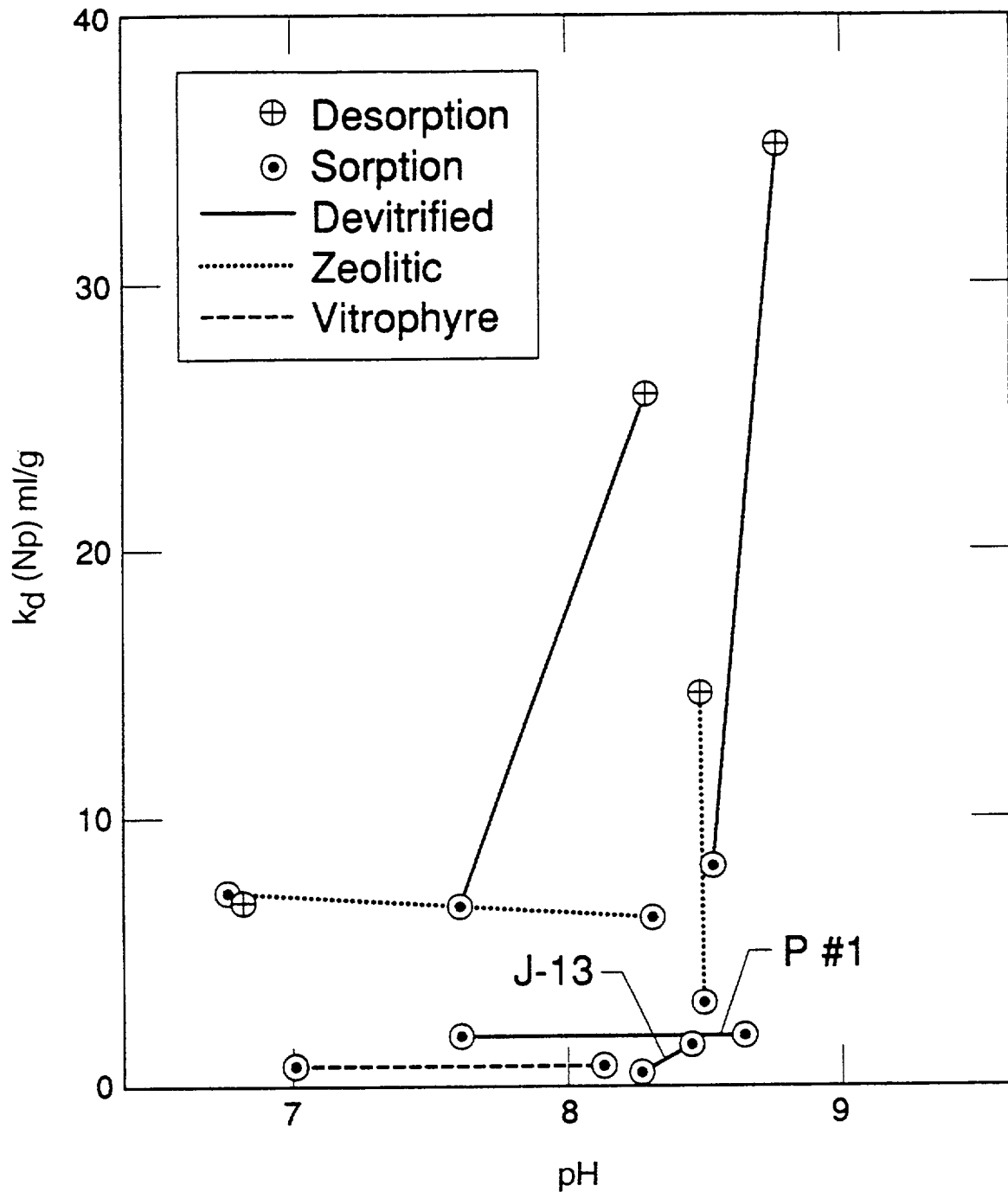


Figure 3-20. Neptunium K_d as a function of pH; (taken from Meijer, 1991).

could be represented. The K_d distributions for cesium are shown in Figures 3-17 and 3-18.

Table 3-26 shows the bulk densities used for the calculation of the retardation factors. Constant values were used rather than distributions because the variability of bulk density is small compared to the variability of the other terms in Equation

3.23. The numbers in Table 3-26 were generated by using the grain densities from Table 2.1-2 of Dudley et al. (1988) and the mean matrix porosities from Table 3-10 of this report ($\rho_b = \rho_g (1 - n)$, where ρ_g is grain density and n is porosity). Bulk density for the tuff saturated zone was loosely based on 40% of the welded value plus 60% of the zeolitic value because Section 3.9.4.2 of DOE (1988) states that the saturated-zone flow path is 40% through the Topopah Spring unit and 60% through the Calico Hills unit.

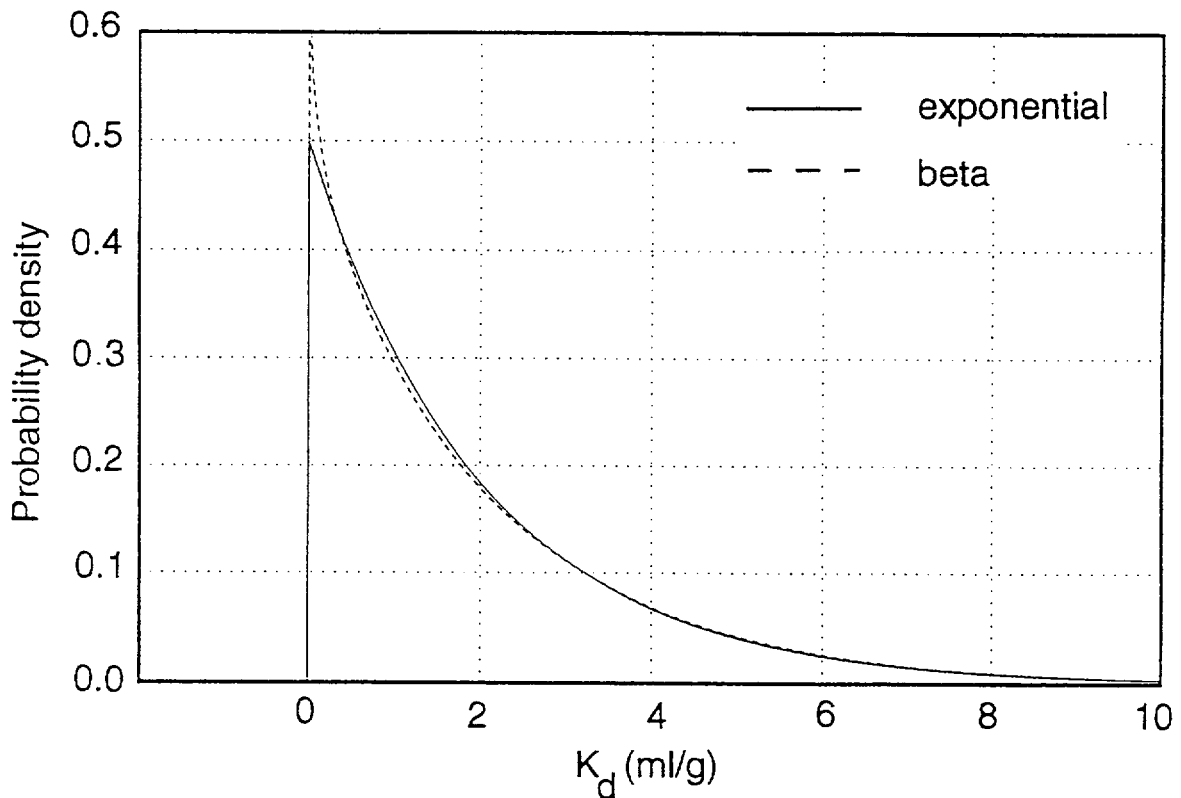


Figure 3-21. Exponential probability density function (Np on devitrified tuff).

3.4.2 Sorption coefficients for the carbonate aquifer

There are no data regarding sorption coefficients for the carbonate aquifer that is below the tuff aquifer in the Yucca Mountain area. As an analog, data from the Culebra dolomite at the Waste Isolation Pilot Plant (WIPP) were used because it is composed of similar carbonate rocks. The K_d values used were provided by A. Meijer of LANL, using data reported in the literature (Lappin et al., 1989; Rechar et al., 1990; MacLean et al., 1978). The distributions used are shown in Table 3-27. The distributions in the table follow the WIPP practice for K_d distributions (Rechar et al., 1990, Appendix A), which is to use histograms for the distributions.

An example of one of these histograms is shown in Figure 3-22, which gives the distribution for the K_d of uranium. The distributions shown in Table 3-27 are quite conservative in that they always have a significant probability of having $K_d = 0$.

Table 3-26
Bulk density used for retardation-factor calculation

Layer	Geohydrologic unit	Bulk density (g/cm ³)
1	Welded	2.30
2	Vitrophyre	2.17
3	Vitric	1.87
4	Zeolitic	1.32
5	Partially welded	1.97
—	Tuff (saturated zone)	1.80

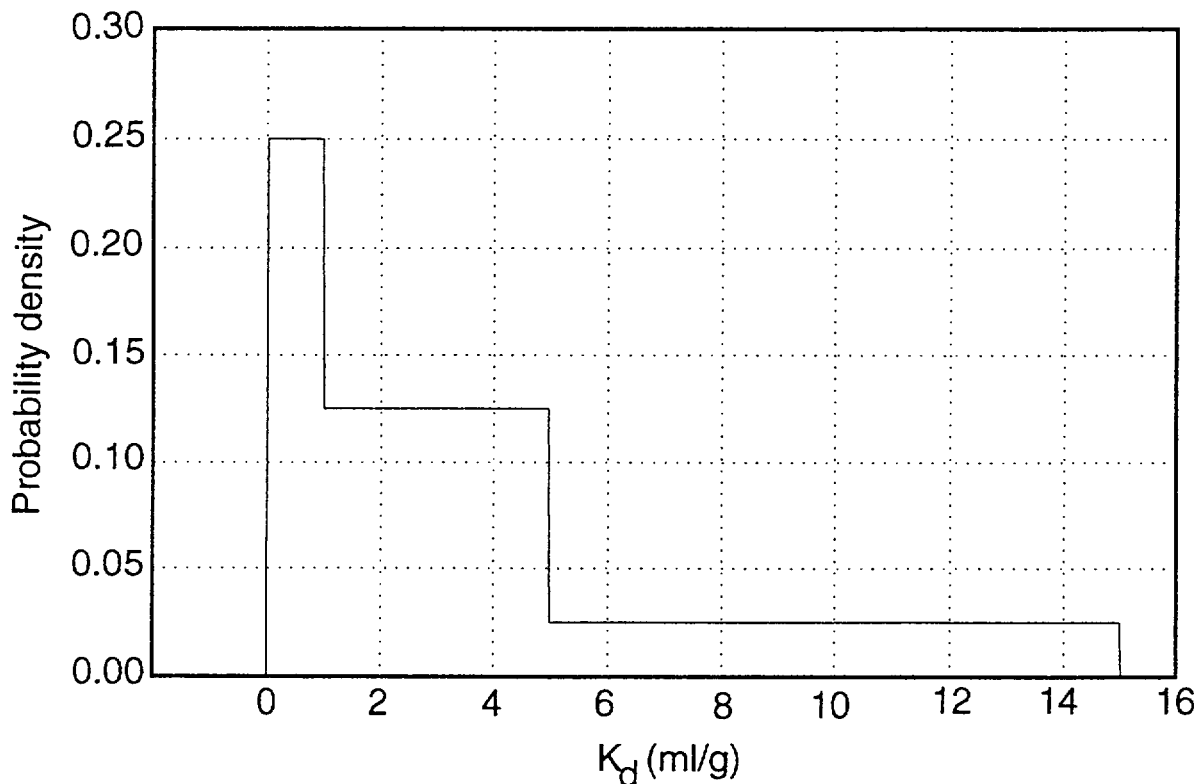


Figure 3-22. Stepwise-uniform probability density function (U on carbonates)

Table 3-27
Probability distributions for K_d in carbonate aquifer
(units are ml/g)

Percentile	Pu	Am, Sn	U, Se	Np	Cs	I, Tc, C
100%	1050	380	15	10	50	0
75%	100	200	5	1	20	0
50%	80	110	3	0.5	10	0
25%	25	100	1	0.1	5	0
0%	0	0	0	0	0	0
Mean	182	150	4	1.6	15	0

Some comments on the values in Table 3-27 follow. 1) The water chemistry is assumed to be oxidizing; if the water were in a reducing state the K_d 's would be larger. 2) In carbonate rocks, much of the carbon would probably precipitate out because of chemical interactions, but our calculations assumed carbon to be transported with no retardation, as shown in the table. 3) Chlorides are present in the Culebra Formation that almost certainly are not present in the carbonate aquifer at Yucca Mountain. Data presented by MacLean et al. (1978) for actinide sorption on limestones in low-chloride waters suggest that the dissimilarity between the WIPP waters and Yucca Mountain waters is not of importance. The bulk density for the rock in the carbonate aquifer was not available, so once again the Culebra dolomite was used as an analog. The validity of this assumption is not known. The Culebra dolomite has a bulk density of 2.8 g/cm³ (Rechard et al., 1990).

Chapter 4

Groundwater Flow and Transport

(Wilson, Gauthier, Robey, Barnard)

A potential repository at Yucca Mountain would be located in partially saturated, fractured tuffs, 200 meters above the water table. Groundwater flow is an inherent, and so far poorly understood, part of Yucca Mountain. Yet groundwater is expected to play an important role in the future performance of a repository, in both waste-container failure and radionuclide transport to the accessible environment.

To analyze the possibility of aqueous releases of radionuclides from the potential repository to the accessible environment, this TSPA couples mathematical models of different parts of the problem: radionuclide releases from the engineered barrier system (EBS), groundwater flow (in both the unsaturated zone and the saturated zone), and radionuclide transport in groundwater. Because little is presently known about groundwater flow at Yucca Mountain, two alternative conceptual models of flow in the unsaturated zone are considered: (1) the composite-porosity model, a model based on Darcy's law (a classical flow model) that allows unrestricted water movement between fractures and the tuff matrix; and (2) the weeps model, a model that depicts essentially all of the percolating water traveling down fractures. These two models were chosen because they represent extremes in matrix/fracture interaction, and could possibly bound the actual flow patterns at Yucca Mountain.

The mathematical models of flow and transport processes, as well as of the Yucca Mountain site, incorporate the following important simplifications. (1) The problem geometry is confined to one-dimensional flow and transport segments. (2) Geologic strata in the unsaturated zone are modeled as homogeneous units with uniform fractures; the saturated zone is modeled as a conglomerate of the tuffaceous and carbonate aquifers. (3) The radionuclide source term (i.e., waste-container degradation and radionuclide releases from the EBS) is modeled by simple functions of some of the important time scales. For example, the "dry-out" time associated with the heat generated during early life of a repository is simply modeled as a delay time before possible container failure. (4) The flow and transport calculations ignore repository thermal effects. (5) Radionuclide retardation during transport is modeled by a simple distribution coefficient (K_d). These simplifications are pragmatic—we are presently unable to use the Monte Carlo technique on nonlinear, nonisothermal, three-dimensional flow and transport problems. But these simplifications can also be justified because our present knowledge of the site and of flow and transport

processes at the site could be insufficient to support using more complex models. Chapter 9 contains further discussion of the simplifications and abstractions made for this TSPA.

This chapter contains a discussion of the aqueous-release problem and a description of each of the models used in the problem analysis. Probabilistic results from the analysis are presented and compared with EPA and NRC performance measures. Deterministic calculations are then examined to show some aspects of the models and the behaviors they predict that are not immediately obvious in the probabilistic calculations.

4.1 Problem development and scenario screening

The scenarios describing the groundwater flow and transport analyses were developed from the FEP diagram for "Nominal Flow in the Presence of the Repository." (See Chapter 3 for an introduction to the concept of a FEP diagram. FEPs are features, events, and processes.) This FEP diagram includes both "Distributed Infiltration," and "Runoff-Producing Events" FEPs. The TSPA problem is in the former category, investigating several aspects of distributed infiltration. Figure 4-1 shows the top portion of the FEP diagram. Viewed from left to right, the branches below the "Distributed Infiltration" FEP indicate progressively deeper locations where the infiltrating water interacts with the surrounding rock matrix, and can thus be considered uniformly distributed for calculational purposes.

The portion of the FEP diagram shown in Figure 4-1 covers FEPs that occur outside the TSPA problem domain. The TSPA groundwater-flow calculations only model Yucca Mountain from the repository horizon down, and Figure 4-1 concerns FEPs above the repository. The boundary conditions in the TSPA calculations are derived from the FEPs shown in this figure.

The leftmost branch of the diagram ("Areal Infiltration") describes FEPs in which infiltrating water is imbibed into the unconsolidated and undifferentiated matrix (e.g., the alluvium) within a few meters of the surface. This scenario assumes that water that percolates farther does so in both the matrix and fractures, and that the pressure heads in each are in equilibrium. This assumption is the basis of the composite-porosity-model component of the TSPA. One path through the FEP diagram that could be modeled by the composite-porosity model is shown by the heavy line labeled ① in Figure 4-1. The box labeled ①, which contains the FEP "Unsaturated/Saturated Flow Plume Established," establishes flow conditions described by the composite-porosity model. These conditions also appear elsewhere in the FEP diagram (all branches ending in ①) and are included in the TSPA

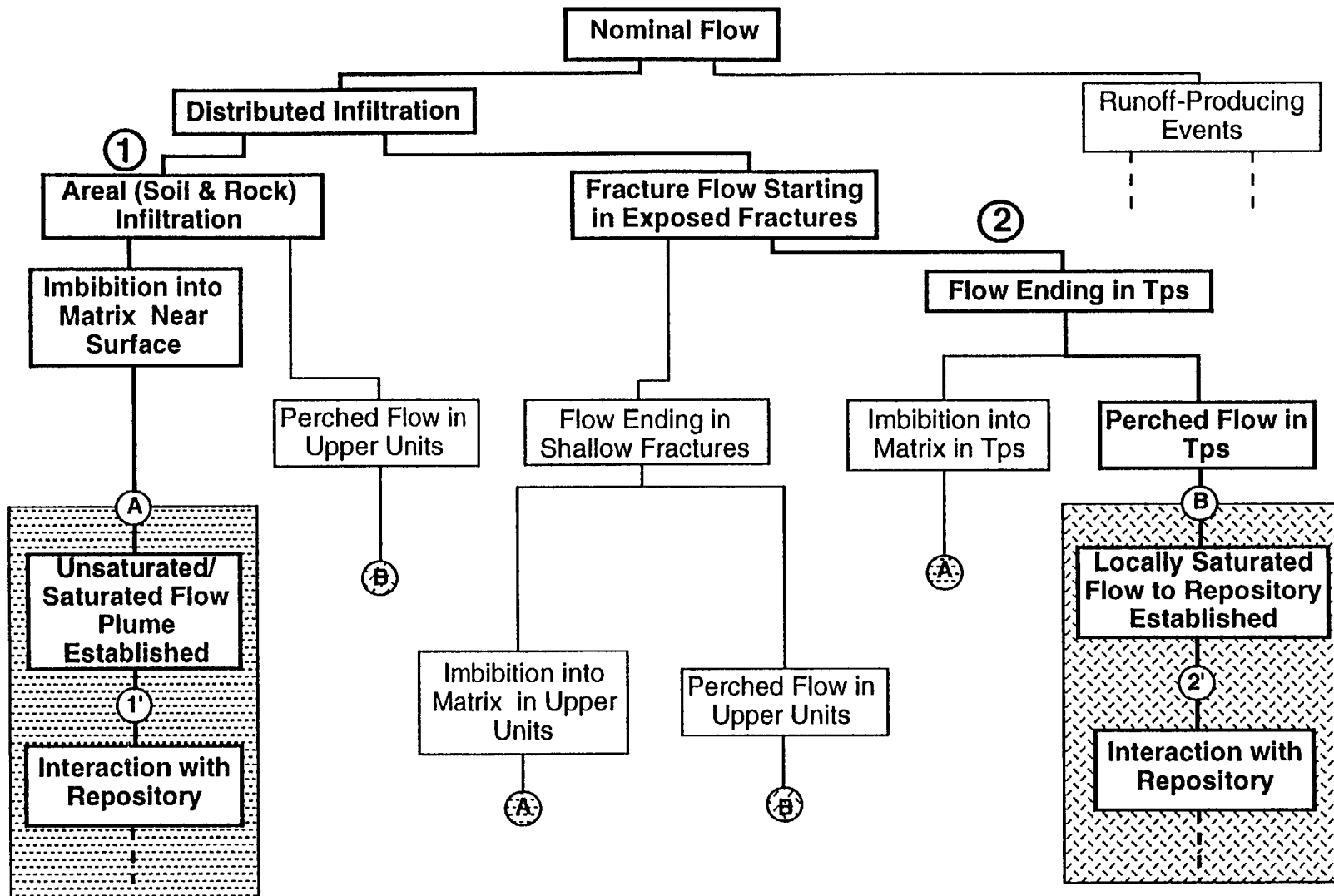


Figure 4-1. Upper section of the Nominal-Flow FEP diagram.

composite-porosity calculation.

The branch labeled "Fracture Flow Starting in Exposed Fractures" addresses fast flow paths through fractures by the percolating water. The branch "Flow Ending in Shallow Fractures" indicates processes in which the water is transported through the undifferentiated surface layers into units such as the Paintbrush nonwelded unit, where it is imbibed by the tuff matrix. The other branch treats fracture flow that reaches the Topopah Spring Member (Tps), where the potential repository is located, before being imbibed by the tuff matrix. (Tps corresponds to the "welded" layer in the stratigraphy used for this TSPA.) These branches represent end-points of a continuum of processes for the fast transport of water from the surface to depth. Locally saturated flow to the repository is the basis for the weeps-model component of the TSPA. One weeps scenario is indicated by the line marked (2) in Figure 4-1, but the other branches that end in "Locally Saturated Flow to Repository Established" (the branches ending in (B)) could also be modeled by the weeps model. As before, the FEP-diagram paths shown in Figure 4-1 are not modeled directly in this TSPA; they only enter into the assumed boundary conditions.

The TSPA composite-porosity calculations are based on the premise that water flow is steady-state. This premise can be justified by assuming that the matrix-imbibition processes in rock above the repository horizon damp any transient-flow fronts that may have originated at the surface. The weeps model, on the other hand, assumes episodic water flow down fractures, because significant matrix imbibition is not allowed by the model.

All the branches in Figure 4-1 end with the FEP "Interaction with Repository." Although the same FEP appears at the end of each branch, the interactions that occur could be different for locally saturated flow as compared with larger-scale saturated/unsaturated conditions. Figures 4-2 and 4-3 expand the FEP diagram from the repository to the water table—the region modeled in the TSPA unsaturated-zone calculations. Figure 4-2 shows FEPs for unsaturated flow, while Figure 4-3 is for locally saturated conditions. Each of the branches in Figure 4-1 (except for "Runoff-Producing Events") is continued by either Figure 4-2 or Figure 4-3.

The FEPs in the leftmost three columns of both continuation figures address thermal effects resulting from the thermal output of the repository. These effects are not directly modeled in the groundwater-flow analysis. Thermal effects are included in the TSPA calculations only insofar as the source-term model contains a time delay when the waste containers are assumed to be hot enough so that no liquid water contacts them. The fourth column in each figure describes FEPs for a cold repository.

Considering the unsaturated flow in Figure 4-2 (labeled (1')), the FEP-diagram

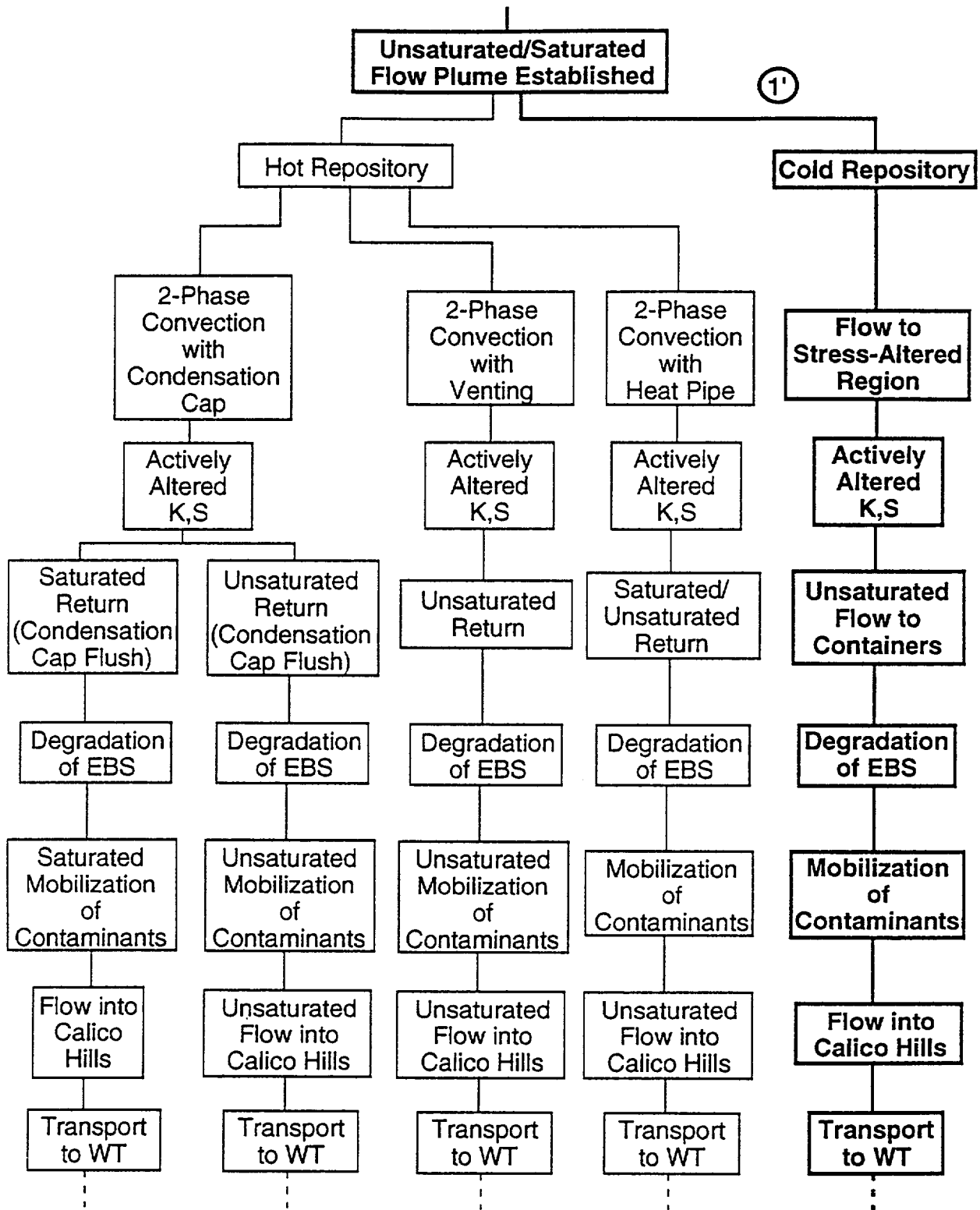


Figure 4-2. Lower part of the Nominal-Flow FEP diagram, for unsaturated conditions.

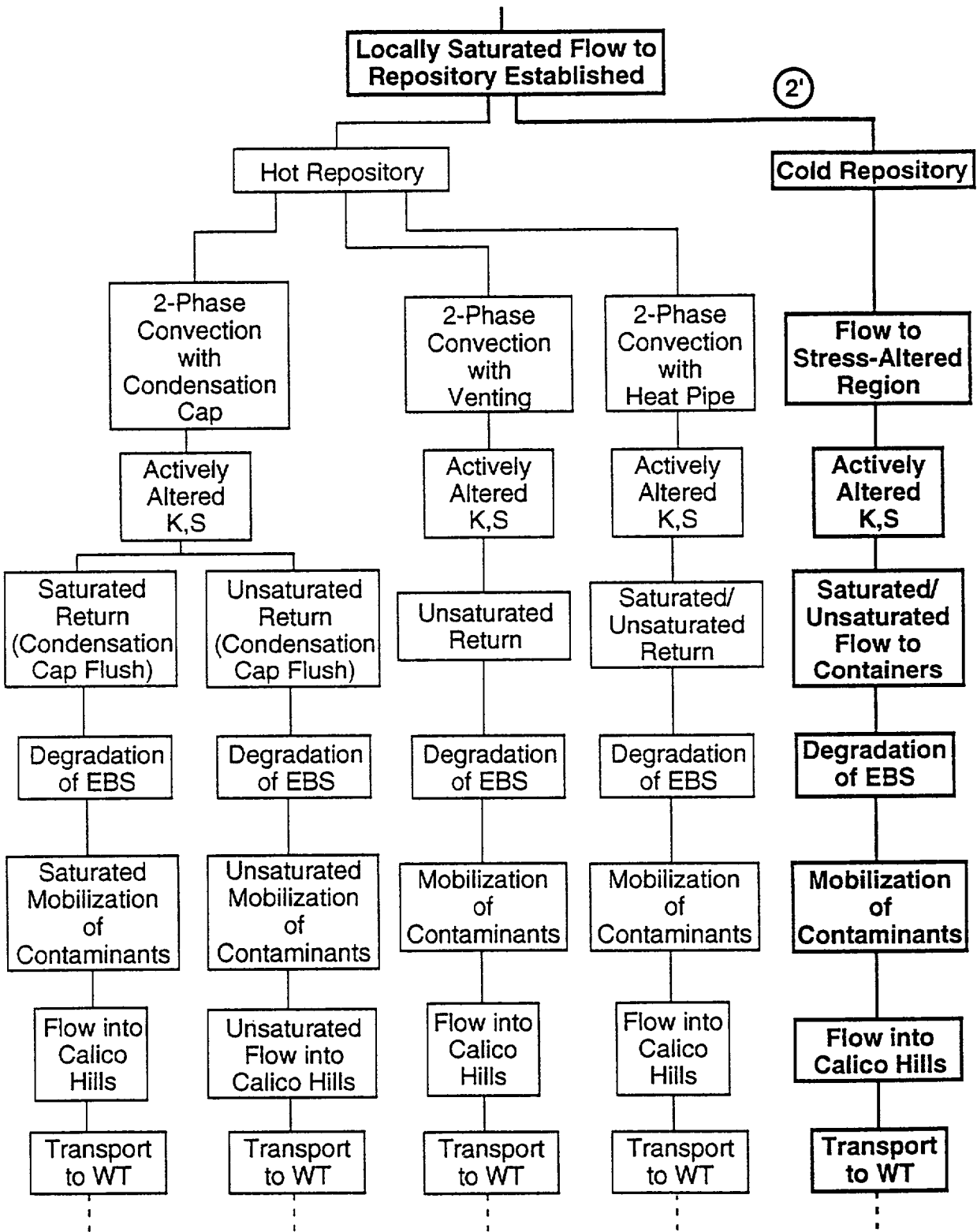


Figure 4-3. Lower part of the Nominal-Flow FEP diagram, for locally saturated conditions.

path shows water flowing into the disturbed rock surrounding the mined repository. Unsaturated flow in this region reaches the containers, which causes degradation of the EBS and mobilization of contaminants. The contaminated groundwater then flows through the Calico Hills formation to the water table. This latter FEP is the primary emphasis of the composite-porosity-model component of the TSPA. Although not shown in this FEP-diagram segment, the complete FEP diagram indicates, and this TSPA considers, flow continuing through the saturated zone to the accessible environment.

Figure 4-3 completes the FEP-diagram path for locally saturated flow. The scenario used for the weeps component of the TSPA is shown as (2') in the figure. Local saturation implies that there is both unsaturated and saturated flow. However, for the purposes of the weeps model, the unsaturated flow is not considered. (A factor is included in the weeps model to describe unsaturated flow into the rock matrix caused by unconnected fractures; however, at that point, the unsaturated flow is not considered further by the model.) The FEP diagram shows that flow occurs in the stress-altered region surrounding the waste packages, resulting in saturated/unsaturated flow to the containers. From here on, the FEP diagram is the same as that described for Figure 4-2.

4.2 Method

Groundwater flow and transport are calculated using the Total-System Analyzer (TSA) (Wilson et al., 1991; Wilson, 1992). The TSA contains separate mathematical models of the following processes:

- 1) groundwater flow in the unsaturated zone (STEADY module of TOSPAC and WEEPTSA, both discussed in Section 4.4),
- 2) radionuclide source term (TRANS module of TOSPAC, discussed in Section 4.3),
- 3) transport in the unsaturated zone (also in the TRANS module of TOSPAC, discussed in Section 4.6), and
- 4) groundwater flow and transport in the saturated zone (also in the TRANS module of TOSPAC, discussed in Sections 4.5 and 4.6).

These models are linked in the TSA to allow simulation of radionuclides from a potential repository to the accessible environment.

The computer programs based on the models are used to perform deterministic calculations; a single set of parameters is used to determine a single result. In order to

consider the uncertainty involved in the parameters, the Monte Carlo method is used. Parameters are sampled from probability distributions, a calculation is performed, the results are saved, and the process is repeated until the appropriate statistics are obtained. Figure 4-4 presents the Monte Carlo method as it is implemented in the TSA. In the TSA, parameters are sampled using Latin-Hypercube sampling (Iman and Shortencarier, 1984).

Uncertainty in the models (as distinct from uncertainty and variability in the parameters) has been only partially addressed in this study, by consideration of two alternative models of flow in the unsaturated zone: (1) the composite-porosity model, and (2) the weeps model. Separate results achieved by using the two different models are presented in Section 4.7.

Figure 4-5 shows how the two different flow models are incorporated in the TSA. Shown in the figure is the coupling of the process models in the TSA, and the input from other phases of this study—specifically, definition of the input-parameter distributions and utilization of the results from more complex process models. At the time of this study, not enough evidence exists to determine which of the alternative conceptual models best represents flow in the unsaturated zone at Yucca Mountain—if either. Chapter 8 discusses combining the results of the two alternative conceptual

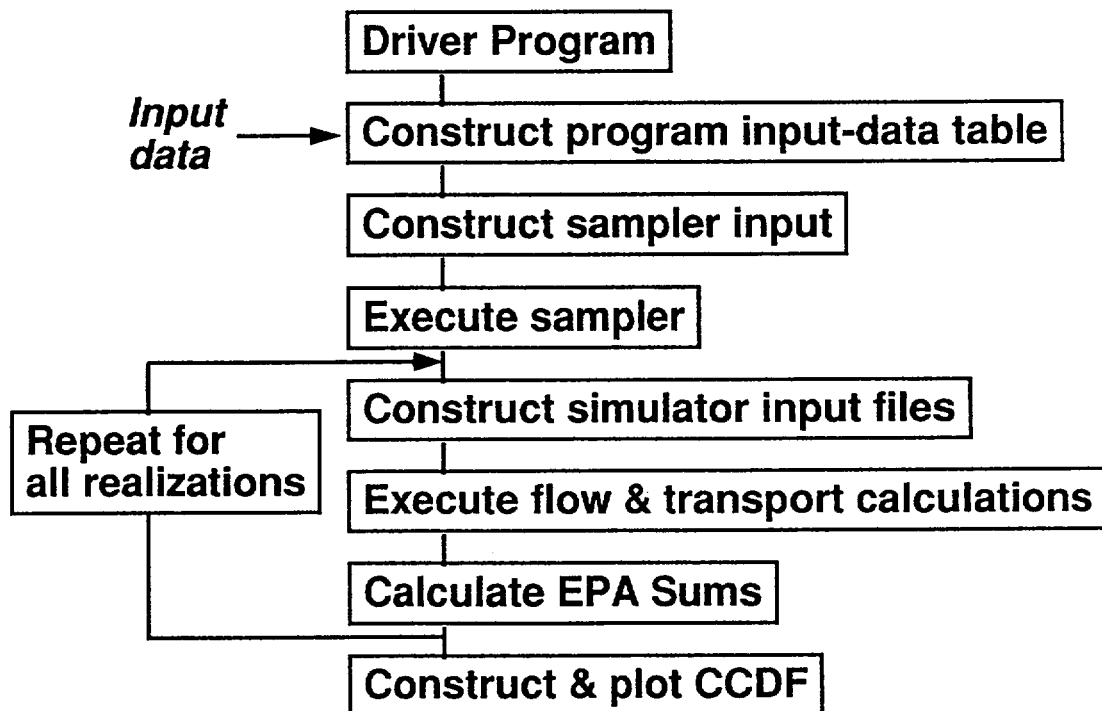


Figure 4-4. Top-level flow chart for the Total-System Analyzer (TSA), showing the loop for performing the Monte Carlo simulation.

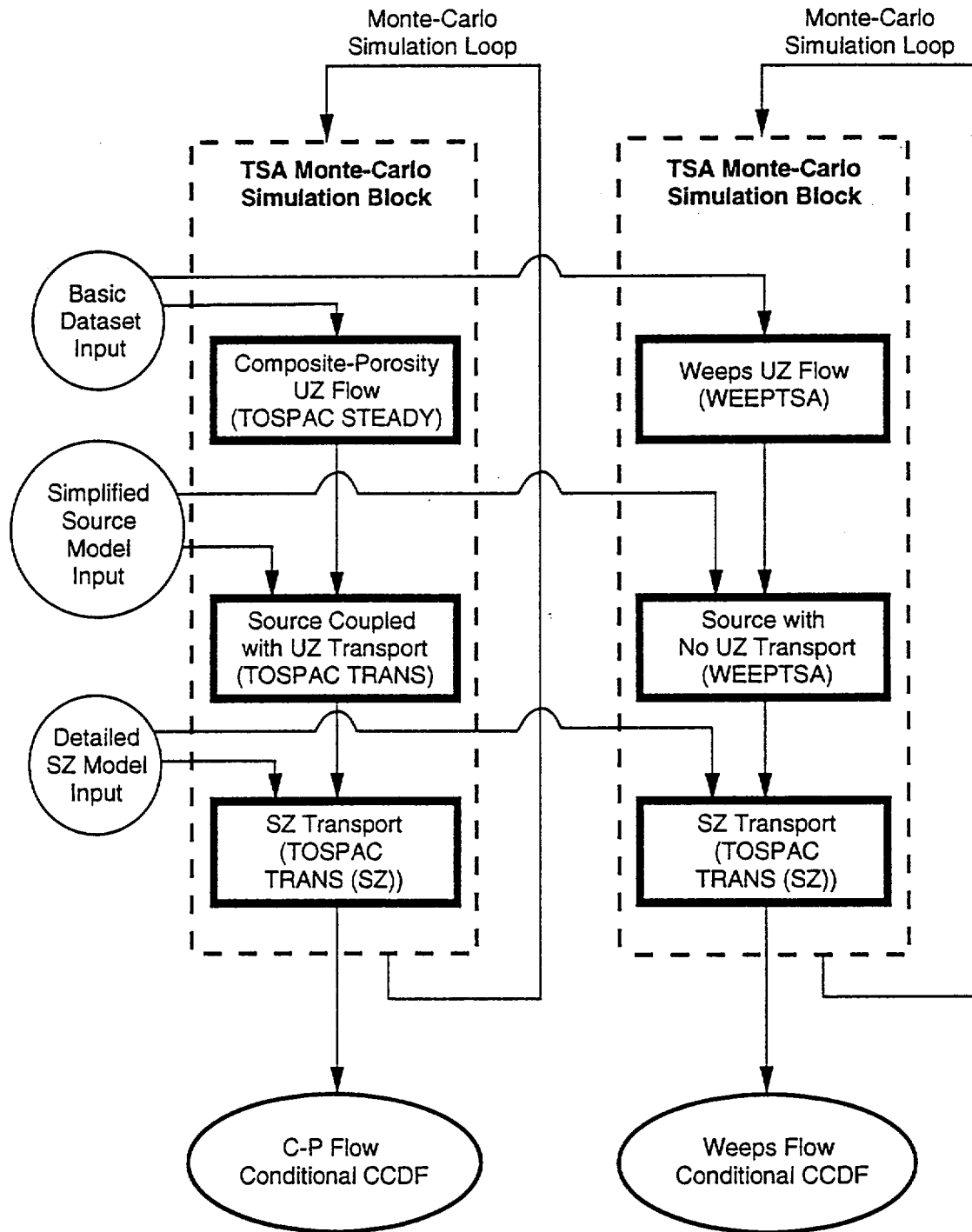


Figure 4-5. Diagram showing how the two alternative conceptual models of flow are implemented in the TSA, including coupling with other models and the input/output interfaces.

models. The conceptual model of flow is also important to the determination of gaseous releases from the potential repository, primarily because of its influence on the source term. Chapter 5 contains a discussion of the effect of groundwater flow on gas-phase releases.

Using the Monte Carlo method, predictions to a probability of one part in 1000 (a criterion from 40 CFR Part 191) require at least 1000 deterministic calculations. Results presented in Section 4.7 follow from 1800 calculations for the composite-porosity flow model (300 for each of six different flow geometries), and 1000 calculations involving the weeps model.

4.3 Radionuclide source term for aqueous releases

The radionuclide source term used in the TSPA calculations of aqueous releases for “nominal” conditions was developed at Lawrence Livermore National Laboratory (LLNL) by William J. O’Connell. The source model is described in detail by O’Connell (1992), but a brief description is included here to make documentation of the TSPA more complete. Note that the notation used here is somewhat different from the notation used by O’Connell (1992).

The source model is a simplified version of the detailed release models being developed at LLNL. For some types of studies, especially those concerned with waste-package or engineered-barrier-system (EBS) design, detailed models are appropriate and needed, but for a total-system performance calculation—and especially for a preliminary total-system performance calculation—a greater level of abstraction is appropriate. There are two basic reasons for this situation. First, there is not yet sufficient information available to be able to characterize in detail the behavior of the repository system. Indeed, the simplified model described below has only 20 input parameters (in addition to some input parameters, such as average water flux and retardation, that are shared with the far-field flow and transport calculation), and yet many of the parameters were set to arbitrary values because the correct values, or likely range of values, are not known. A detailed EBS model could require dozens or even hundreds of input parameters. The second reason for using a simplified source model is to reduce the computational load. Complicated calculations of the chemical reactions involved in failure of the waste containers, dissolution of the spent fuel, and transport of the dissolved waste in the near field would add considerably to the amount of computer time and analyst time required for the calculations.

The source model described here is directly applicable to the composite-porosity water-flow model. Some modifications were necessary to apply this source model to the weeps model; those modifications are described in Section 4.4.4. Figure 4-6

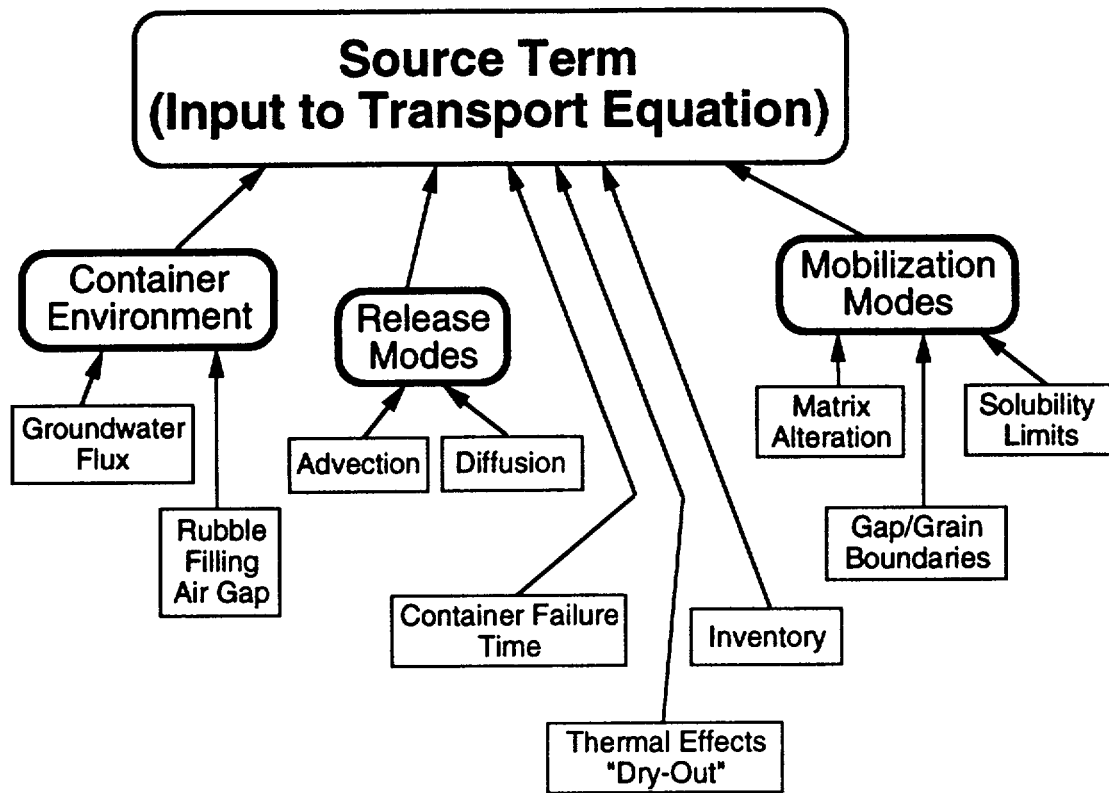


Figure 4-6. Important factors included in the model of the radionuclide source term.

presents schematically some of the important factors that go into the source model.

The source model described in this section can be applied to most waste-container designs considered for a repository at Yucca Mountain. For the calculations in this report, we assume the reference container and repository layout as given in the Yucca Mountain Site Characterization Plan (SCP; DOE, 1988) and the Site Characterization Plan Conceptual Design Report (SCP-CDR; MacDougall et al., 1987). Figure 4-7 illustrates a vertically emplaced waste container, and shows some of the terms used in this section.

The following subsections contain brief descriptions of the radionuclide inventory, waste-container environments, and some of the physical processes involved in radionuclide releases from the EBS. The processes included are container wetting after the thermal dry-out period, container failure, radionuclide mobilization, and radionuclide transport out of the container. The source model is broken into several submodels that are highly abstracted representations of the processes. Each process submodel is parameterized very simply in one of two ways—either by three time scales, or by two time scales and a water-flow rate. A start time t_0 and a ramp-up time t_1 are used as parameters for all submodels. For some of the submodels, the

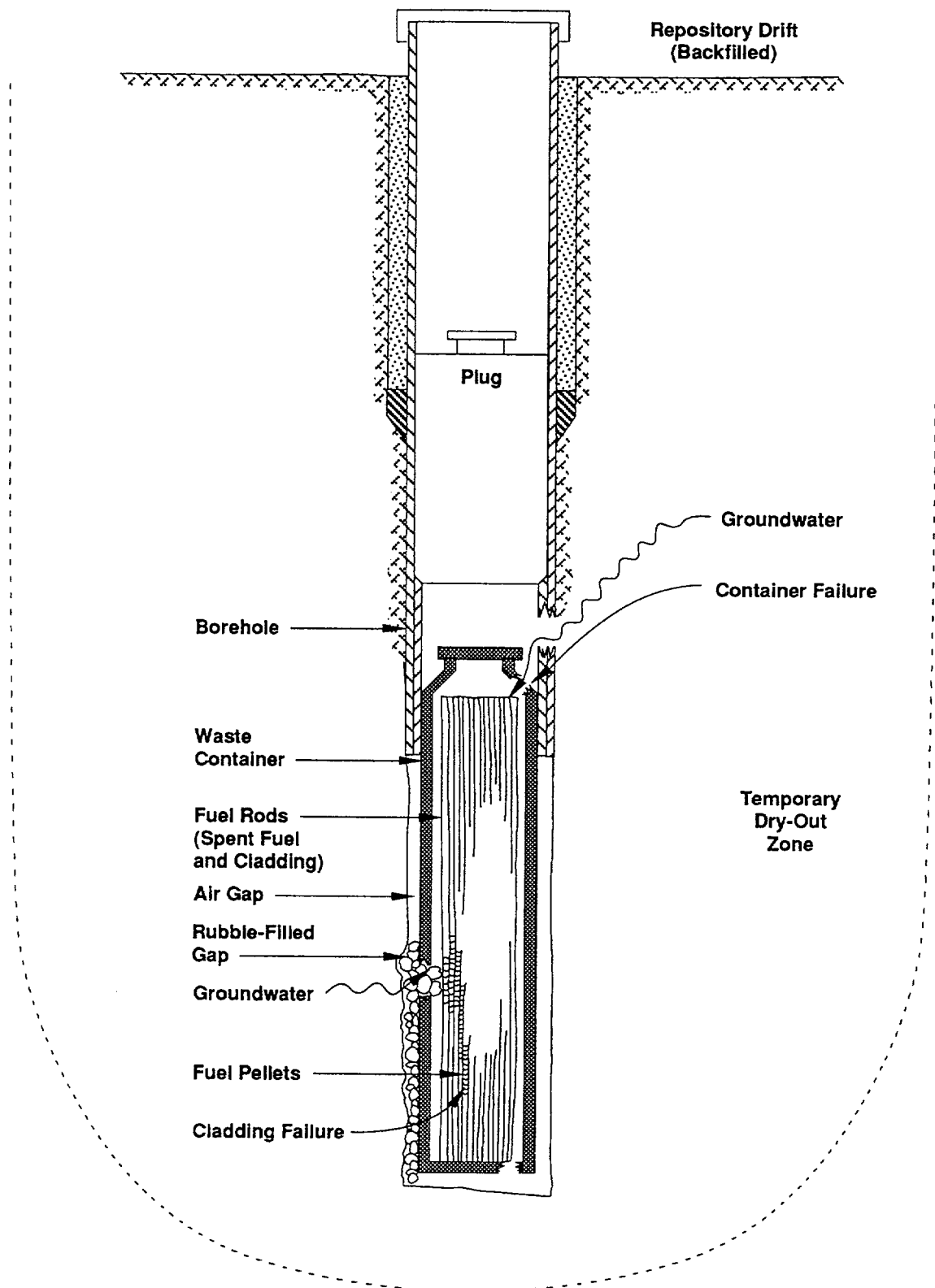


Figure 4-7. One concept for a vertically emplaced waste container.

third parameter is a fall-off time t_2 . When the fall-off time would be very long, a water-flow rate W is used as the third parameter, in place of fall-off time. When a submodel is parameterized by three times, t_2 is always taken to be larger than t_1 —that is, ramp-up is assumed to be faster than the fall-off.

4.3.1 Radionuclide inventory

Wilson (1991) lists 39 radionuclides that are potentially important to include in total-system performance calculations. Those 39 nuclides and a few others are included in the human-intrusion and volcanism calculations discussed in Chapters 6 and 7 of this report. The human-intrusion and volcanism calculations model direct releases to the surface, in which the only limitation on releases is the inventory involved. Thus, all nuclides with non-negligible inventory were included. For the “nominal” aqueous and gaseous releases, however, source release rates and transport velocities are additional limitations on the amount of radioactivity reaching the accessible environment. Thus, based on these limitations and the results of many preliminary calculations, it was decided to consider only ten radionuclides (only nine by aqueous release) in the nominal-case calculations.

Table 4-1 shows the nine nuclides considered for aqueous release. Also shown are the inventories used, the half-lives, the NRC limits, the EPA limits, and the release type (“s” for solubility-limited or “a” for alteration-limited). The tenth nuclide is ^{14}C , which was considered for gaseous release (Chapter 5). The data in Table 4-1 were taken from Wilson (1991). The data sources are given in Wilson’s report, but the principal source is Roddy et al. (1986). The inventories follow from the as-

Table 4-1. Radionuclides included in the aqueous-release calculations.

Species	Inventory (Ci/MTHM)	Half-life (yr)	Activity (Ci/mol)	NRC limit (Ci/MTHM-yr)	EPA limit (Ci/MTHM)	Release type
^{234}U	1.89	2.445×10^5	1.46	1.89×10^{-5}	0.1	s
^{243}Am	1.54×10^1	7.380×10^3	4.84×10^1	1.41×10^{-4}	0.1	s
^{239}Pu	3.08×10^2	2.406×10^4	1.49×10^1	3.00×10^{-3}	0.1	s
^{237}Np	1.12	2.140×10^6	1.67×10^{-1}	1.67×10^{-5}	0.1	s
^{135}Cs	3.51×10^{-1}	2.300×10^6	1.55×10^{-1}	1.67×10^{-5}	1.	a
^{129}I	2.95×10^{-2}	1.570×10^7	2.28×10^{-2}	1.67×10^{-5}	0.1	a
^{126}Sn	7.15×10^{-1}	1.000×10^5	3.58	1.67×10^{-5}	1.	s
^{99}Tc	1.23×10^1	2.130×10^5	1.68	1.22×10^{-4}	10.	a
^{79}Se	3.81×10^{-1}	6.496×10^4	5.50	1.67×10^{-5}	1.	a

sumption of 60 percent pressurized-water-reactor (PWR) spent fuel with burnup of 33,000 megawatt-days per metric ton of heavy metal (MWd/MTHM) and 40 percent boiling-water-reactor (BWR) spent fuel with burnup of 27,500 MWd/MTHM. The 60/40 distribution of PWR and BWR spent fuel follows from data in the SCP; additionally, there should be a small fraction of glassified high-level waste, but the glass waste is neglected in this TSPA. The spent fuel was assumed to have been discharged from the reactor 10 years previously. The nominal-case calculations assume a total repository inventory of 70,000 MTHM of waste, and therefore, the inventories and the NRC and EPA limits presented in the table must be multiplied by 70,000. The NRC limits are based on 10 CFR 60.113(a)(1) (NRC, 1983). The quantity being limited by the NRC in that regulation is the release rate from the EBS, and the limits are based on the inventory 1000 years after repository closure. The EPA limits are based on 40 CFR Part 191, Appendix A (EPA, 1985), and pertain to cumulative releases to the accessible environment over a period of 10,000 years after emplacement in the repository.

The nuclides in Table 4-1 are grouped by decay chain, though only one nontrivial chain is included. In some cases (^{234}U and ^{237}Np), the nuclides being used in the calculations experience significant ingrowth during the course of 10,000 years. Because the parent radionuclides were not included in the calculations, the ingrowth was added at the start. That is, the inventories listed in the table for those two radionuclides are not the actual values 10 years after discharge from the reactor, but rather the values that would result when their parent radionuclides decay completely. For ^{234}U , the principal parent is ^{238}Pu ; for ^{237}Np , the principal parents are ^{241}Pu and ^{241}Am .

4.3.2 Container environments and types of releases

Two types of releases from waste containers are included in the source model: advective releases and diffusive releases. Advective releases are assumed to occur if a waste container is in a locally wet part of the repository, where water is running in fractures and seeping onto the container. A simple "flow-through" model is assumed in calculating the advective releases. Diffusive releases are assumed to occur if the air gap surrounding the container in its emplacement borehole has been partially filled with rubble, thus creating a pathway for waste to undergo molecular diffusion out of the container (if the container has failed). For simplicity, the height of the rubble in the borehole is assumed to be the same as the height of the water in the container, simplifying the estimate of the fraction of the spent fuel in a given container that contributes to diffusive releases. Figure 4-8 illustrates the two types

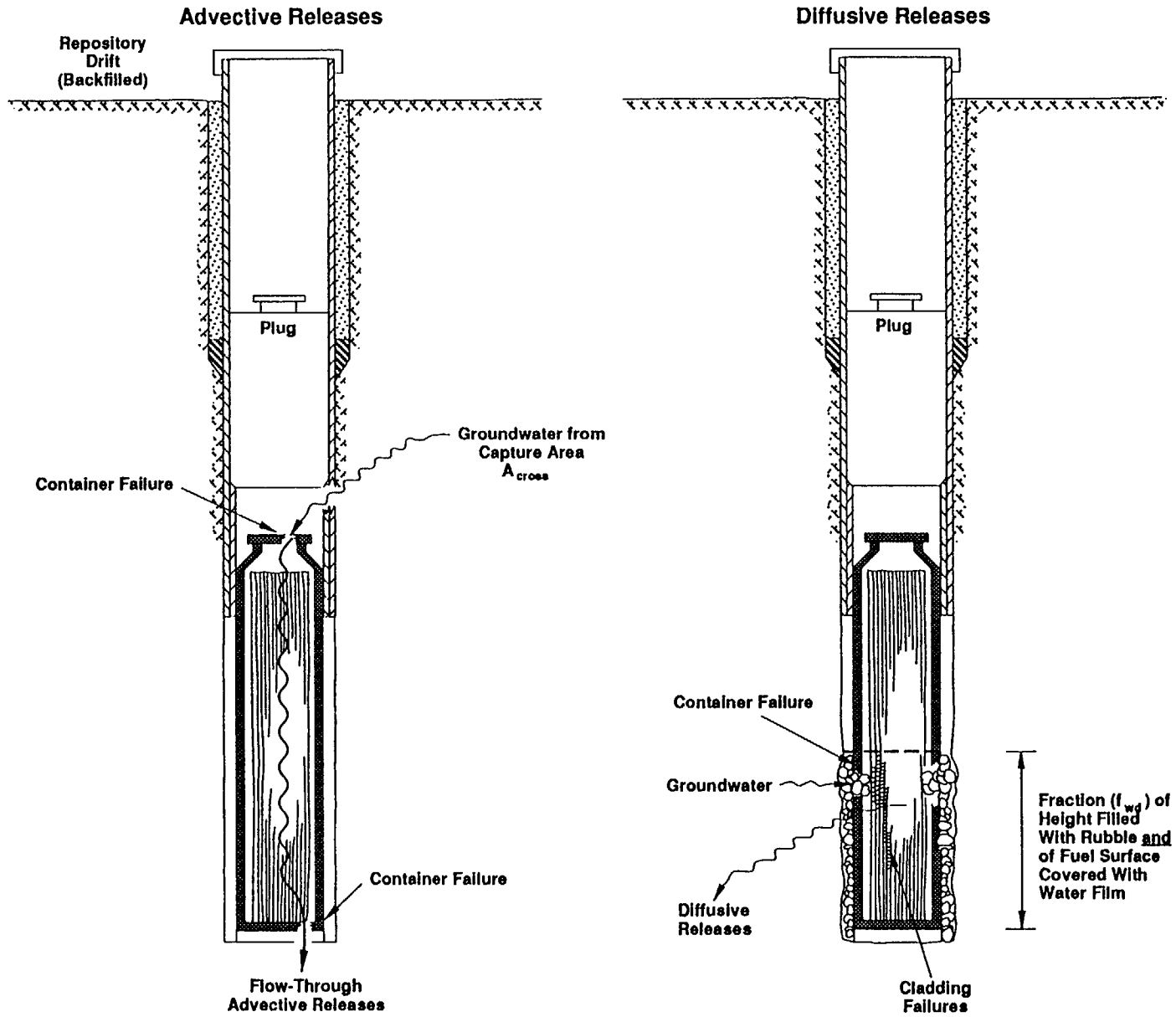


Figure 4-8. Two release mechanisms included in the source-term model.

of releases considered in the source-term model.

The fraction of containers in seepage areas is denoted by f_s and the fraction of containers with rubble filling at least part of their air gap is denoted f_r . The model assumption is that f_s is also the fraction of containers experiencing some advective releases and f_r is the fraction of containers experiencing some diffusive releases. With these two fractions we can divide the waste containers into four categories:

- 1) Containers with both advective and diffusive releases. The fraction of containers in this category is $f_s f_r$.
- 2) Containers with only advective releases. The fraction of containers in this category is $f_s(1 - f_r)$.
- 3) Containers with only diffusive releases. The fraction of containers in this category is $(1 - f_s)f_r$.
- 4) Containers with no releases. The fraction of containers in this category is $(1 - f_s)(1 - f_r)$.

Containers in seepage areas are referred to as wet, while containers with no seepage flux are referred to as moist.

The fraction of containers with some rubble in their air gap, f_r , is a user-supplied input parameter in the model. The fraction of containers in seepage areas (that is, with water dripping on them), f_s , is calculated from a simple model. The basic assumption that allows an estimate of f_s is that the spatial distribution of water fluxes follows a log-normal distribution (Chesnut, 1992). The log-normal distribution is defined by two input parameters: the percolation rate q (Section 3.2.3), and the coefficient of variation, here denoted by v (v is a specific model parameter and should not be confused with the general coefficient of variation, CV, discussed in Chapter 3). Note that q does not represent the water flux at any point, but rather the average over the repository area. It is also assumed that there is a threshold flux value, q_0 , above which fracture flow (seepage) is initiated. In the composite-porosity flow model, this threshold flux is given by the saturated hydraulic conductivity of the tuff matrix of the layer in which the repository resides.

The log-normal distribution is used to determine what fraction of the repository area has water running in the fractures, and thus what fraction of the waste containers are considered to be in wet environments with water seeping onto them. The rest of the waste containers are assumed to be in regions where the rock matrix is not saturated and are thus considered to be in moist environments. The resultant

expression for f_s is as follows:

$$f_s = P[q > q_0] = \frac{1}{2} \operatorname{erfc} \left(\frac{\ln q_0 - \mu}{\sqrt{2}\sigma} \right), \quad (4.1)$$

where erfc is the complementary error function, μ is the mean of the spatial flux distribution in log space, and σ is the standard deviation of the spatial flux distribution in log space. The mean and standard deviation in log space can be related to the previously described input parameters as follows:

$$\mu = \ln q - \frac{1}{2} \ln(v^2 + 1), \quad (4.2)$$

$$\sigma = \sqrt{\ln(v^2 + 1)}. \quad (4.3)$$

The average flux for those containers subjected to seepage flow is given by

$$q' = q \cdot f_s^{-1} \cdot \frac{1}{2} \operatorname{erfc} \left(\frac{\ln q_0 - \mu - \sigma^2}{\sqrt{2}\sigma} \right). \quad (4.4)$$

It is assumed that q_0 of that flux is carried by the porous matrix, so that the average flux available for seepage flow is given by

$$q_s = q' - q_0. \quad (4.5)$$

This quantity is the amount of water flux that is used in calculating advective releases for those containers that have advective releases.

4.3.3 Container wetting and failure

After waste containers are emplaced in a repository, radioactive decay is expected to generate enough heat to dry out the region surrounding the repository. As the decay progresses, the heat should subside, and groundwater should reenter the repository and eventually contact all the containers. Water is expected to be the major cause of container failure; sometime after groundwater contacts the containers, they will degrade and eventually fail.

The resaturation of the entire repository after the thermal dry-out period is described by two parameters, the beginning time of the resaturation (t_{rb}) and the duration of the resaturation (t_{rd}). It is assumed that no waste is released before time t_{rb} because all the containers are hot and dry. During the period from time t_{rb} to $t_{rb} + t_{rd}$, the containers are cooling enough that more and more of them are wetted. After wetting, the containers start to fail, with a typical lifetime of t_c .

Container wetting and failure together make up one of the process submodels referred to earlier. The three time parameters just introduced are used for the three

submodel time scales. The start time is given by the beginning of the resaturation period t_{rb} , the ramp-up time is given by the smaller of t_{rd} and t_c , and the fall-off time is given by the larger of t_{rd} and t_c :

$$t_{0,c} = t_{rb}, \quad t_{1,c} = \min\{t_{rd}, t_c\}, \quad t_{2,c} = \max\{t_{rd}, t_c\}. \quad (4.6)$$

The subscript c stands for the "container wetting and failure" submodel.

4.3.4 Modes of waste mobilization

The radionuclides making up the spent fuel are divided into two groups: low-solubility elements for which mobilization (that is, dissolution) is solubility-limited and high-solubility elements for which mobilization is alteration-limited. Table 4-1 shows the appropriate group for each radionuclide. Alteration refers to chemical alteration (oxidation) of the UO_2 fuel matrix. The assumption is that as the uranium changes its oxidation state, the other elements, which are present in the fuel matrix as trace impurities, become liberated and are free to dissolve in water. Apted et al. (1990) contains a discussion of this assumption. In addition, the high-solubility nuclides are assumed to have a fraction f_p of their inventories in the pellet/cladding gap and the grain boundaries within the fuel matrix. This fraction is available for quicker release because it is not necessary for fuel-matrix alteration to occur before it can be dissolved.

As stated previously, glass waste is not included in the present source model; all 70,000 MTHM of waste is taken to be spent fuel. Also, only a portion of the spent fuel is being modeled—the most important portion, to be sure—the spent fuel pellets themselves. The fuel-rod cladding and the fuel-assembly structural parts also have significant amounts of radioactivity (see, e.g., Wilson, 1991) but to include releases from them would require adding additional submodels to the source model. For the present study, the only nuclide that would be affected by adding such additional submodels is ^{14}C , because none of the nine nuclides listed in Table 4-1 has a significant portion of its inventory outside the spent fuel pellets.

The time scales for the alteration-limited-mobilization submodel are given here, but solubility-limited mobilization is lumped together with transport out of the container and discussed in the next subsection. There are several cases for the waste-mobilization time scales because they are different for matrix releases and for gap/grain-boundary releases, and they are different for the different transport types (advective, diffusive, and combination advective/diffusive). In all cases the start and ramp-up times (t_0 and t_1) are taken to be zero; the processes are being represented by a single time scale, the fall-off time t_2 . Note, however, that zero

start and ramp-up times do not mean that waste mobilization starts at time zero—mobilization starts after container failure; the various time scales are convolved later. In the following, an m subscript refers to mobilization of the nuclides in the waste matrix, p (for “prompt”) refers to mobilization of the gap/grain-boundary fraction, s (for “seepage”) refers to advective releases, d refers to diffusive releases, and c refers to combination advective/diffusive releases.

For advective releases:

$$t_{0,m,s} = 0, \quad t_{1,m,s} = 0, \quad t_{2,m,s} = 1/(a_m f_{ws}), \quad (4.7)$$

$$t_{0,p,s} = 0, \quad t_{1,p,s} = 0, \quad t_{2,p,s} = 1/(a_p f_{ws}), \quad (4.8)$$

where a_m is the matrix-alteration rate, a_p is the prompt-alteration rate, and f_{ws} is the fraction of the waste-form surface area wetted. The idea is that the matrix alteration proceeds at a rate a_m , but only part of the waste is contacted by water and is releasing its waste to the water. The parameters a_m , a_p , and f_{ws} are input parameters.

For diffusive releases:

$$t_{0,m,d} = 0, \quad t_{1,m,d} = 0, \quad t_{2,m,d} = 1/(a_m f_{wd}), \quad (4.9)$$

$$t_{0,p,d} = 0, \quad t_{1,p,d} = 0, \quad t_{2,p,d} = 1/(a_p f_{wd}), \quad (4.10)$$

where f_{wd} is the fraction of the waste-form surface area wetted and participating in diffusive releases (Figure 4-8).

For combination advective/diffusive releases:

$$t_{0,m,c} = 0, \quad t_{1,m,c} = 0, \quad t_{2,m,c} = 1/(a_m \max\{f_{ws}, f_{wd}\}), \quad (4.11)$$

$$t_{0,p,c} = 0, \quad t_{1,p,c} = 0, \quad t_{2,p,c} = 1/(a_p \max\{f_{ws}, f_{wd}\}). \quad (4.12)$$

4.3.5 Radionuclide transport out of the waste container

Next, time scales are required for the amount of time it takes the nuclides to get out of a container after they have been mobilized. As already mentioned, the advective-release model is a simple flow-through model, in which it is assumed for simplicity that water can enter the container at the top, flow through, and exit out the bottom. The time scale for this process is just given by the volume of water in the container divided by the rate at which water flows through (volume divided by volume per unit time gives a time). Thus, for advective, alteration-limited releases,

$$t_{0,t,s} = 0, \quad t_{1,t,s} = 0, \quad t_{2,t,s} = \frac{Ad_{film}f_{ws}}{A_{cross}f_{in}q_s}, \quad (4.13)$$

where A is the total surface area of the spent fuel rods in a container, d_{film} is the thickness of the water film on the wetted part of the spent-fuel surface, A_{cross} is the water-capture area (that is, the amount of area around a waste container from which the water flux is gathered and funneled into the container), and f_{in} is the fraction of the flux through A_{cross} that actually gets into the waste package. It can be seen that $Ad_{film}f_{ws}$ gives the volume of water inside the waste container and $A_{cross}f_{in}q_s$ gives the volume rate at which water flows through. Recall that q_s is the average seepage flux in the vicinity of containers that have seepage flux, as discussed previously. In Equation 4.13, the t subscripts refer to transport out of the container.

For the advective, solubility-limited releases, the turnover time ($t_{2,t,s}$ above) is neglected, and the rate at which waste is carried away is calculated. This is simply given by the rate at which water flows through, multiplied by the solubility limit (assuming that the water leaving the waste container is saturated with the waste elements). For now, let us define W_s as the water-flow rate:

$$W_s = A_{cross}f_{in}q_s . \quad (4.14)$$

W_s (and the corresponding diffusive quantities W_{dm} and W_{dw} defined below) are multiplied by the solubility of each nuclide later.

The time scales for diffusive transport out of a waste container and through the rubble-filled air gap around the container are based on work by Ueng and O'Connell (1992). Using a Laplace-transform method for an idealized problem setup, they expressed the near-field transport solution in terms of a series of time scales

$$\tau_i = \frac{RL^2}{D\mu_i^2} , \quad (4.15)$$

where μ_i are the solutions of

$$\mu = \alpha \cot \mu . \quad (4.16)$$

R is the retardation factor due to adsorption; L is the width of the rubble-filled air gap; and D is the diffusion coefficient for transport through the rubble-filled air gap. It would probably be preferable to use different retardation factors for this near-field transport than are used for the far-field transport, but for simplicity (and in the absence of detailed information about near-field conditions) the same values were used for both. Sorption and the values used to represent it are discussed in Section 3.4. The diffusion coefficient in rubble is expected to be significantly different than the diffusion coefficient in intact rock (Conca, 1990); therefore, different diffusion coefficients are used in this TSPA for the calculation of diffusion-release time scales and for the calculation of far-field transport (Sections 4.5 and 4.6). Two values of rubble

diffusion coefficients were used, one for a wet container environment (D_{wet}) and one for a moist container environment (D_{moist}); this leads to two sets of diffusion times from Equation 4.15. Note also that, because the retardation factor is different for different nuclides, the diffusion time scales are different for different nuclides. Lastly, α is given by

$$\alpha = \frac{RaL}{Ad_{film}} . \quad (4.17)$$

R , L , A , and d_{film} have already been defined; a is the effective diffusion area of the rubble, so that aL represents the volume of water in the rubble. It can be seen that α is the retardation factor times the ratio of the volume of water in the rubble to the volume of water in the container. Previously, the volume of water in the container was given as $Ad_{film}f_{wd}$, with a factor (f_{wd}) reflecting the fact that only a fraction of the spent fuel is covered with water. The factor f_{wd} does not appear in Equation 4.17 because the same fraction is assumed to apply to the water in the rubble. A simple picture is being used in which rubble fills the air gap to some height and a water film covers the fuel rods to the same height (Figure 4-8).

With all these definitions in place, we can now present the time scales used in the submodel for diffusive transport out of a waste container. The two longest time scales from Equation 4.15 are used for the ramp-up and fall-off time scales:

$$t_{0,t,d} = 0 , \quad t_{1,t,d} = \tau_2 = \frac{RL^2}{D_{moist}\mu_2^2} , \quad t_{2,t,d} = \tau_1 = \frac{RL^2}{D_{moist}\mu_1^2} . \quad (4.18)$$

Note that diffusive releases with no advective releases take place in a moist container environment, so D_{moist} is used for the diffusion coefficient.

As with advective releases, the solubility-limited case is handled a little differently than just described. Solubility-limited releases are characterized by two time scales and a water-flow rate rather than by three time scales. The first time (the start time) is set to zero, just as in Equation 4.18 above. The second time (the ramp-up time) is as above, but for a constant-concentration source it turns out that it is appropriate to use $\mu = \pi$ instead of the expression given in Equation 4.16. That is,

$$t_{0,t,dm} = 0 , \quad t_{1,t,dm} = \frac{RL^2}{D_{moist}\pi^2} \quad (4.19)$$

is used for solubility-limited diffusive releases. The effective water-flow rate for diffusive releases is given by

$$W_{dm} = \frac{f_{wd}aD_{moist}}{L} . \quad (4.20)$$

Equations 4.19 and 4.20 may be deduced from Equation 7 of Ueng and O'Connell (1992), which is an expression for the radionuclide release rate from a constant-concentration source. The *dm* subscripts refer to moist diffusive transport.

Combination advective/diffusive transport is handled differently for the alteration-limited and solubility-limited cases. For nuclides with alteration-limited mobilization, the advective and wet-diffusive time scales are combined as shown below. For nuclides with solubility-limited mobilization, the advective and wet-diffusive releases are calculated separately, and then added.

First, consider the case of alteration-limited waste mobilization. The time scales in Equation 4.13 characterize the advective transport, and the time scales in Equation 4.18, with D_{wet} substituted for D_{moist} , characterize the diffusive transport. Let us call the latter time scales $t_{i,t,w}$, $i = 0, 1, 2$ (*w* for "wet"). Whichever process, advection or diffusion, is fastest (i.e., has the smallest time scales) should dominate the releases. Therefore, the time scales are combined in such a way as to emphasize whichever is smallest. The algorithm used is

$$t_{0,t,c} = 0, \quad (4.21)$$

$$\frac{1}{t_{2,t,c}} = \frac{1}{t_{2,t,s}} + \frac{1}{t_{2,t,w}}, \quad (4.22)$$

$$t_{1,t,c} = \begin{cases} t_{1,t,s} & \text{if } t_{2,t,s} < t_{2,t,w}, \\ t_{1,t,w} & \text{otherwise.} \end{cases} \quad (4.23)$$

For the case of solubility-limited waste mobilization, we simply define quantities analogous to those in Equations 4.19 and 4.20, only using D_{wet} instead of D_{moist} :

$$t_{0,t,dw} = 0, \quad t_{1,t,dw} = \frac{RL^2}{D_{wet}\pi^2}, \quad W_{dw} = \frac{f_{wda}D_{wet}}{L}. \quad (4.24)$$

The *dw* subscripts refer to wet diffusive transport.

4.3.6 Convolution of the processes

Having defined time scales for container wetting and failure, for waste mobilization, and for near-field transport, the next step is to combine those time scales into a set of overall time scales for each of the three release types, advective, diffusive, and combination. The combination is done separately for alteration-limited mobilization and for solubility-limited mobilization.

For alteration-limited advective releases, we have the following:

$$t_{0,adv,a} = t_{0,c} + t_{0,m,s} + t_{0,t,s}, \quad (4.25)$$

$$t_{2,adv,a}^2 = t_{2,c}^2 + t_{2,m,s}^2 + t_{2,t,s}^2 , \quad (4.26)$$

$$t_{1,adv,a}^2 = t_{x,c}^2 + t_{x,m,s}^2 + t_{x,t,s}^2 . \quad (4.27)$$

In the last expression, the x subscripts have the following meaning. Equation 4.27 is the same as Equation 4.26 except that whichever of $t_{2,c}$, $t_{2,m,s}$, $t_{2,t,s}$ is largest is replaced by the corresponding term with subscript 1. Thus, in Equation 4.27 two of the x 's are 2 and one of the x 's will be 1. The reasoning behind the three expressions is as follows. In Equation 4.25 the three start times are simply added together. This makes sense because the start times are not intended to be absolute times, but rather amounts of time, and the three time lags are cumulative. The combination of fall-off times in Equation 4.26 reflects the fact that the slowest process (with the largest time scale) is the limiting process, and so the combination time scale should get the largest contribution from the largest component time scale. Equation 4.27 for the ramp-up time is the hardest to explain. The ramp-up time for the slowest process is combined with the fall-off times for the faster processes because the faster processes are probably already in their long-time modes while the slowest process is still in its ramp-up phase.

There is an equivalent set of advective-release time scales for the prompt (gap/grain-boundary) fraction of those nuclides that have a prompt fraction:

$$t_{0,adv,p} = t_{0,c} + t_{0,p,s} + t_{0,t,s} , \quad (4.28)$$

$$t_{2,adv,p}^2 = t_{2,c}^2 + t_{2,p,s}^2 + t_{2,t,s}^2 , \quad (4.29)$$

$$t_{1,adv,p}^2 = t_{x,c}^2 + t_{x,p,s}^2 + t_{x,t,s}^2 , \quad (4.30)$$

where the x 's in the third expression have the same meaning as before.

For solubility-limited advective releases, there are fewer quantities to combine. The time scales for container wetting and failure must be combined with the time scales for near-field transport and the effective water-flow rate. This is done as follows:

$$t_{0,adv,s} = t_{0,c} + t_{0,t,s} , \quad (4.31)$$

$$t_{1,adv,s}^2 = t_{2,c}^2 + t_{1,t,s}^2 , \quad (4.32)$$

$$W_{adv} = W_s . \quad (4.33)$$

The reasoning is similar to that given above for alteration-limited advective releases.

The application of the above combination algorithms to the diffusive and combination releases follows the same reasoning given above, so they are not repeated here. The net result is the following sets of time scales and effective water-flow rates.

For alteration-limited diffusive releases: $t_{0,dif,a}, t_{1,dif,a}, t_{2,dif,a}$.

For prompt-fraction diffusive releases: $t_{0,dif,p}, t_{1,dif,p}, t_{2,dif,p}$.

For solubility-limited moist-diffusive releases: $t_{0,difm,s}, t_{1,difm,s}, W_{difm}$.

For alteration-limited combination releases: $t_{0,com,a}, t_{1,com,a}, t_{2,com,a}$.

For prompt-fraction combination releases: $t_{0,com,p}, t_{1,com,p}, t_{2,com,p}$.

For solubility-limited wet-diffusive releases: $t_{0,difw,s}, t_{1,difw,s}, W_{difw}$.

4.3.7 Generic shape functions

So far, the basic idea of describing the releases for a given component in terms of three time scales or two time scales and a flow rate has been presented. Time scales and flow rates have been defined for nine different release components. To conclude, we must describe how those time scales and flow rates are used and how the nine release components are added together to form the final radionuclide source term.

A major simplifying assumption in the source model is that the exact shape of the release-rate curve is not as important as its time scales. Based on that assumption, we define "generic shape functions" that have the general shape expected of a release-rate curve and that take the sets of time scales and flow rates as parameters. Two generic functions are defined, one with three time-scale parameters for the alteration-limited releases, and one with two time-scale parameters and one flow-rate parameter for the solubility-limited releases.

Figure 4-9 shows the generic shape function for alteration-limited releases. The releases are zero up until the start time t_0 , then they ramp-up linearly until time $t_0 + t_1$, and after that they fall off exponentially with e -folding time t_2 . If the generic shape function is called F , the equations are as follows:

$$F(t; t_0, t_1, t_2) = \begin{cases} 0 & \text{for } t \leq t_0, \\ B(t - t_0)/t_1 & \text{for } t_0 < t \leq t_0 + t_1, \\ B \exp[-(t - t_0 - t_1)/t_2] & \text{for } t > t_0 + t_1. \end{cases} \quad (4.34)$$

The function is normalized so that its integral is equal to one, $\int_0^\infty F(t; t_0, t_1, t_2) dt = 1$, implying

$$B = (\frac{1}{2}t_1 + t_2)^{-1}. \quad (4.35)$$

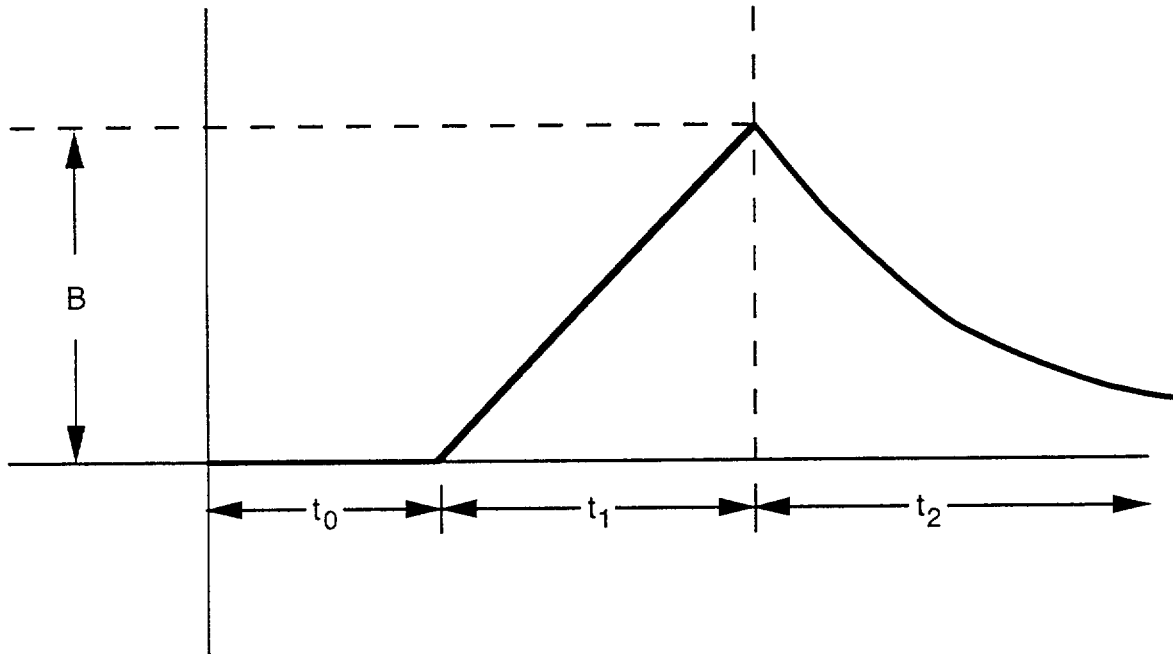


Figure 4-9. The generic shape function for alteration-limited releases.

In the final release-rate expression, the generic function F is multiplied by the appropriate inventory; the above normalization ensures that the releases integrated over time add up to the right amount.

Figure 4-10 shows the generic shape function for solubility-limited releases. The releases are zero until the start time t_0 , then they ramp-up linearly until time $t_0 + t_1$, and after that they remain constant. This generic function is denoted G , and it is defined by

$$G(t; t_0, t_1, W) = \begin{cases} 0 & \text{for } t \leq t_0, \\ W(t - t_0)/t_1 & \text{for } t_0 < t \leq t_0 + t_1, \\ W & \text{for } t > t_0 + t_1. \end{cases} \quad (4.36)$$

Clearly, releases cannot continue at a constant rate forever since there is a finite inventory. For the release of solubility-limited radionuclides, it is necessary to keep track of the inventory and set the release rate to zero after the inventory is exhausted.

4.3.8 Combining the release components

For the radionuclides with alteration-limited releases, there are six components to put together to get the release rate: the matrix and prompt fractions for each of

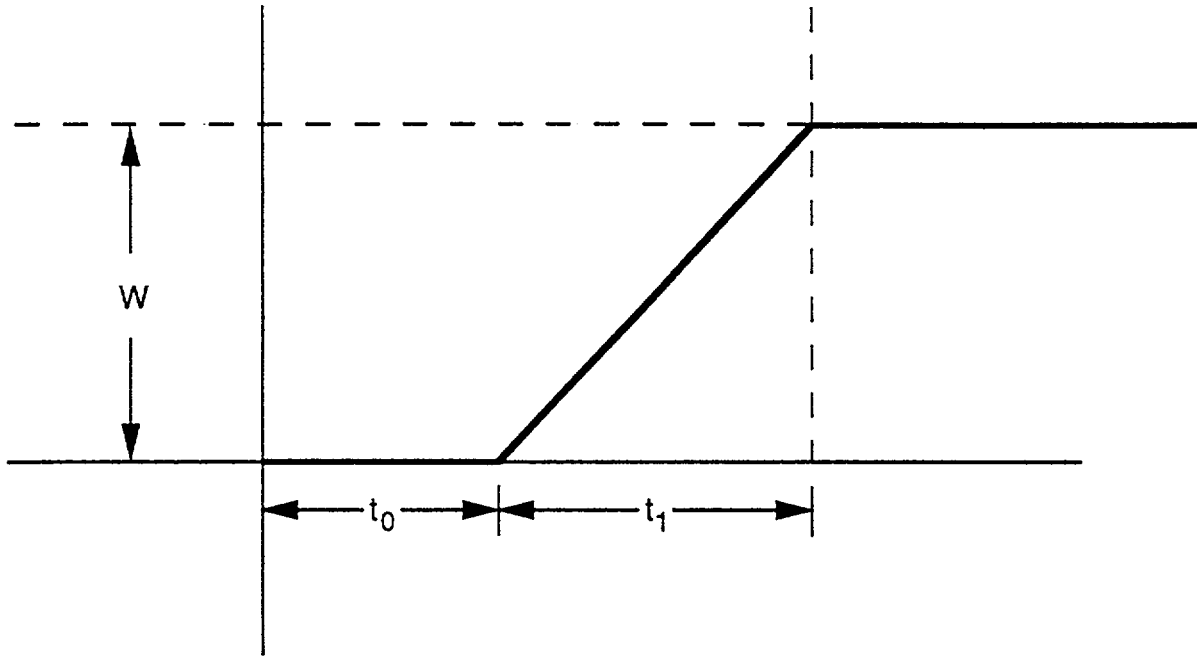


Figure 4-10. The generic shape function for solubility-limited releases.

the three release types. Let us call the normalized release rate F_{tot} . Then

$$F_{tot}(t) = (1 - f_p)F_{matrix}(t) + f_p F_{prompt}(t) , \quad (4.37)$$

with

$$\begin{aligned} F_{matrix}(t) = & f_s(1 - f_r) F(t; t_{0,adv,a}, t_{1,adv,a}, t_{2,adv,a}) \\ & + (1 - f_s)f_r F(t; t_{0,dif,a}, t_{1,dif,a}, t_{2,dif,a}) \\ & + f_s f_r F(t; t_{0,com,a}, t_{1,com,a}, t_{2,com,a}) , \end{aligned} \quad (4.38)$$

$$\begin{aligned} F_{prompt}(t) = & f_s(1 - f_r) F(t; t_{0,adv,p}, t_{1,adv,p}, t_{2,adv,p}) \\ & + (1 - f_s)f_r F(t; t_{0,dif,p}, t_{1,dif,p}, t_{2,dif,p}) \\ & + f_s f_r F(t; t_{0,com,p}, t_{1,com,p}, t_{2,com,p}) . \end{aligned} \quad (4.39)$$

To get the actual release rate for a radionuclide, the normalized release rate F_{tot} is multiplied by its inventory:

$$\Sigma(t) = I_0(t)F_{tot}(t) . \quad (4.40)$$

In this equation, $\Sigma(t)$ is the release rate for a given radionuclide if the radionuclide has alteration-limited releases. $\Sigma(t)$ is inserted into the transport equation as a source

term. $I_0(t)$ is the inventory of the nuclide. The 0 subscript indicates that this inventory is calculated by applying the radioactive decay equations to the initial inventory $I_0(0)$ (which is given in Table 4-1), without subtracting the releases. That is, $I_0(t)$ is the total amount of the radionuclide in question at time t , including all that has been released and all that is still inside the waste containers.

For the radionuclides with solubility-limited releases, there are three release components—one for each release type. The normalized release rate is given by

$$\begin{aligned}
 G_{tot}(t) = & f_s G(t; t_{0,adv,s}, t_{1,adv,s}, W_{adv}) \\
 & + (1 - f_s) f_r G(t; t_{0,difm,s}, t_{1,difm,s}, W_{difm}) \\
 & + f_s f_r G(t; t_{0,difw,s}, t_{1,difw,s}, W_{difw}) .
 \end{aligned}
 \tag{4.41}$$

Note that the coefficients in this combination are different from the coefficients in Equations 4.38 and 4.39. The third term is not the combination advective/diffusive releases, as it was before, but only the diffusive part of the combination. The advective part is now in the first term.

The normalization of the release rate means something different than it did for the alteration-limited-release formulas. G_{tot} is an effective water-flow rate, and has to be multiplied by the effective concentration of a radionuclide to get the release rate for the radionuclide:

$$\Sigma(t) = N_{cans} S G_{tot} ,
 \tag{4.42}$$

where $\Sigma(t)$ is the release rate for a radionuclide if the nuclide has solubility-limited releases, N_{cans} is the number of waste containers in the repository, and S is the effective solubility limit of the radionuclide in question. The number of waste containers appears in the formula because the effective water-flow rates given above were calculated for a single waste container. "Solubility limit" is modified by "effective" because a solubility limit applies to all the isotopes of an element, not to a particular radionuclide. If there is more than one significant isotope of an element, the concentration must be partitioned among them. For example, suppose an element has a solubility limit of 1 and there are two isotopes, in the ratio of 60 percent isotope A and 40 percent isotope B . Then the effective solubility of A is 0.6 and the effective solubility of B is 0.4. Because of radioactive decay and generation, the partitioning among isotopes of an element can change with time. Thus, S may be a function of time even if changes in the chemical environment are neglected. For the present study, no more than one isotope of any element was considered (see Table 4-1). To avoid having to do extra calculations to determine the partitioning as a function of time, the conservative approach of using the maximum partition for the 10,000-year

period of interest was used. Of the nuclides listed in Table 4-1, the only ones for which partitioning is of concern are ^{234}U , ^{239}Pu , and ^{243}Am (note that partitioning is not an issue for the alteration-limited nuclides because it is assumed that their solubility is high enough that it is not a factor). From Roddy et al. (1986), the amounts of all isotopes of those three elements at 100 yr and at 10,000 yr were obtained. At 100 yr, ^{234}U makes up about 0.028 percent of the uranium (by moles), ^{239}Pu makes up about 64 percent of the plutonium, and ^{243}Am makes up about 0.72 percent of the americium. At 10,000 yr, ^{234}U makes up about 0.034 percent of the uranium, ^{239}Pu makes up about 75 percent of the plutonium, and ^{243}Am makes up almost 100 percent of the americium. The partitioning factors at 10,000 yr were used to adjust the solubility limits since they are higher than the ones at early time. The only one of the three that changes substantially during 10,000 years is the partitioning factor for ^{243}Am . In our procedure, ^{243}Am releases are overestimated at early times; for the first thousand years or so, there is a great deal of ^{241}Am , so most americium releases during that period would be in the form of ^{241}Am . ^{241}Am is not included in the transport calculations because it has a rather short half-life and most decays away before it can be transported to the accessible environment.

4.3.9 Parameter values for the source model

Table 4-2 shows the values used for the input parameters to the source model. These values are particular to the source model and they were provided for the most part by William J. O'Connell of LLNL. A single value was used for some of the parameters, while probability distributions were used for others. Use of a single value does not necessarily imply that the value of the parameter is well-known. On the contrary, in some cases (such as the coefficient of variation of the spatial flux distribution, v) the value used is almost purely speculative because little or no data are available. It was decided that, for the present TSPA study, probability distributions would be attributed to one key variable for each of the basic processes modeled. Where these probability distributions were used, the log-uniform distribution was chosen because it is a simple distribution requiring only lower and upper limits to be defined and because it represents well the idea of a quantity being uncertain over several orders of magnitude.

The repository area is taken from Rautman et al. (1987). The number of waste containers is based on 70,000 MTHM of spent fuel, with 2.1 MTHM per container. (The amount of spent fuel per container will vary depending on fuel age, burnup, consolidation, etc. We follow Apted et al., 1990, in assuming 2.1 MTHM per container.) The value for the prompt inventory fraction is at the upper end of the values

Table 4-2. Values for source-model parameters.

Model parameter	Distribution	Distribution parameters ^a	Mean value
Repository area, A_{rep} (m ²)	—	—	5.61×10^6
Number of waste containers, N_{cans}	—	—	33,300
Amount of waste in repository (MTHM)	—	—	70,000
Prompt inventory fraction, f_p	—	—	0.02
Fraction of boreholes with rubble, f_r	—	—	0.5
Fraction of seepage entering container, f_{in}	—	—	0.5
Fraction of fuel wet with seepage, f_{ws}	—	—	0.5
Fraction of fuel wet and diffusing, f_{wd}	—	—	0.5
Beginning of resaturation period, t_{rb} (yr)	—	—	300
Duration of resaturation period, t_{rd} (yr)	—	—	1000
Container lifetime when wet, t_c (yr)	log-uniform	500, 10000	3170
Matrix-alteration rate, a_m (yr ⁻¹)	log-uniform	5×10^{-5} , 1×10^{-3}	3.17×10^{-4}
Prompt-alteration rate, a_p (yr ⁻¹)	—	—	0.5
Effective diffusion area, a (m ²)	—	—	0.172
Spent-fuel surface area, A (m ²)	—	—	140
Water-collection area, A_{cross} (m ²)	—	—	2
Rubble thickness, L (cm)	—	—	3
Water-film thickness, d_{film} (mm)	—	—	1
Moist diffusion coefficient, D_{moist} (m ² /yr)	log-uniform	3×10^{-6} , 3×10^{-4}	6.45×10^{-5}
Wet diffusion coefficient, D_{wet} (m ² /yr)	log-uniform	9×10^{-4} , 9×10^{-3}	3.52×10^{-3}
Flux coefficient of variation, v	—	—	1.3
²³⁴ U solubility, S (mol/ℓ)	log-uniform	7.1×10^{-11} , 2.3×10^{-8}	4.0×10^{-9}
²⁴³ Am solubility, S (mol/ℓ)	log-uniform	1.2×10^{-11} , 3.8×10^{-9}	6.6×10^{-10}
²³⁹ Pu solubility, S (mol/ℓ)	log-uniform	1.6×10^{-10} , 5.1×10^{-8}	8.8×10^{-9}
²³⁷ Np solubility, S (mol/ℓ)	log-uniform	5.9×10^{-11} , 1.9×10^{-8}	3.3×10^{-9}
¹²⁶ Sn solubility, S (mol/ℓ)	log-uniform	1.0×10^{-9} , 3.2×10^{-7}	5.5×10^{-8}
Percolation rate, q	see Table 3-7		

^a Parameters for the log-uniform distribution are minimum, maximum.

that have been suggested for it, and there is an SCP “goal” for f_p to be less than 0.02 (SCP, Table 8.3.5.9-3). The various other fractions (f_r , f_{in} , f_{ws} , f_{wd}) are simply set to the middle of the possible range, 0.5. The resaturation-time parameters are based on thermal modeling of the spatial array of waste packages by Johnson and Montan (1990). The two parameters represent the variation in the time when waste containers are wetted: some containers are wetted as early as 300 yr and others are wetted as late as 1300 yr. A 9500-year range was used for the container-lifetime distribution to reflect the great uncertainty in container performance. The upper end of the range for matrix-alteration rate is based on laboratory experiments of spent-fuel leaching; Apted et al. (1990) contains a discussion. The lower bound was chosen a factor of 20 lower to reflect the fact that there is much uncertainty. The choice of a factor of 20 is subjective. The value 0.5 yr^{-1} for the alteration rate of the prompt fraction is simply a small number that spreads the releases out over 2 years. The

actual value is immaterial; the 2-yr alteration time is so much smaller than the other time scales in the problem that the other time scales are the limiting factors.

The effective diffusion area is given by the waste-container surface area—approximately 9 m^2 —reduced by the product of the effective porosity and the saturation of the rubble (i.e., the moisture content of the rubble; see Ueng and O'Connell, 1992). The value for the surface area of the fuel rods in a container was taken from design data tabulated in DOE (1987). The value of 2 m^2 for the water-collection area is an estimate of how much area might be expected to drain into a container. The value is subjective. For comparison, the cross-sectional area of a waste container is approximately 0.34 m^2 , so the assumed water-collection area is about six times as large as the geometrical-intercept area. We follow Apted et al. (1990) and Ueng and O'Connell (1992) in taking 3 cm as the rubble thickness (L). (The SCP-CDR shows 3.8 cm as the design air-gap width.) The water-film thickness on a spent-fuel surface under unsaturated conditions is unknown. It presumably will depend on surface roughness, capillarity, and water surface tension. A value of 1 mm is used here.

The typical diffusion coefficient in water is $3 \times 10^{-2} \text{ m}^2/\text{yr}$ (e.g., Travis et al., 1984). This coefficient would be the upper bound on what is possible for D_{moist} and D_{wet} . Diffusion in porous media varies because of tortuosity and constrictivity effects. Anderson (1979) reports values in the neighborhood of $3 \times 10^{-3} \text{ m}^2/\text{yr}$ in fractured basalts. The far-field transport calculations (Section 4.6), used a diffusion coefficient of $3.16 \times 10^{-3} \text{ m}^2/\text{yr}$ (including reduction by a tortuosity-constrictivity factor of 10). Under "wet" conditions, the diffusion coefficient might be nearly as high as the pure-water number, but under "moist" conditions, the effective diffusion coefficient in rubble is reduced by several orders of magnitude (Conca, 1990). The distributions used for D_{moist} and D_{wet} reflect these considerations. The distribution of "wet" diffusion coefficients goes from a little below to a little above the far-field value. The distribution of "moist" diffusion coefficients is broader and its maximum value is below the minimum "wet" value. The specific values used for the ranges are subjective, but reflect the expectations.

The value of 1.3 for the coefficient of variation of the spatial flux distribution is an arbitrary selection, chosen to give a skewed distribution.

Each solubility distribution goes from a factor of 100 below a "nominal" value to a factor of 3 above the nominal value. The nominal values for uranium and the other actinides are the highest steady-state values seen in several series of spent-fuel measurements (Wilson, 1987, 1990a, 1990b). The variability as a function of temperature and other test conditions is substantial, and the variability in calculated solubilities under a range of relevant conditions (Wilson and Bruton, 1989) is even

greater. The range chosen here, two and a half orders of magnitude for each solubility distribution, is greater than that of the experiments and less than that of the calculations. The nominal value for tin is an estimate. The partitioning factors discussed previously for ^{234}U , ^{239}Pu , and ^{243}Am are already included in the solubility values listed in Table 4-2.

4.4 Unsaturated-zone flow models

The unsaturated zone at Yucca Mountain consists of several hundred meters of stratified, fractured tuffs. Two conceptual models of groundwater flow through partially saturated, fractured rock were considered in this study: the composite-porosity model (also known as the equivalent-continuum model), and a model of significant fracture flow known as the “weeps” model. Figure 4-11 presents an overview of how the two models fit together in the TSA, and some of the parameters that are important to each.

The different models are included in this study for two reasons. First, the models represent two extremes in the description of matrix/fracture interaction. The composite-porosity model forces flow to be shared between the matrix and the frac-

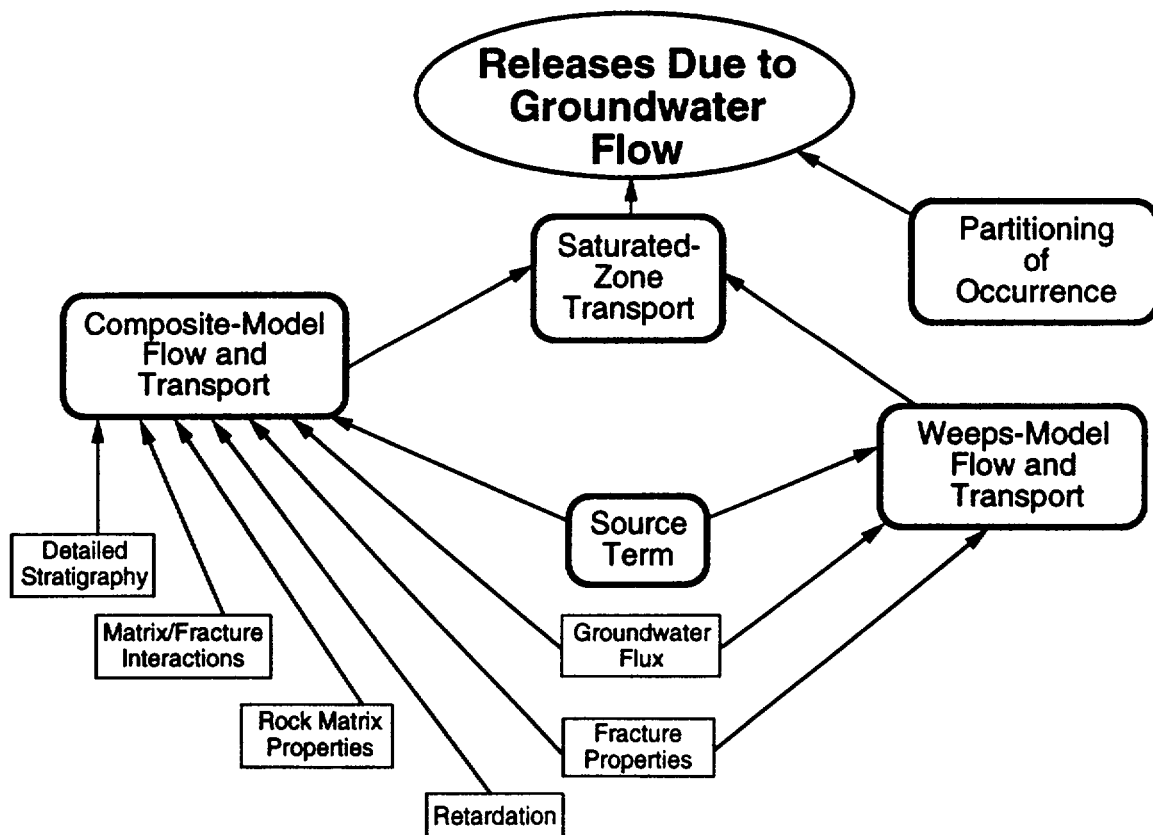


Figure 4-11. Important factors included in the two groundwater-flow models.

tures (the distribution determined by capillary forces); the weeps model precludes flow in the matrix, restricting it to the fractures. The actual matrix/fracture interaction within Yucca Mountain is unknown. It could vary spatially and temporally. It could vary on a scale smaller than that which can be sampled, and thus never be known exactly. We suspect the gross behavior of the groundwater flow at Yucca Mountain falls somewhere between the two descriptions. By considering the two models, we hope to bound the realm of physical possibility.

Second, it is of interest to determine how the choice of a conceptual model of flow influences the end results of a TSPA, and to demonstrate methods for handling alternative conceptual models. A flow model affects the results in a nontrivial way, because the flow model influences all the major release mechanisms. Groundwater flow is, of course, the basis for aqueous radionuclide transport. But groundwater is also currently believed to be a major cause for waste-container degradation (Section 4.3); to a large extent it determines the radionuclide source term, and thus, both gaseous and aqueous releases. And, to a certain extent, groundwater flow influences the impact of human-intrusion scenarios. (For instance, drilling in the vicinity could intercept radionuclides transported by groundwater from the containers.) Consideration of alternative conceptual models—especially bounding models—allows a more complete picture of the possible performance of a potential repository at Yucca Mountain.

4.4.1 Composite-porosity model of unsaturated flow

The composite-porosity model is built into the computer program TOSPAC (Dudley et al., 1988; Gauthier et al., 1992b), which is used by the TSA. TOSPAC incorporates the composite-porosity model in formulations of Darcy's law (for solving steady-state flow with the STEADY module) and Richards' equation (for solving transient flow with the DYNAMICS module). The composite-porosity model is also built into NORIA-SP (Hopkins, Eaton, and Bixler, 1991) and LLUVIA-II (Eaton and Hopkins, 1992), computer programs that model flow in two dimensions and that were used in this study to examine the assumption of one-dimensional flow inherent in TOSPAC (Chapter 9). NORIA-SP and LLUVIA-II use the composite-porosity model in a generalized form of Richard's equation.

For a complete discussion of the composite-porosity model, see Peters and Klavetter (1988) and Dudley et al. (1988). What follows is a general discussion of how the composite-porosity model represents flow, and the model assumptions that are significant to this study. An illustration of how the composite-porosity model could predict flow in Yucca Mountain is given in Figure 4-12.

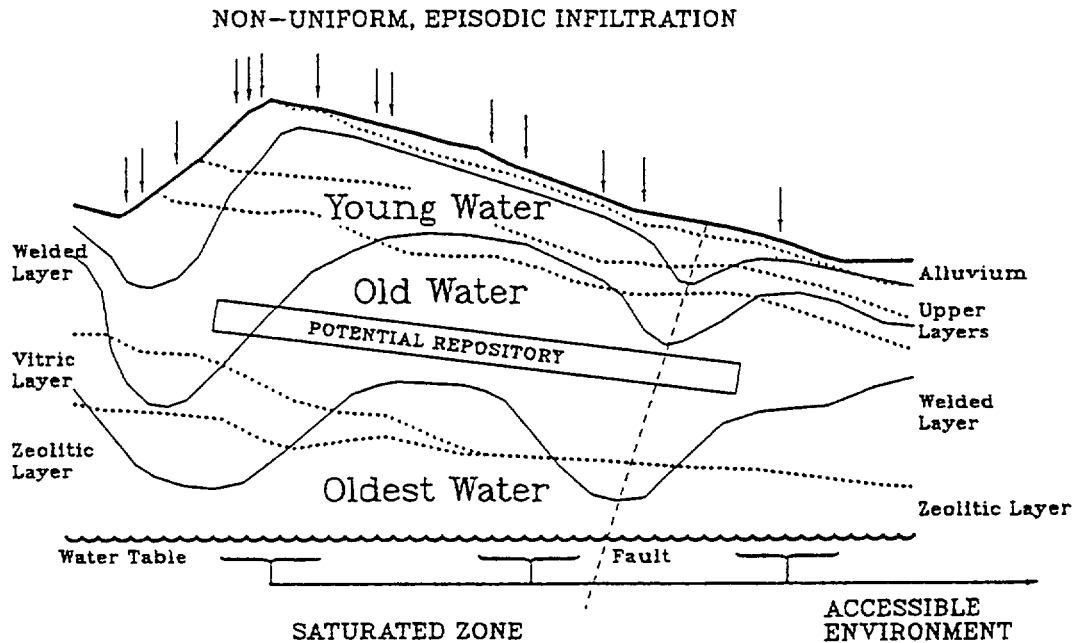


Figure 4-12. A conceptual model of composite-porosity flow at Yucca Mountain.

The composite-porosity model describes flow driven by gravity and capillary forces. The description of capillary forces is based on capillary-bundle theory, a classical theory of flow through unsaturated porous media (see, e.g., de Marsily, 1986). Several methods based on classical theory exist for modeling flow in fractured, porous media, such as discrete-fracture modeling and dual-porosity models. The major assumption that differentiates the composite-porosity model from other models of flow is the equilibrium assumption: the flow in the fractures must be closely coupled with the flow in the rock matrix (i.e., at any given location, no barrier exists to impede the interaction of flow in matrix and flow in the fractures; matrix and fractures are in complete communication). Figure 4-13 shows the difference between flow down a fracture when there is strong matrix/fracture coupling and when matrix/fracture coupling is weak.

The equilibrium assumption is enforced in the composite-porosity model by requiring the pressure head in the matrix to equal the pressure head in the fractures at any given location in the composite material.

A corollary to the equilibrium assumption is that one of the major parameters of Darcy's law, hydraulic conductivity (K), can be described separately for the matrix and fractures, then combined in an area-weighted average. For example, Darcy's law in one dimension is configured by the composite-porosity model as follows:

$$q = -K \left(\frac{\partial \psi}{\partial z} + 1 \right) \quad (4.43)$$

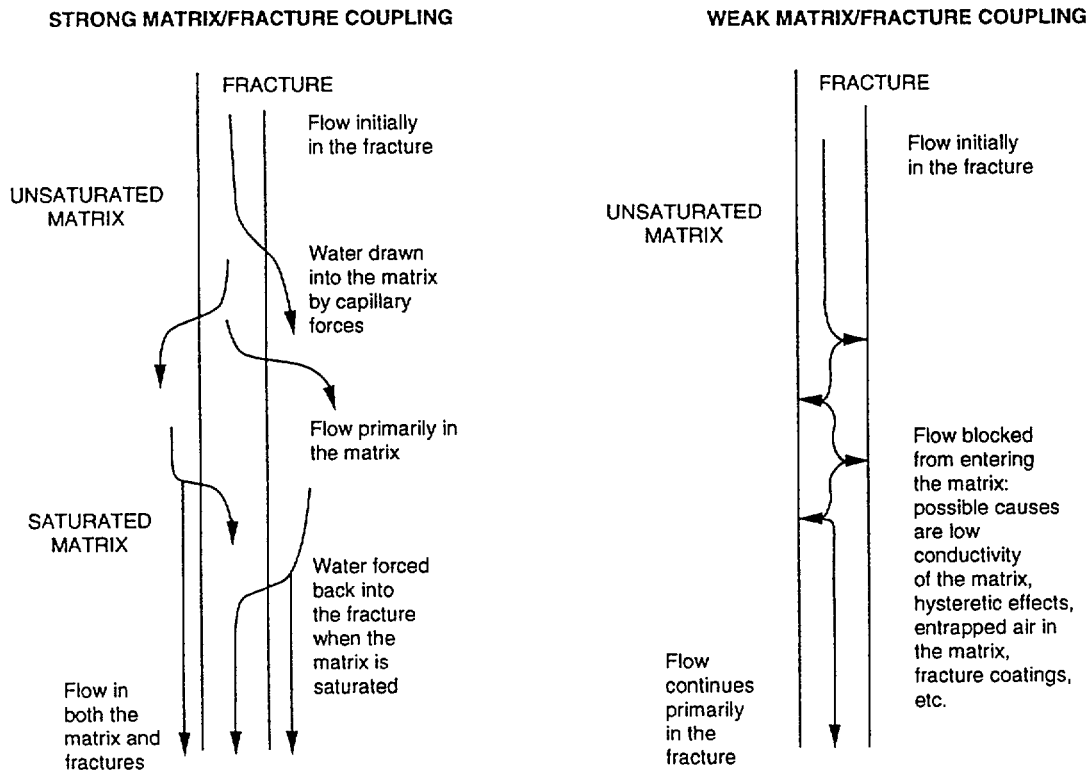


Figure 4-13. How the strength of the matrix/fracture coupling influences flow, and factors that contribute to weak matrix/fracture coupling.

$$\Rightarrow q = -\frac{A_m K_m + A_f K_f}{A_m + A_f} \left(\frac{\partial \psi}{\partial z} + 1 \right), \quad (4.44)$$

where q is the groundwater flux or Darcy velocity (through the composite medium), ψ is the pressure head (the same in the matrix and fractures for this model), z is the elevation, A_m and A_f are the cross-sectional areas of the one-dimensional column for the matrix and fractures, respectively, and K_m and K_f are the hydraulic conductivities of the matrix and fractures, respectively.

In the STEADY module of TOSPAC, Darcy's law is solved iteratively for pressure head using a finite-difference method. Knowing the pressure head, saturation and hydraulic conductivity are calculated from characteristic curves described according to van Genuchten (1980). The calculations are performed directly from van Genuchten's equations so that the most accurate values are used, minimizing the tendency for numerical instability. Different characteristic curves are used for the matrix and the fractures (Section 3.3), allowing different water fluxes and velocities to be calculated for the matrix and fractures. Also for numerical stability, the derivative of Equation 4.44 is used in STEADY, making the equation more closely resemble the conservation-of-mass formulation.

For the purposes of this study, the major consequence of the composite-porosity

model is as follows: flow occurs in the smallest pores, where the strongest capillary forces reside (capillary forces are expressed in the composite-porosity model by the characteristic curves, and are typically strongest in the matrix). If the small pores are saturated, then flow occurs also in the larger pores (e.g., the fractures). Thus, when the characteristic curves used to describe the hydrologic properties of the matrix and fractures are dissimilar, as is the case in this study, flow tends to reside primarily in the matrix until the flux exceeds the saturated conductivity of the matrix, at which point the matrix is (almost completely) saturated, and significant flow occurs in the fractures.

For transient flow, gross measures (such as water-pulse travel time) could be unable to distinguish between the composite-porosity model and other models. With the composite-porosity model, however, the physics of the water flow could be incorrect. With the composite-porosity model, a large pulse of water applied at the boundary would travel primarily through the matrix (where the strongest capillary forces reside) before overflowing into the fractures. Modeled with a discrete-fracture model or a dual-porosity model, a water-pulse would travel primarily through the fractures (where typically the conductivity is greatest) before imbibing into the matrix.

For steady-state flow, the composite-porosity model gives the same results as other classical models if the boundary conditions are consistent with equal matrix and fracture pressures. Other boundary conditions (for example, specifying a flux in the fractures at a boundary but specifying no flow for the matrix) can lead to a zone (small or large, depending on the matrix/fracture coupling strength) of disequilibrium between the matrix and fracture pressures. Models that allow the matrix and fractures to be completely decoupled (e.g., the weeps model, discussed below), can achieve markedly different steady-state-flow solutions. This TSPA only considered steady-state groundwater flow for the composite-porosity calculations. (Although the percolation rate was randomly selected from a probability distribution for each calculation—Section 3.3.)

As part of this study, deterministic calculations were performed using the mean values of all the parameters (parameter values are discussed in Section 4.4.2; the deterministic calculations are discussed in Section 4.8). From these average-parameter calculations, examples of the flow results using the composite-porosity model have been selected, and are discussed below.

Figure 4-14 shows the calculated saturation for one of the columns used to represent the unsaturated zone at Yucca Mountain. The column extends from 10 meters above the repository horizon down to the water table. The rate of percolation is

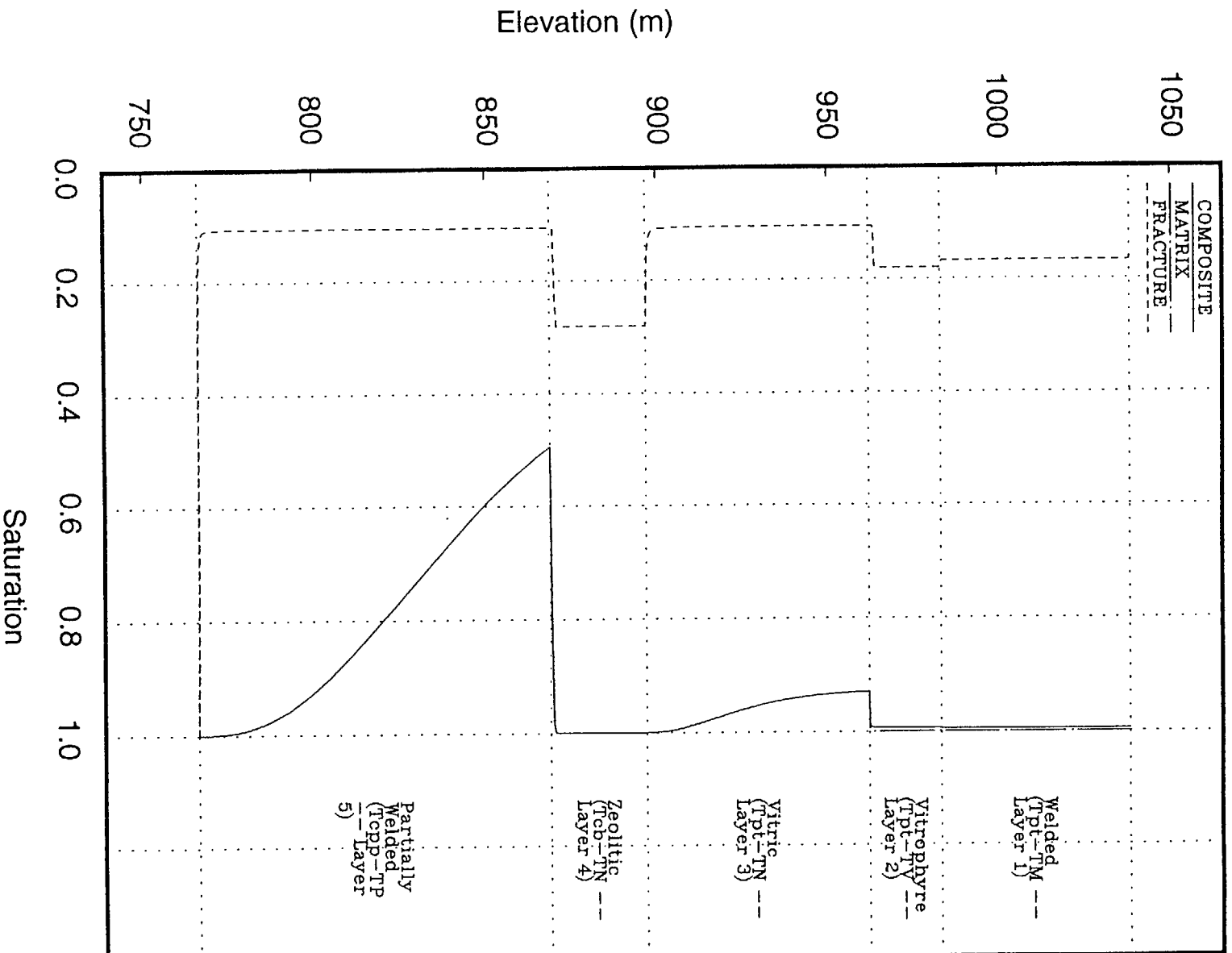


Figure 4-14. Saturation versus elevation, given an influx of 1 mm/yr (0.001 m/yr); calculated using the STEADY module of TOSPAC and the composite-porosity model of flow.

1 mm/yr. The figure shows the matrix to be near complete saturation in much of the column; only the units with highly conductive rock matrix—the vitric and partially welded units—are unsaturated. The units with partially saturated matrix show the fractures to be at residual saturation. The units with saturated matrix show higher saturations in the fractures. The lower boundary condition (at the water table) is a pressure head of zero, which corresponds to complete saturation in both the matrix and fractures.

Figure 4-15 shows the average linear water velocity (the pore-water velocity) of groundwater for the same problem. The water velocity in the composite medium is approximately 10 mm/yr (0.01 m/yr). This “composite” velocity approximates the velocity of a nonsorbing tracer in a closely coupled matrix/fracture system, implying a tracer travel time of approximately 25,000 years over the 250-m distance. The water velocities are much different in the matrix and the fractures for most of the units, however. The units that show higher saturations in the fractures have significant fracture-water velocities; for the other units, the fracture-water velocity is nil.

4.4.2 Parameters for the composite-porosity flow model

The composite-porosity model as implemented in TOSPAC requires a description of the porous medium, including the physical dimensions and the hydrologic properties. To allow comparison with other TSPA participants, the transect of Yucca Mountain between drill holes USW H-5 and USW G-4, and USW G-4 and UE-25a #1 was used as the basis for representing the stratigraphy of the unsaturated zone for the composite-porosity models. For the TOSPAC/TSA calculations, six one-dimensional vertical columns were defined within the boundaries of the transect to form the basis for six calculational meshes.

Figure 4-16 shows the transect with the locations of the six vertical columns for the TOSPAC/TSA calculations. The locations of the columns were determined so that each column represented one-sixth of the area of the repository. Figure 4-17 shows the division of the repository block into six equal sub-areas, and the resulting position of the columns within these sub-areas along the specified transect.

Elevations of stratigraphic boundaries for each column were calculated by linear interpolation from the elevations of the boundaries at the drill holes. (Note that there is a 14-m offset at the Ghost Dance Fault that has been taken into account.) Figure 4-18 shows the six columns used for the composite-porosity model in this study. The top of each column is 10 meters above the repository horizon. Elevations for each of the units within each column, and at each drill hole, are presented in Table 4-3. USW G-4 was not included as a constraint on the linear interpolation,

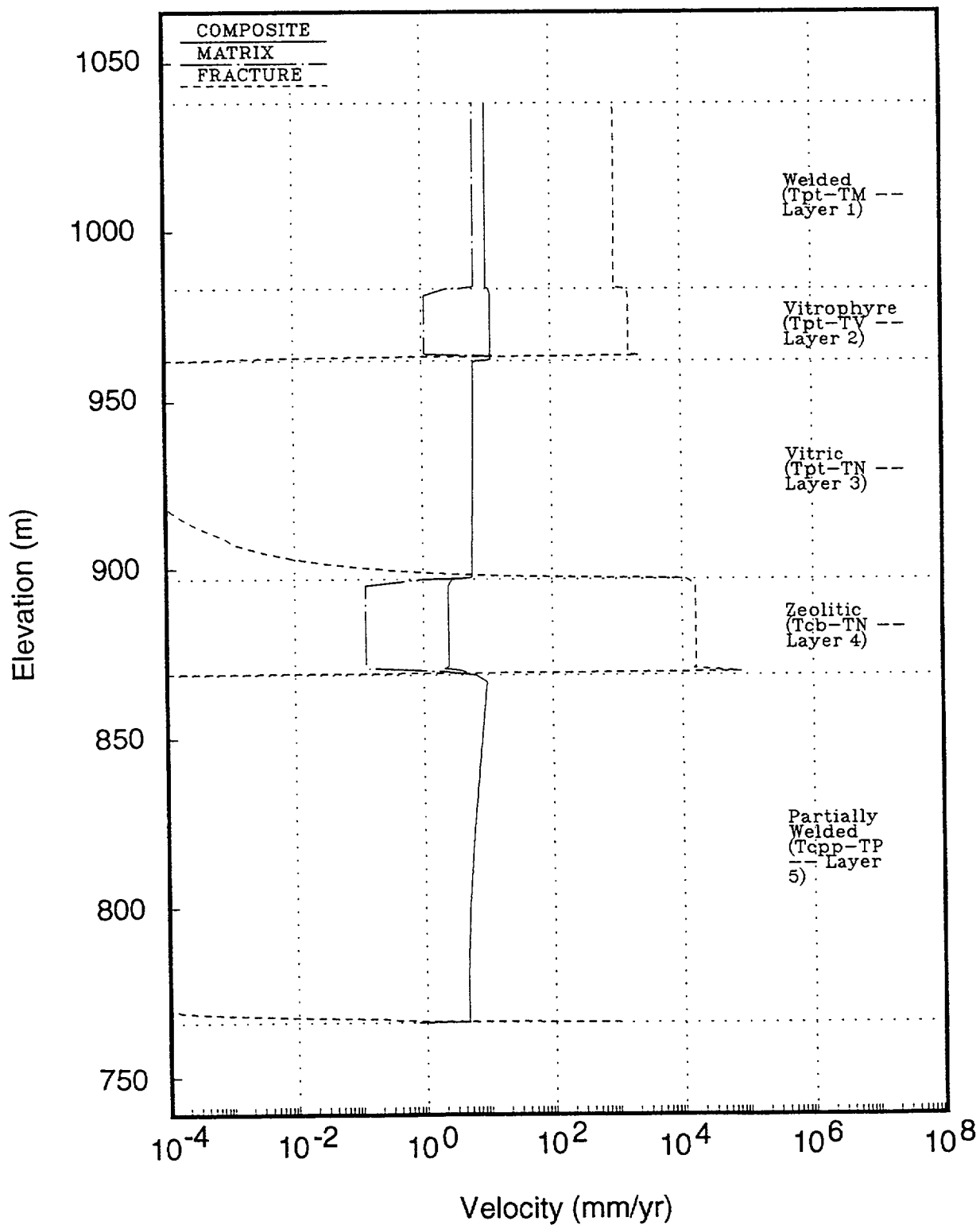


Figure 4-15. Groundwater velocity given an influx of 1 mm/yr (0.001 m/yr); calculated using the STEADY module of TOSPAC and the composite-porosity model of flow.

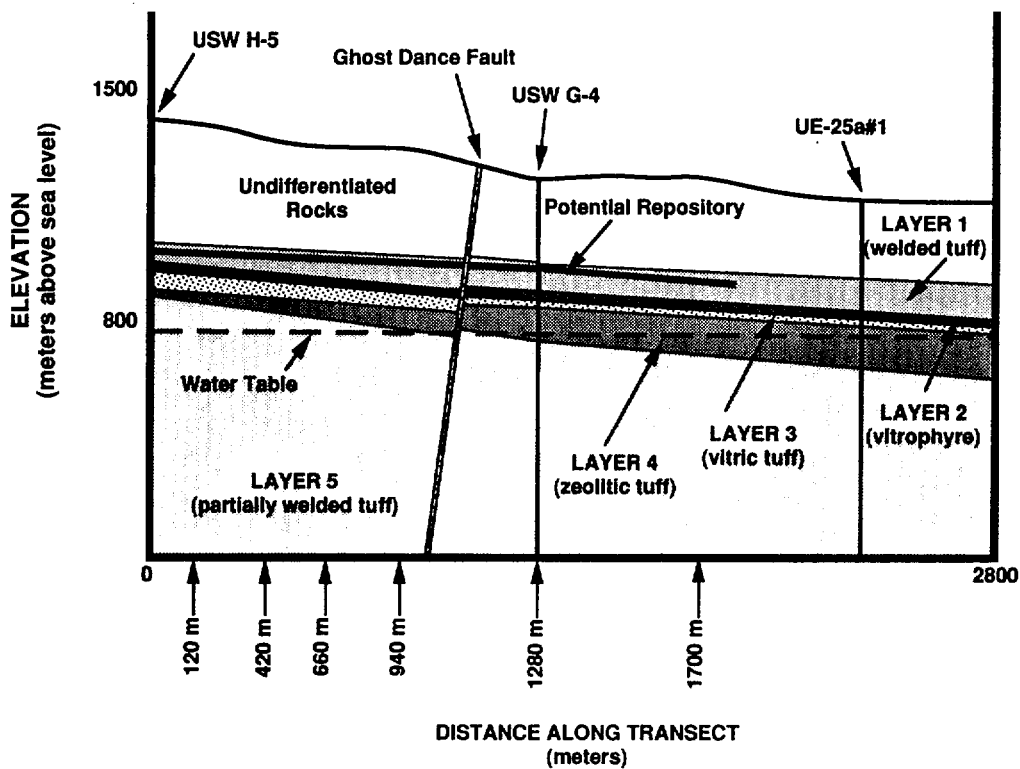


Figure 4-16. Transect of Yucca Mountain between drill holes USW H-5 and USW G-4, and USW G-4 and UE-25a #1, showing the idealized stratigraphy and the locations of the six vertical columns for the composite-porosity flow (TOSPAC/TSA) calculations.

and its elevations do not correspond exactly to the linear interpolation.

Table 4-4 lists the parameters used for the composite-porosity model of groundwater flow in the unsaturated zone. Chapter 3 contains discussion of the parameters that are described by probability distributions and how the distributions were chosen. The remainder of this subsection contains a discussion of the other parameters.

The water-density and compressibility parameters used by the composite-porosity model are standard values (e.g., Freeze and Cherry, 1979), although the standard compressibility has been multiplied by water density and the acceleration caused by gravity to get the necessary units (Gauthier et al., 1992b). The hydrologic properties that are specified for the bulk materials are the fracture porosity and the bulk compressibility. The hydrologic properties that are specified for the matrix materials are the porosity, the relative-hydraulic-conductivity function (like the water-retention function, a "characteristic curve" of the material), and the saturated hydraulic conductivity. For this study, the van Genuchten parameters (van Genuchten, 1980) were used to specify the relative-hydraulic-conductivity function: S_r , the residual saturation; S_s , complete saturation (ideally taken to be one); α_{vG} , specifying the air-entry pressure; and β_{vG} , a slope parameter that provides a mea-

Table 4-3. Elevations^a used for the composite-porosity model of the UZ.

Location	Elevation at top of layer...						Water table
	1	Rep. ^b	2	3	4	5	
USW H-5	1478 ^c	1035	996	974	905	885	770
120 m E (Col. 1)	1038 ^d	1028	983	962	897	869	766
420 m E (Col. 2)	1021 ^d	1011	950	932	877	827	755
660 m E (Col. 3)	1007 ^d	997	923	907	861	794	747
940 m E (Col. 4)	990 ^d	980	893	879	843	756	737
1099 m E Ghost Dance	1309 ^c	971	875	863	832	734	731
1099 m W Ghost Dance	1309 ^c	971	889	877	846	748	731
1280 m E (Col. 5)	966 ^d	956	877	864	836	— ^e	731
1313 m E USW G-4 ^f	1270 ^c	961	869	860	836	— ^e	731
1700 m E (Col. 6)	930 ^d	920	848	835	813	— ^e	730
UE-25a #1	1199 ^c	(875)	811	798	784	— ^e	729

^a In meters.

^b The repository is modeled as a 5-m-thick layer.

^c Ground surface.

^d Top of simulated column.

^e Below the water table.

^f Not used in the linear interpolation.

Table 4-4. Parameters used by the composite-porosity model.

Model parameter	Distribution	Distribution parameters	Mean value
Water density (kg/m ³)	—	—	1000
Water compressibility (m ⁻¹)	—	—	4.3 × 10 ⁻⁶
Bulk-rock compressibility (m ⁻¹)	—	—	0
Matrix porosity, n_m	see Tables 3-10 and 3-17		
Matrix van Genuchten S_s	—	—	1
Matrix van Genuchten S_r	see Table 3-19		
Matrix van Genuchten α_{vG}	see Table 3-18		
Matrix van Genuchten β_{vG}	see Table 3-12		
Matrix saturated conductivity, K_s	see Table 3-8		
Fracture compressibility (m ⁻¹)	—	—	0
Fracture porosity, n_f	see Table 3-23		
Fracture van Genuchten S_s	—	—	1
Fracture van Genuchten S_r	see Table 3-21		
Fracture van Genuchten α_{vG}	see Table 3-20		
Fracture van Genuchten β_{vG}	see Table 3-14		
Fracture saturated conductivity, K_s	see Table 3-14		
Percolation rate, q	see Table 3-7		
Lower-boundary pressure head (m)	—	—	0

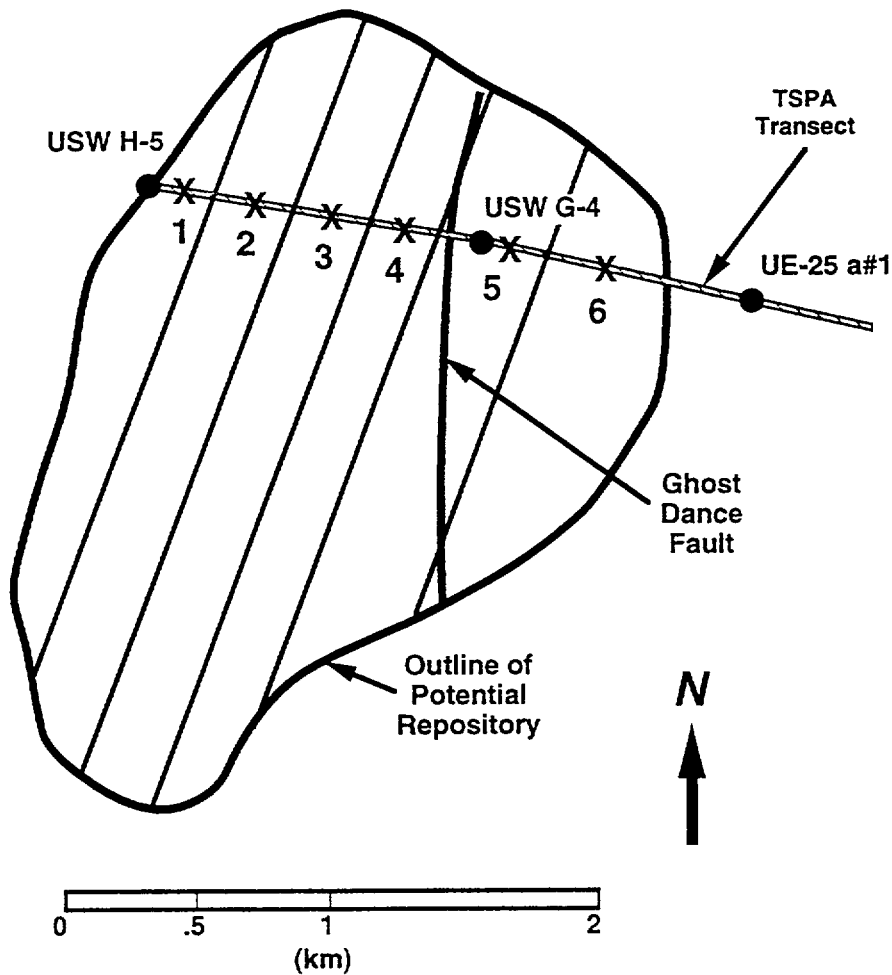


Figure 4-17. Map of the boundary of the potential repository at Yucca Mountain, showing the division of the repository into six equal-area subregions, and the locations of the six vertical columns for the composite-porosity flow (TOSPAC/TSA) calculations.

sure of the pore-size distribution within the material. Similar information must be provided for the fracture "materials." For TOSPAC, the water viscosity is implicit in the characteristic curve. TOSPAC also requires percolation rate (a steady-state flux) and a pressure head defined at the bottom of the flow column to find a unique solution. The bottom pressure head of 0 m specifies saturated conditions—i.e., the water table.

4.4.3 Weeps model of unsaturated flow

The weeps model is embodied in the WEEPTSA program in the TSA. More details on the weeps model may be found in Gauthier et al. (1992a). Its adaptation for use in the TSA is discussed by Wilson (1992). The following is a brief discus-

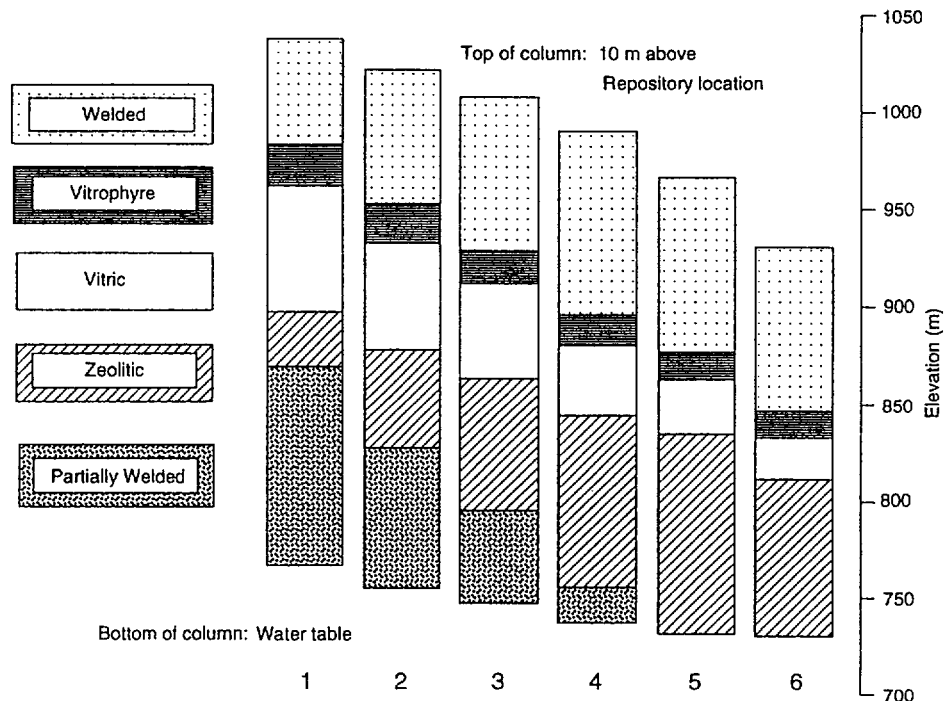


Figure 4-18. Stratigraphies of the six vertical columns used for the composite-porosity flow (TOSPAC/TSA) calculations.

sion of how the weeps model represents flow, and how the model assumptions are significant to this study.

The weeps model describes a system in which the fractures support flow independently of the matrix. The weeps model is illustrated in Figure 4-19. The model is based on the idea that a finite amount of water infiltrates Yucca Mountain each year and, because of little or no interaction between the matrix and the fractures, a significant amount of the water flows through fractures (weeps) down to the water table.

Supporting evidence for significant fracture flow at Yucca Mountain is circumstantial. Secondary mineralization on the walls of fractures has been reported at Yucca Mountain (Carlos, 1985) and these deposits could indicate prior fracture flow. Continuous water seepage from a fracture occurs at G-tunnel (located at Rainier Mesa approximately 30 km to the northwest of Yucca Mountain) in unsaturated welded tuff similar to the tuffs at Yucca Mountain. A rate of infiltration of between 0.5 and 4.5 mm/yr (Montazer and Wilson, 1984) has been suggested, which is greater than the saturated conductivity of much of the matrix in the welded tuffs (Peters et al., 1984, measured saturated conductivities to be less than 1 mm/yr for the welded tuff matrix). If this amount of water is percolating through the welded tuff ma-

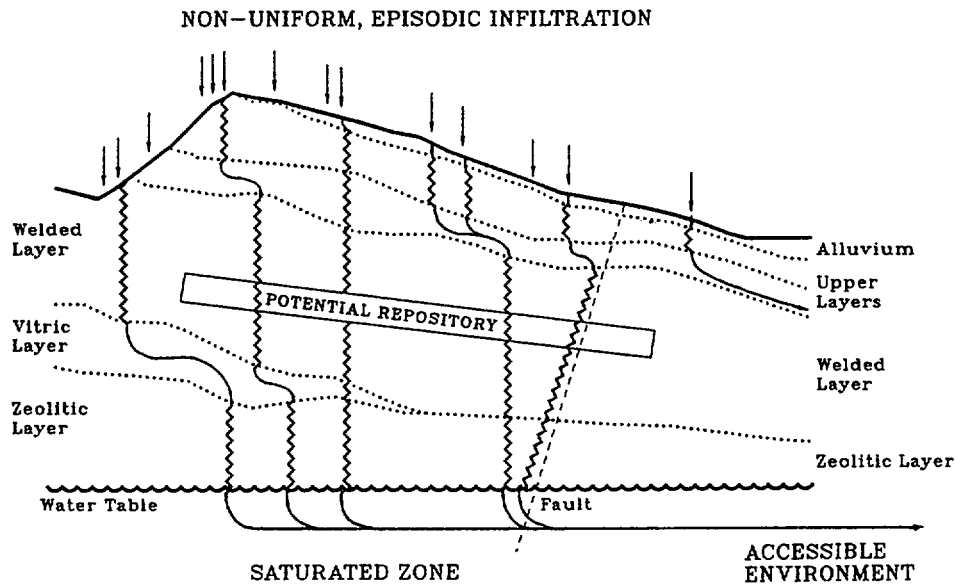


Figure 4-19. A conceptual model of significant fracture flow (weeps) at Yucca Mountain.

trix, the matrix should be saturated; however, in-situ matrix saturations reported by the Yucca Mountain Reference Information Base, Version 4 (RIB 1.4.2), are approximately 60 percent. Radioactive ^{36}Cl has been reported in the Topopah Spring unit at drill hole USW UZ-6 (Norris, 1990). ^{36}Cl is a remnant of the atmospheric testing of nuclear weapons that took place within the last 50 years, and its presence deep inside Yucca Mountain suggests groundwater travel times much shorter than should occur when flow is predominantly through the matrix. And finally, ambiguous evidence for fracture flow has been reported at USW UZ-1 (Whitfield, Thordarson, and Hammermeister, 1990). Water contaminated with drilling fluids, presumably from USW G-1, was found at the bottom of dry-drilled USW UZ-1, suggesting that the fluids had flowed the 300-m distance through the fractures within 3 years. But no evidence of weeping fractures was seen through a camera lowered into USW UZ-1.

For significant fracture flow to occur, specific conditions and features must exist to initiate flow in fractures, then sustain the flow. Surface conditions at Yucca Mountain that could contribute to initiating flow in fractures include the following: annual cycles of infiltration; spatial variation in precipitation causing large localized pulses of water; runoff through washes causing large, localized pulses; and direct precipitation on, or runoff over, outcroppings of fractured tuffs. Subsurface features within Yucca Mountain that could contribute to the initiation of fracture flow in underlying strata include heterogeneities; buried topographical features (e.g., paleowashes); undulations in nonwelded geologic units (causing water to perch above

fractured, welded geologic units); dip of the geologic units and the conductivity contrast between geologic units (causing lateral diversion of flow that eventually results in locally saturated conditions); and the pinching out of geologic units that carry significant flow. Conditions that reduce matrix/fracture coupling and work to retain water in fractures include the following: short time scale of flow (e.g., flow in pulses, with large amounts of water passing through fractures with large apertures); low hydraulic conductivities in the matrix; hysteretic effects that slow the wetting of the matrix; coatings on the fracture walls (Gallegos, Thoma, and Smith, 1992); and capillary or other barriers (e.g., parallel dry fractures) that restrict lateral movement of water by imbibition into the matrix (resulting in a localized saturated zone around the flowing fracture). The above conditions are known to exist at Yucca Mountain; however, whether they actually contribute to significant fracture flow is speculative.

Because of the lack of data, quantification of groundwater flow and the impact of flow on a potential repository at Yucca Mountain using the weeps model is through deduction. In other words, although we do not yet know how (or if) significant fracture flow behaves at Yucca Mountain, we can deduce that in the broadest sense it must behave according to the following rules: (1) a finite amount of water infiltrates the mountain, (2) the water is distributed among a number of fractures, and the number of fractures is a function of the the amount of infiltrating water and the amount of water carried by each fracture, (3) the number of containers that are contacted by flowing fractures is a function of the number of flowing fractures and the geometry of fracture and container locations.

The amount of water entering Yucca Mountain (V_{in}) is estimated as the product of the percolation rate (q) and the area of the potential repository ($A_{rep} = 5.61 \times 10^6$ m²): $V_{in} = qA_{rep}$. For 1 mm/yr, the average percolation rate used in this study, V_{in} would be 5610 m³/yr.

Fractures can only pass so much water in a year. An estimate of the number of major flowing fractures at Yucca Mountain starts by determining the hydraulic conductivity (K_f) associated with a given fracture aperture, using a parallel-plate model:

$$K_f = \frac{\rho g}{\mu} \frac{b^2}{12}, \quad (4.45)$$

where b is the flow aperture, and $\rho g/\mu$ is the product of water density ($\rho = 1000$ kg/m³) and gravity ($g = 9.76 \times 10^{15}$ m/yr²) divided by the dynamic water viscosity ($\mu = 3.16 \times 10^4$ kg/m-yr at 20° centigrade), and is equal to 3.09×10^{14} m⁻¹yr⁻¹. The flow aperture is used in this equation rather than the physical fracture aperture because the fracture need not be flowing at capacity, that is, need not be saturated.

We define the flow aperture as the aperture required to pass the water flowing through the fracture as if the fracture were flowing at capacity.

Next, the water-flow rate (Q_f) through the fracture can be estimated using an elaboration of Darcy's law that contains a description of turbulence caused by nonlaminar flow (Ward, 1964):

$$q_f + 0.55\sqrt{\frac{\rho}{\mu g}}K_f q_f^2 = K_f \frac{\partial h}{\partial l} \quad (4.46)$$

$$\implies q_f = \frac{Q_f}{A_f} = \frac{-1 + \sqrt{1 + 2.2K_f\sqrt{\frac{\rho}{\mu g}}K_f \frac{\partial h}{\partial l}}}{1.1\sqrt{\frac{\rho}{\mu g}}K_f}, \quad (4.47)$$

where q_f is the flux through the fracture, Q_f is the rate of flow through the fracture (the quantity of interest), A_f is the area of the fracture perpendicular to flow ($A_f = b w_f$, where w_f is the transverse length of the fracture), and $\partial h/\partial l$ is the hydraulic gradient. We assume that the hydraulic gradient is one—water flow is dominated by gravity, and not affected by capillary forces or by the weight of water ponded above.

The number of flowing fractures (N_{weeps}) and the water-flow rate through a single fracture (V_{weep}) are now calculated as follows:

$$N_{weeps} = \frac{V_{in}}{Q_f} \times C \times F, \quad (4.48)$$

$$V_{weep} = \frac{V_{in}}{N_{weeps}/C} = \frac{Q_f}{F}, \quad (4.49)$$

where C is the connectivity factor, and F is the weep-episode factor.

The connectivity factor (C) indicates the fraction of fractures that are actually connected from the surface to the water table. It is effectively used to decrease the number of weeps, because we strongly suspect that not all fracture paths are connected. Assuming that some fracture paths are unconnected, two interpretations are possible for determining the water-flow rate through the connected fractures: (1) the unconnected fractures do not flow and the water they would carry is added to the water carried by the connected fractures, or (2) the unconnected fractures carry water that is ultimately absorbed by the matrix and exhaled from the mountain as vapor. The latter interpretation is used in this study.

The weep-episode factor (F) is the inverse of the fraction of the time the weeps are flowing. For example, if weeps flow only 17 days out of the year (the mean of the assumed distribution), then the weep-episode factor is $365.25/17 = 21.5$; if

weeps flow one month out of the year, the weep-episode factor is 12. The weep-episode factor is effectively used to increase the number of weeps, while decreasing the average flow rate through each weep.

In the above equations, the number of weeps and the water-flow volume are most sensitive to the flow aperture. Because the amount of water carried by a fracture varies as the cube of the flow aperture, small changes in the flow aperture result in large changes in the water-flow rate, and the fractures with the largest flow apertures dominate the flow and can be considered as representative of the flow system. Figure 4-20 shows the major flow variables for fractures of three different apertures.

Once the number of flowing fractures is determined, a geometric argument, as outlined in Figure 4-21, is used to estimate the number of fractures that could come in contact with waste containers. The area in which a flowing fracture affects a waste container ($A_{contact}$) is estimated by the size of the fracture and the exposed area of a waste container. $A_{contact}$ is defined as the area about a circle of diameter d_{can} (the diameter of a waste container, 0.66 m) in which a line of length w_f , with a given orientation, will contact the circle; with any larger area, it is possible to place the line such that they do not touch. It is easier to visualize the converse problem, which is

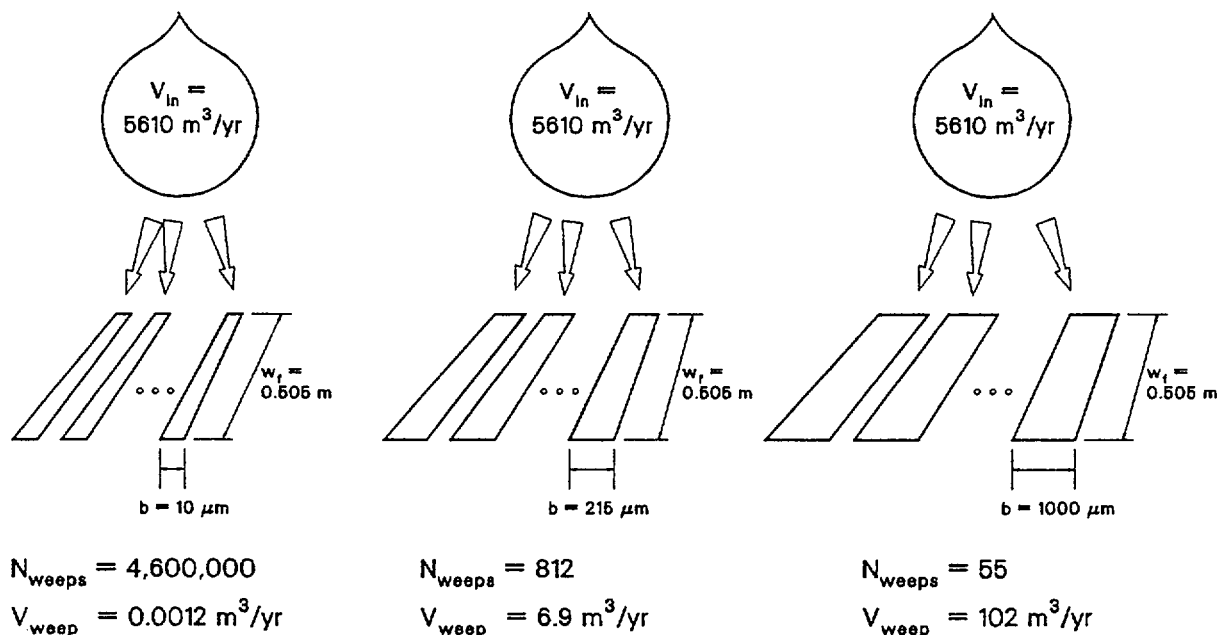


Figure 4-20. Estimates of some weeps-model parameters for three different sizes of fractures.

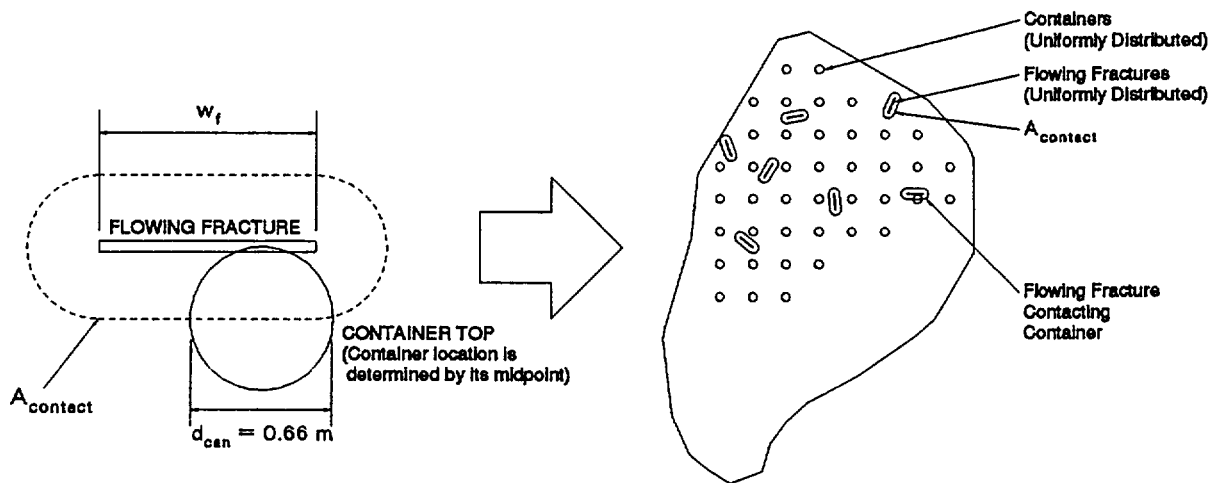


Figure 4-21. Geometric considerations in calculating the number of containers contacted by flowing fractures.

shown in the figure: $A_{contact}$ is given in terms of locating a circle (by its midpoint) with respect to a line. The probability of a given flowing fracture contacting a waste container ($P_{contact}$) is then the product of the total number of waste containers in the repository and the ratio of the area of contact and the area of the repository. The expected number of flowing fractures contacting containers ($N_{contact}$) is calculated assuming a binomial distribution. The equations are as follows:

$$A_{contact} = w_f d_{can} + \pi \left(\frac{1}{2} d_{can}\right)^2, \quad (4.50)$$

$$P_{contact} = N_{cans} \frac{A_{contact}}{A_{rep}}, \quad (4.51)$$

$$N_{contact} = N_{weeps} P_{contact}, \quad (4.52)$$

$$\sigma_{contact} = \sqrt{N_{weeps} P_{contact} (1 - P_{contact})}, \quad (4.53)$$

where N_{cans} is the total number of containers in the potential repository ($N_{cans} = 33,300$) and $\sigma_{contact}$ is the standard deviation of the assumed binomial distribution.

As shown below, maximizing the number of containers contacted by flowing fractures maximizes releases. We can therefore make the conservative assumption that no two flowing fractures contact the same container—i.e., that the number of flowing fractures contacting containers is equal to the number of containers contacted by flowing fractures ($N_{contact}$)—until all containers are contacted by flowing fractures.

It is interesting to note that when all containers are contacted by flowing fractures ($N_{contact} \geq N_{cans}$), the amount of water that contacts a container averages out

to be the influx through the contact area, reduced by the connectivity factor:

$$\frac{N_{contact}}{N_{cans}} V_{weep} = q A_{contact} C . \quad (4.54)$$

This result is to be expected for a uniform spatial distribution of the infiltrating water.

As an example of how the weeps model works, consider flow through fractures using the average values of parameter distributions used in this study (Section 4.4.5). The average fracture has an aperture of 215 μm and a transverse length of 0.505 m ($A_f = 1.09 \times 10^{-4} \text{ m}^2$). For this fracture, the flow rate (Q_f) is calculated to be 74.3 m^3/yr . Thus, to pass 5610 m^3/yr (V_{in}) requires 76 of these fractures. Assume that 50 percent of the fractures ($C = 0.5$) are connected from the surface to the water table, (50 percent of the water, carried by unconnected fractures, is absorbed by the matrix) and that fractures only flow for 17 days out of the year ($F = 21.5$). With these additional assumptions, 812 fractures ($76 \times 0.5 \times 21.5$) are required to pass the 5610 m^3/yr , with the water-flow volume (V_{weep}) through one of these fractures averaging 6.91 m^3/yr . The area in which a weep could contact a container ($A_{contact}$) is 0.675 m^2 , and the probability of a weep contacting a container ($P_{contact}$) is 0.00421. The expected number of containers contacted by weeps ($N_{contact}$) is 4 (actually, 3.42), with a standard deviation of 2 (actually, 1.85). Therefore, the weeps model predicts that if the percolation rate at Yucca Mountain is 1 mm/yr for the next 10,000 years, and if the size of the major flowing fractures is 215 μm by 0.505 m, then approximately 4 containers would be subject to groundwater flow, and *only* these 4 containers would fail and release radionuclides (both aqueous and gaseous) within 10,000 years.

The curves shown in Figure 4-22 were calculated using the mean values and the worst-case values of the weeps-model parameters (except, of course, for the flow aperture). The curves show how the number of containers contacted varies with the size of the flowing fractures, and therefore, the number of flowing fractures. The basic conclusion of the weeps model is that *larger* flow apertures imply *fewer* flowing fractures, and *fewer* flowing fractures imply *fewer* containers subjected to fracture flow. As shown by the one-standard-deviation bound (the dashed lines), there is little statistical uncertainty in these numbers.

In terms of radionuclide releases, the weeps model predicts a similar relationship. The *larger* the flow apertures, the *fewer* containers subjected to groundwater flow, thus the *lower* the releases. This relationship is shown in Figure 4-23, with the curves calculated using the mean values, as well as the worst-case values, for all parameters in the source-term and weeps models (except, of course, for the flow aperture). Also shown in Figure 4-23 are the contributions of the aqueous and

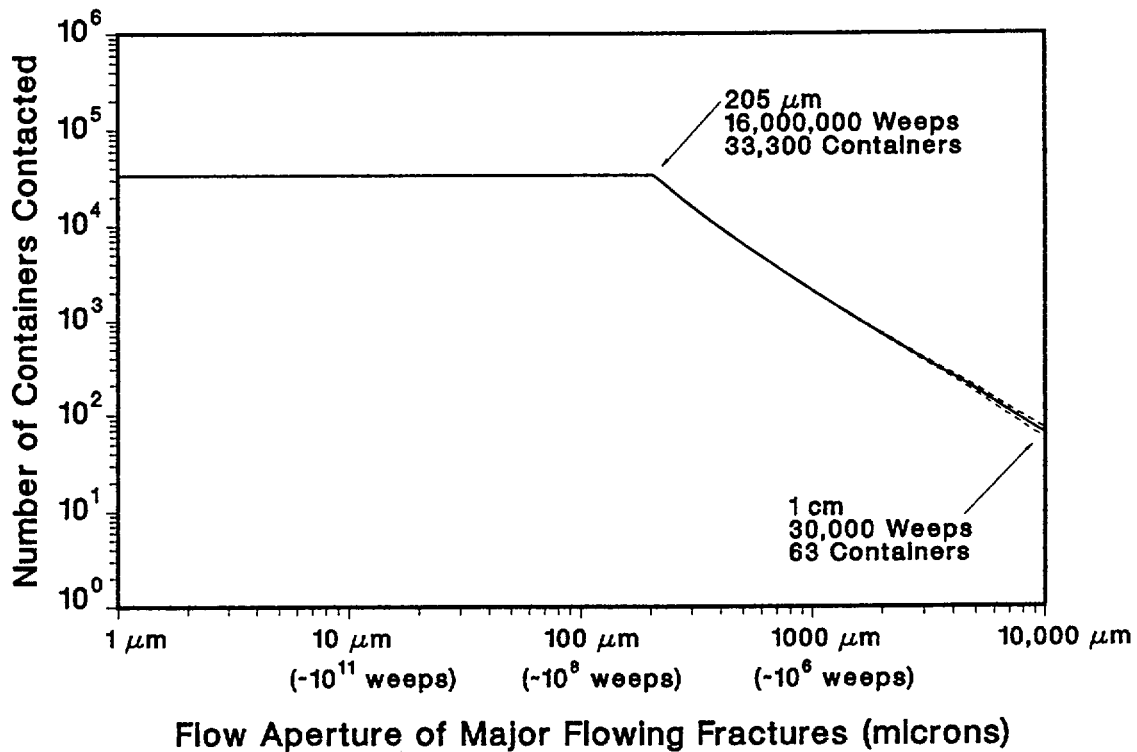
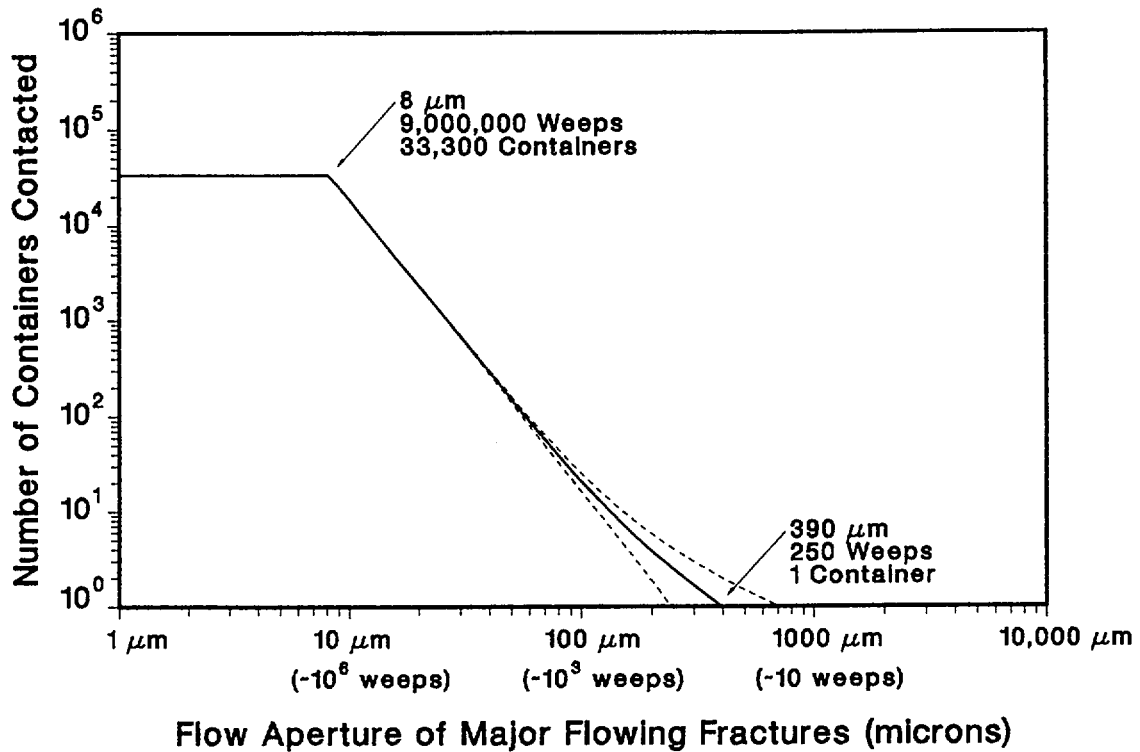


Figure 4-22. Relationship between the flow aperture of the major flowing fractures (weeps), the number of flowing fractures, and the number of waste containers contacted; the dashed lines indicate plus or minus one standard deviation. (a) Derived from the mean values of weeps-model parameters. (b) Derived from the worst-case extreme values of weeps-model parameters.

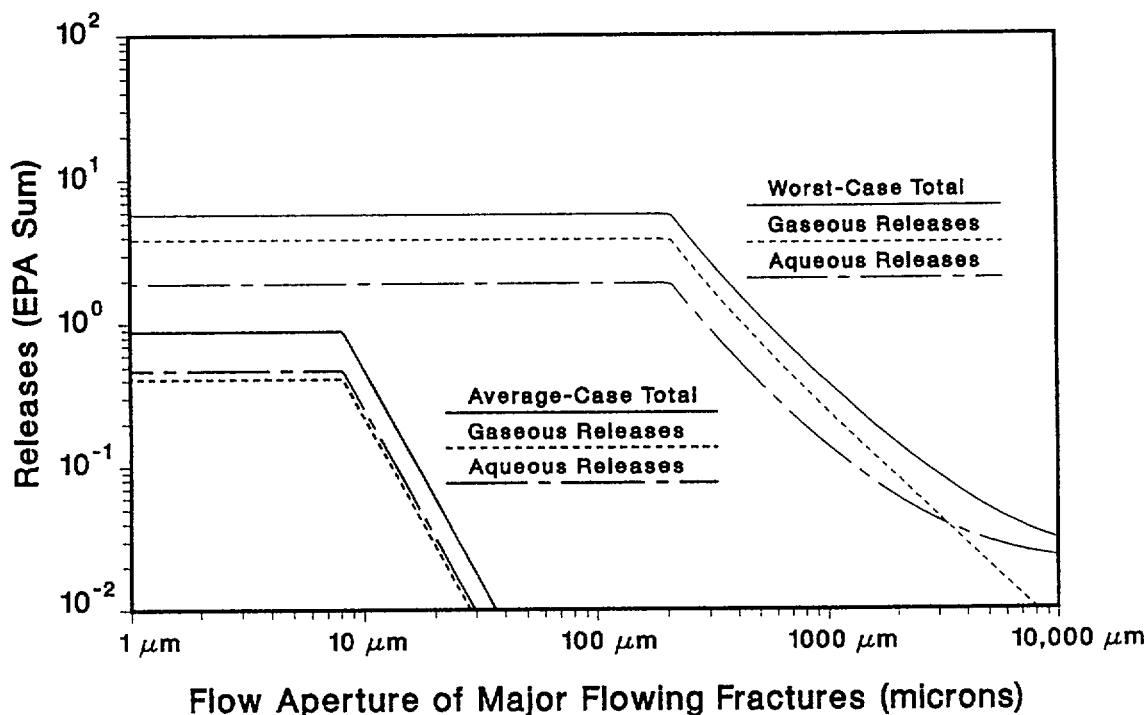


Figure 4-23. Relationship between the flow aperture of the major flowing fractures, the number of flowing fractures, and the resulting releases from the potential repository. The thick curves represent results derived from the mean values of weeps- and source-model parameters; the thin curves are derived from the worst-case extreme values of weeps- and source-model parameters.

gaseous components to the total releases. (Gaseous releases—releases of ^{14}C —were calculated as described in Section 5.2.)

The percolation rate of 1 mm/yr used for the mean-value figures is the mean of the exponential distribution of percolation rates used in this study. Higher percolation rates would cause the curves shown in Figures 4-22 and 4-23 to be shifted to the right (as for the worst-case curves, which used a percolation rate of 39 mm/yr).

In the weeps model, it is assumed that only containers contacted by weeps fail and release radionuclides. The source term for radionuclides is basically the same as that used by the composite-porosity model, with changes discussed in Section 4.4.4. Transport of radionuclides through the unsaturated zone is assumed to be at a time scale much shorter than 10,000 years, and is modeled as instantaneous—i.e., releases from the source are treated as releases from the unsaturated zone. Releases from the source are reduced by an arbitrary “absorption factor.” The absorption factor is included in the model to take into account that some of the nuclides released from waste containers might not make it to the water table, at least not within 10,000 years.

Radionuclides could be carried into dead-end fractures or simply drawn out of the fractures *en route*, either because of imbibition of solute-bearing water into the tuff matrix (absorption) or because of diffusion of the radionuclides into the matrix-pore water (matrix diffusion).

Many of the assumptions supporting the weeps model could prove false, not the least of which is that significant fracture flow exists at Yucca Mountain. However, assuming the general validity of the model, several assumptions within the model have direct consequences to this study. First, all the weeps are approximately the same size; i.e., carry approximately the same amount of water. Second, only containers contacted by weeps fail. Although this assumption limits the source term, often severely, it is reasonable that containers not subjected to groundwater flow could remain intact for 10,000 years or even longer. Third, flow does not switch from one fracture to another, or from one set of fractures to another (on the scale of the distance between containers). Fourth, the percolation rate is not a function of fracture size. Fifth, weeps and waste containers are uniformly distributed throughout the plane of the repository. Sixth, flow is not concentrated by the disturbed zone.

4.4.4 Adaptation of the source model for weeps

The source model defined in Section 4.3 was designed for composite-porosity flow. Application to weeps flow necessitated two changes.

The first change involved elimination of diffusive releases from the source term. This change maintains consistency with the weeps-model philosophy that the rock matrix is essentially decoupled from the flow and diffusive transport would be at best inconsequential.

A variation of the weeps/source model would be to assume locally saturated conditions where a weep contacts a waste container, and allow diffusive transport in the near field. Variations of this kind were not investigated in the current study, but they are not expected to make a large difference in the results because an important feature of the weeps model is that only a subset of the waste containers releases waste (Section 4.4.3). Other variations on the weeps/source model are also possible. For example, gaseous releases from some of the unwetted containers could be allowed, but this possibility was not investigated in this TSPA.

The part of the source model that is modified for the weeps calculations is the transport out of the waste container (Section 4.3.5). In Equations 4.13 and 4.14, the quantity $A_{cross} f_{in} q_s$ represents the volume of water per unit time that is flowing through a waste container. Recall that q_s is calculated by using a log-normal spatial flux distribution (see Equations 4.2 through 4.5). This calculation is unnecessary

for the weeps model because the water-flow rate for a waste container contacted by weeps is calculated within the weeps model: $A_{cross} f_{in} q_s$ is replaced by V_{weep} (see Equation 4.49) or, in the case where more than a single weep is contacting a container, by $q A_{contact} C$ (Equation 4.54). The amount of water actually contacting the waste could be reduced by a factor f_{in} as was done previously (Equation 4.13), but for the current study it is simply assumed that all the water flowing past a container does contact waste. The fraction of containers engaging in advective releases, f_s (see Equation 4.1), is set equal to the fraction of containers contacted by weeps. In the notation of the previous subsection, $f_s = \min\{N_{contact}/N_{cans}, 1\}$ (see Equations 4.51 and 4.52). The fraction of containers engaging in diffusive releases, f_r , is set to zero.

The second change involved scaling releases to reflect that only a fraction of the waste containers could be releasing radionuclides. To scale the overall release rate properly, the release-rate formulas are scaled by the factor f_s (see Equations 4.38, 4.39, and 4.41). Because of the way the generic release functions are defined, the alteration-limited releases (using Equation 4.38 or 4.39) are already properly scaled over all time—i.e., only a fraction f_s of the total inventory is released. For the solubility-limited nuclides, however, the generic release function remains at a constant release rate after an initial ramp-up period (Figure 4-10). Because the rate never decreases, it is necessary to keep track of how much has been released, and cut off releases when the inventory has been exhausted. For the weeps model, releases must be cut off when f_s times the inventory has been exhausted. To enforce this condition in the simplest way, the inventories of the solubility-limited nuclides are reduced by the factor f_s at the beginning of the calculation.

4.4.5 Parameters for the weeps model

Table 4-5 contains a list of the parameters used in WEEPTSA, the TSA implementation of the weeps model.

The weeps model, as implemented, is “nondimensional,” and does not require a detailed geometry. The area of the repository is taken from Rautman, Whittet, and South (1987). Container diameter is taken from the reference container in the SCP. The number of waste containers is calculated from the 70,000 MTHM planned for the potential repository and an assumed 2.1 MTHM for each container (Apted et al., 1990). The percolation-rate distribution is taken from Section 3.3. These values are the same as those used for the composite-porosity model.

The fracture-aperture distribution (actually the flow-aperture distribution) is estimated from a number of sources. Peters et al. (1984) measured an aperture of 6 μm in the laboratory. Klavetter and Peters (1986) used a log-normal distribution

Table 4-5. Parameters used by the weeps model.

Model parameter	Distribution	Distribution parameters ^a	Mean value
Fracture aperture, b (m)	log-uniform	$1 \times 10^{-5}, 1 \times 10^{-3}$	2.15×10^{-4}
Horizontal length, w_f (m)	uniform	0.01, 1	0.505
Weep-episode factor, F	log-uniform	1, 100	21.5
Connectivity factor, C	uniform	0, 1	0.5
Absorption factor, A	uniform	0, 1	0.5
Hydraulic gradient, $\partial h/\partial \ell$	—	—	1
Area of the repository, A_{rep} (m ²)	—	—	5.61×10^6
Container diameter, d_{can} (m)	—	—	0.66
Number of containers, N_{cans}	—	—	33,300
Percolation rate, q	see Table 3-7		

^a Parameters for the uniform and log-uniform distribution are minimum, maximum.

of apertures, with a mean aperture of 25 μm . Sinnock, Lin, and Brannen (1984) reported apertures between 71 μm and 89 μm . Zimmerman et al. (1988) calculated apertures between 36 μm and 190 μm . Because of the uncertainty in this parameter, a log-uniform distribution over a wide range was used in this study. The distribution reaches to values higher than those mentioned in order to include extreme cases, for example apertures of faults.

Quantitative information concerning the transverse length of a fracture is unavailable. Qualitatively, an average length of 1 m appears reasonable, with a tremendous range of variability. A uniform distribution best represents the uncertainty in this parameter. The decision to place the distribution range to be less than or equal to 1 m is based on several observations. First, geometric considerations suggest that an upper bound be placed on the transverse length; e.g., it is probably unrealistic to suppose that all the water in a 100-m-long weep would contact a single container. Second, we are most interested in the transverse length of the fracture that is filled with water, and this length must be less than or equal to the actual transverse length. Finally, although the weeps model is relatively insensitive to this parameter, shorter lengths require more flowing fractures (for a given percolation rate), and result in more containers being contacted by flowing fractures; thus, lengths shorter than 1 m are conservative.

The hydraulic gradient is set to one, implying that weep flow is dominated by gravity, and not affected by capillary forces or by the weight of water ponded above.

The distribution of the weep-episode factor (F) is unknown. The periodicity of an episode is assumed to be one year, based on the opinion that most infiltration occurs because of snowmelt in the winter or early spring, when evapotranspiration and runoff are minimal (Flint, 1989). The distribution represents a likelihood of the

episodes lasting any duration between 3.65 and 365 days a year, skewed toward the shorter durations. Shorter durations are conservative because they result in more flowing fractures.

The connectivity factor (C) and the absorption factor (A) are completely unknown. The distributions selected for these parameters reflect maximum uncertainty. These factors are included in the weeps model as place-savers for potentially more realistic future models.

The same source parameters were used for the weeps calculations as for the composite-porosity calculations (Tables 4-1 and 4-2), with the exceptions mentioned above— f_r is set to zero, and f_{in} , A_{cross} , v_r , and all of the parameters relating to diffusive releases are no longer used. There may be value in defining different distributions for some of the parameters (such as container lifetime and percolation rate) for the weeps calculations, rather than using the same distributions as the composite-porosity calculations, but such changes were not investigated for this TSPA.

4.5 Saturated-zone flow models

Radionuclide solutes from a repository at Yucca Mountain could be subjected to flow and transport first in the unsaturated zone, and then in the saturated zone. In this TSPA, flow and transport in the unsaturated zone and the saturated zone are considered separately, because of the difficulty in modeling these regimes in a coupled fashion.

The saturated-zone model used in this study is based on a regional flow model that is inherently two-dimensional in the horizontal plane. To utilize the model, the following steps were taken:

- 1) the model was reproduced and analyzed using the computer program STAFF-2D (Huyakorn et al., 1991), producing a distribution of groundwater travel times for the saturated zone, and
- 2) the distribution of groundwater travel times gained from the detailed STAFF2D effort was transferred to the simpler TRANS module of TOSPAC for inclusion in the TSA calculations.

4.5.1 Saturated flow using Czarnecki's model

To determine the groundwater travel times in the saturated zone, a two-dimensional flow model of the saturated zone was constructed, and the transport of solutes was modeled from points directly below the repository out to the accessible-

environment boundary (Figure 4-24). Transport was calculated both with and without dispersion. This subsection contains a discussion of the two-dimensional model, some two-dimensional transport calculations, and the rationale for choosing the travel-time distribution calculated without dispersion for inclusion in subsequent TSA calculations (Section 4.5.2).

Only a few of the most important parameters for the models used in this study are included in the final probability distribution of the groundwater travel times. No attempt was made to model radioactive decay, adsorption, or other processes specific to the type of solute; these parameters are factored into the TSPA at a later stage (Section 4.5.2).

A model that established the general flow patterns over a broad area encompassing the Nevada Test Site was developed by Waddell (1982). The information from these flow patterns was used to generate a smaller flow model including Yucca Mountain and extending approximately 70 km to Death Valley (Czarnecki and Waddell, 1984; Czarnecki, 1985). This two-dimensional model, as developed by Czarnecki and Waddell ("Czarnecki's model") and used in this TSPA, considers the general geology of the region and is calibrated to match the observed hydraulic heads of the

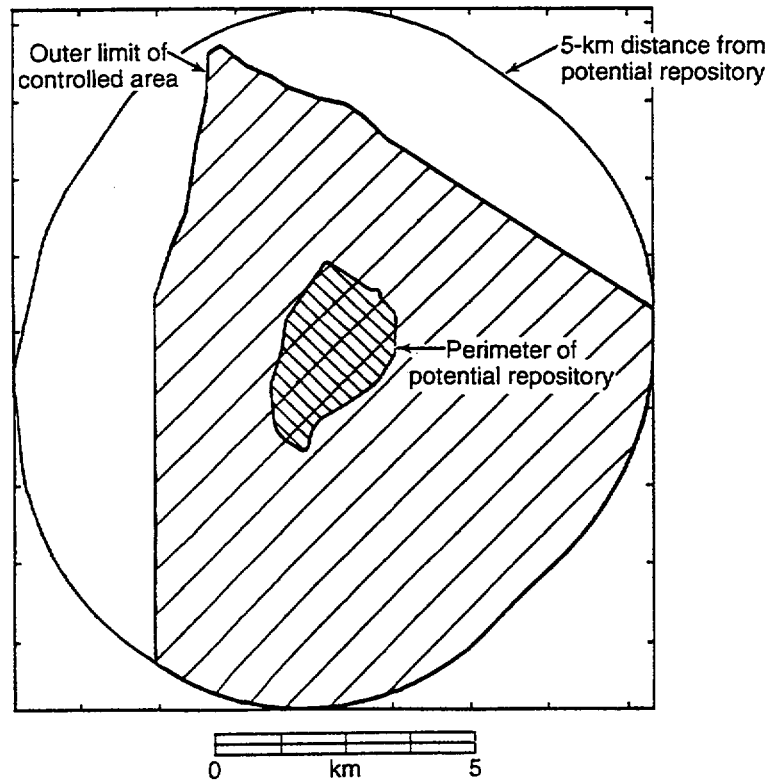


Figure 4-24. Map of region surrounding the potential repository at Yucca Mountain; the area outside the shaded region is the accessible environment. (After Figure 9 of Rautman et al., 1987.)

aquifer. Figure 4-25 shows the location of the observed hydraulic heads for the region considered by Czarnecki's model. In Figure 4-26, the hydraulic properties and boundary conditions used in the model are illustrated. Figure 4-27 shows the calculated hydraulic heads.

Czarnecki's two-dimensional model treats the geologic strata in the third dimension (depth) as single composite medium. Several layers actually exist, including at least two aquifers: the tuff aquifer and the deeper carbonate aquifer. The tuff aquifer is generally assumed to have much slower velocities than the carbonate aquifer. A scarcity of information remains regarding interaction between the two aquifers, which would mean models that include the two aquifers discretely would be speculative.

Czarnecki's flow model was duplicated using the STAFF2D computer program. No attempt was made to vary the flow properties according to any probability distribution because such models would have a low likelihood of matching the hydraulic heads observed in the field.

The flow model generates Darcy velocities, which then must be converted to pore-water velocities for the transport codes by dividing the Darcy velocity by the porosity. Four drill holes were identified from the area within and downstream of the potential repository (UE-25b #1, USW G-4, USW G-3 and J-13), and using porosity data from these drill holes (Tipton, 1991), an average porosity of 17.6 percent was calculated. Porosity in other areas (e.g. upstream of the repository) was set to the same value; during the simulations, no transport took place through these other areas, making the porosity unimportant there.

Two types of dispersion occur during transport: molecular diffusion and hydrodynamic dispersion. Molecular diffusion is caused by the random motions of individual molecules. Although the molecular diffusion varies because of tortuosity and pore size, Anderson (1979) states that values are of the order of 10^{-10} m²/s (approximately 3×10^{-3} m²/yr). A molecular diffusion of 5×10^{-3} m²/yr was used in the STAFF2D transport models as this value was mentioned specifically by Anderson. (This value was inadvertently different than that used for the transport calculations described in Section 4.6; however, as is discussed below, it was decided not to incorporate any dispersion in the travel-time distribution, making the choice of a diffusion coefficient moot. Furthermore, molecular diffusion is negligible compared to the assumed hydrodynamic dispersion.)

Hydrodynamic dispersion (also known as kinematic or mechanical dispersion) is a mechanical process caused by advection. Hydrodynamic dispersion D_h is generally taken to be proportional to water velocity v , with the coefficient of propor-

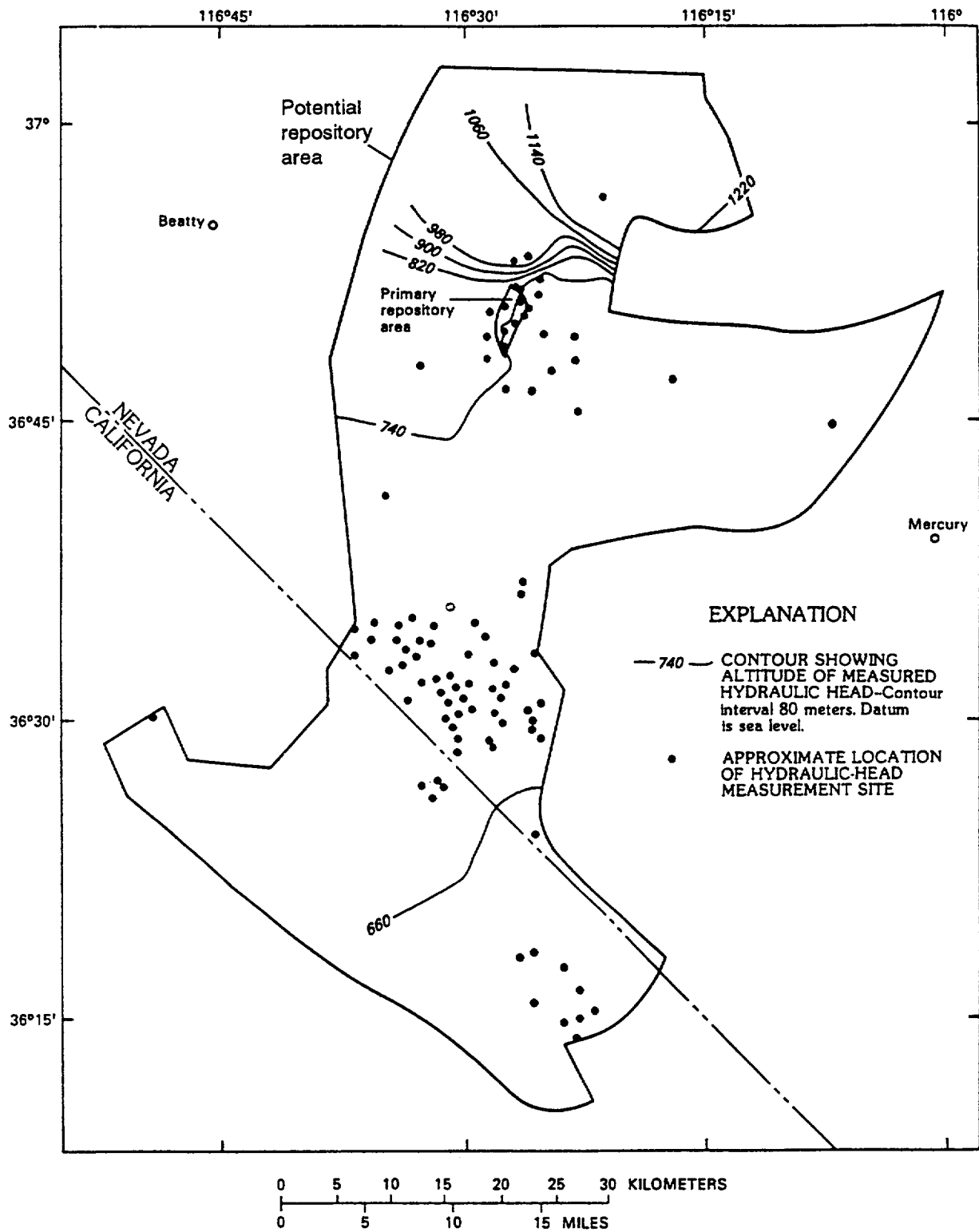


Figure 4-25. Map of region modelled by Czarnecki and Waddell, showing location of hydraulic-head measurement sites and the potential repository. (Taken from Figure 3 of Czarnecki and Waddell, 1984.)

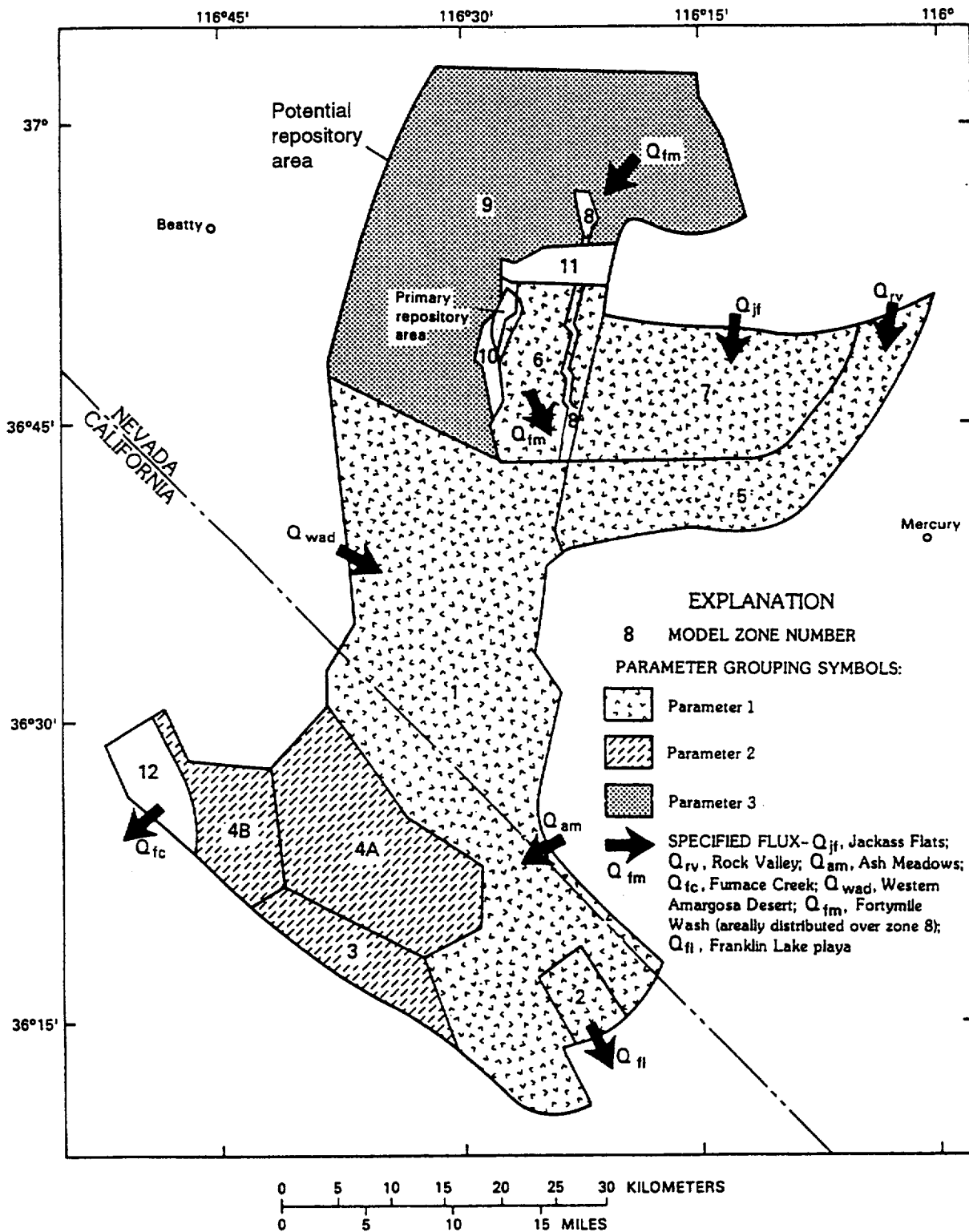


Figure 4-26. Map of region modelled by Czarnecki and Waddell, showing layout of the hydraulic properties and boundary conditions. (Taken from Figure 4 of Czarnecki and Waddell, 1984.)

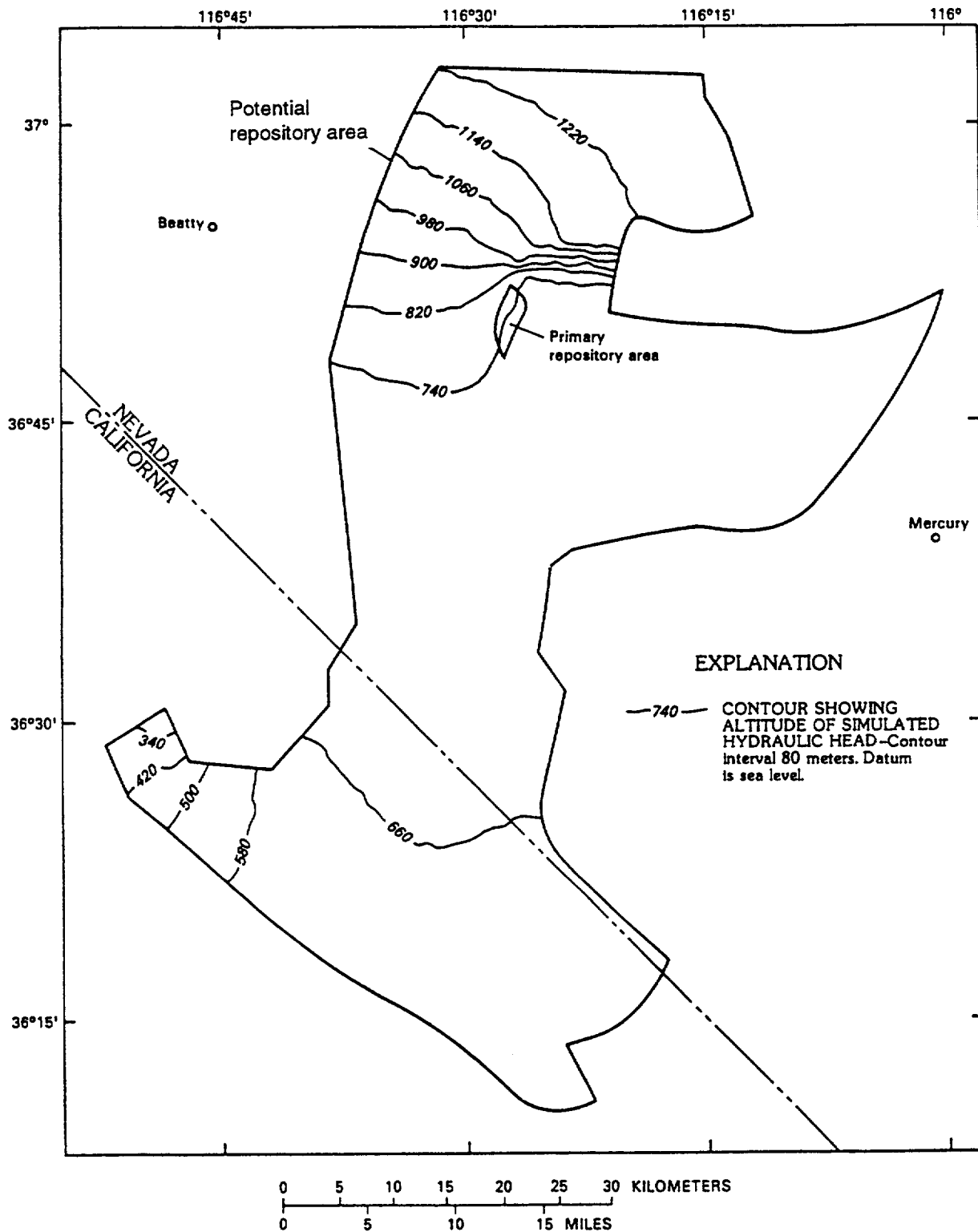


Figure 4-27. Map of region modelled by Czarnecki and Waddell, showing simulated hydraulic heads. (Taken from Figure 5 of Czarnecki and Waddell, 1984.)

tionality called the dispersivity α : $D_h = \alpha|v|$. Dispersivity may be different in the longitudinal direction (along the flow, α_L) and the transverse direction (perpendicular to flow, α_T). Dispersivity could be proportional to the distance over which it is measured (de Marsily, 1986). Anderson (1979) lists several studies of fractured basalt that show α_L in the range of 30.5 to 91 meters and α_T/α_L on the order of 1. The ratio α_T/α_L is usually lower in other studies, but a ratio of 1 could be reasonable in fractured tuffs because of the high tortuosity (compared with sediments) and the relatively low water velocities. A ratio of 1 was used for this study.

Two major sources of uncertainty were considered for the saturated zone. The first source of uncertainty is based upon the actual point of release within the repository and the path taken to the accessible environment. A uniform distribution of waste within the repository was assumed. The other parameter studied was the amount of dispersion present. Results were calculated using dispersivities of 0, 30, 60 (originally considered the most representative value), and 500 meters.

Because of numerical instability problems, zero dispersivity could not be modeled using STAFF2D, and therefore, a separate particle-transport computer program was written that does not include diffusion or hydrodynamic dispersion. The particle-transport code uses the flow field produced by a STAFF2D calculation and transports particles at the pore-water velocities with no molecular diffusion or hydrodynamic dispersion. 500 particles were released at random locations directly beneath the repository and tracked to the accessible environment. The times required for each particle were used to obtain a distribution of travel times, which is shown as the "No Dispersion" curve in Figure 4-28.

STAFF2D also includes its own transport model, which was used to produce and track a pulse release of solute directly under the repository. The solute was transported, and by calculating the amount that reached the accessible environment at each time step, a distribution of travel times was produced. Because the solute concentrations must be continuous, the pulse release could not be completely resolved by the calculational mesh, resulting in an inaccuracy caused by the numerical solution technique called "numerical diffusion."

Figure 4-28 also shows the three travel-time distributions obtained with the STAFF2D transport model. Because the particle method includes no dispersion, its travel-time distribution has a smaller range of travel times than the STAFF2D transport models. The STAFF2D transport simulations with dispersivity also include numerical diffusion and thus produced excessively broad predictions of travel times. Increase of dispersivity by almost an order of magnitude from 60 to 500 meters results in a broader distribution of travel times, but the relatively small change

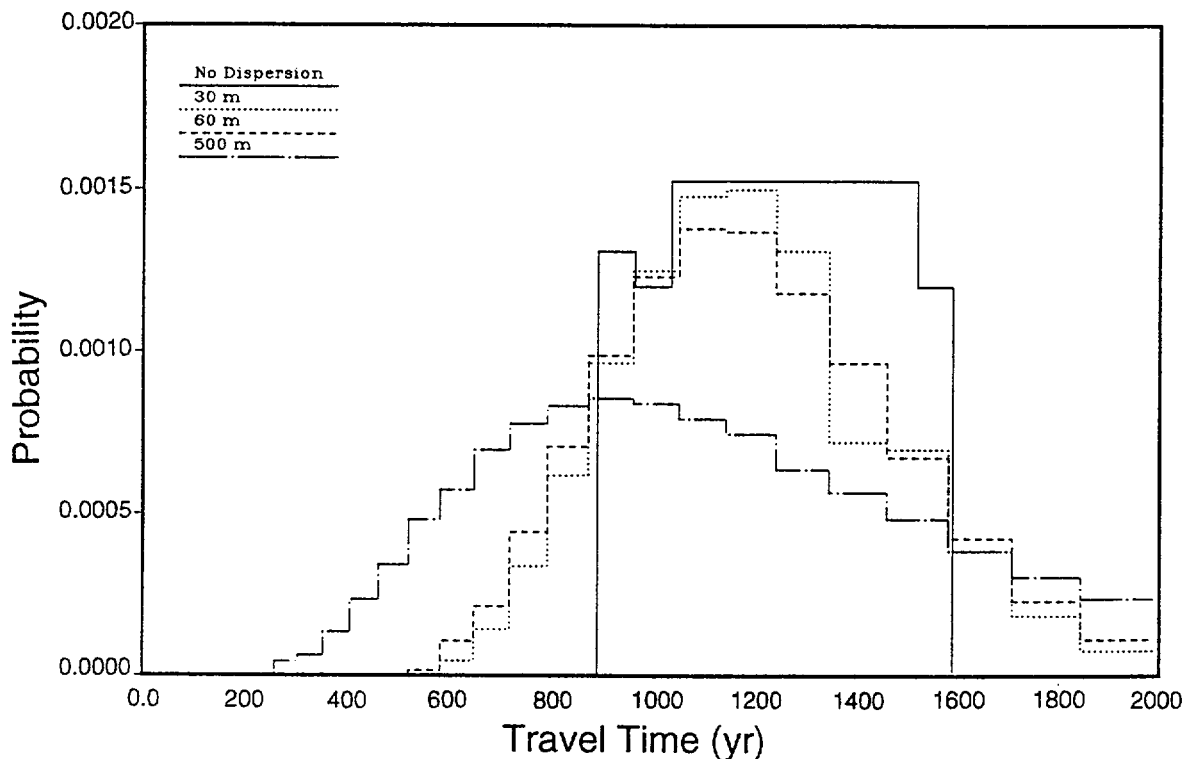


Figure 4-28. Histogram of saturated-zone travel times from the potential repository to the accessible environment: the solid line represents the results of tracking 500 particles from random locations beneath the potential repository to the accessible environment; the two dashed lines represent results of solute-transport calculations with 30- and 60-m dispersivity; the dotted line represents results of a solute-transport calculation with 500-m dispersivity.

shows that travel times are not very sensitive to the dispersivity. The distributions for 30- and 60-m dispersivities are very similar. This fact implies that the differences between the 30-m and 60-m distributions and the particle distribution result primarily from numerical diffusion. Because the probability distribution from the particle method does not have numerical diffusion, it is considered to be the most accurate model and was used to establish the velocity distribution for the TSA saturated-zone calculations. (With no dispersion included in the travel times, radionuclide dispersion during transport through the saturated zone has been modeled separately in the TSA calculations, as discussed in the next subsection.)

4.5.2 TSA model of saturated flow

Czarnecki's model of the saturated zone is a two-dimensional plane, 1000 m thick, consisting of a combination of the tuffaceous aquifer and the carbonate aquifer, and covering the general area around the potential repository and out beyond the

accessible environment. For the TSA calculations, the saturated-zone model was simplified to a one-dimensional flow tube 5125 m in length. Although the exact orientation is not significant, the flow tube is assumed to reach from inside the southeastern repository boundary, south by southeast to the accessible environment (see Figure 4-24). The flow tube extends 100 m upstream and 5000 m downstream of a 25-m-long "point source" region underlying the potential repository. The area of the flow tube is assumed to be 3000 m horizontally by 1000 m vertically; 3000 m is approximately the maximum length of the potential repository, and 1000 m is the depth assumed in Czarnecki's model. (Cross-sectional area is used to determine a representative concentration, but has no effect on the quantity of primary interest, the cumulative release to the accessible environment.) Figure 4-29 shows the saturated-zone geometry as used in the TSA for this study.

Both unsaturated-zone flow models—the composite-porosity model and the weeps model—were coupled to the same one-dimensional saturated-zone model. For every calculation, radionuclides released from the repository were distributed uniformly within the point-source region of the flow tube underlying the repository. Figure 4-30 shows how the releases from the six one-dimensional columns used by the composite-porosity model of the unsaturated zone were inserted into the TSA

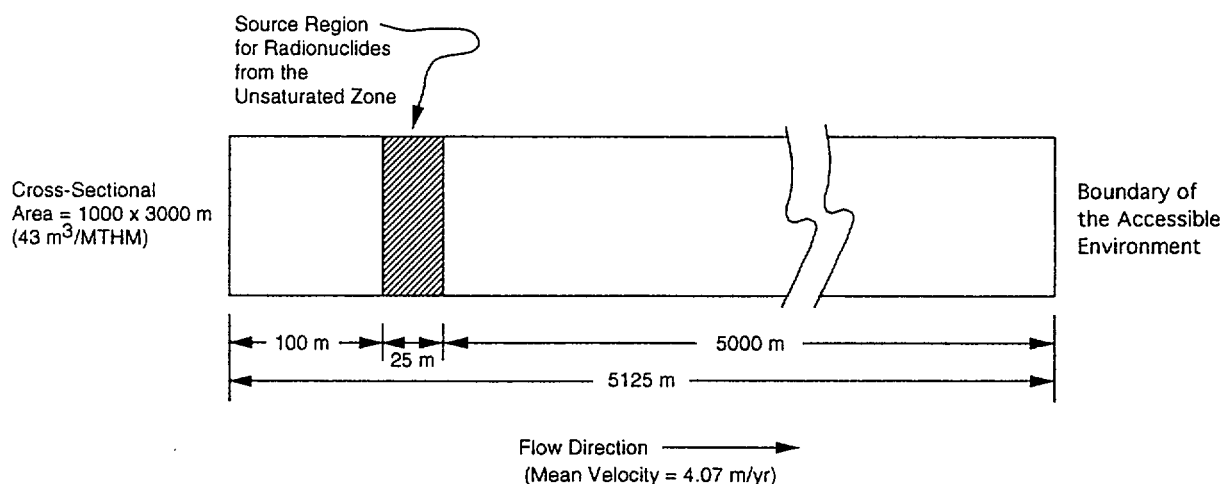


Figure 4-29. Geometry of the horizontal flow tube used in TSA calculations to model the saturated zone.

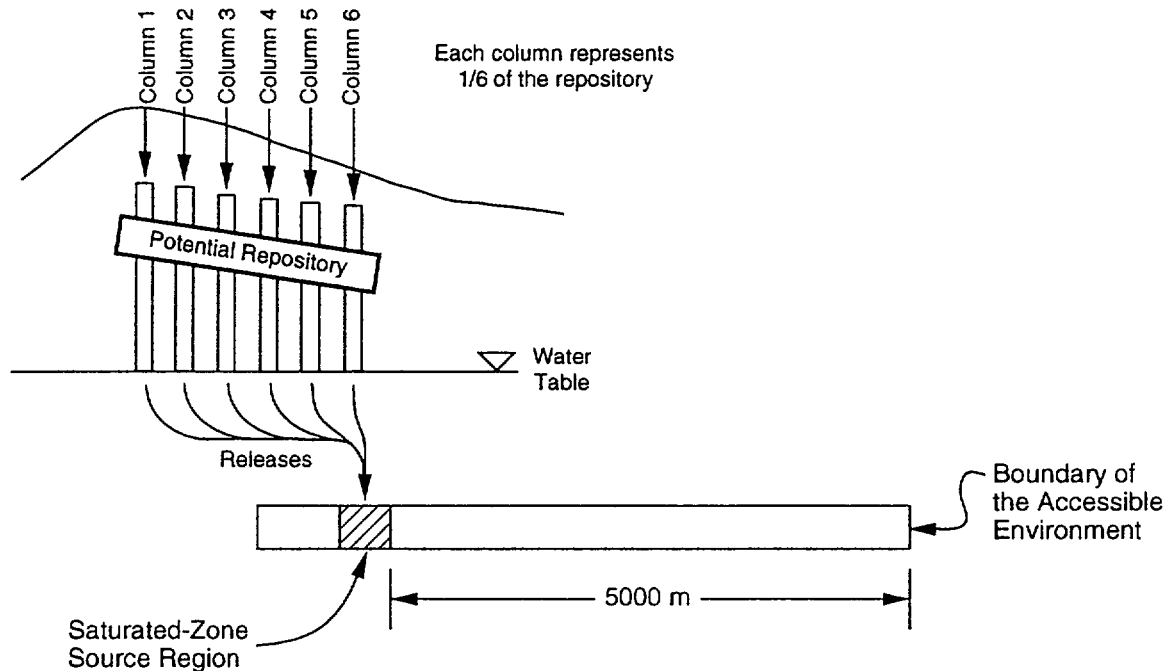


Figure 4-30. Coupling of the six vertical columns for the composite-porosity flow (TOSPAC/TSA) calculations with the horizontal flow tube used in TRANS/TSA calculations to model the saturated zone.

saturated-zone model. Figure 4-31 illustrates the coupling between the “nondimensional” weeps model and the TSA saturated-zone model.

The TRANS module of TOSPAC (Section 4.6) is used by the TSA to model transport in the saturated zone. The water velocities deduced from Czarnecki’s model were input parameters to TRANS (discussed below). The TRANS flow tube can pass through materials with different water velocities and porosities for both the matrix and fractures. In this study only one material was used, the same average of tuffaceous and carbonate materials used in Czarnecki’s model. Matrix and fracture quantities were not specified separately, as the Czarnecki values are a composite of the two.

As discussed in Section 4.5.1, using Czarnecki’s saturated-zone flow model in two dimensions, particles were distributed randomly within the potential repository boundary, released, and timed to the accessible environment. The resulting travel-time distribution implicitly contained the different distances traveled by each particle. The travel-time distribution was transformed into a velocity distribution for input to the TSA saturated-zone calculation by taking each travel time and dividing it into 5000 m to get an effective velocity. By doing this calculation, the distribution of travel times for the one-dimensional TSA calculations is the same as the distribu-

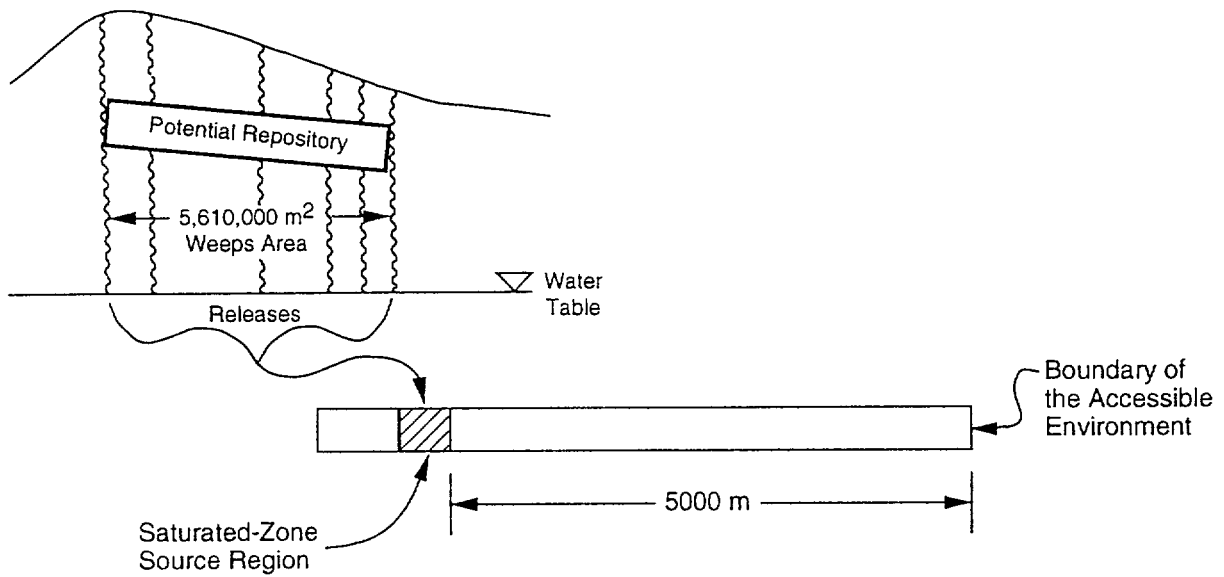


Figure 4-31. Coupling of the weeps-model (WEEPTSA) calculations with the horizontal flow tube used in TRANS/TSA calculations to model the saturated zone.

tion of travel times for Czarnecki's flow model. The resulting histogram of effective velocities is shown in Figure 4-32. Also shown in the figure is a beta distribution that is a fit to the histogram. The beta distribution is the distribution that was actually used in the TSA saturated-zone calculations.

4.5.3 Parameters for the saturated-zone flow model

Table 4-6 contains the parameters used by the TRANS module of TOSPAC in the TSA for modeling flow in the saturated zone. Water velocity is taken from the distribution shown in Figure 4-32. The porosity distribution was defined by a compilation of available porosity data (Section 4.5.1), fitted with a beta distribution.

Table 4-6. Parameters used to model the saturated zone.

Model parameter	Distribution	Distribution parameters ^a	Mean value
Groundwater velocity, v (m/yr)	beta	3.2, 5.9, 0.84, 2.87	4.07
Bulk porosity, n_b	beta	0.09, 0.29, 0.737693, 1.36935	0.175

^aParameters for the beta distribution are min, max, α , and β .

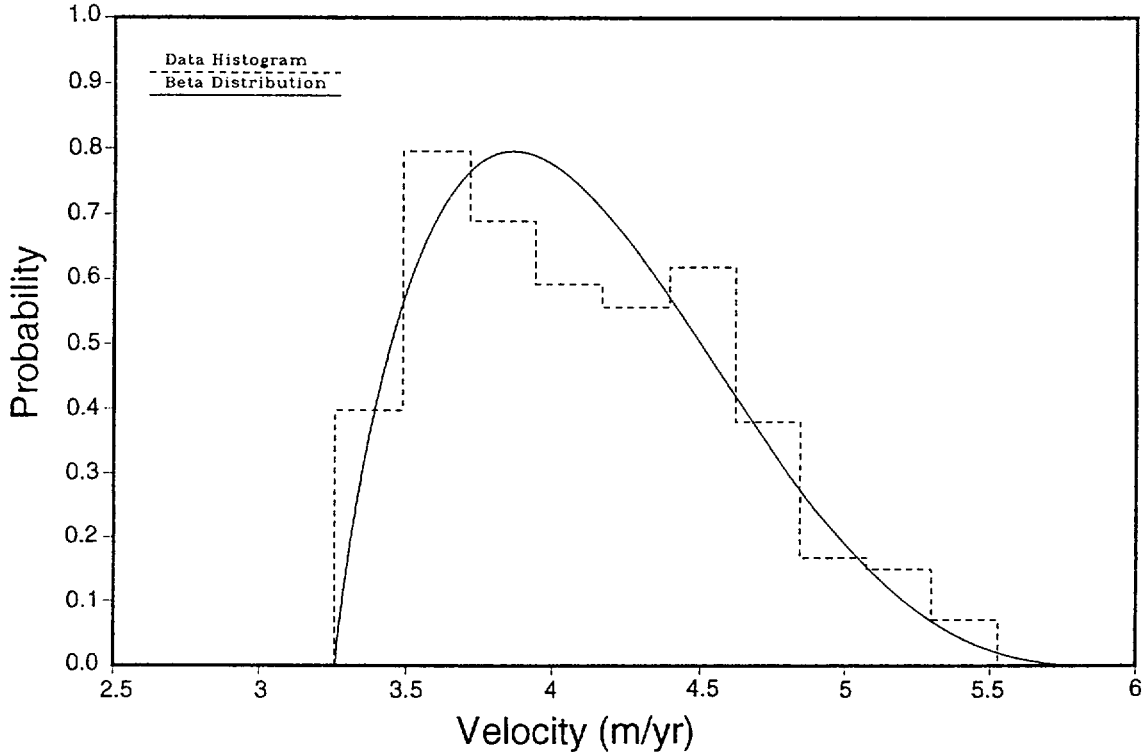


Figure 4-32. Probability density function of the effective water velocities used in the TRANS/TSA model of the saturated zone.

4.6 Transport model

4.6.1 The TOSPAC transport model

The transport model used by the TSA for this study is implemented in the TRANS module of the computer program TOSPAC; for a complete discussion of the model, see Dudley et al. (1988). The following is a general discussion of how the model represents transport, and the model assumptions that are significant to this study.

TRANS is a one-dimensional dual-porosity model of solute transport, containing two generalized advection-dispersion differential equations. The equation for solute transport through a rock matrix is as follows:

$$\begin{aligned}
 \frac{\partial}{\partial t}(R_m^i \theta_m C_m^i) &= -\frac{\partial}{\partial z}(C_m^i q_m - \theta_m D_m^i \frac{\partial C_m^i}{\partial z}) && \text{[Advective and Dispersive Terms]} \\
 &- \lambda^i R_m^i \theta_m C_m^i + \lambda^{i-1} R_m^{i-1} \theta_m C_m^{i-1} && \text{[Decay and Production Terms]} \\
 &+ \Sigma_m^i && \text{[Source Term]} \\
 &+ X^i, && \text{[Matrix/Fracture Transfer Term]}
 \end{aligned}
 \tag{4.55}$$

where R is the retardation factor, θ is the moisture content, C is concentration (the

unknown for which the equation is being solved), q is the groundwater flux, D is the dispersion coefficient, z is the elevation, λ is the radioactive-decay rate, Σ is the source term (zero everywhere except in the repository region), and X is the transfer term. The superscript i indicates a particular radionuclide and the subscript m indicates the matrix material. The equation for transport through the fractures is similar; a subscript f is simply substituted for the m subscript and the sign of the transfer term is reversed. The two equations are solved for the concentration of each radionuclide at a given problem time, and the solutions are joined via the transfer term (X). As indicated, the equations consist of terms describing the following phenomena: (1) movement of dissolved radionuclides in groundwater by advection and dispersion (including both molecular diffusion and hydrodynamic dispersion), (2) radioactive decay and production (when decay chains are specified) of radionuclides, (3) injection of radionuclides (when a source internal to the calculational mesh is specified—an external source is handled by a boundary condition), and (4) movement of radionuclides between the matrix and the fractures.

The dispersion factor is a combination of molecular diffusion and hydrodynamic dispersion, and is defined separately in the matrix and the fractures as follows:

$$D_m^i = \frac{D^i}{\tau_m} + \alpha_{Lm}|v_m|, \quad [\text{Matrix Diffusion and Dispersion}]$$

$$D_f^i = \frac{D^i}{\tau_f} + \alpha_{Lf}|v_f|, \quad [\text{Fracture Diffusion and Dispersion}] \quad (4.56)$$

where D is the free diffusion coefficient in water, τ is the tortuosity-constrictivity factor, α_L is the longitudinal hydrodynamic dispersivity, and v is the pore-water velocity, or average linear velocity of the groundwater. Hydrodynamic dispersion occurs only downstream in the direction of flow, diffusion occurs both upstream and downstream.

The retardation factor describes the geochemical effect of radionuclide adsorption to the surface of the porous medium through which it is being transported. The retardation factor is discussed in Section 3.4.

The transfer term allows an approximation of the two-dimensional movement of solute between matrix and fracture "pores" in the one-dimensional TRANS. Two processes are included in the transfer term: advective transfer, in which radionuclides follow the movement of water between the matrix and fractures, and diffusive transfer, in which radionuclides follow the concentration gradient between the ma-

trix and fractures. The equation for the transfer term is as follows:

$$X^i = \left(\frac{\partial \theta_m}{\partial t} + \frac{\partial q_m}{\partial z} \right) C^i(b) \quad [\text{Advective Coupling}]$$

$$+ \gamma_d \frac{\theta_m D^i / \tau_m}{a^2} (C_f^i - C_m^i), \quad [\text{Diffusive Coupling}] \quad (4.57)$$

where $C(b)$ is the concentration of a given radionuclide at the matrix/fracture boundary, a is one half of the distance between the centerlines of adjacent fractures (i.e., one half the fracture spacing), and γ_d is the matrix/fracture coupling factor, an input variable that is used to set the strength of the interaction between the matrix and fractures. In this study, only one setting ($\gamma_d = 1$) was used for the matrix/fracture coupling. The value of $C(b)$ depends on whether water is flowing from matrix to fractures or vice-versa, and it is defined as follows:

$$C^i(b) = \begin{cases} C_f^i & \text{if } X_{advective}^i > 0 ; \\ C_m^i & \text{if } X_{advective}^i < 0 . \end{cases} \quad (4.58)$$

The equations in TRANS apply to both the unsaturated zone and the saturated zone, and TRANS was used in this study to model both regions. For modeling the unsaturated zone, the hydrologic parameters—percolation rate (q), pore-water velocity (v), and moisture content (θ)—are supplied by the composite-porosity model as programmed in the STEADY module of TOSPAC (Section 4.4.1); for modeling the saturated zone, the hydrologic parameters are contained in the input file and are given in Table 4-6. In this study, TRANS is used to model the unsaturated zone only for the composite-porosity model; for the weeps model, transport in the unsaturated zone is assumed to be instantaneous (radionuclides released from the EBS are immediately injected into the saturated zone). TRANS is used to model the saturated zone for both the composite-porosity model and the weeps model.

Figure 4-33 presents an example of the results of a single transport calculation using TRANS. The calculation involved transport in the unsaturated zone, based on the composite-porosity model of flow, with the stratigraphy of Column 1. The mean values of all the parameters of the flow, source, and transport models were used. (Section 4.8 contains a discussion of these average-case problems; note that they extend for 1,000,000 years into the future).

The figure shows the distribution in space and time of the radionuclide ^{79}Se . The lines orthogonal to the elevation axis coincide with points in the calculational mesh. The dark bands are regions of closely spaced calculational mesh points that coincide with the boundaries between strata. The lines orthogonal to the time axis correspond to user-specified snapshots of the concentration data. The peak in the

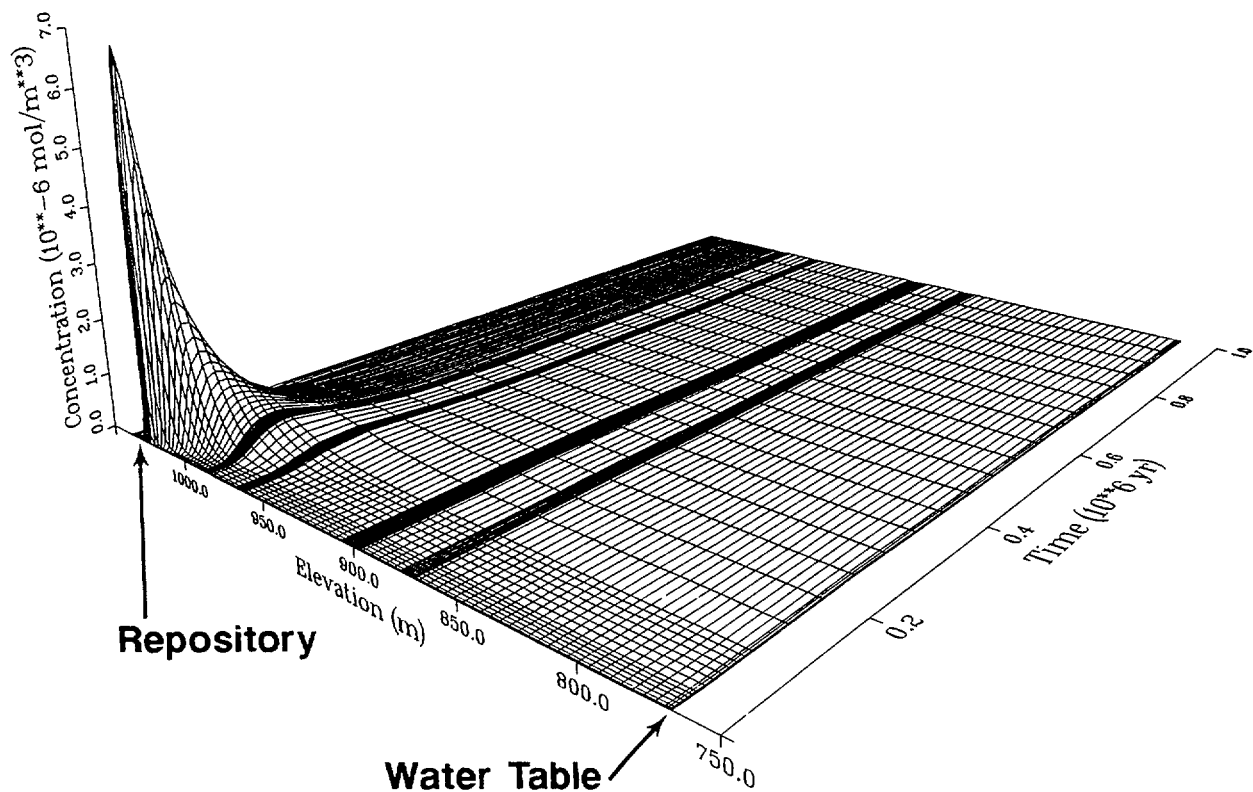


Figure 4-33. Concentration surface of ^{79}Se over time and elevation in the unsaturated zone, as calculated by the TSA radionuclide transport model, TRANS, using the composite-porosity flow field from Column 1.

figure represents ^{79}Se being released from the repository. As time increases, the ^{79}Se is transported downstream and begins to decay (^{79}Se has a half-life of 65,000 years). Because of the linear scale, it is not obvious that some ^{79}Se reaches the lower boundary (766-m elevation).

Figure 4-34 presents the concentration of ^{79}Se as it is transported through the saturated zone. The ^{79}Se in this figure comes directly from the ^{79}Se that reaches the lower boundary in Figure 4-33. The radionuclides are injected at a distance of 5000 m from the boundary of the accessible environment; the boundary of the accessible environment is located at 0 m. The concentration peak is approximately 8 orders of magnitude lower in Figure 4-34 than it is in Figure 4-33. Much of the ^{79}Se has decayed away or been adsorbed in the unsaturated zone; however, the concentration is also significantly reduced by dilution in the 1000-m thick saturated zone. No dark bands occur in the plot because a single material was used to model the saturated zone, and it required only a uniform calculational mesh.

Figure 4-35 shows the concentration of ^{79}Se in time and space as it is transported through the saturated zone using the releases generated with the weeps model. (The surface represented in the figure is not particularly smooth because of the coarse

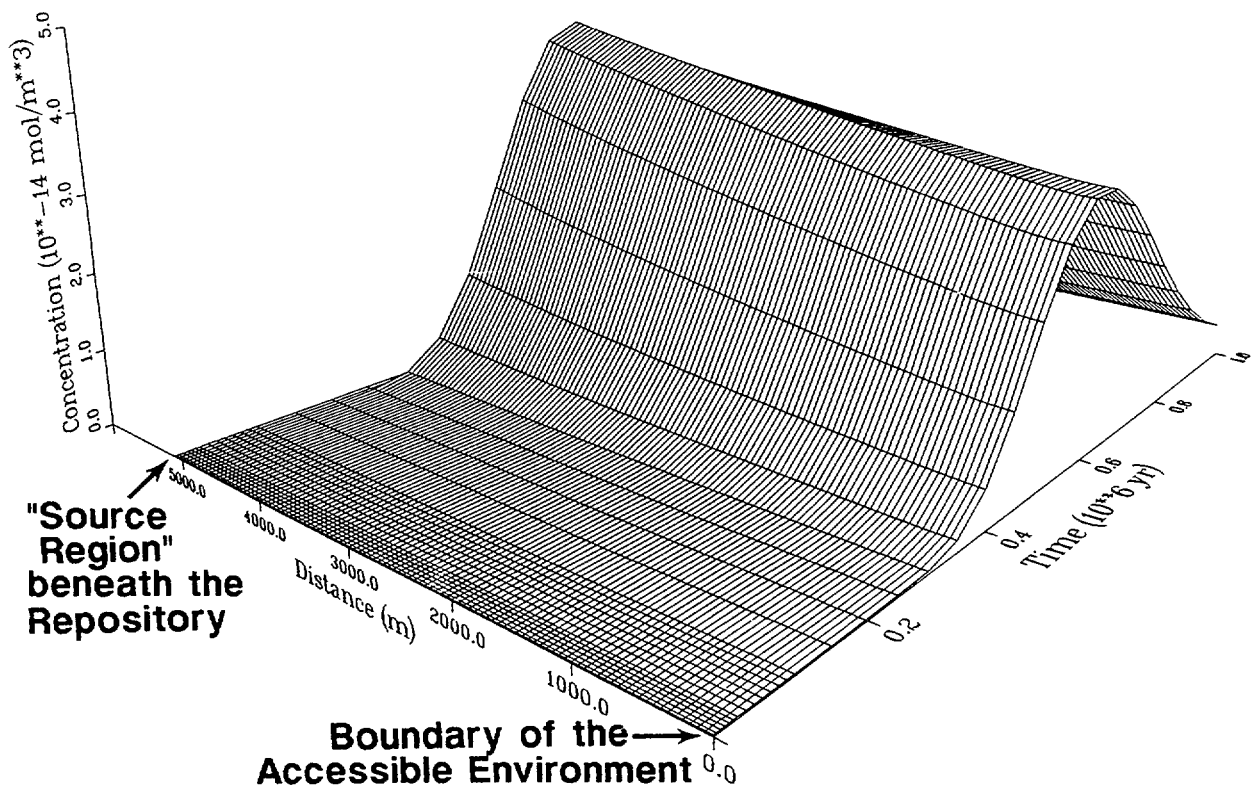


Figure 4-34. Concentration surface of ^{79}Se over time and distance in the saturated zone, as calculated by the TSA radionuclide transport model, TRANS, using the ^{79}Se that reached the bottom boundary of Column 1.

spacing of data points.) Transport through the unsaturated zone is assumed to be instantaneous in the weeps model; hence, only transport through the saturated zone is considered. The figure shows a concentration peak of approximately 10^{-11} mol/m³ directly under the repository. This peak is higher than the peak in Figure 4-34, because the unsaturated zone is not a significant barrier to radionuclide transport in the weeps model.

Radionuclide releases are calculated in TRANS from changes in concentration at the problem boundary, indicating the amounts of radionuclides leaving the problem domain. Section 4.8 contains a discussion of radionuclide releases from the same transport calculation that produced the concentration surfaces shown in Figures 4-33, 4-34, and 4-35. (The results are shown later in Figures 4-46 and 4-50.)

The TRANS module of TOSPAC can simultaneously solve for the transport of up to 50 radionuclides. Nine radionuclides (Table 4-1) were considered for the aqueous-release part of this study.

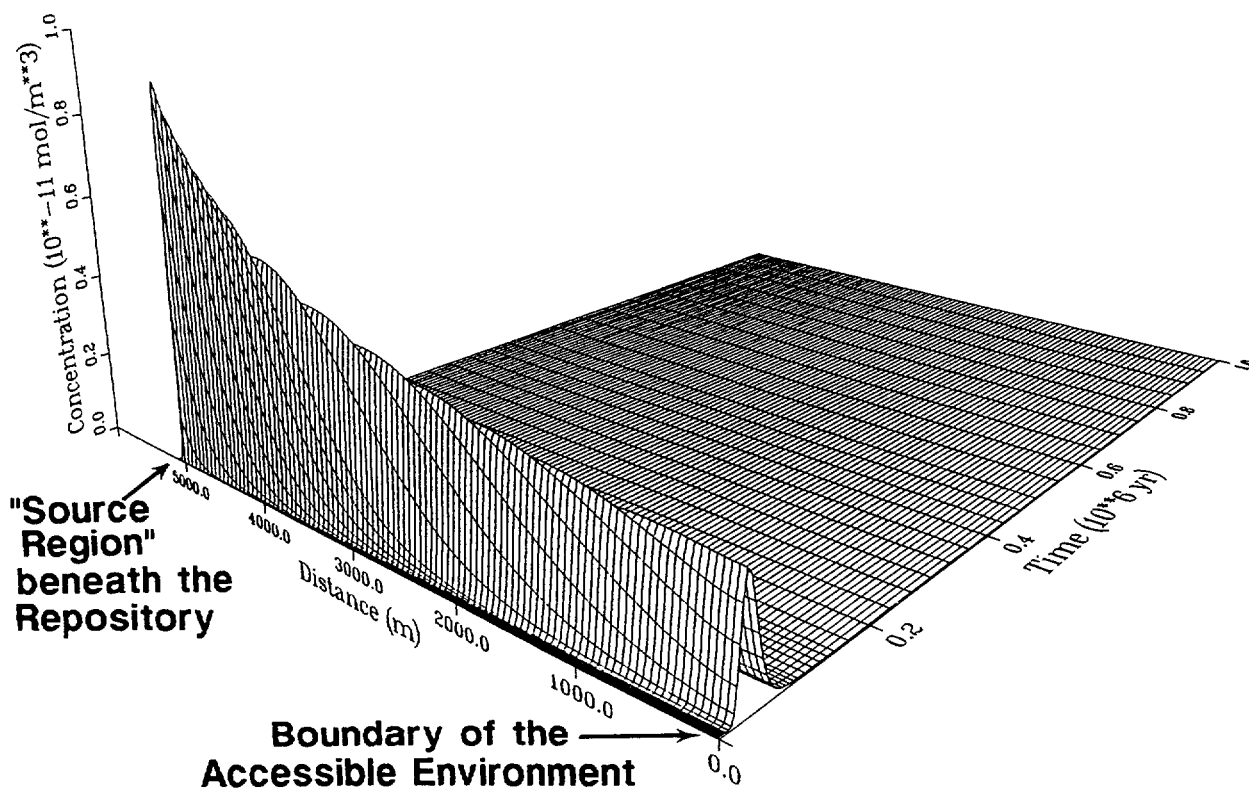


Figure 4-35. Concentration surface of ^{79}Se over time and distance in the saturated zone, as calculated by the TSA radionuclide transport model, TRANS, using the ^{79}Se released by the weeps model.

4.6.2 Parameters for the transport model

Table 4-7 presents the parameters used by TRANS for modeling transport of radionuclides. For unsaturated-zone transport, TRANS uses the same geometry and calculational mesh that are used in the flow calculation by STEADY (Section 4.4.2). For saturated-zone transport, TRANS uses the geometry defined in Section 4.5.2.

The diffusion coefficient is a standard value for diffusion in water; for example, see Travis et al. (1984).

A study of tortuosity for diffusion in tuff by Daniels et al. (1982) found values near 10. This value has commonly been used in performance-assessment calculations (e.g., Dudley et al., 1988, and Barnard and Dockery, 1991). Fracture tortuosity is set to 1, as the tortuosity of a fracture path is likely to be small compared to the tortuosity of a matrix path. (Note that a tortuosity of 10 was used for the combination of matrix and fractures constructed for the saturated-zone calculations.)

The appropriate value to use for dispersivity is uncertain, as discussed already in Section 4.5.1. Dispersivity could be sensitive to the scale over which it is measured (de Marsily, 1986). No data are available from the Yucca Mountain site, so we were forced to estimate the dispersivity from information in the literature. De Marsily, in

Table 4-7. Parameters used to model transport.

Model parameter	Distribution	Distribution parameters ^a	Mean value
Diffusion coefficient, D (m ² /yr)	—	—	3.16×10^{-2}
Matrix tortuosity factor, ^b τ_m	—	—	10
Fracture tortuosity factor, ^b τ_f	—	—	1
UZ dispersivity, ^b α_L (m)	uniform	10, 25	17.5
SZ dispersivity, α_L (m)	log-uniform	50, 500	195
Fracture distribution coefficient, ^{b,c} K_a	—	—	0
Matrix distribution coefficient, ^{b,c} K_d	see Table 3-7		
Bulk density, ^b ρ_b	see Table 3-26		
Fracture spacing, welded (m)	—	—	0.0353
Fracture spacing, vitrophyre (m)	—	—	0.0281
Fracture spacing, vitric (m)	—	—	0.500
Fracture spacing, zeolitic (m)	—	—	0.625
Fracture spacing, partially welded (m)	—	—	0.227
Matrix/fracture coupling factor, ^b γ_d	—	—	1
Matrix velocity correlation length ^b	—	—	0
Fracture velocity correlation length ^b	—	—	0

^a Parameters for the uniform and log-uniform distributions are minimum, maximum.

^b For all layers.

^c For all radionuclides.

his discussion of hydrodynamic dispersion, gives a rule of thumb that longitudinal dispersivity tends to be approximately one tenth of the flow-path length. The distribution used for dispersivity in the unsaturated-zone calculations is based on this rule of thumb. The unsaturated-zone flow-path length for the six columns used varies from 185 m to 257 m. For simplicity, it was decided to sample from dispersivities between 10 m and 25 m, and to use the same distribution for each of the columns and in each of the geologic units, rather than trying to match the actual flow-path length. A uniform distribution was used in the absence of any information about the actual shape of the distribution. For a saturated-zone flow-path of 5000 m to the accessible environment, the rule of thumb implies a dispersivity of 500 m. This value is high compared to typical measured values (Anderson, 1979, lists values for fractured basalt ranging from 30.5 m to 91 m), but then measurements over a 5000-m distance are unusual. Because of the great uncertainty, it was decided to assume a log-uniform distribution between the two extremes, rounded to 50 m and 500 m.

The last two parameters listed in the table, the coupling factor and the velocity correlation length, are particular to the TOSPAC transport model, and the reader is referred to Dudley et al. (1988) for a full description of their meaning. By setting the velocity correlation length to zero, we are forcing the TOSPAC dispersion model to use the standard $D_h = \alpha_L|v|$ for hydrodynamic dispersion (except that hydrodynamic

dispersion is always set to zero upstream of the source). The coupling-strength parameter γ_d was discussed briefly above. Choosing 1 for its value causes a strong enough matrix/fracture coupling that the matrix and fracture concentrations are essentially always in equilibrium ($C_m = C_f$), even at the highest percolation rates considered in this study. The fracture spacings listed in Table 4-7 are used only in calculating the matrix/fracture coupling strength (Equation 4.57). The results are not sensitive to the fracture spacing (unless γ_d is reduced—see Dudley et al., 1988), so a single value was used for each unit rather than defining a probability distribution. The saturated-zone transport calculations lumped the matrix and fractures into a single equivalent porous medium, so no fracture spacing was required and the matrix/fracture coupling term had no effect in those calculations.

4.7 Results

Primary results of the determination of the aqueous releases of radionuclides from a potential repository at Yucca Mountain were achieved by Monte Carlo simulation using the models described in Sections 4.3 through 4.6. The Monte Carlo simulations were conducted over a time frame of 10,000 years to allow comparison with the EPA performance measure. (Also, longer time frames would have greatly increased computing costs. Selected deterministic calculations have been made, however, which simulate a period of 1,000,000 years. See the examples in Sections 4.4 and 4.6, and the discussion in Section 4.8.) The intent of this section is to describe the gross behavior of the models with the entire input-parameter distributions. In Section 4.8, deterministic calculations are examined to show the more detailed behavior of the individual models.

It should be stressed that the determination of the aqueous releases of radionuclides from a potential repository at Yucca Mountain is an evolving endeavor, dependent on the validity of the models used and the accuracy of the input data. The results presented in this chapter are not final. They are offered to provide insight into the TSPA process in general, and into the present state of modeling aqueous-release mechanisms at Yucca Mountain.

The results are presented in terms of three performance measures: the Environmental Protection Agency containment standard (EPA, 1985); the Nuclear Regulatory Commission limit for release rates from the Engineered Barrier System; and, the NRC-established minimum for pre-waste-emplacement groundwater travel time (both NRC, 1983). None of these performance measures is entirely applicable to a rigorous comparison with TSPA results: the EPA standard has been remanded back to the EPA by U. S. District Court and is currently being rewritten; the EBS is being

designed to meet the NRC release-rate criterion, so a release model that shows a violation of that criterion is probably unrealistic; and the groundwater-travel-time criterion applies to pre-waste-emplacment conditions, whereas the TSPA calculations are intended to represent future conditions (the water percolation rate, in particular, is thought to be lower under present conditions than assumed here.) The performance measures are used in this discussion solely as a background for presenting the results; these results are too preliminary to be used as evidence for or against regulatory acceptance.

Because of the uncertainty in the applicable conceptual model of flow for Yucca Mountain, the results are presented separately for the composite-porosity model and the weeps model. The results show aqueous releases within 10,000 years to be surprisingly similar for both flow models when judged against the EPA release limit. However, when judged against the NRC performance measures, the two models show quite different behavior.

4.7.1 Comparison of results using the composite-porosity model with performance measures

For the composite-porosity model, 1800 separate deterministic calculations were made using the STEADY (unsaturated, steady-state flow), TRANS (radionuclide source and unsaturated-zone transport), and TRANS (saturated-zone transport) modules of TOSPAC in the TSA; 300 realizations were calculated for each of the six columns described in Section 4.4.2. The number of calculations was chosen as a compromise between minimizing computer time and maximizing the number of realizations for the columns on the eastern half of the repository block, from where we believed most of the releases would come in 10,000 years. The method used for combining the results of the six columns is discussed in Chapter 8. For each calculation, the cumulative amounts of radionuclides released at the following boundaries in 10,000 years were saved: (1) the engineered barrier system (effectively, the boundary of the source region), (2) the water table (the boundary of the unsaturated zone), and (3) the accessible environment.

The remanded EPA standard (EPA, 1985) specifies probabilities that cumulative releases of radionuclides to the accessible environment shall not exceed certain levels (see Table 4-1) within 10,000 years. Figure 4-36 presents conditional CCDFs for aqueous releases from the EBS, from the unsaturated zone, and to the accessible environment, as calculated by the TSA using the composite-porosity model of flow. The plot shows the probability of achieving a given release in terms of the EPA sum. The EPA sum is the sum of the ratios of the cumulative release of a radionuclide and

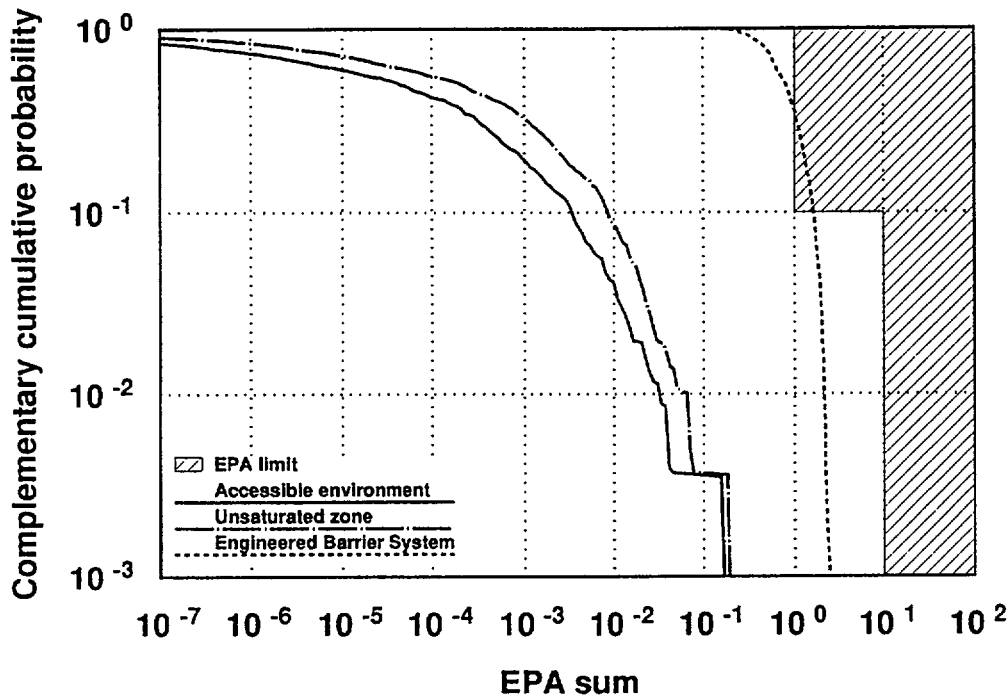


Figure 4-36. Conditional CCDFs for aqueous releases, calculated using the composite-porosity model of flow. Shown are partial EPA sums calculated using releases from the EBS, releases from the unsaturated zone, and releases to the accessible environment.

the EPA-prescribed limit for that radionuclide, as given in the following equation:

$$M = \sum_i \frac{Q_i}{L_i}, \quad (4.59)$$

where M is the normalized cumulative release (the EPA sum), Q_i is the cumulative radioactivity of the i th radionuclide released to the accessible environment within 10,000 years, and L_i is the EPA limit for the i th radionuclide (given in Table 4-1 for the radionuclides used in this study). The quotient Q_i/L_i is known as the EPA ratio for radionuclide i . The cross-hatched area in Figure 4-36 indicates regions where the EPA limit is exceeded; however, it applies only to releases to the accessible environment (the normalized releases from the EBS and from the unsaturated zone are not actually EPA sums because they do not represent releases to the accessible environment). Also, note that the EPA sums shown in Figure 4-36 are really *partial* EPA sums because they include only aqueous releases and not releases by other mechanisms.

The figure indicates that the calculated aqueous releases to the accessible environment are approximately two orders of magnitude below the EPA limit. The

releases to the water table are well below those from the EBS, indicating that the unsaturated zone is a significant barrier to the release of radionuclides. A number of processes contribute to this obstacle, including the generally long travel time associated with the composite-porosity model (a median of approximately 70,000 years, and a mean of approximately 500,000 years, as discussed below); the close coupling of the matrix and fractures afforded by the composite-porosity model, and our modeling of the matrix/fracture coupling factor in TRANS, allowing significant matrix diffusion of radionuclides; and the retardation of most radionuclides by adsorption. As indicated on the plot, however, the saturated zone adds little additional impediment to the radionuclides. Although matrix diffusion and radionuclide retardation are just as operable in the saturated zone, the groundwater travel time for the present saturated-zone model is only about 1200 years and the unretarded radionuclides are transported relatively quickly through the saturated zone to the accessible environment.

As mentioned previously, the number of deterministic calculations used in the Monte Carlo simulation has a direct bearing on the resolution of a given probability. At the extremely low probabilities, only a few calculations are contributing to the CCDFs. The sharp jump in the unsaturated-zone and saturated-zone curves at a probability of approximately 0.003 is caused by the lack of resolution when only a few realizations have relatively high releases.

Figure 4-37 shows the conditional CCDFs for the total release to the accessible environment, and for the major radionuclides contributing to the total release. Figure 4-38 offers a pie chart showing the contribution of the major radionuclides to the mean partial EPA sum. The figures indicate that ^{99}Tc and ^{129}I dominate the releases. Several reasons combine to produce this situation. First, ^{99}Tc and ^{129}I are highly soluble. Second, ^{99}Tc and ^{129}I are released from the waste form at the matrix-alteration rate—the fastest rate considered. And perhaps most significantly, of the ten radionuclides included in this study, only ^{14}C , ^{99}Tc , and ^{129}I were considered nonsorbing, and therefore their transport was unretarded through both the unsaturated and saturated zones. (^{14}C was not considered for aqueous releases in this study and is therefore absent from Figures 4-37 and 4-38—see Chapter 5.)

Figure 4-39 illustrates performance of the source model with composite-porosity flow, based on the NRC release-rate limit from the EBS of one part in 10^5 per year (10 CFR 60.113; see Table 4-1 for a list of the NRC release-rate limits for the nuclides included in this study). In the figure, the NRC limit is normalized to 1, and a CCDF of peak normalized release rates has been constructed. Results from both the composite-porosity model and the weeps model are shown. Values greater than 1

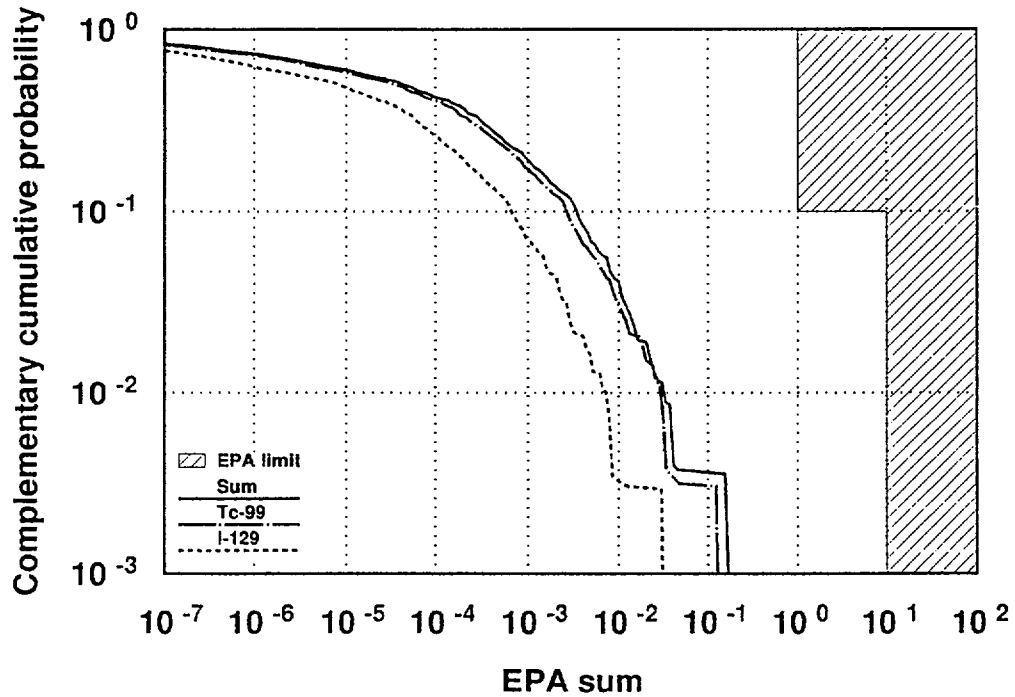


Figure 4-37. Conditional CCDF for aqueous releases to the accessible environment, calculated using the composite-porosity model of flow. Also shown are probability distributions of the EPA ratios of ^{99}Tc and ^{129}I .

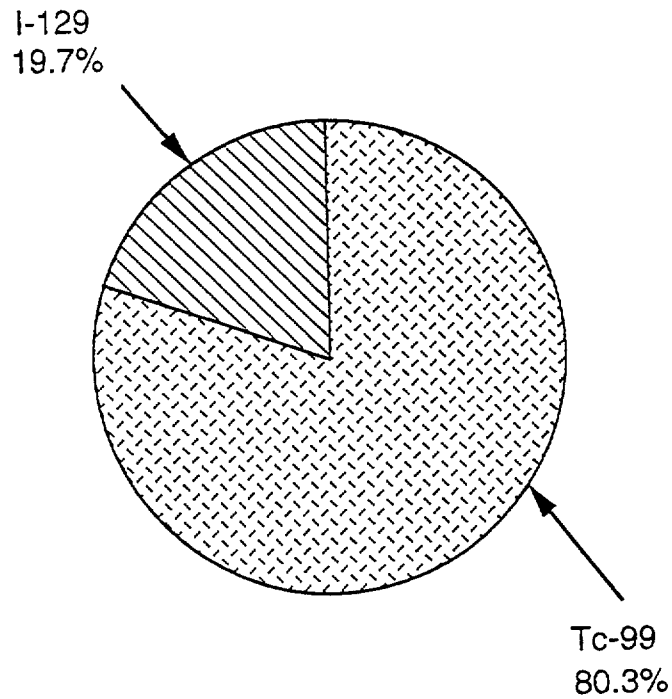


Figure 4-38. Contribution of individual radionuclides to the mean partial EPA sum, calculated using the composite-porosity flow model.

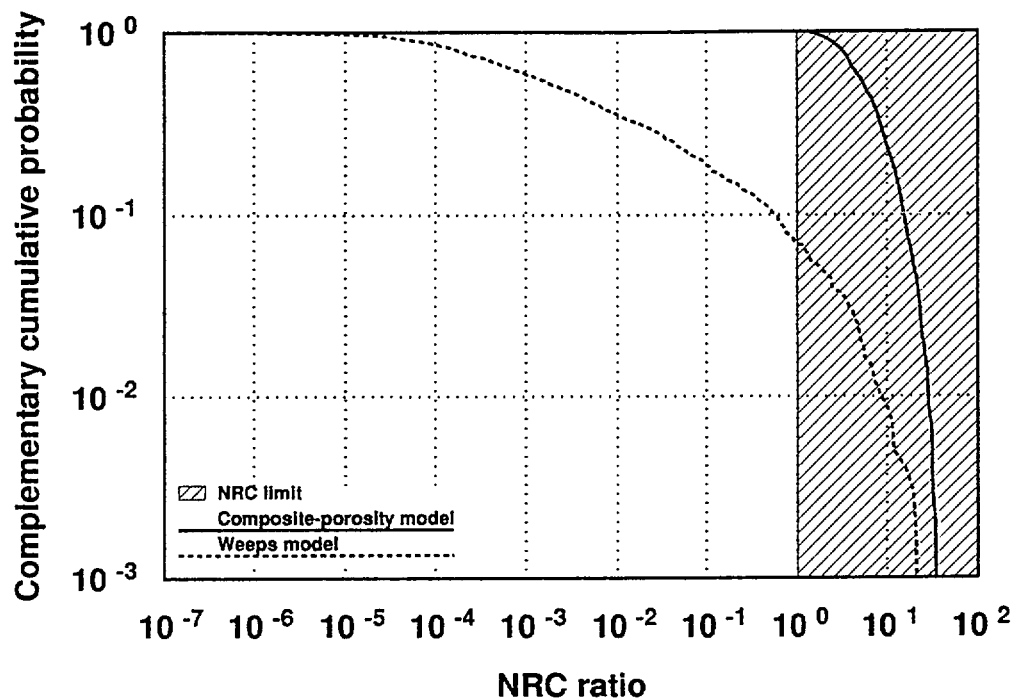


Figure 4-39. Probability distributions of the NRC ratio, calculated for the composite-porosity model and for the weeps model.

exceed the NRC limit, and the probability of exceeding this value can be determined from the CCDF. The EBS will be designed to meet the NRC limit; therefore, the intent of this figure is not to show compliance with the NRC limit, rather the intent is as follows: (1) to indicate how the source model used in this TSPA behaves given the composite-porosity flow, (2) to determine the extent to which releases from the EBS contribute to releases to the accessible environment in 10,000 years, and (3) to offer a quantitative basis for comparing the behavior of the source-term models for composite-porosity flow and for weeps flow.

For the source model used, ^{99}Tc has the highest normalized release rate, so the NRC ratios shown in Figure 4-39 for the composite-porosity model are the NRC ratios for ^{99}Tc . As shown, exceeding the NRC limit is certain, given the source model and parameter distributions that were used. As modeled, excessive releases result from the assumption that matrix alteration allows rapid dissolution of volatile radionuclides and from the neglect of the container and cladding as barriers to transport out of a waste container. Also, the composite-porosity model produces a widespread flow field that contacts all the containers.

It is worth noting that the distribution of percolation rates used could be unrealistically high for the composite-porosity model, because of lateral diversion of flow

in the units above the repository. The Paintbrush nonwelded unit has properties of a capillary barrier, and could divert water in such a way as to keep the percolation rate from exceeding the saturated conductivity of the matrix in the "welded" layer (Ross, 1990; Prindle and Hopkins, 1990). For these simulations, percolation rate was assumed to have an exponential distribution with a mean of 1 mm/yr. The matrix saturated conductivity of the welded layer was assumed to have an exponential distribution with a mean of 0.66 mm/yr. Thus, the percolation rate exceeds the saturated conductivity of the matrix in a majority of the Monte Carlo realizations. If the Paintbrush nonwelded unit is effective as a capillary barrier, it would be more realistic to keep the percolation rate equal to or less than the saturated conductivity of the welded matrix.

Although our source model for composite-porosity flow is shown to exceed the NRC limit, the EPA limit is not exceeded (Figure 4-36). That is, the high releases from the EBS do not necessarily result in high releases to the accessible environment in 10,000 years. The relatively uniform percolation field dictated by the composite-porosity model subjects a large number of containers to destructive conditions that result in high releases from the EBS, but this same flow field moves so slowly that the released radionuclides remained trapped in the mountain for very long periods of time (see the discussion of Figure 4-36).

Figure 4-40 shows distributions of travel time for an unretarded tracer. Travel times through the unsaturated zone and through the saturated zone are shown separately in the figure. The total travel time would be a combination of the two, but because the unsaturated-zone travel time is so much longer than the saturated-zone travel time, the combination curve would be very similar to the unsaturated-zone curve. Because the weeps model carries the assumption of zero travel time in the unsaturated zone, the curve for the saturated zone also represents the total travel time for an unretarded tracer in the weeps model (Section 4.7.2). The curves represent a combination of travel-time distributions from 1800 unsaturated-zone calculations and 1000 saturated-zone calculations.

Figure 4-40 may be thought of as a comparison of our water-flow models with the NRC criterion requiring a minimum groundwater travel time (GWTT) along the fastest path of likely radionuclide transport of at least 1000 years (10 CFR 60.113). These travel-time results are presented as an illustration of the properties of the models being used, and not as a formal estimate of compliance with the NRC GWTT criterion. Three factors must be kept in mind in comparing our results with the NRC regulation. (1) The NRC criterion relates to *pre-waste-emplacement* groundwater travel time. The water-flux distribution used for this study is intended to repre-

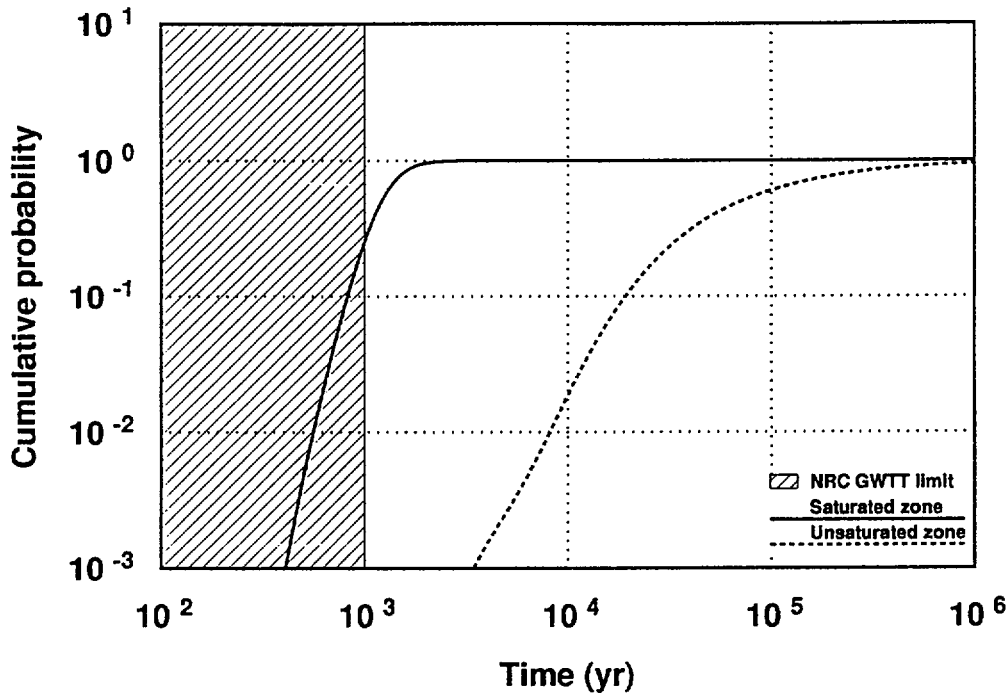


Figure 4-40. Distributions of travel times for an unretarded tracer through the unsaturated zone (with composite-porosity flow) and through the saturated zone.

sent the distribution of possible flux values over the next 10,000 years, which is likely to be higher than the distribution of values at the present time. As already discussed, neither of these distributions is well-known. (2) The NRC regulation governs groundwater travel time from the disturbed zone to the accessible environment. We have not attempted to define the disturbed zone for our problem, but have simply calculated travel times from the repository to the accessible environment. (3) The travel-time distributions presented in Figure 4-40 are distributions of the travel time of a nonsorbing tracer. Tracer travel time could be the best quantity to represent paths of "likely radionuclide travel," but this interpretation is controversial.

The median tracer travel time through the unsaturated zone is approximately 70,000 years, while the mean travel time is a very long 500,000 years. (The median can be read off the plot; the mean is calculated from the data that were used to make the plot.) The mean is longer than the median because some extremely long travel times are included in the data. All the unsaturated-zone travel times shown are greater than 2000 years, and 98 percent are greater than 10,000 years. The median travel time for the saturated zone is approximately 1200 years, while the mean travel time is 1300 years. For the saturated zone alone, approximately 75 percent of the travel times are in excess of 1000 years.

4.7.2 Comparison of results using the weeps model with performance measures

For the weeps model, 1000 separate deterministic calculations were made by the TSA using WEEPTSA (radionuclide source and unsaturated-zone fracture flow) coupled with the TRANS (saturated-zone transport) module of TOSPAC. The number of calculations was chosen so that a probability of 10^{-3} could be achieved when building a CCDF.

Figure 4-41 presents a comparison of releases generated by the weeps model with the (remanded) EPA release standard. Shown are conditional CCDFs for aqueous releases from the EBS, from the unsaturated zone, and to the accessible environment. The plot shows the probability of achieving a given release in terms of the partial EPA sum. Again, the cross-hatched area indicates infringement on the EPA limit, but it only applies to releases to the accessible environment.

The figure shows that aqueous releases to the accessible environment are about one order of magnitude below the EPA limit. Indeed, releases directly from the EBS are about one order of magnitude below the EPA limit. As shown in the figure, once radionuclides are released from the waste containers, there is little obstruction to reaching the accessible environment. The difference between the releases from

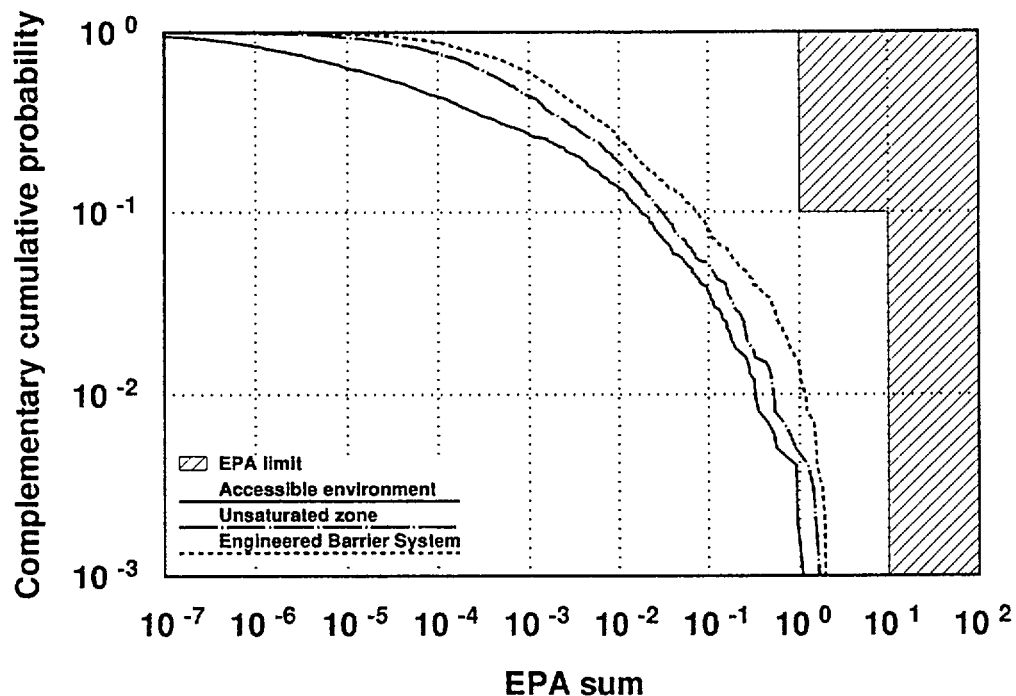


Figure 4-41. Conditional CCDFs for aqueous releases, calculated using the weeps model of flow. Shown are partial EPA sums calculated using releases from the EBS, releases from the unsaturated zone, and releases to the accessible environment.

the EBS and the unsaturated-zone is entirely caused by the absorption factor in the weeps model that estimates the fraction of radionuclides that is transported to the water table down the weeps (the remaining fraction being assumed to remain behind in the unsaturated zone, at least on a time scale of 10,000 years). The absorption factor was described by a uniform distribution between 0 and 1 (for maximum uncertainty), and thus the unsaturated-zone-release curve averages a factor of two less than the EBS curve. The difference between the releases from the unsaturated zone and to the accessible environment is a reflection of the saturated-zone travel time. The difference is slightly greater than that seen for the composite-porosity model (Figure 4-36), because sorbing radionuclides are only retarded in the saturated zone with the weeps model, while strongly sorbing nuclides do not even reach the saturated zone within 10,000 years with the composite-porosity model. As with the results for the composite-porosity model, the CCDF for releases to the accessible environment is not greatly different from the CCDF for releases to the saturated zone because the saturated-zone travel times (see Figures 4-28 and 4-40) assumed for this study for ^{99}Tc and ^{129}I are small compared to the EPA time period of 10,000 years.

Comparison of Figure 4-41 with Figure 4-36 indicates that while releases to the accessible environment calculated using the weeps model are greater than releases calculated using the composite-porosity model, releases from the EBS are much lower. The reason is significant: weep flow contacts fewer containers than composite-porosity flow. And in the weeps model, containers not subjected to flow do not fail.

In Figure 4-42, the major radionuclides that contribute to the total releases to the accessible environment are represented by individual CCDFs. The dominant radionuclides are again the nonsorbing radionuclides ^{99}Tc and ^{129}I , as shown also in the pie-chart in Figure 4-43. For the weeps model, however, several other radionuclides contribute slightly to the results: ^{79}Se , ^{234}U , and ^{237}Np . These other radionuclides are relatively weakly sorbing and are therefore not strongly retarded in the saturated zone. The saturated zone still provides a significant barrier for most of these additional, weakly sorbing radionuclides (if not, ^{79}Se would have releases comparable to ^{99}Tc and ^{129}I) and even more so for the other radionuclides considered in this study.

Figure 4-39, above, illustrates peak release rates from an EBS subjected to weep flow. In the figure, the releases are normalized to the NRC release-rate limit. ^{99}Tc has the highest peak normalized release rate for many realizations, but for some combinations of parameters other radionuclides are higher (see, e.g., Figure 4-51 in the next section). As shown, a 7 percent probability of exceeding the NRC limit was

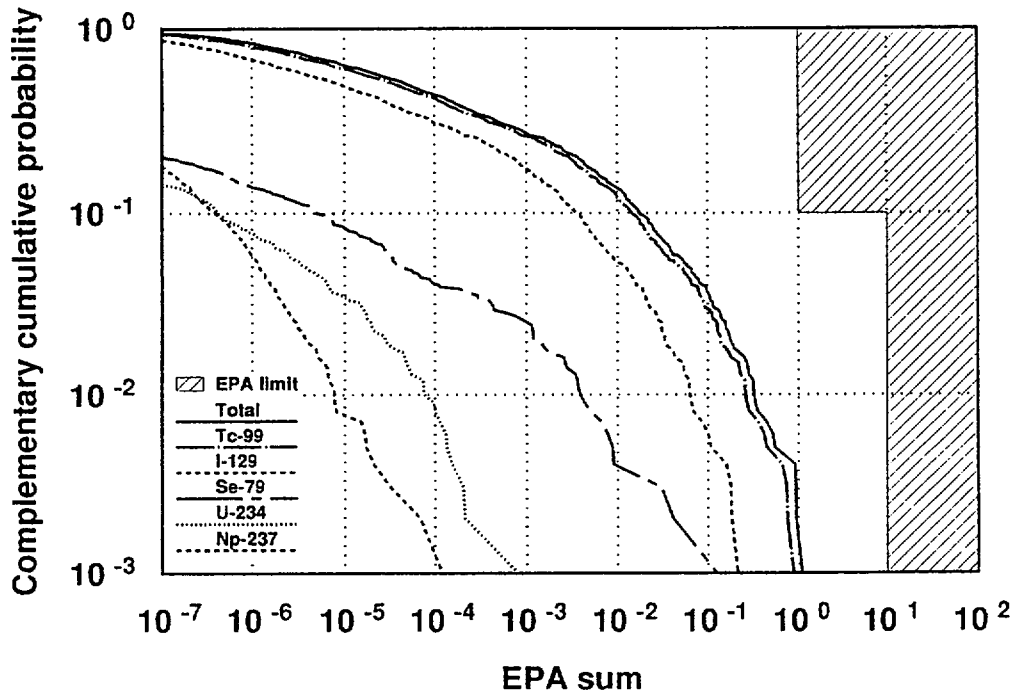


Figure 4-42. Conditional CCDF for aqueous releases to the accessible environment, calculated using the weeps model of flow. Also shown are probability distributions of the EPA ratios of ^{99}Tc , ^{129}I , ^{79}Se , ^{234}U , and ^{237}Np .

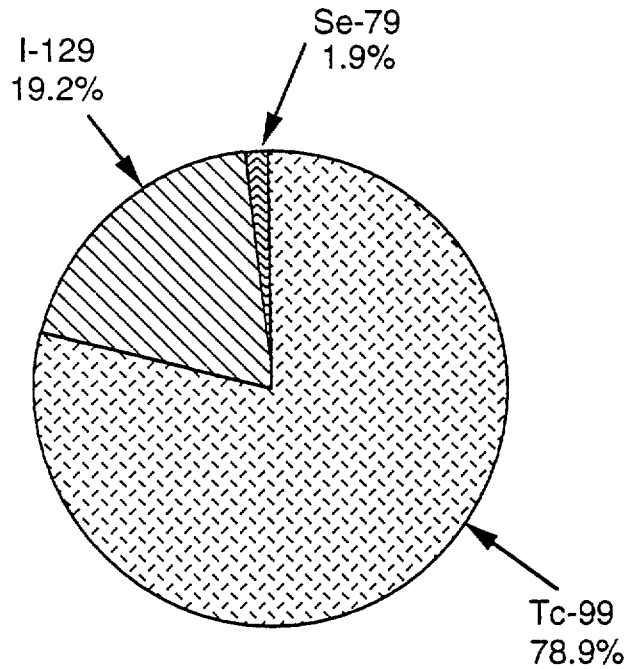


Figure 4-43. Contribution of individual radionuclides to the mean partial EPA sum, calculated using the weeps model.

calculated for the source model used. This result is in direct contrast with the results shown for the composite-porosity model. Releases from the EBS are constrained by the relatively few containers subjected to flow using the weeps model.

The distribution of travel times for an unretarded tracer in the weeps model is illustrated in Figure 4-40, above. In the weeps model, the travel time in the unsaturated zone is neglected (taken to be zero), so the weeps-model travel time is just given by the saturated-zone travel time. As shown, the probability of a travel time less than 1000 years is approximately 25 percent, for the saturated-zone model used.

If we put aside, for the moment, questions surrounding whether the models represent accurately the processes and whether parameters are defined correctly for the models, these results lead to an interesting situation. Both flow models used in this study indicate that a potential repository at Yucca Mountain does not exceed the (remanded) EPA standard for aqueous releases. Composite-porosity flow at Yucca Mountain meets the EPA limit despite release rates from the EBS substantially in excess of the NRC limit. The reason for meeting the EPA limit is that, with composite-porosity flow, travel times are very long—well above the NRC's minimum groundwater travel time. On the other hand, weeps flow at Yucca Mountain is found to produce EBS release rates well below the NRC limit, while calculated travel times are close to the NRC's minimum groundwater travel time. The reason here is that, with weeps flow, few containers are subjected to groundwater flow, fail, and release waste.

The containment and GWTT requirements prescribed by the NRC are useful as performance surrogates; they provide insight into how the models describe the subsystems of the potential repository and the site. However, the NRC requirements do not necessarily indicate whether a repository will meet the EPA total-system standard.

4.7.3 Conditional CCDFs for aqueous releases

Figure 4-44 directly compares the conditional CCDFs for aqueous releases resulting from using the composite-porosity and weeps models of flow. The weeps model results in higher probabilities of greater releases over 10,000 years, although the curves are surprisingly similar given the considerable differences between the two flow models. Neither model predicts releases in excess of the EPA limits. The closest prediction to excessive releases is still an order of magnitude less than the limit, and then at very low probabilities. Chapter 8 discusses combining these CCDFs into a single CCDF for aqueous releases.

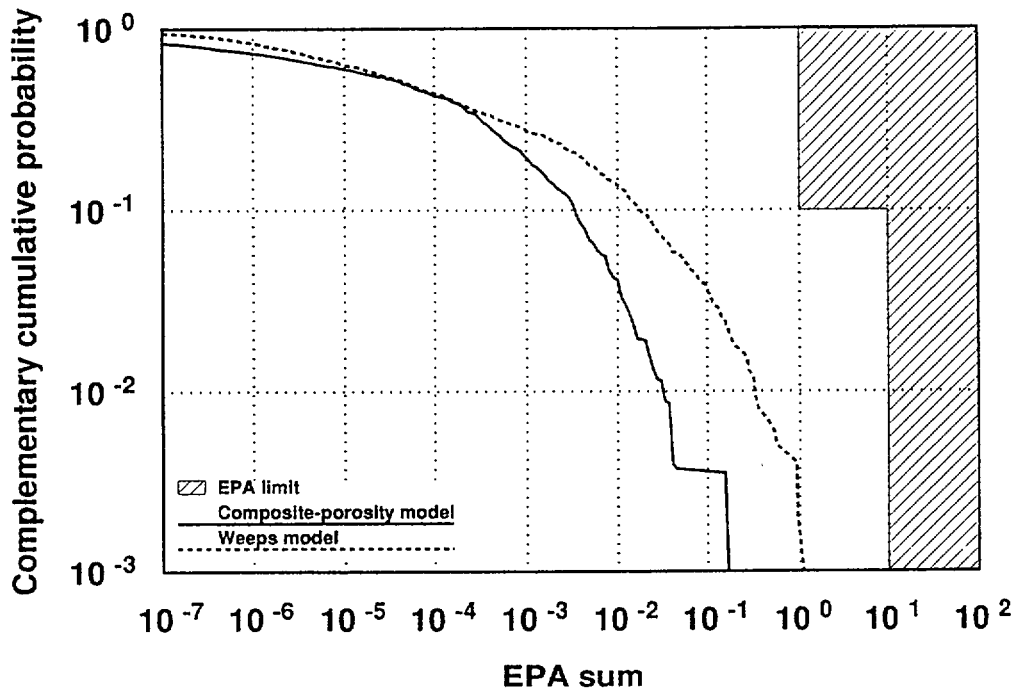


Figure 4-44. Conditional CCDFs for aqueous releases. Shown are the distributions for the composite-porosity model and for the weeps model.

Figure 4-44 appears to imply that there is little to differentiate between the composite-porosity flow model and the weeps flow model in terms of performance. However, the similarity between the CCDFs resulting from the two models is, for the most part, a coincidence, dependent on the 10,000-year time period prescribed by the EPA and on the particular parameter distributions used for this study (the aqueous-release CCDFs of Wilson, 1992, are quite different for composite-porosity flow and for weeps flow). Comparison with the NRC performance measures (above) indicates that the two models show widely different behaviors. The composite-porosity model causes slow, continuous releases from the EBS, with relatively high concentrations of radionuclides dispersed throughout the mountain during a leisurely trip to the accessible environment. The weeps model causes a pulse of releases from a relatively small number of containers; for the most part, the nonsorbing radionuclides reach the accessible environment quickly, while the retarded radionuclides trickle out in relatively low concentrations. Additional analysis (Section 4.8) indicates that, after 10,000 years, the weeps model predicts a repository that is still largely intact; however, the composite-porosity model predicts a repository that is continuing to degrade. One consequence of this behavior is that the conditional CCDFs presented in Figure 4-44 allow comparison of site performance with the EPA standard, but they

are not particularly useful in understanding the models or the site. Another consequence is that, in the long run, fracture-flow pathways (if they exist) could prove beneficial in preserving a repository by limiting the number of containers subjected to groundwater flow.

4.8 Analysis of the average case

Part of the TSPA effort is to investigate the consequences of using mean values of parameters in the various process models. The term "average" case is used to describe the situation in which the mean values of all the parameters in all the models are used. We use the word average here in the mathematical sense; we are *not* attempting to investigate the expected state of a potential repository at Yucca Mountain.

The purposes of analyzing the average case are threefold: (1) to compare the average of the probabilistic calculations (Section 4.7) with the calculation using mean parameter values; (2) to examine the behavior of the repository farther into the future than was done with the probabilistic calculations; and, (3) to provide release-rate data for an independent calculation of potential radiation dose to human inhabitants (the dose calculations are to be presented in a forthcoming report from Pacific Northwest Laboratory).

Deterministic, average-case calculations to produce release-rate data included the following cases. A description of the analysis of each case is contained in the indicated section.

- 1) aqueous releases with composite-porosity flow (Section 4.8.1),
- 2) aqueous releases with weep flow (Section 4.8.2),
- 3) gaseous releases with composite-porosity-derived source (Chapter 5),
- 4) gaseous releases with a weeps-derived source (Chapter 5).

The average-case calculations were conducted over a simulated 1,000,000-year time span, rather than the 10,000-year time span of the probabilistic calculations described in Section 4.7. A longer time scale was chosen because many radionuclides have half-lives much greater than 10,000 years (Table 4-1), and a potential dose-based regulation might not have the same time limit as the release-based standard. Also, an evaluation of trends in the results presented in Section 4.7 indicates that release rates could increase after 10,000 years. We are interested in examining these long-term trends. A caution should be mentioned here, however. Predictions of events up to 1,000,000 years in the future carry even greater uncertainty than predictions

of events for 10,000 years. These results are offered to suggest, not foretell, possible occurrences.

Table 4-8 contains a comparison of the results from the average deterministic calculation and the results from the probabilistic calculations discussed in the previous section. The results are in terms of the partial EPA sums for cumulative release over 10,000 years. In almost every case, the calculations using the average parameter values result in significantly lower releases than the average of the results produced by the probabilistic calculations. This pattern indicates that combinations of extreme parameter values in the probabilistic calculations have produced results that greatly outweigh average behavior—a characteristic of nonlinear problems. For example, with the composite-porosity flow model, many combinations of parameters produce minimal or no releases, but a few combinations of parameters produce releases that are orders of magnitude greater than the average behavior (because of realizations with unusually high percolation rates, low radionuclide retardations, etc.).

The results shown in Table 4-8 caution us that average parameters in nonlinear models could severely underpredict average behavior, if the conditions that produce the extreme results exist. Therefore, behavior with average parameters may not be an acceptable measure of performance. This conclusion is another reason why the average-case calculations should not be construed to represent the expected future of a potential repository at Yucca Mountain.

4.8.1 Average composite-porosity-flow case

For the composite-porosity-flow case, a deterministic calculation was produced for each of the six columns specified in Section 4.4.2. The releases from the six columns were summed to get the total release. Release rates to the accessible environment are shown in Figure 4-45. Of interest is that for the average parameters, releases are negligible until sometime after 5000 years. As with the Monte Carlo simulation, the dominant radionuclides at 10,000 years are ⁹⁹Tc and ¹²⁹I, and indeed, these radionuclides dominate releases for 500,000 years. After 500,000 years, ⁷⁹Se,

Table 4-8. Comparison of deterministic and probabilistic calculations (EPA sums).

Problem	Deterministic solution	Probabilistic mean
Composite-porosity, aqueous	1×10^{-7}	2×10^{-3}
Weeps, aqueous	4×10^{-5}	1×10^{-2}
Composite-porosity, gaseous	0.3	0.5
Weeps, gaseous	4×10^{-5}	2×10^{-2}

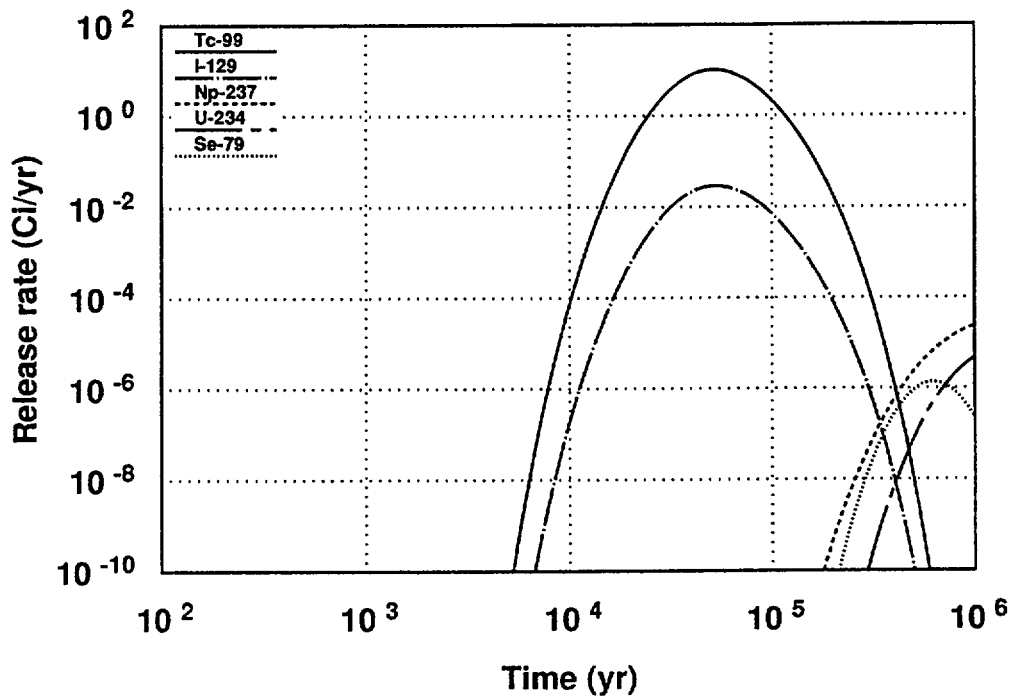


Figure 4-45. Release rates to the accessible environment for radionuclides released using the composite-porosity flow model with mean values for all parameters.

^{237}Np , and ^{234}U become important.

Release rate to the accessible environment is an important quantity because the release rates for all radionuclides to a large extent determines the radiation dose to a population, and the time of the maximum release rate typically corresponds to the time of the maximum dose to a population from a given radionuclide. In this case, the maximum dose would probably come from ^{99}Tc and ^{129}I , which both peak at approximately 60,000 years—well beyond the current EPA time period of 10,000 years. At 60,000 years, approximately 10 Ci/yr of ^{99}Tc and 0.03 Ci/yr of ^{129}I are being released to the accessible environment from the entire repository.

Figure 4-46 presents cumulative aqueous releases to the accessible environment in terms of the EPA ratio. The EPA ratio is shown in Equation 4.59; in general, values exceeding 1, at 10,000 years, exceed the EPA limit. Despite the lower EPA limit specified for ^{129}I (0.1 Ci/MTHM EPA limit), ^{99}Tc (10 Ci/MTHM EPA limit) still dominates the releases by this measure because of its much greater inventory. The total cumulative release approaches a partial EPA sum of one, but not until 100,000 years (well after 10,000 years) because of the extremely long groundwater travel times associated with composite-porosity flow (see below). No other nuclides contribute significantly to this measure within 1,000,000 years.

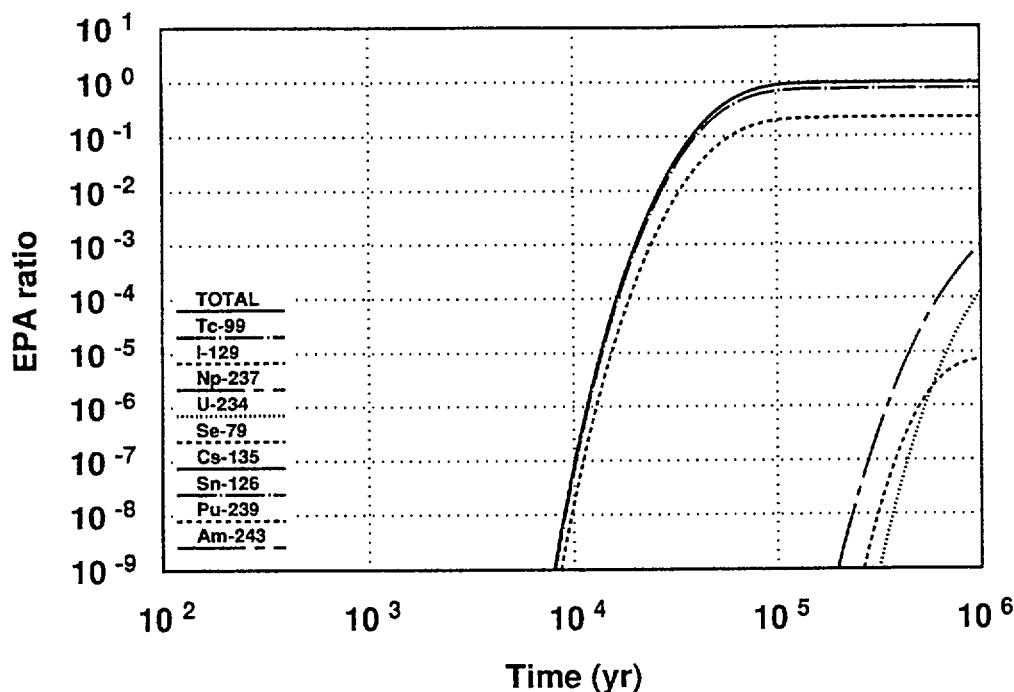


Figure 4-46. Cumulative releases to the accessible environment (in terms of the EPA ratio), calculated using the composite-porosity flow model with mean values for all parameters.

The aqueous release rates from the EBS are plotted in terms of the NRC ratio in Figure 4-47. In the figure, release rates are divided by their respective NRC limits (Table 4-1). Therefore, values over 1 exceed the NRC limit. As before, this information is presented to indicate the behavior of the source model, to determine what effect the releases from the EBS have on releases to the accessible environment, and to allow comparison of the source releases in the composite-porosity model and the weeps model.

With the composite-porosity model, maximum release rates from the EBS occur in the neighborhood of 4000 years. ⁹⁹Tc and ⁷⁹Se exceed the NRC release-rate limit; ¹³⁵Cs approaches the limit. ⁹⁹Tc exceeds the limit for the time period between 800 and 20,000 years. The excessive EBS releases contribute to excessive releases to the accessible environment (Figures 4-45 and 4-46), but only after a long time delay. The long time delay is primarily the result of the long GWTT afforded by composite-porosity flow (below). In the figure, release rates for several radionuclides abruptly drop to zero when their total inventory in the repository is exhausted.

The distribution of travel times for an unretarded tracer is presented in Figure 4-48. Results for both the composite-porosity model and the weeps model

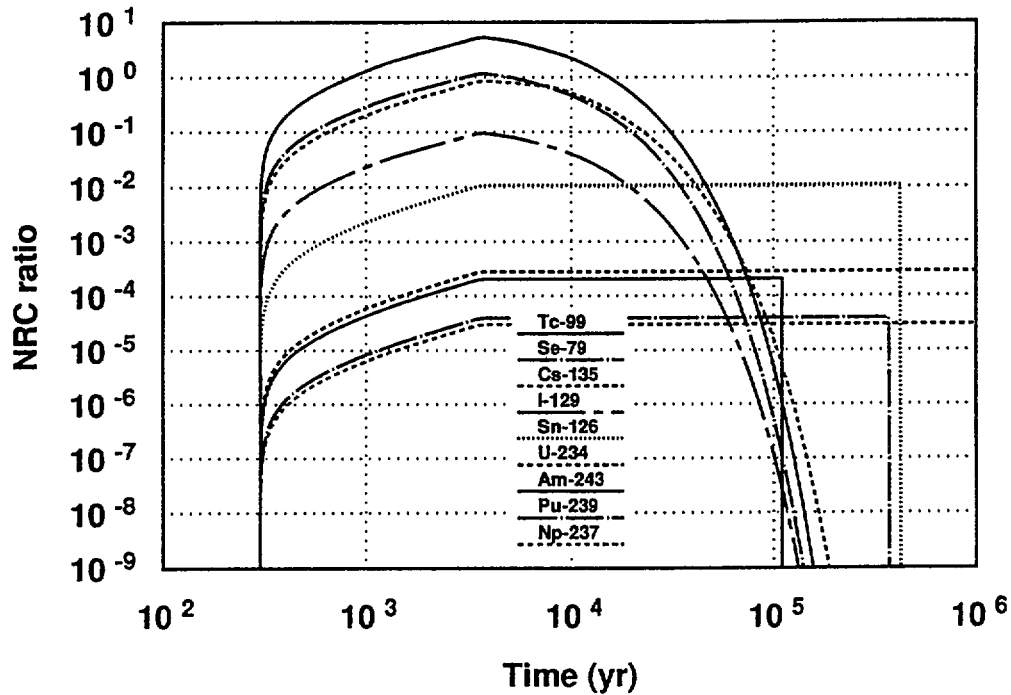


Figure 4-47. Release rates from the EBS (normalized to the NRC limit), calculated using the composite-porosity flow model with mean values for all parameters.

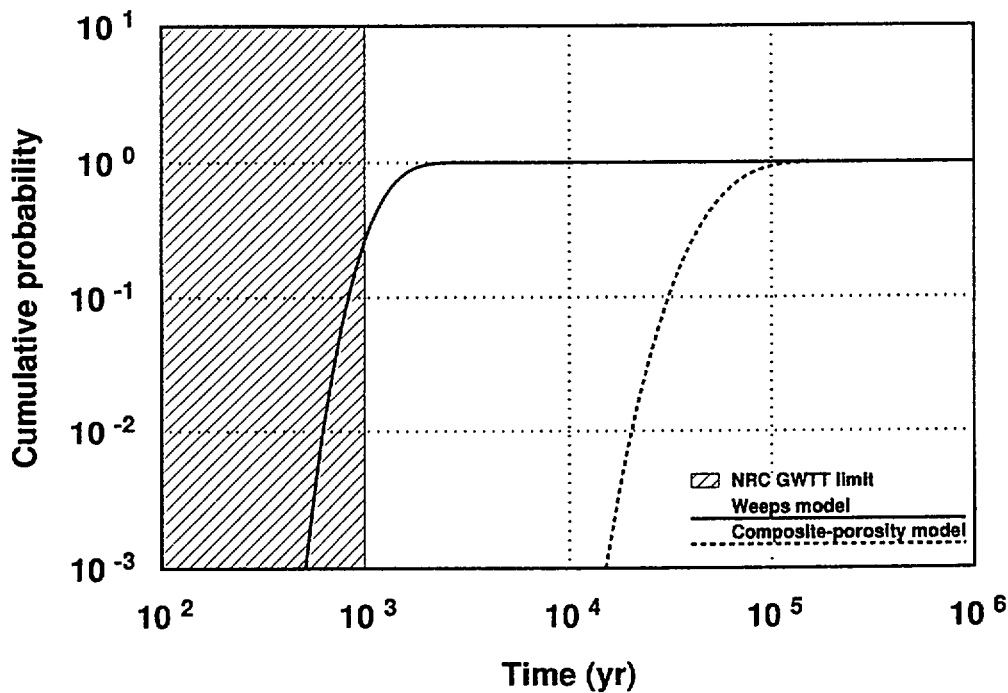


Figure 4-48. Distributions of travel times for an unretarded tracer from the repository to the accessible environment, for the composite-porosity model and for the weeps model. Calculated using mean values for all parameters.

are shown. In the figure, values less than 1000 years indicate infringement on the NRC-established minimum GWTT requirement along the fastest path of likely radionuclide transport (but see the caveats in Section 4.7.1).

The travel times for the composite-porosity model were calculated with the nonsorbing-tracer method from a single deterministic calculation for each column. The curves approximate the travel-time distributions of ^{99}Tc and ^{129}I . The spread is caused by dispersion of the tracer during transport. The median travel time for the composite-porosity model is approximately 60,000 years, and the mean travel time is similar, indicating a relatively symmetric distribution. (The median can be read off the plot; the mean is calculated from the data that were used to make the plot.) The composite-porosity model produces travel times much greater than the minimum required by the NRC, and the long travel times are primarily responsible for the long delay in releases at the accessible environment (discussed above).

Comparison of the travel-time distribution for the average composite-porosity case with the travel-time distribution for the Monte Carlo composite-porosity calculations (Figure 4-40) shows the average-parameter case to have less variance than the Monte Carlo case. Thus, as expected, a greater probability of both fast and slow travel times results from the Monte Carlo calculations. The median of the Monte Carlo simulations is at a somewhat longer time (70,000 years) and the mean (500,000 years) is at a much longer time. An exponential distribution was used for the percolation rate, and the mean of the distribution (which was the value used for the average case) is at a higher value than the median. The Monte Carlo simulations therefore sampled more from percolation rates lower than the mean, resulting in more long travel times.

4.8.2 Average weeps-flow case

Figure 4-49 presents release rates to the accessible environment for the average weeps-flow case. Releases begin before 1000 years, and peak for ^{99}Tc , the dominant radionuclide, at approximately 5000 years, when slightly more than 0.01 Ci/yr is being released from the entire repository. ^{79}Se has the next greatest release rate, 10^{-4} Ci/yr peaking at approximately 40,000 years. As with the Monte Carlo simulation, the dominant radionuclides at 10,000 years are ^{99}Tc and ^{129}I . After 100,000 years, ^{234}U , ^{237}Np , and ^{135}Cs are most important.

According to the figure, maximum dose to a population can be expected in the neighborhood of 5000 years, with ^{99}Tc being the most offending radionuclide. (Although the dose from ^{129}I could be significant because of the propensity for the human body to retain this element.)

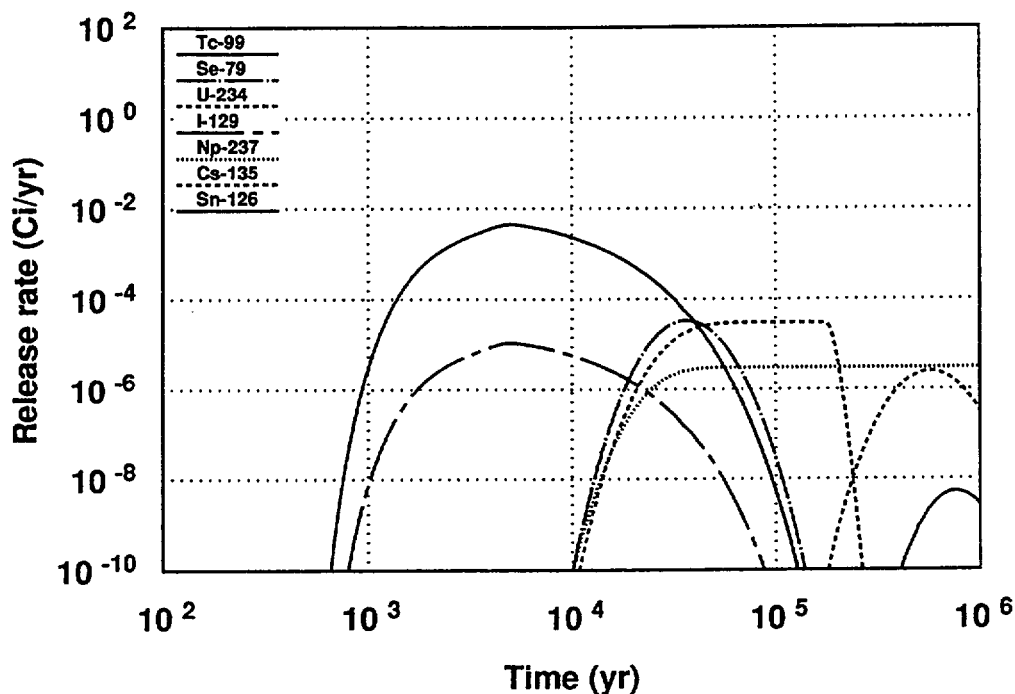


Figure 4-49. Release rates to the accessible environment for radionuclides released using the weeps model with mean values for all parameters.

In comparison with Figure 4-45, note that the maximum release rates for the weeps model occur at much earlier times than those for the composite-porosity model; however, the maximum release rates are of much lesser magnitude. The earlier release times for the weeps model are caused by the assumption of instantaneous transport through the unsaturated zone. The lower release rates are the direct result of lower releases from the EBS, which are explained below.

The cumulative aqueous releases to the accessible environment calculated using the weeps model, in terms of the EPA ratio, are presented in Figure 4-50. By this measure, ⁹⁹Tc dominates the releases for the first 40,000 years, after which ²³⁴U dominates. At 1,000,000 years the cumulative releases are still increasing slowly; however, the releases are still well below a partial EPA sum of one.

Comparison of Figure 4-50 for the weeps model with Figure 4-46 for the composite-porosity model, shows that the weeps model results in much lower releases. With the weeps model, releases are constrained by the limited number of waste containers that are contacted by flowing fractures. A basic assumption behind the weeps model is that flow does not switch from one fracture (or set of fractures) to another over time. Topological conditions and precipitation patterns could be stable enough to make this assumption reasonable for a 10,000-year period; however, this

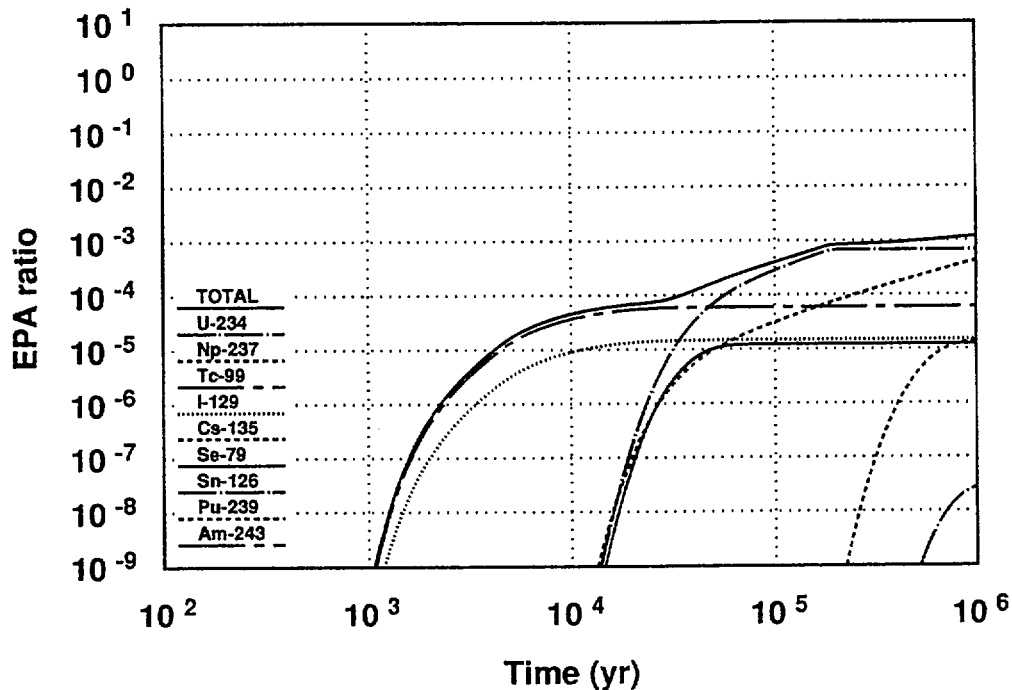


Figure 4-50. Cumulative releases to the accessible environment (in terms of the EPA ratio), calculated using the weeps model with mean values for all parameters.

assumption is even more tenuous over a 1,000,000-year period. If flow does switch to new fractures, different waste containers could be contacted, and if the total contact time is sufficient for the containers to fail, greater releases of the volatile, matrix-alteration-released radionuclides (e.g., ^{99}Tc , ^{129}I , ^{79}Se , and ^{135}Cs) could result. But even with flow switching from fracture to fracture, approximately the same releases for the nonvolatile, solubility-limited radionuclides (e.g., ^{234}U and ^{237}Np) could be expected, because these radionuclides in total would see approximately the same amount of water—which determines their releases—independent of their container of residence.

The aqueous release rates from the EBS are plotted in terms of the NRC ratio in Figure 4-51. Maximum releases from the EBS occur in the neighborhood of 4000 years. Release rates are much lower than for the composite-porosity model (Figure 4-47), and none of the radionuclides exceeds the NRC release-rate limit. One interesting feature of Figure 4-51 is that the release rates from the solubility-limited nuclides are much higher, relative to the alteration-limited nuclides, than they were in Figure 4-47. In fact, the highest release rate is for one of the solubility-limited nuclides, ^{126}Sn . The high release rates for solubility-limited nuclides result from the very large amount of water flowing through the assumed 215- μm fractures.

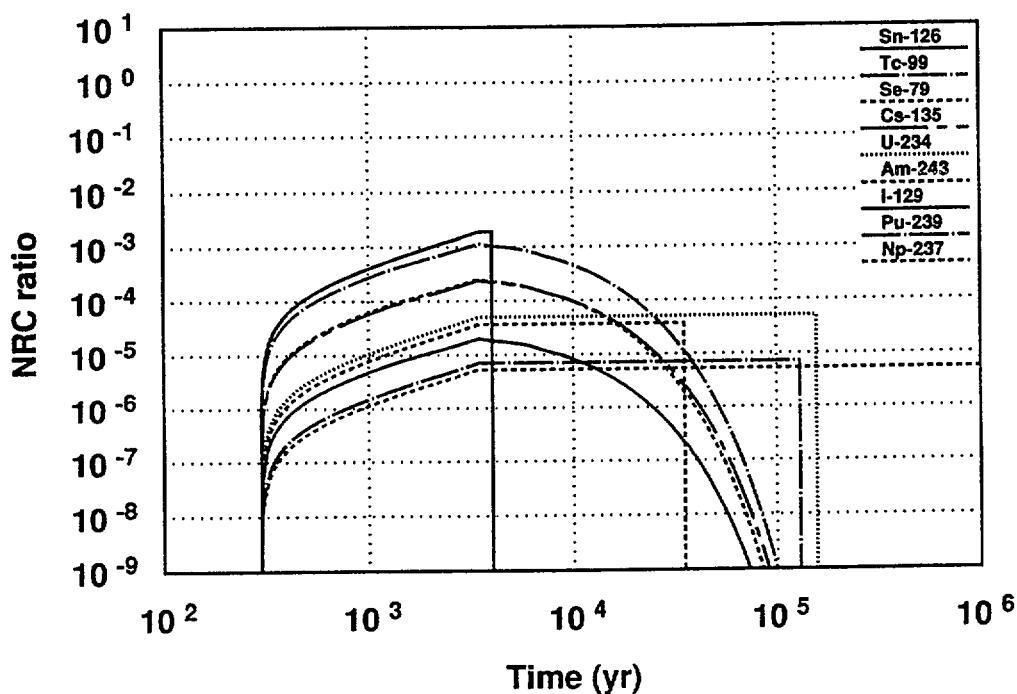


Figure 4-51. Release rates from the EBS (normalized to the NRC limit), calculated using the weeps model with mean values for all parameters.

Only a few waste containers are contacted, but the ones that are contacted average approximately $7 \text{ m}^3/\text{yr}$ of water pouring through them. The source releases for alteration-limited advection, as defined in Sections 4.3 and 4.4.4, are insensitive to the water-flow rate, whereas the source releases for solubility-limited advection are directly proportional to the water-flow rate. Thus, for a high enough water-flow rate through a waste container, the solubility-limited releases can exceed the alteration-limited releases, as happened in this "average" weep-flow calculation. This effect is not realistic, but it is conservative. It results from failure to take the fuel-matrix-alteration rate into account in the solubility-limited-release model (the alteration rate should limit the quantity of ^{126}Sn available for dissolution).

The distribution of travel times for an unretarded tracer in the weeps-flow case, as well as the composite-porosity-flow case, are presented in Figure 4-48, above. (Section 4.8.1 contains a description of the figure and the calculations that produced it.) The NRC-established minimum GWTT requirement along the fastest path of likely radionuclide transport (10 CFR 60.113) is 1000 years. The weeps-flow tracer travel time can be seen to infringe on the NRC limit approximately 25 percent of the time. (Again, these results are presented to help explain the weeps model—especially with respect to releases of radionuclides—rather than as a determination

of compliance with the GWTT criterion. The weeps model represents an extremely conservative assumption about unsaturated-zone travel time.) The median travel time for the weeps model is approximately 1500 years, while the mean travel time is 1300 years. The median being longer than mean implies that the distribution is skewed slightly toward shorter values.

The travel-time distribution for the weeps model results entirely from flow through the saturated zone, and can be explained as follows. With a pore-water velocity of 4.07 m/yr (the mean of the saturated-zone velocity distribution), a non-sorbing tracer would cover the 5000 m to the accessible environment in 1230 years (that is, in 1230 years, approximately half of the tracer would have reached the accessible environment). With the diffusion and hydrodynamic dispersion built into the model, the tracer concentration spreads as it moves, and thus, 25 percent of the tracer reaches the accessible environment before 1000 years.

Chapter 5

Gas Flow and Transport

(Wilson, Barnard)

Gaseous releases of ^{14}C in the form of $^{14}\text{CO}_2$ are expected to be important for a partially saturated repository (see, e.g., Park and Pflum, 1990; Van Konynenburg, 1991). A significant amount of ^{14}C is in the spent-fuel inventory. In Chapter 4 it is pointed out that the radionuclide source model being used assumes rapid releases (higher than the NRC containment criterion in 10 CFR Part 60 would allow) of the highly soluble species from the EBS because of oxidation alteration of the spent-fuel matrix. ^{14}C also falls into the alteration-limited release category and, because gas transport times tend to be much shorter than water transport times, there is potential for large (in terms of EPA ratio) releases of ^{14}C to the accessible environment.

Figure 5-1 shows schematically some of the important factors that go into the gaseous flow and transport calculations.

The analysis of gaseous release and transport is very similar to the analysis of

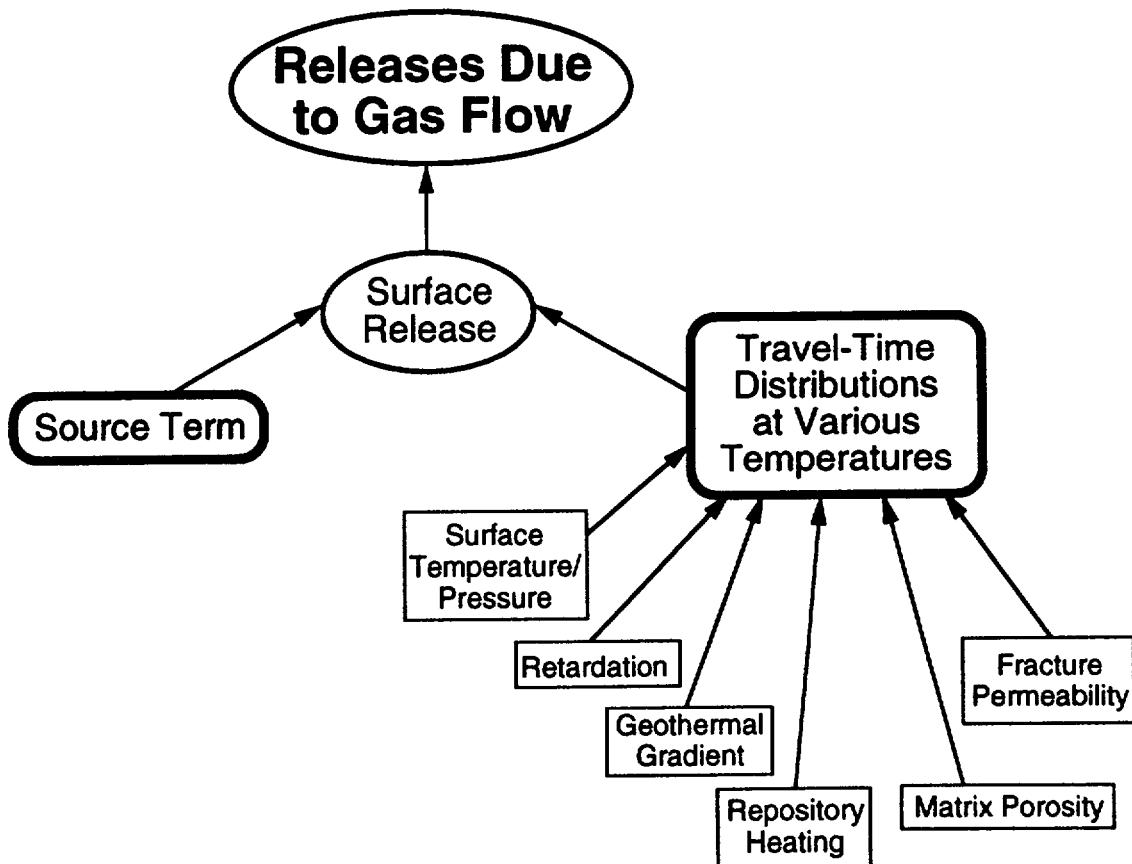


Figure 5-1. Factors included in the gas-flow problem.

aqueous release and transport in Chapter 4. Models are needed for release of ^{14}C from the EBS, for gas flow, and for transport of $^{14}\text{CO}_2$. These models are discussed in the following sections. The models are combined with probability distributions of their input parameters to generate probability distributions of the performance measures (the EPA ratio and the NRC ratio), which are then compared to the prescribed limits.

The probabilistic calculations were performed using the Monte Carlo method, in which “realizations” of the system are successively generated by random sampling from the input probability distributions. For each realization, the releases of radionuclides to the accessible environment in 10,000 years were calculated. The results from all realizations were used to determine the probability distributions of the releases.

As for aqueous releases, the Monte Carlo simulation of gaseous releases was done with the TSA computer program (Wilson et al., 1991; Wilson, 1992). A flow diagram of the method is shown in Figure 5-2. As shown in the figure, there are two separate calculations of gaseous releases, corresponding to the two conceptual models of unsaturated-zone water flow (the composite-porosity model and the weeps model—see Chapter 4). Even though water flow is not directly of interest in the gas-flow calculation, it influences the gaseous releases from the EBS because waste mobilization and release from the waste containers is dependent on contact of liquid water with the waste containers. For simplicity, the gas- and water-flow calculations in this TSPA were performed separately. In a more sophisticated treatment, gas and water flow would be coupled.

5.1 Problem development and scenario screening

The scenario describing the TSPA gas flow and transport analysis was developed from the same FEP diagram as was used for the groundwater-flow problem. The upper-level FEPs for this scenario are the same as for groundwater flow, e.g., “Distributed Infiltration” and “Imbibition into Matrix Near Surface,” and are shown in Figure 4-1. As with the groundwater-flow problem, the composite-porosity and weeps models are considered to be the two mechanisms important to release of radionuclides from the EBS. All the branches of the FEP diagram in Figure 4-1 end with the FEP “Interaction with the Repository.” Figure 5-3 shows the subsequent FEPs; no distinction is made here between container failure occurring in the composite-porosity model and that occurring in the weeps model.

As Figure 5-3 shows, the same two conditions for the repository—“Hot Repository” and “Cold Repository”—appear in the gas-flow FEP diagram as in the water-

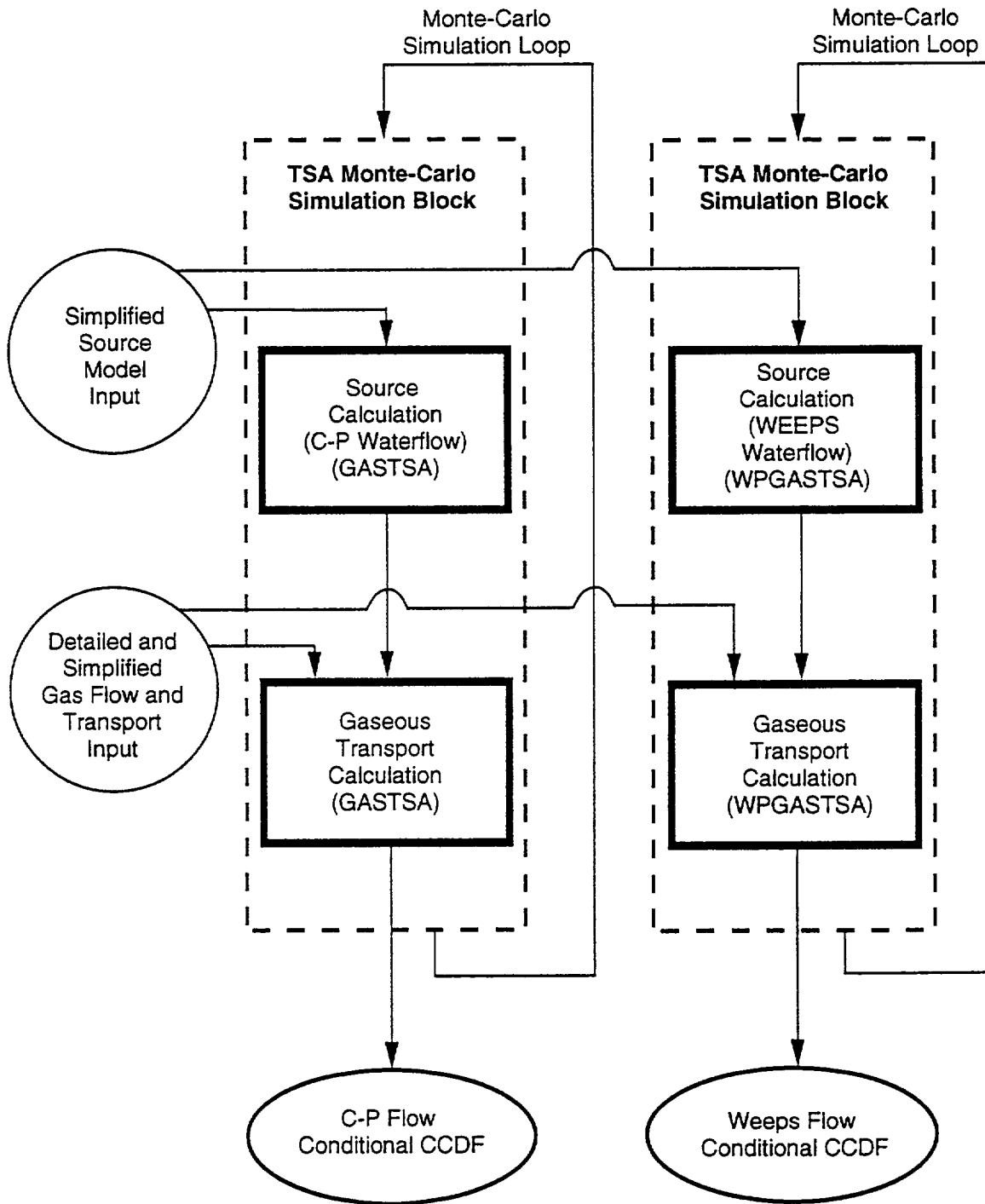


Figure 5-2. Flow diagram for the two TSA gaseous-transport simulations, one for composite-porosity water flow and one for weeps water flow. (Only the source calculations are different; the transport calculations in GASTSA and WPGASTSA are identical.)

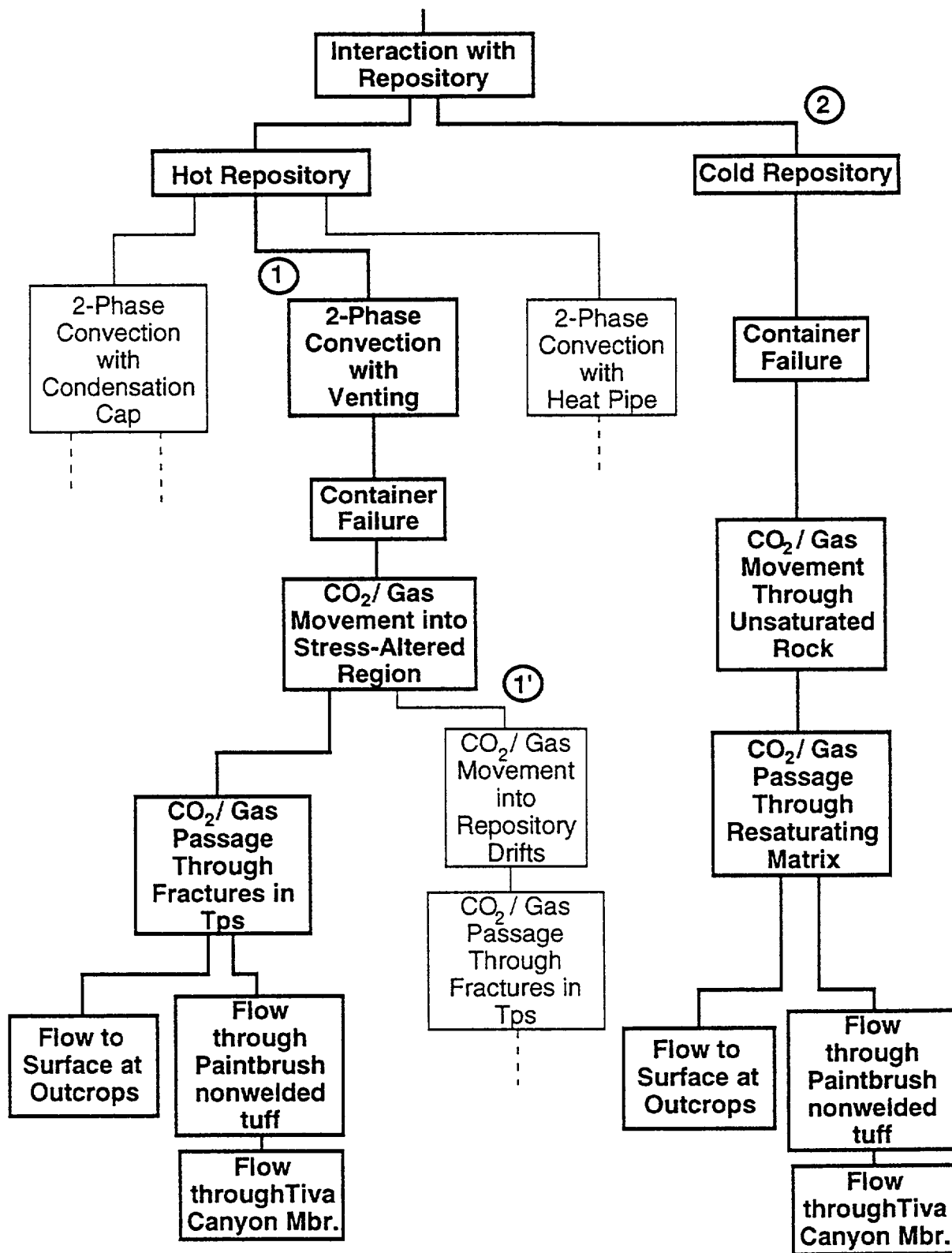


Figure 5-3. FEP diagram for nominal gas flow.

flow FEP diagrams (Figures 4-2 and 4-3). For the "Hot Repository" FEPs, the same two-phase processes are included as for groundwater flow. The gas-flow and water-flow FEPs are both part of the same FEP diagram, but Figure 5-3 shows only the gas-flow part and Figures 4-2 and 4-3 show only the water-flow part. The paths applicable to the TSPA gas-flow analysis are shown as ① and ② in Figure 5-3. The scenario that would most likely produce fast and large releases would occur from venting gas to the surface.

The TSPA gas-release calculation considers only the release of ^{14}C , in the form of $^{14}\text{CO}_2$. It is assumed that the $^{14}\text{CO}_2$ has formed in the spent fuel from chemical and radiolytic processes occurring since discharge of the fuel from the reactors. The gas inventory includes that available at the time the waste package is breached and that formed later due to alteration of the fuel. Gas is released to the rock surrounding the waste packages by failure of those packages. It is assumed that either unsaturated or saturated groundwater conditions could cause these failures. After a waste package is breached, the $^{14}\text{CO}_2$ escapes into the surrounding rock. The rock surrounding the waste packages will be disturbed by the construction of the repository. The most likely effect of this disturbance is to alter the stress fields such that there could be more or larger fractures. In addition, the backfilled repository drifts represent rock volumes that are considerably different from the country rock. The gas can be expected to move into this volume.

The mechanism specified in the TSPA analysis for gas to move from the repository to the surface is flow through connected fractures or faults. Flow through the Topopah Spring Formation (Tps), the Paintbrush nonwelded tuff, and the Tiva Canyon Member are listed separately because of the likely differences in the flow rates. The Paintbrush nonwelded tuff is probably much less fractured than the Tps Formation and therefore would have lower gas-flow rates. The Tiva Canyon Member is probably similar to the Tps. In addition, the Topopah Spring has outcrops in Solitario Canyon, so it is possible that some of the gas flow can avoid the Paintbrush and Tiva Canyon entirely.

The radionuclide release-vs.-time has a component for the promptly released fraction, and one for the gas released due to fuel-matrix alteration. In addition, the curve shape depends on the assumptions made about what happens to the gas when it first escapes from the waste packages. If it goes directly into the connected fractures, the release will be as described above. If it goes into the repository drifts before moving into the fractures, the prompt-release fraction can be damped, and the alteration-release fraction can occur over a longer time. This process is not considered in the TSPA analysis, but is shown in Figure 5-3 as path ①'.

5.2 Radionuclide source term for gaseous releases

The radionuclide source term for gaseous releases is essentially the same as the source term for aqueous releases, which was already described in Sections 4.3 and 4.4.4 (for composite-porosity water flow and weeps water flow, respectively). This TSPA includes two different Monte Carlo simulations of gaseous release, flow, and transport. The flow and transport calculations are the same for the two simulations, but different assumptions are used in calculating the source releases because the source model is dependent on the choice of groundwater-flow model. The parts of the source model that are the same as given in Chapter 4 will not be repeated; only the additional information needed to complete the specification of the gaseous source term will be presented.

Table 5-1 gives inventory and general information for ^{14}C in spent fuel. The data sources are the same as given previously for Table 4-1 and additionally Park and Pflum (1990). Note that ^{14}C is the only radionuclide considered to be transported in gaseous form (Van Konynenburg, 1989). In the release calculations, there is no attempt to distinguish between gaseous and aqueous mobilization of ^{14}C in the waste container. One of the basic assumptions in the transport calculations is that carbon dioxide in the air is in equilibrium with bicarbonate in the water (and other aqueous carbon species; at the pH of groundwater in Yucca Mountain, bicarbonate is expected to be the predominant form of dissolved carbon). This implies that, whether the ^{14}C is initially released in gaseous or aqueous form, it will quickly come to equilibrium and be transported primarily via the gas flow. This assumption will be discussed more fully in the next section.

The inventory figures in Table 5-1 could be high. Van Konynenburg (1991) re-examined the assumptions of Roddy et al. (1986) regarding ^{14}C production during reactor operation, and he suggested the following revised inventory numbers

Table 5-1. Some ^{14}C data.

Quantity	Value
Inventory (Ci/MTHM)	1.54
Inventory in fuel matrix (Ci/MTHM)	0.58
Inventory in cladding (Ci/MTHM)	0.51
Inventory in assembly hardware (Ci/MTHM)	0.45
Half-life (yr)	5729
Activity (Ci/mol)	62.4
NRC limit (Ci/MTHM-yr)	1.67×10^{-5}
EPA limit (Ci/MTHM)	0.1
Release type	alteration-limited

(his figures for PWR and BWR inventories have been combined in a 60%/40% ratio, consistent with the other inventory numbers used for this study): fuel-matrix inventory, 0.58 Ci/MTHM (unchanged); cladding inventory, 0.26 Ci/MTHM (about half the value in Table 5-1); and assembly-hardware inventory, 0.17 Ci/MTHM (about 38 percent of the value in Table 5-1). Van Konynenburg's revised inventories were not adopted for this TSPA, but should be considered for use in future TSPA studies.

Aside from the gaseous nature of the ^{14}C releases, the other major difference between ^{14}C releases and releases of the other nuclides being modeled (see Table 4-1) is that ^{14}C has a significant fraction of its inventory outside the fuel pellets. As shown in the table, there are significant amounts of ^{14}C in the fuel-rod cladding and in the fuel-assembly hardware in addition to the UO_2 fuel matrix. As already mentioned in Section 4.3, ideally there would be source submodels to describe releases from the cladding and the fuel-assembly hardware, but they are not included at the present time. For this TSPA, the releases from cladding and hardware were neglected except for the important quick-release part of the cladding releases (Park and Pflum, 1990; Wilson, 1991). It should be reasonable to neglect these releases because they should be small compared to releases from the fuel matrix (Wilson, 1991, estimated the time scales for releases from cladding and fuel-assembly hardware to be greater than 60,000 yr—much greater, in the case of cladding releases—whereas the fuel-matrix-alteration time scale used in this study to determine the rate of releases from the fuel matrix varies from 1,000 yr to 20,000 yr—see Table 4-2).

The quick-release fraction of the ^{14}C inventory comes from an oxidation layer on the surface of the fuel-rod cladding (Van Konynenburg et al., 1985, 1987). The ^{14}C comes off in gaseous form and is available for release as soon as the waste container has failed (release does not require cladding failure because it is on the outside of the cladding). The quick-release inventory of ^{14}C should be released earlier than the gap/grain-boundary inventory, but the source model being used has no provision for including the cladding as a barrier (i.e., the cladding-failure time is being neglected), so for these calculations the quick-release ^{14}C and the gap/grain-boundary ^{14}C were lumped together into the "prompt" inventory fraction f_p . It is uncertain how much of the ^{14}C inventory might come off in the initial pulse upon container failure, but a recent review by Park and Pflum (1990) suggests that it might be as much as 5 percent of the ^{14}C inventory. The gap/grain-boundary fraction is also uncertain, but the aqueous-release calculations assumed it to be 2 percent. For compatibility, 2 percent was also assumed for ^{14}C , but only 2 percent of the fuel-matrix portion rather than 2 percent of the whole inventory.

As a result of the assumptions discussed above, the following numbers were

adopted. The quick-release fraction of the ^{14}C inventory was assumed to vary between 0.5 percent and 5 percent of the total inventory; i.e., between 0.0077 Ci/MTHM and 0.077 Ci/MTHM, since a total inventory of 1.54 Ci/MTHM is being assumed (Table 5-1). The gap/grain-boundary fraction was assumed to be 2 percent of the fuel-matrix inventory of 0.58 Ci/MTHM; this amount comes to 0.012 Ci/MTHM. The combination of quick-release and gap/grain-boundary inventories thus varies from 0.019 Ci/MTHM to 0.089 Ci/MTHM. The fuel-assembly-hardware part of the inventory (0.45 Ci/MTHM) is neglected entirely and most of the cladding inventory (0.51 Ci/MTHM) is also neglected, except for the quick-release part of the cladding inventory. The total modeled ^{14}C inventory consists of the matrix part (0.58 Ci/MTHM) plus the quick-release part (from 0.0077 Ci/MTHM to 0.077 Ci/MTHM), so the ^{14}C inventory varies from 0.58 Ci/MTHM to 0.65 Ci/MTHM. The prompt fraction is the quotient of the combined quick-release and gap/grain-boundary inventories, and the total inventory; therefore, the prompt fraction varies from 0.03 to 0.14 ($0.019/0.58 \approx 0.03$ and $0.089/0.65 \approx 0.14$). Uniform probability distributions were used and a correlation was built into the sampling so that if a high prompt fraction was chosen for a realization then a high value for the inventory was also chosen. This information is summarized in Table 5-2.

The source-term calculation proceeds exactly as described in Sections 4.3 and 4.4.4, with the following exception: The time scales for transport out of the waste container ($t_{i,t,x}$, where $i = 0, 1, 2$ and $x = s, d, c, dm, \text{ or } dw$) are set to zero. That is, the amount of time it takes the ^{14}C to get out of the waste container after it has been mobilized is neglected. This change is not significant because the transport times, as defined in Section 4.3, are small in most cases anyway, so that the other time scales (for container failure, for fuel-matrix alteration, etc.) determine the behavior. The reason for making the change is that the time for gas to get out of a waste container is probably small compared to the time for liquid to get out of a waste container. Some work has been done on modeling diffusion of gases, including carbon dioxide, out of a breached waste container (Light et al., 1990; Pescatore,

Table 5-2. Probability distributions assumed for ^{14}C inventory.

Model parameter	Distribution	Distribution parameters ^a	Mean value
^{14}C inventory, I_0 (Ci/MTHM)	uniform	0.58, 0.65	0.0615
^{14}C prompt fraction, f_p	uniform	0.03, 0.14	0.085

Note: a rank correlation of 0.9 was assumed between I_0 and f_p .

^a Parameters for the uniform distribution are minimum, maximum.

1990), but that work generally assumes that the container is mostly intact except for a few pinholes or cracks. That assumption is not consistent with the assumptions made for the aqueous-release source model in Section 4.3, where the waste container as a barrier was neglected after failure. To be consistent, it is neglected here, for gaseous releases, as well. Clearly, though, future work should include more realistic container models for both aqueous and gaseous releases.

5.3 The gas-flow model

Benjamin Ross and his coworkers at Disposal Safety Incorporated have been developing a gas-flow model of Yucca Mountain under contract to Sandia National Laboratories. The most comprehensive calculations to date of gas flow within Yucca Mountain are reported by Ross et al. (1992). The TSPA calculation of ^{14}C transport uses their results directly. In this section, an overview of the gas-flow model and its major assumptions will be given; a discussion of how those results are used within the TSA will be given in the following section.

The Ross et al. computer model, called TGIF, is a two-dimensional, steady-state model of gas flow within Yucca Mountain. The major assumptions that go into the gas-flow model are:

- Thermodynamic equilibrium exists among air, water vapor, and water.
- The gas is saturated with water vapor.
- Changes in partial pressure of water vapor are accommodated by changes in gas composition, with the total pressure remaining nearly constant.
- Molecular diffusion resulting from gradients of water-vapor partial pressure has a negligible effect on gas flow.
- The porous matrix and fractures could be treated together as an equivalent porous medium.
- The presently available results assume steady-state conditions. There are at least two important implications of this assumption. First, there must be a steady water source (presumably surface infiltration) to replenish the water that the moist underground air carries out into the atmosphere. Second, atmospheric temperature, humidity, and pressure are assumed constant (in time, not in space) in the calculations. The diurnal and annual variations are neglected and average values are used.

See Ross et al. (1992) for additional details.

In addition to describing the model, Ross et al. present results of a series of detailed calculations of gas flow in Yucca Mountain, both under ambient conditions and with a repository present, providing additional thermal driving force. For the detailed calculations that were made, four east-west cross-sections were used. Figure 5-4 shows a plan view of the potential repository area with a grid superimposed. The four east-west grid lines that cross the potential repository area indicate the locations of the four model cross-sections. Figures 5-5 through 5-8 show the four cross-sections. The most important features affecting the gas flow are:

- The assumed repository. Repository heating is very important in driving the gas flow.
- The layer of nonwelded tuff, labeled PTn in the figures. It is between two layers of welded tuff labeled TSw and TCw; TSw corresponds to "welded" in Figure 4-16. The nonwelded tuff probably has lower permeability than the welded tuff because it is not as heavily fractured. Because of the lower permeability it could act as a confining layer, slowing flow to the surface.
- The surface topography. Under ambient conditions, the temperature, humidity, and pressure differences between the atmosphere and the subsurface gas are important in driving the gas flow. At high repository temperatures, repository-induced thermal driving tends to overwhelm the topographic effects, but they are never negligible.

The lower boundary of the welded tuff (TSw in the figures) is used as the lower boundary of the calculational mesh because there is probably a permeability reduction there, too, leading to little gas flow downward into the nonwelded tuff. The western boundary of the calculational mesh is at the trough of Solitario Canyon, which is probably a natural flow boundary; the eastern boundary of the calculational mesh is set far away from the assumed repository so that that boundary condition will have little effect on the solution near the repository.

Figures 5-9 and 5-10 show examples of the calculational results for the predicted gas-flow pathlines, Figure 5-9 for ambient conditions and Figure 5-10 for a repository heated to a uniform temperature of 330 K (approximately 30 K above ambient). The calculations show air being drawn in at lower elevations and then expelled at higher elevations. Repository heating can cause large convection cells to form. In the simulations shown, the permeability of the nonwelded tuff (shown as a narrow shaded band) was set to 1 percent of the permeability of the welded

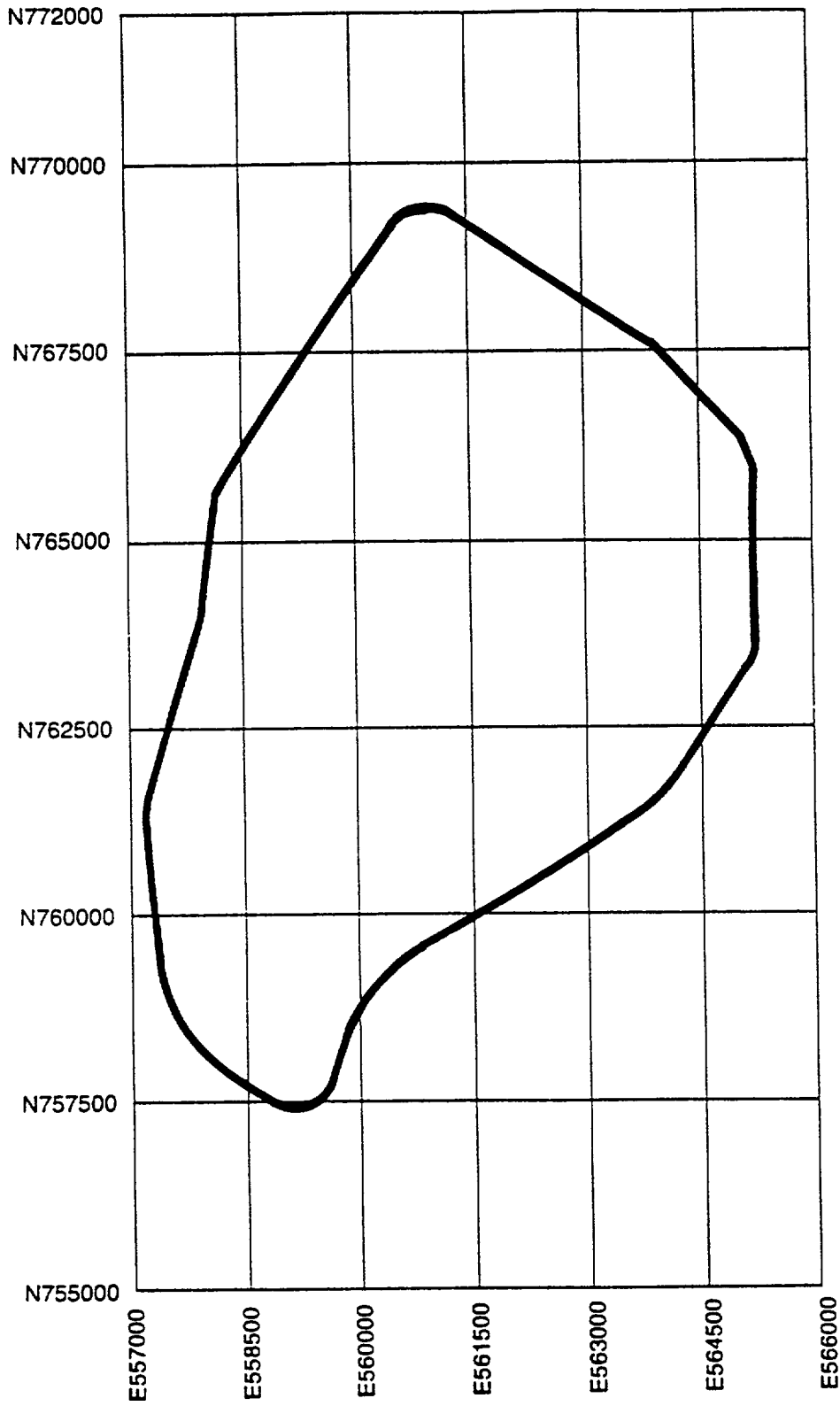


Figure 5-4. Map of the repository (taken from Figure 6-1 of Ross et al., 1992).

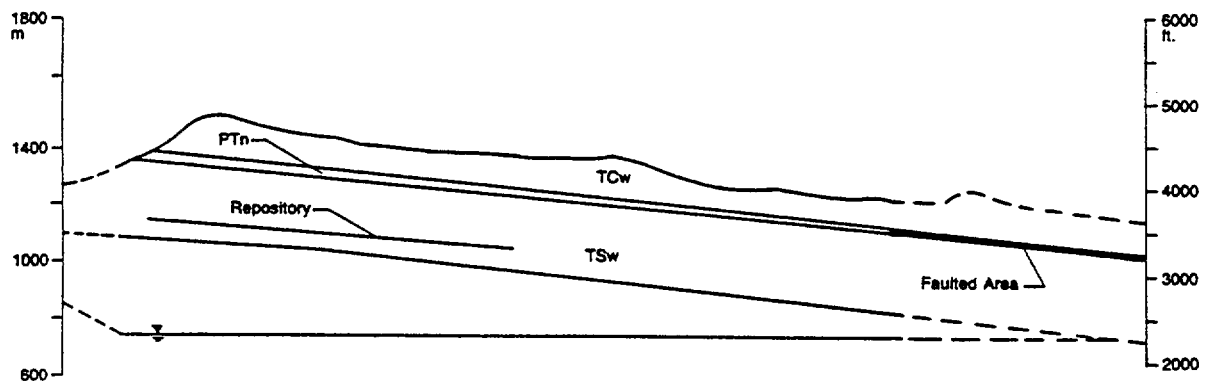


Figure 5-5. Geometry of cross-section N760000 (taken from Figure 6-2 of Ross et al., 1992).

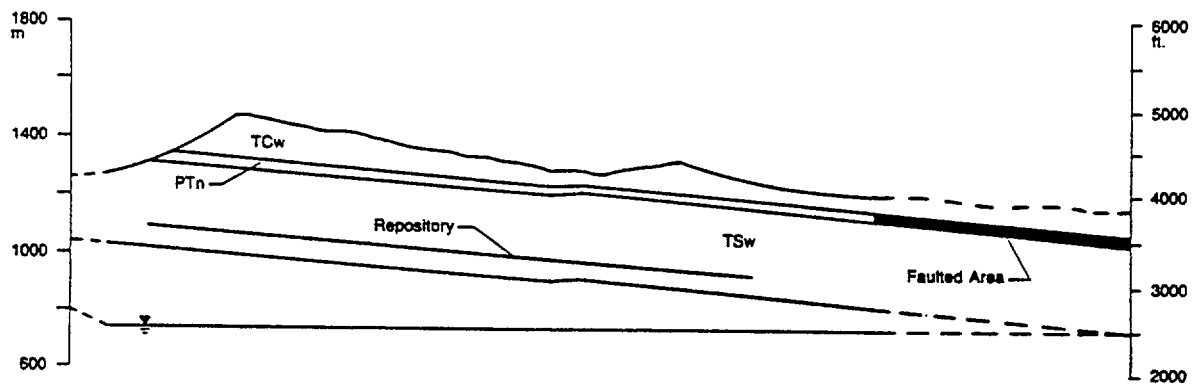


Figure 5-6. Geometry of cross-section N762500 (taken from Figure 6-3 of Ross et al., 1992).

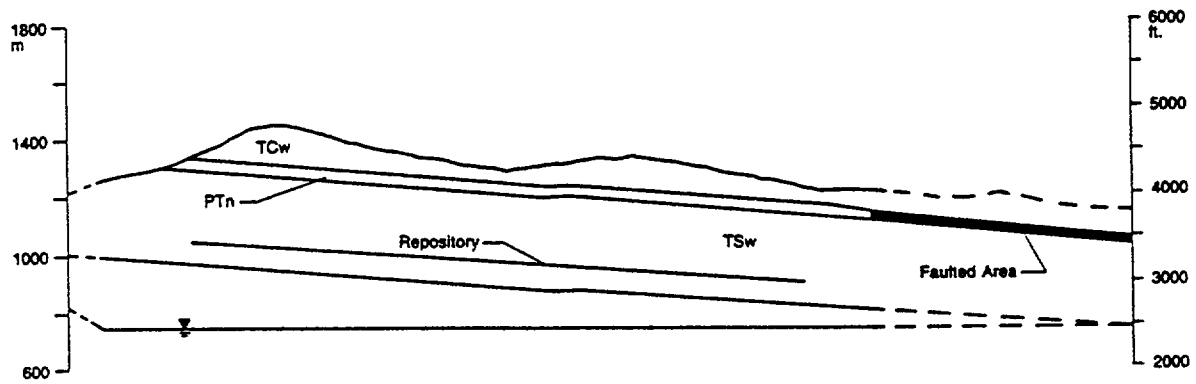


Figure 5-7. Geometry of cross-section N765000 (taken from Figure 6-4 of Ross et al., 1992).

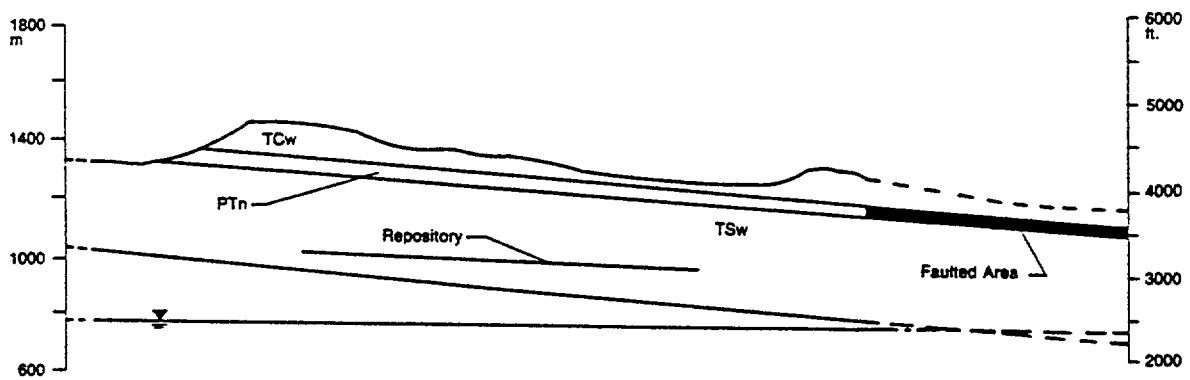


Figure 5-8. Geometry of cross-section N767500 (taken from Figure 6-5 of Ross et al., 1992).

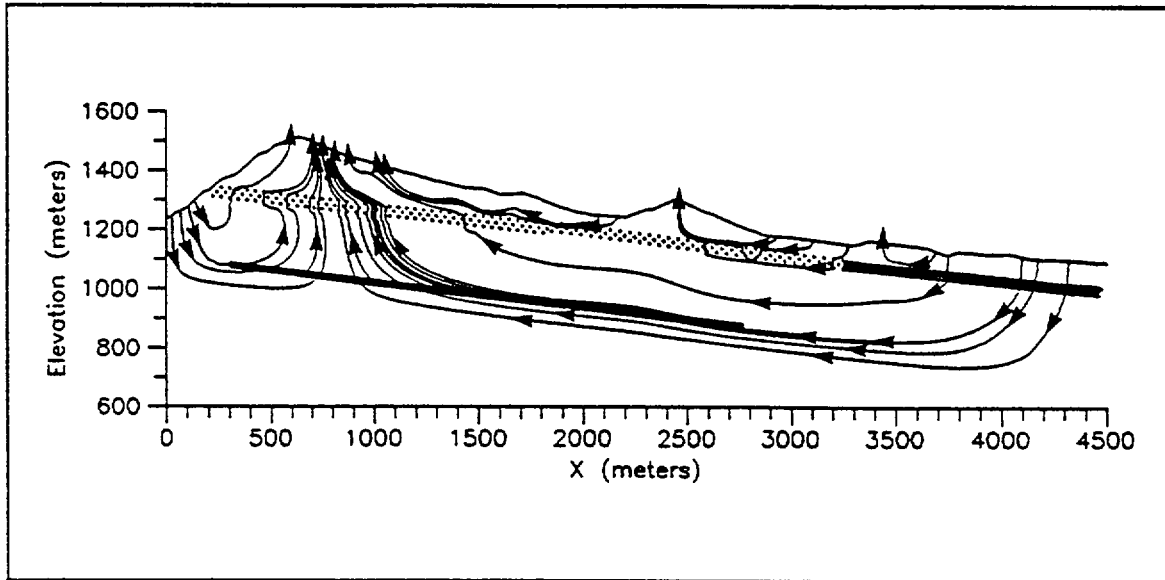


Figure 5-9. Path lines with ambient temperature and nonwelded/welded permeability ratio of 0.01 (0.1 in faulted area). Cross-section N762500. (Taken from Figure 6-13 of Ross et al., 1992.)

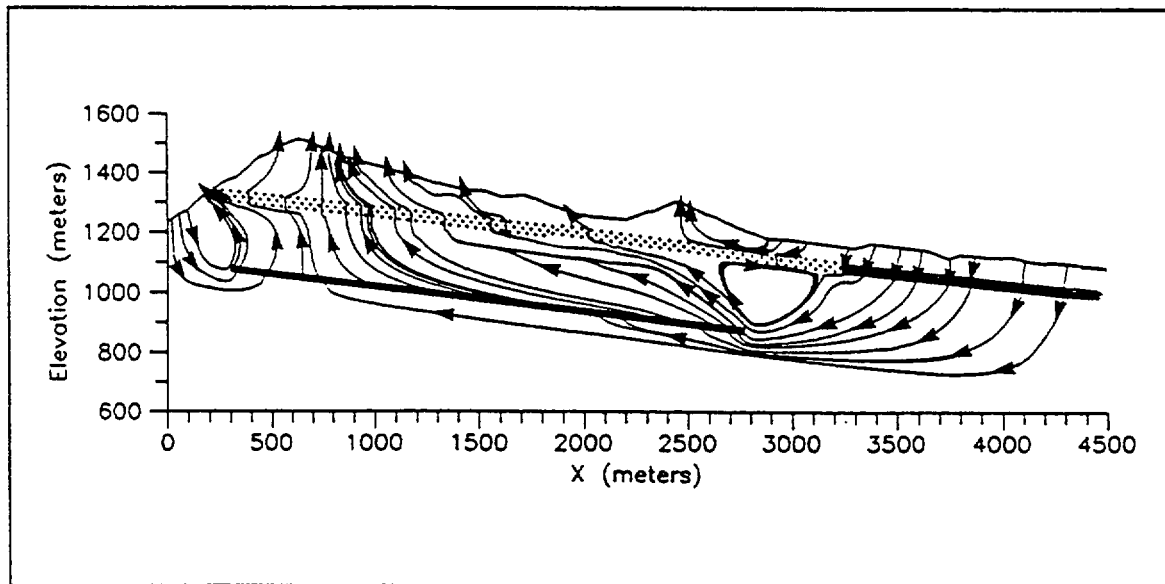


Figure 5-10. Path lines with the repository heated to 330 K and nonwelded/welded permeability ratio of 0.01 (0.1 in faulted area). Cross-section N762500. (Taken from Figure 6-14 of Ross et al., 1992.)

tuff. This choice is somewhat arbitrary, and simulations were also performed using other values for the permeability ratio (Ross et al., 1992; Lu et al., 1991). The results for permeability ratio of 1 percent were used as the base case in the transport calculations described in the next section. This choice was made because Thorstenson (1991) observed that naturally occurring ^{14}C abundances differ above and below the nonwelded unit (at drill hole USW UZ-1), which implies that the air-flow systems above and below are fairly independent. In the simulations, the nonwelded layer is fairly effective as a semi-confining layer that separates the mountain into two flow systems, but more so as the permeability ratio decreases. Thorstenson's measurements of ^{14}C abundance also provide some qualitative validation of the gas-flow model, because the measurements found ^{14}C abundances of a fourth to a half of the modern abundance, and the calculated ^{14}C travel times for ambient conditions are a few times the half-life of 5700 yr. Permeability will be discussed more later, but for now let us note that the gas-flow equations used are linear in the permeability, so the absolute value does not affect the pathlines shown in Figures 5-9 and 5-10, but only the relative values for the different layers.

Additional considerations enter into the calculation of transport of carbon dioxide to the surface. The ^{14}C travel time from repository to surface is sensitive to the permeability values chosen for the rock layers and to the assumptions made concerning geochemical retardation, so those two topics will be discussed next. Note that transport of ^{14}C is assumed to be entirely by advection; i.e., diffusion is neglected. With the values used for permeability, this assumption is reasonable, but if a much lower value were used for permeability then it would be necessary to include diffusion.

Montazer et al. (1986) measured air permeabilities in two boreholes, USW UZ-1 and UE-25a#4. The permeabilities were derived from an analysis of air-pressure fluctuations in the boreholes; they represent large-scale field measurements and should be applicable to the large-scale flow calculations of interest. Values of $7 \times 10^{-13} \text{ m}^2$, $8 \times 10^{-13} \text{ m}^2$, and $1 \times 10^{-11} \text{ m}^2$ in the Topopah Spring welded unit and $2 \times 10^{-11} \text{ m}^2$ in the Tiva Canyon welded unit were reported. Ross et al. adopted a value of 10^{-11} m^2 for their calculations. Thordarson (1983) reported a permeability of $1 \times 10^{-12} \text{ m}^2$ for Topopah Spring welded tuff, from pump tests on well J-13, where the Topopah Spring unit is in the saturated zone (these are also large-scale field measurements, but less applicable because of possible differences between the saturated zone and the unsaturated zone). Tsang and Pruess (1987) made site-scale gas-flow calculations for Yucca Mountain. They used a permeability of $2 \times 10^{-14} \text{ m}^2$, but the source of that number was not stated. Buscheck and Nitao (1988), in a study of hydrothermal

effects for EBS design, used a permeability of $3 \times 10^{-13} \text{ m}^2$, but the origins of the number are unclear. The mean of the distribution used for fracture permeability (the matrix permeability being negligible in comparison) of the "welded" layer in the water-flow calculations for this TSPA is $5 \times 10^{-14} \text{ m}^2$. (To calculate this value requires information on fracture conductivity from Table 3-14 and information on fracture density from Table 3-23.) In using different permeability in this chapter than in the previous chapter we are not necessarily being inconsistent, because the appropriate value for unsaturated water flow could be different from the appropriate value for gas flow. Such a difference could occur because the gas flow is primarily through the largest fractures while the water flow is primarily through smaller fractures. It is important to reconcile these numbers in the future, though, by acquiring more data on the distribution of fracture apertures. Clearly, there is quite a bit of uncertainty about the correct permeability to use. In the TSPA calculations, this uncertainty is partially taken into account by use of a "retardation/permeability factor" that will be discussed in the next section.

The permeability of the nonwelded layer is also important to the calculation of ^{14}C travel time. As mentioned earlier, Ross et al. made calculations for several values of the nonwelded/welded permeability ratio, but we have adopted as our base case the simulations that had a nonwelded permeability that was 1 percent of the welded permeability, or 10^{-13} m^2 . Montazer et al. (1986) reported permeability values for the Paintbrush nonwelded unit from $2 \times 10^{-14} \text{ m}^2$ to $7 \times 10^{-12} \text{ m}^2$. It was decided that for this TSPA no variations on the permeability ratio would be included, so all of our gas-release results assume that the nonwelded tuff has a permeability two orders of magnitude smaller than the welded tuff. Variations on this parameter are left to future work.

For retardation, Ross et al. made some theoretical calculations of the geochemistry of carbon dioxide in air in equilibrium with bicarbonate in water. They found retardation factors in the range of 30 to 75, depending on the type of tuff and the temperature (see Figure 5-11). They used the calculated temperature-dependent retardation factors in their calculation of travel times for ^{14}C from repository to surface. There are several uncertainties in the retardation-factor calculation, including uncertainty about the dominant chemical reactions, uncertainty about the water composition in the unsaturated zone, and uncertainty about the pH of unsaturated-zone water. Also, it has been suggested that precipitation of calcite could provide a significant retardation factor (Codell and Murphy, 1992) and it is quite possible that there is some sorption of the carbon dioxide on the rock in addition to the reaction with the water; strong sorption has been observed on iron and aluminum oxides

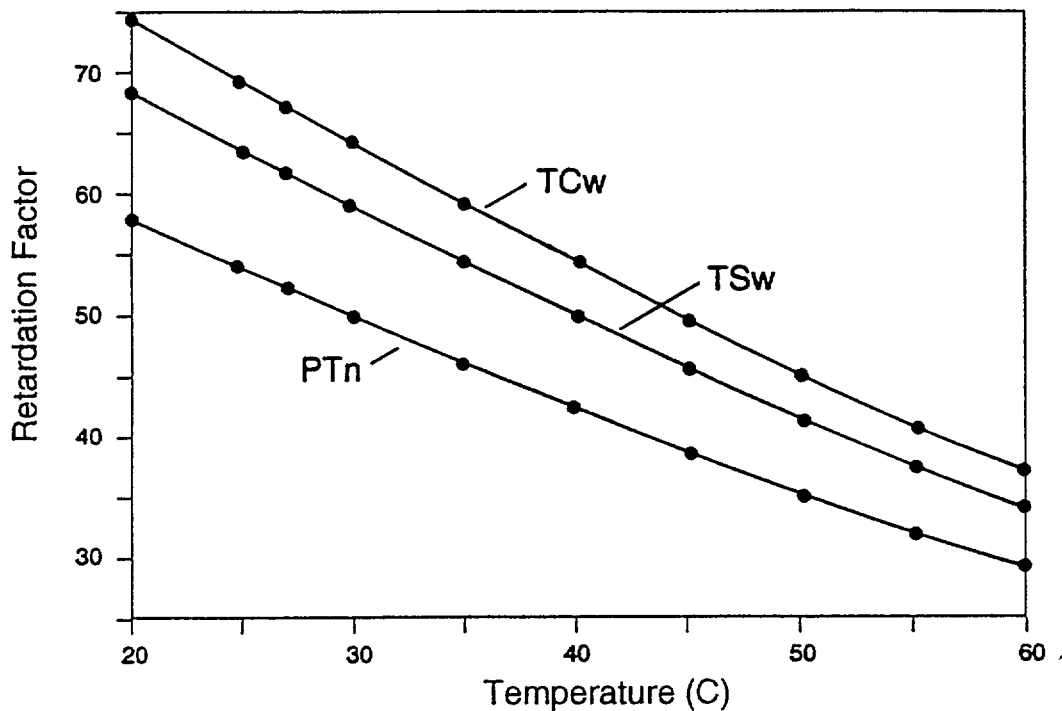


Figure 5-11. Retardation factor as a function of temperature for all units (taken from Figure 4-2 of Ross et al., 1992).

(Russell et al., 1975; Schulthess and McCarthy, 1990). The amount of uncertainty in retardation is unclear, but some account of the uncertainty will be taken in defining the "retardation/permeability factor" referred to above.

5.4 Adaptation of gas flow and transport for the TSA

The method used in the TSA for calculating gaseous releases has been described briefly elsewhere (Wilson, 1992); it will be presented in somewhat more detail here. The gaseous transport calculation is based directly on results from Ross et al. (1992). That report includes distributions of ^{14}C travel time from the repository to the earth's surface calculated using the gas-flow model described in the previous section. The report includes travel-time distributions for three steady-state repository temperatures, 300 K (ambient temperatures), 315 K, and 330 K. Ross et al. have also calculated the travel-time distribution for 360 K; those results are not included in the report, but were used for this study along with the other three distributions. The four travel-time distributions are shown in Figure 5-12. It can be seen that the travel-time distribution is bimodal—the cumulative distribution function rises, then levels off, then rises again. The first rise (or lower travel times) represents ^{14}C that originates near the western end of the repository and has a relatively short travel

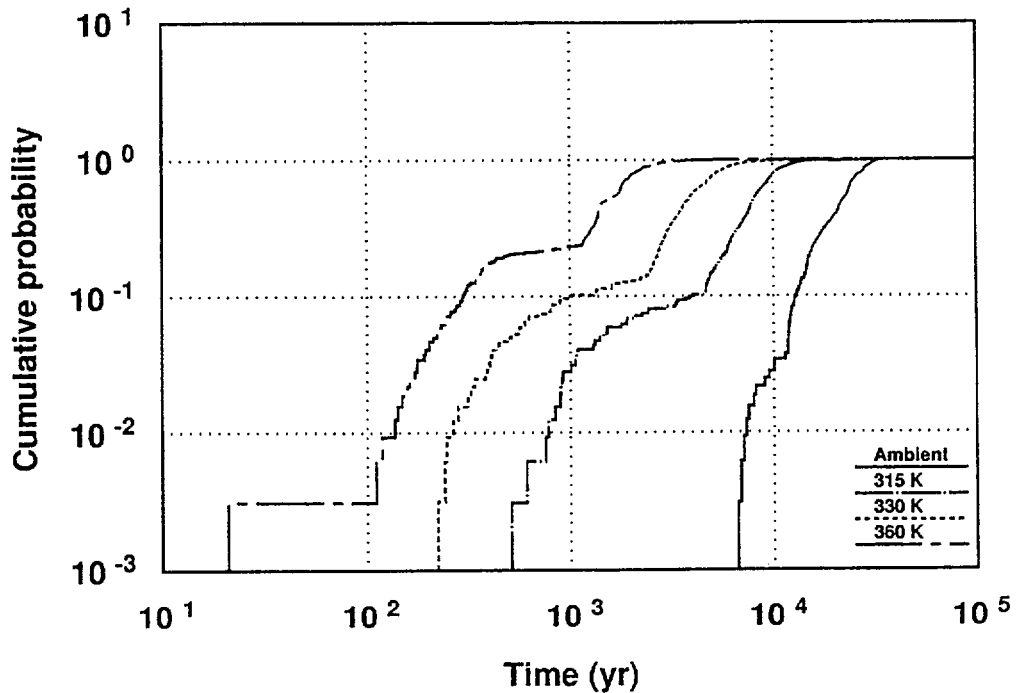


Figure 5-12. The four ^{14}C travel-time distributions.

path out the face of Solitario Canyon without having to go through the nonwelded layer. See the short pathlines at the left of Figure 5-10. Note also that Figure 5-9, for ambient conditions, has none of those short pathlines, and correspondingly the first mode in the ambient curve of Figure 5-12 occurs at a lower cumulative probability and is much less prominent than it is in the heated-repository curves. The second mode, which contains most of the probability in all four cases, represents the majority of the ^{14}C , which has longer pathlines and has to go through the nonwelded layer to reach the surface.

A number of approximations are necessary to use these results for a calculation of ^{14}C release in the TSA. The repository temperature is not in steady state, but declines slowly with time as the radioactivity decays away. To represent this process with four steady-state travel-time distributions entails a certain amount of error. To mitigate this error, approximations were made in such a way as to err on the conservative side (that is, in such a way as to increase releases). The first step was to identify the points in time corresponding to the four repository temperatures. This was accomplished by using results of Tsang and Pruess (1987). The Tsang and Pruess results are not directly comparable to the Ross et al. results because a number of different assumptions were made. In particular, as has already been mentioned,

Ross et al. use a value of gas permeability that is three orders of magnitude higher than that used by Tsang and Pruess (for the welded tuff; Tsang and Pruess used the same permeability for welded and nonwelded tuff). The higher permeability leads to higher gas velocities in the Ross et al. calculations. One effect of the higher velocities should be a greater rate of repository cooling, so that for a given time the Tsang and Pruess temperature is expected to be higher than the Ross et al. temperature would be. Therefore, associating the Ross et al. temperatures with the Tsang and Pruess temperatures is inconsistent, but should be conservative. (Conservative because the temperature at a given time is taken to be higher than it would be if the temperature were calculated using the Ross et al. values, and higher temperatures imply higher gas velocities and therefore shorter ^{14}C travel time to the surface.) It is possible that repository cooling is primarily dominated by heat conduction through the rock, in which case the Tsang and Pruess temperature could be a good approximation of the Ross et al. temperature.

The temperature history of the repository, as reported by Tsang and Pruess (1987) is shown in Figure 5-13. Also shown in the figure is a dashed line indicating the temperature history assumed for the TSPA gas-release calculations. Since ^{14}C travel-time distributions were only available for four temperature values, the dashed line is a "stair-step" curve. The 360-K travel-time distribution was used from the beginning of the calculation until a time of 2400 yr, the 330-K distribution was used from 2400 yr until 4800 yr, and the 315-K distribution was used after 4800 yr. If calculations were extended beyond 10,000 yr, the 300-K distribution would be used for times past 10,000 yr. It would be preferable to have distributions for additional temperatures so that the temperature discretization would not be as gross, but by always taking the travel-time distribution from a higher temperature than is expected at a given time, conservatism is maintained. The first part of the calculation may not be entirely conservative, since the Tsang and Pruess temperature goes above 360 K for a time. However, the transport calculation is conservative in another way, too. The temperature field should be declining with time rather than remaining constant. The decline in temperature has two effects: (1) During the course of transport from repository to surface, temperatures could decline significantly; the method being used for the transport calculations instead assumes that the temperature field remains fixed as it was at the time of release. This choice was made only for pragmatic reasons—travel-time distributions including effects of cooling *en route* were not available. (2) Using steady-state temperature profiles overestimates the spatial extent of the temperature field. That is, when the repository temperature is at 360 K, the high-temperature region has not spread out as far from the repository

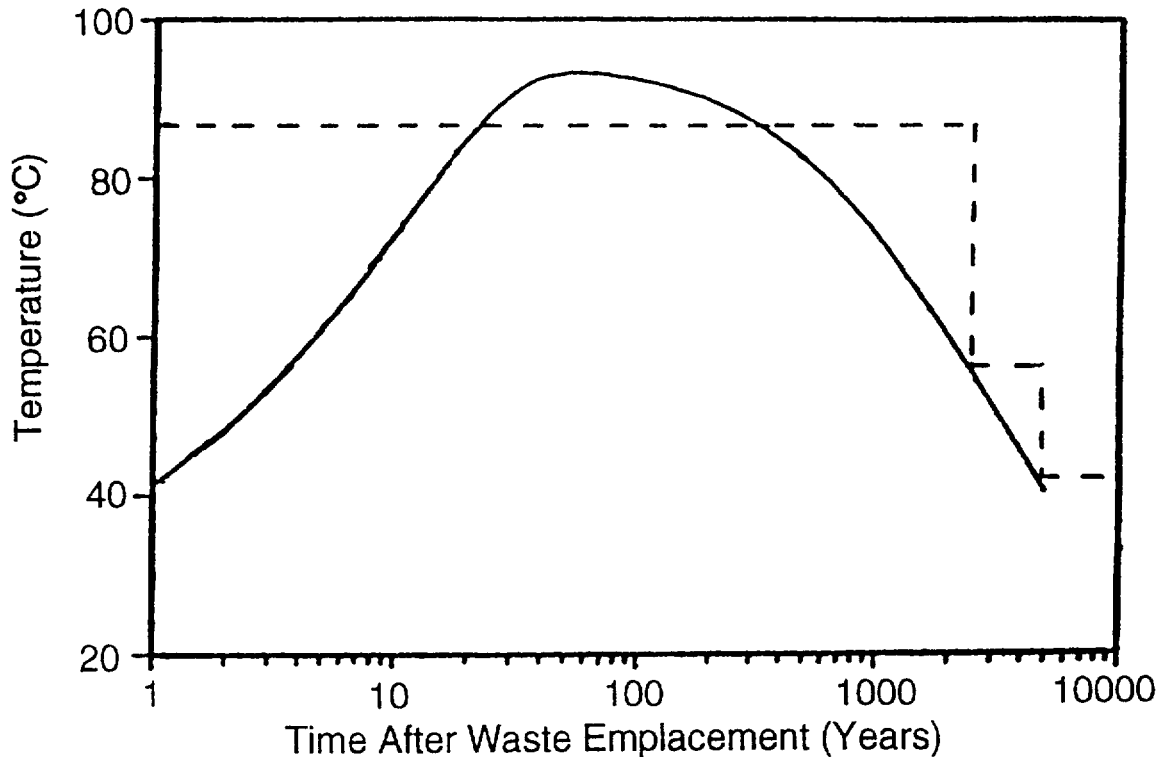


Figure 5-13. Temperature vs. time after waste emplacement at the center of the repository (taken from Figure 4 of Tsang and Pruess, 1987). Dashed line shows the TSA approximation.

as a steady-state temperature field with the repository at 360 K. The consequence of this effect is similar to that of the first effect: the ^{14}C , during its migration to the surface, should see lower temperatures than we are assuming. This shortcoming is another result of using steady-state calculations to determine the travel-time distributions.

The calculation of ^{14}C gaseous release proceeds as follows. The release rate from the source, $\Sigma(\tau)$, is calculated using the radionuclide source model described in Section 5.2; τ is the time of release from the source. At each time τ , there is a distribution of travel times, $P(t;\tau)$, where t is the travel time to the surface (see Figure 5-12). Of the ^{14}C released at time τ , the fraction that escapes to the atmosphere within the EPA time period is calculated as an integral over the travel-time distribution. The formula used for the calculation can be written as

$$R = \int_0^T d\tau \Sigma(\tau) \int_0^{T-\tau} dt P(t;\tau) e^{-\lambda t} , \quad (5.1)$$

where R is the cumulative release to the accessible environment, T is the EPA time period (10,000 yr), and λ is the decay rate of ^{14}C . As indicated in the equation and as discussed above, the travel-time distribution P depends on the release time τ . P

is normalized so that $\int_0^\infty P(t; \tau) dt = 1$.

In calculating the integral over the travel-time distributions, the distributions were regarded as discrete rather than continuous. That is, each of the four travel-time distributions consisted of a list of 323 ^{14}C travel times; rather than do some sort of smoothing or interpolation, the travel-time density function was taken to be a sum of 323 delta functions. (This is why the cumulative distribution functions in Figure 5-12 are stair-steps instead of smooth curves.) Then, for example,

$$\int_0^T P(t; \tau) e^{-\lambda t} dt = \sum_{n=1}^N \frac{1}{323} e^{-\lambda t_n} , \quad (5.2)$$

where $\{t_n, n = 1, \dots, 323\}$ are the calculated travel times for release-time τ , and $\{t_n, n = 1, \dots, N\}$ are the travel times smaller than T (only travel times t between 0 and T contribute to the integral.)

To take into account the uncertainties in permeability and retardation discussed in the previous section, a "retardation/permeability factor" is introduced; let us denote the factor by F . This factor is a multiplication factor for the travel-time distributions. The travel times are directly proportional to the retardation factor (remember, though, that the retardation is not a simple constant; see Figure 5-11) and inversely proportional to the permeability (permeability is not a simple constant, either, but varies from geologic unit to geologic unit). The factor F represents the deviation from the "base" values:

$$F = (R/R_b) \cdot (k_b/k) , \quad (5.3)$$

where R is the retardation factor, R_b is the base retardation factor, k is the permeability, and k_b is the base permeability. If the retardation is multiplied by some factor everywhere and the permeability is multiplied by some other factor everywhere, then F is the ratio of those two factors. F is used by multiplying all the travel times by it. For example, for the travel-time distribution $\{t_n, n = 1, \dots, 323\}$ of Equation 5.2, the adjusted travel-time distribution would be $\{F t_n, n = 1, \dots, 323\}$.

We wanted to assign a distribution to F that would represent the uncertainty in k and R . A log-uniform distribution from 0.5 to 10 was chosen. The reason for selecting a maximum of 10 is that some of the field-measured permeability values for the Topopah Spring welded tuff are as small as about one tenth of the base value of 10^{-11} m^2 . It could be that the lower values (longer travel times) are more representative, but additional data are needed. For now, a log-uniform distribution is used to represent the great uncertainty. The lower bound of 0.5 for F is less based on hard data; it is intended to represent the possibility of retardation factors lower

than the base values. (Also, the permeability could be higher than the base value.) In fact, higher retardation factors are probably more likely than lower ones, and if ^{14}C retardation is better quantified in the future it could move the F distribution upward.

The important factors going into the gas flow and transport calculation are summarized in Table 5-3.

5.5 Results

For each of the conceptual models of groundwater flow, composite-porosity and weeps, a Monte Carlo simulation of 1000 realizations was performed, using the models and parameter distributions described above. For the gaseous-release calculations associated with composite-porosity water flow, the repository was not divided into six columns, as it was for the aqueous-release calculations (Section 4.4.2). For both gaseous-release simulations, the repository was treated as a whole.

The conceptual model of groundwater flow enters in because interaction of groundwater with the waste containers could be an important element in the mobilization of ^{14}C . The "quick-release" part of the ^{14}C inventory can be released without water being present (Van Konynenburg et al., 1985, 1987), and the fuel-matrix alteration process that liberates the ^{14}C in the UO_2 matrix could be able to proceed without water being present (but perhaps at a lower rate; little is known about the effect of water on the matrix-alteration rate). Regardless of whether water is important to ^{14}C mobilization, it certainly is important to the processes that lead to container failure.

Figure 5-14 shows the conditional CCDFs for normalized gaseous releases to the accessible environment for the two Monte Carlo simulations. Aqueous releases in the weeps model were higher than in the composite-porosity model (Figure 4-44), so it is

Table 5-3. Probability distributions assumed for ^{14}C transport.

Model parameter	Distribution	Distribution parameters ^a	Mean value
Base permeability for welded (m^2)	—	—	10^{-11}
Base permeability for nonwelded (m^2)	—	—	10^{-13}
Base retardation factors	see Figure 5-11		
Times for 360-K travel-time dist. (yr)	—	0 to 2400	—
Times for 330-K travel-time dist. (yr)	—	2400 to 4800	—
Times for 315-K travel-time dist. (yr)	—	4800 to 10,000	—
Times for 300-K travel-time dist. (yr)	—	over 10,000	—
Retardation/permeability factor, F	log-uniform	0.5, 10	3.2

^a Parameters for the log-uniform distribution are minimum, maximum.

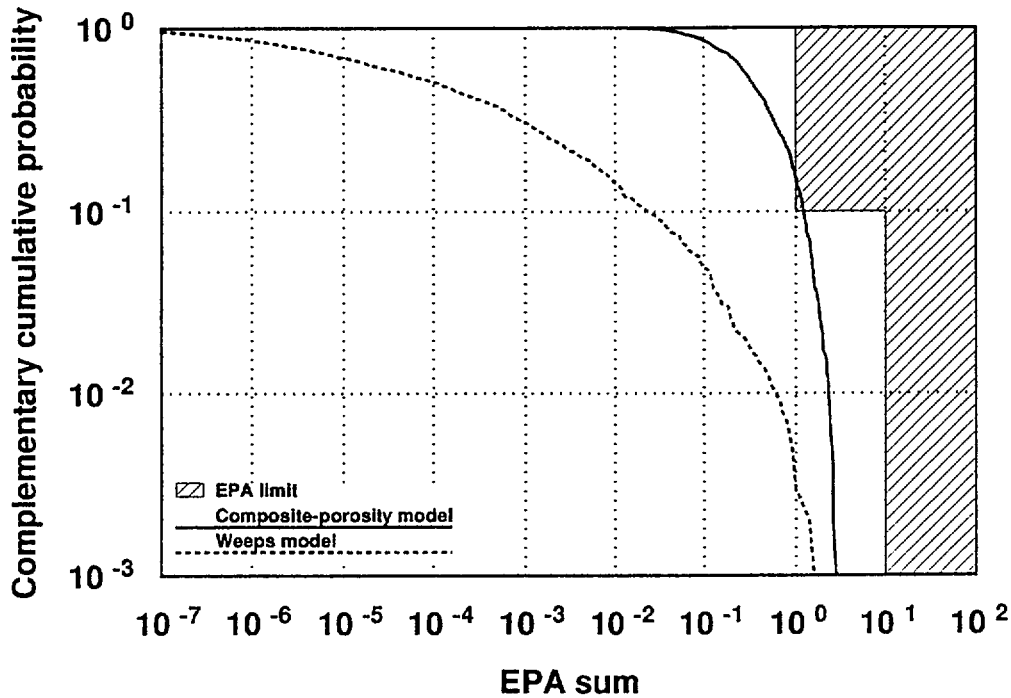


Figure 5-14. Conditional CCDFs for gaseous releases. Shown are the distributions for the composite-porosity model and for the weeps model.

surprising at first that for gaseous releases they are reversed—gaseous releases in the composite-porosity model are higher than in the weeps model. The reason for this has already been mentioned in another context in Section 4.7: In the weeps model it is assumed that only a subset of waste containers is contacted by flowing water, and only that subset fails and releases radionuclides. In the composite-porosity model, more waste containers are contacted by water and fail, releasing radionuclides. In realizations with high values of the fuel-matrix alteration rate, it is possible for all of the ^{14}C to be released from the waste containers within 10,000 yr and for most of it to be released to the surface. It is also possible for all waste containers to be contacted by water and release all of their ^{14}C in a weeps realization, but with the parameter distributions being used (see Table 4-5) the probability of that occurrence is fairly low.

It can be seen from Figure 5-14 that the calculated gaseous releases assuming the composite-porosity water-flow model exceed the 1985 EPA limits (represented by the shaded region). This result should be kept in perspective. Remember that, for this first attempt at a total-system performance assessment, a number of conservative assumptions have been made. Some of the assumptions (e.g., neglecting the container and cladding as barriers in the source-release calculation, using the sim-

ple stair-step approximation of repository temperature in the transport calculation) are merely pragmatic and could be handled better in future calculations as better modeling capabilities are developed. Other assumptions (e.g., use of the simple matrix-alteration model of waste mobilization, use of a mean water flux of 1 mm/yr) require additional data to determine their validity or to determine the appropriate parameter values. In cases like these, we often feel that the choices made were conservative, but we will not know for sure until more data become available.

Some additional information helps to provide a better understanding of the results. Figure 5-15 shows the CCDFs for NRC ratio (ratio of peak release rate from the EBS to the NRC release-rate limit in 10 CFR 60.113). It can be seen that the NRC release-rate limit is exceeded almost 80 percent of the time for the composite-porosity model and about 3 percent of the time for the weeps model (with the assumptions used). This shows that source release rates are relatively high. This clearly shows that the source model being used is overly conservative; these high NRC ratios could be reduced to a more realistic estimate by improving the model. Some possibilities for improvement include improved modeling of the container and cladding barriers, applying different container-failure distributions to "wet" and "moist" containers, and determining whether the matrix-alteration model of waste mobilization is correct. Note also that the percolation-rate distribution assumed could be unrealistically high for the composite-porosity model (see Section 4.7.1), which increases composite-porosity releases by putting more waste containers in "wet" conditions. It is likely that, if the number of high NRC ratios were reduced, then the number of high EPA sums would be reduced, so that the composite-porosity curve in Figure 5-14 would no longer exceed the EPA limits. To complete the discussion of the NRC containment requirements of 10 CFR 60.113, note that the "substantially complete containment" requirement is met because the source model being used has no releases before 300 yr.

Figure 5-16 shows conditional CCDFs for gaseous releases from the EBS and gaseous releases to the accessible environment (i.e., without and with transport to the surface included) assuming the composite-porosity water-flow model. The corresponding curves for the weeps water-flow model are shown in Figure 5-17. In these figures, the curves for releases to the accessible environment are the same as the curves in Figure 5-14. Figures 5-16 and 5-17 show that little is gained by the transport to the surface. The ^{14}C travel times are too short to reduce the releases significantly. As was mentioned in the description of the transport calculations in the preceding section, a number of approximations were made (using the Tsang and Pruess temperature history when the Ross et al. temperatures would probably be

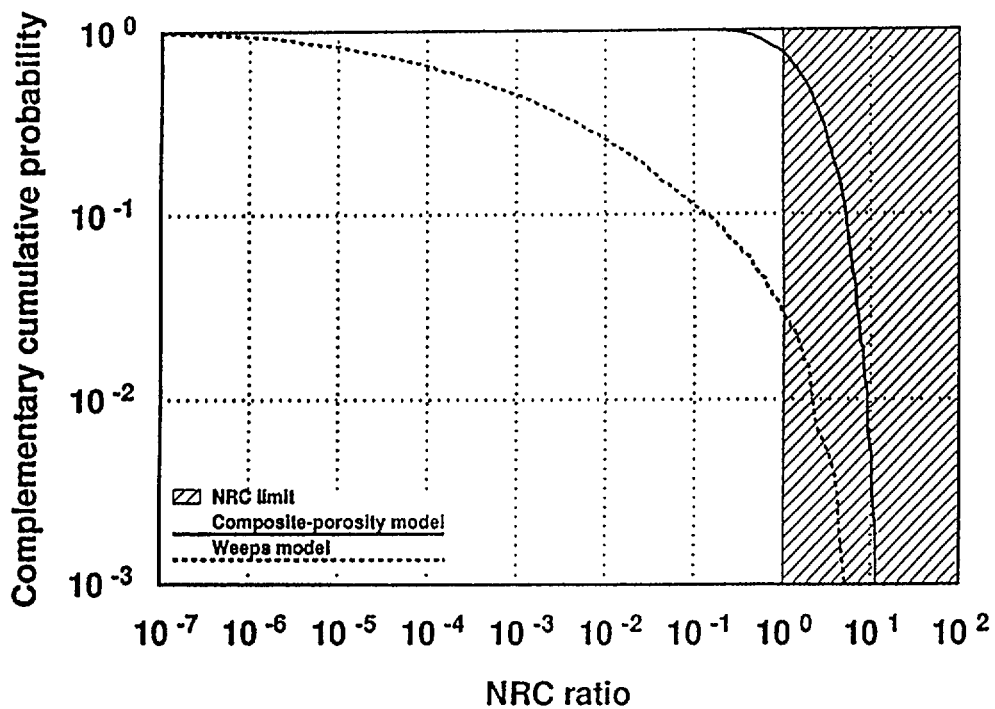


Figure 5-15. Probability distributions of the NRC ratio, calculated for the composite-porosity model and for the weeps model.

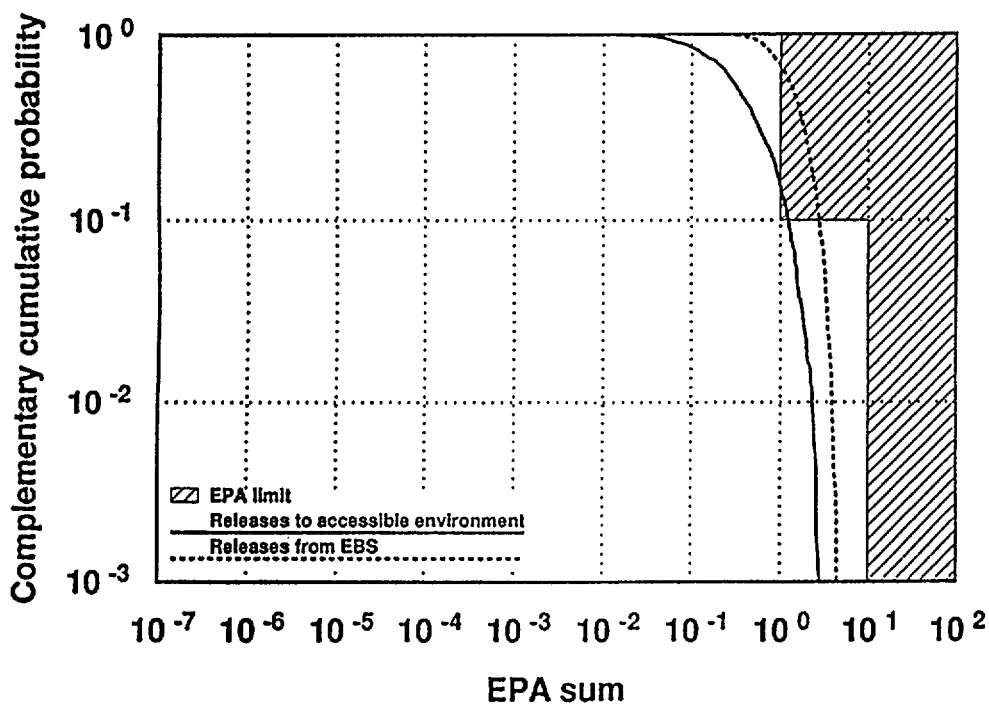


Figure 5-16. Conditional CCDFs for gaseous releases, calculated using the composite-porosity model for water flow. Shown are partial EPA sums calculated using releases from the EBS and releases to the accessible environment.

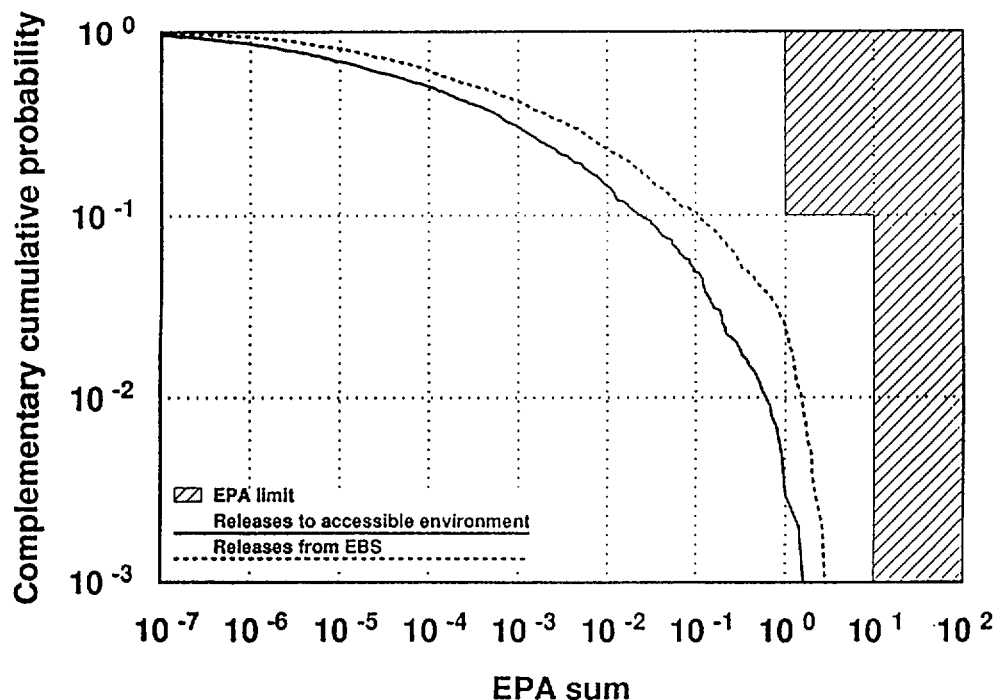


Figure 5-17. Conditional CCDFs for gaseous releases, calculated using the weeps model for water flow. Shown are partial EPA sums calculated using releases from the EBS and releases to the accessible environment.

lower, using a ^{14}C travel-time distribution for a higher temperature at each time, using travel-time distributions calculated for steady-state conditions), each of them in such a way as to overestimate the releases. Refining the transport model would undoubtedly reduce the EPA ratios for releases to the accessible environment (which would increase the separation between the EBS and accessible-environment curves), but there is probably much more potential for reducing the EPA ratios by refining the source model (which would move both curves to the left).

To conclude, Park and Pflum (1990) and Van Konynenburg (1991) have argued that, for a partially saturated repository, it will be difficult (i.e., expensive) to meet the EPA and NRC release criteria for ^{14}C , because heavy reliance must be placed on the EBS to reduce ^{14}C releases. They also point out that even the entire ^{14}C inventory would be negligible compared to the natural ^{14}C background. From the results presented in this section, it seems quite likely that more realistic release and transport models for ^{14}C would reduce releases to the accessible environment to below the EPA limits. To reduce EBS release rates below the NRC limit could require adding additional barriers to ^{14}C releases in the EBS. However, such considerations should be studied using more realistic release models than were used here.

5.6 Analysis of the average case

To go along with the average-case aqueous-release calculations reported in Section 4.8, corresponding calculations were made for gaseous releases. As stated before, the "average" case is the case for which all the parameters are assigned the means of their respective probability distributions; it is not intended to represent the expected state of a repository at Yucca Mountain. The reasons for investigating the average case are given in Section 4.8. The results are shown in Figures 5-18 through 5-23. Gaseous releases were only calculated for 20,000 yr rather than for 10^6 yr as the average-case aqueous calculations were. Nothing is lost by this reduction because the half-life of ^{14}C is only 5700 yr, which means that most of it will decay away within 20,000 yr. (The average-case aqueous calculations were extended to such a large time so that the peak release rates to the accessible environment could be observed for some of the nuclides. The peak release rate for ^{14}C occurs within 20,000 yr.) The "wiggles" in the accessible-environment-release curves (Figures 5-18 and 5-19) are artificial, caused by the switches from one ^{14}C travel-time distribution to another. These switches occur at 2400 yr, 4800 yr, and 10,000 yr (see Table 5-3).

As with the probabilistic calculations, releases are higher for the composite-porosity model than for the weeps model. For the composite-porosity model, the

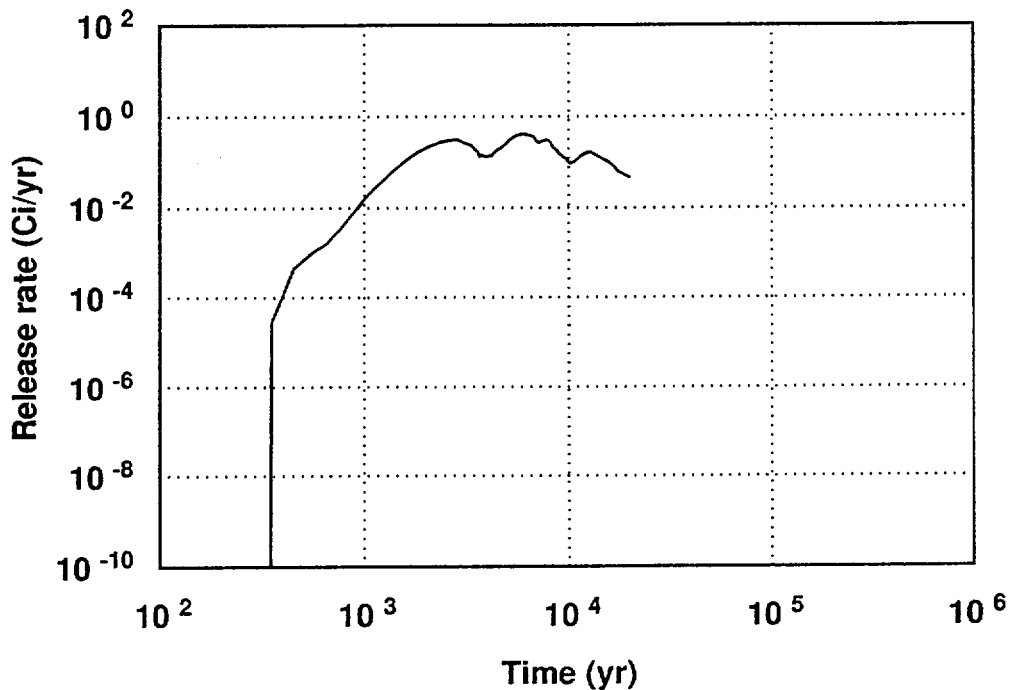


Figure 5-18. Release rate to the accessible environment for gaseous ^{14}C , using the composite-porosity model for water flow and mean values for all parameters.

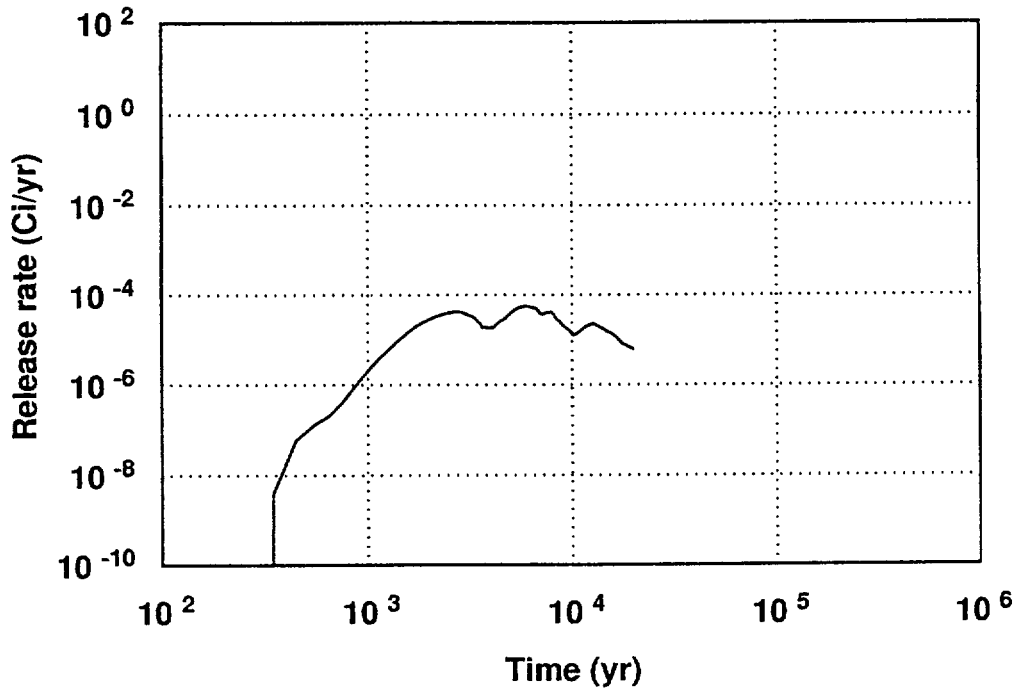


Figure 5-19. Release rate to the accessible environment for gaseous ^{14}C , using the weeps model for water flow and mean values for all parameters.

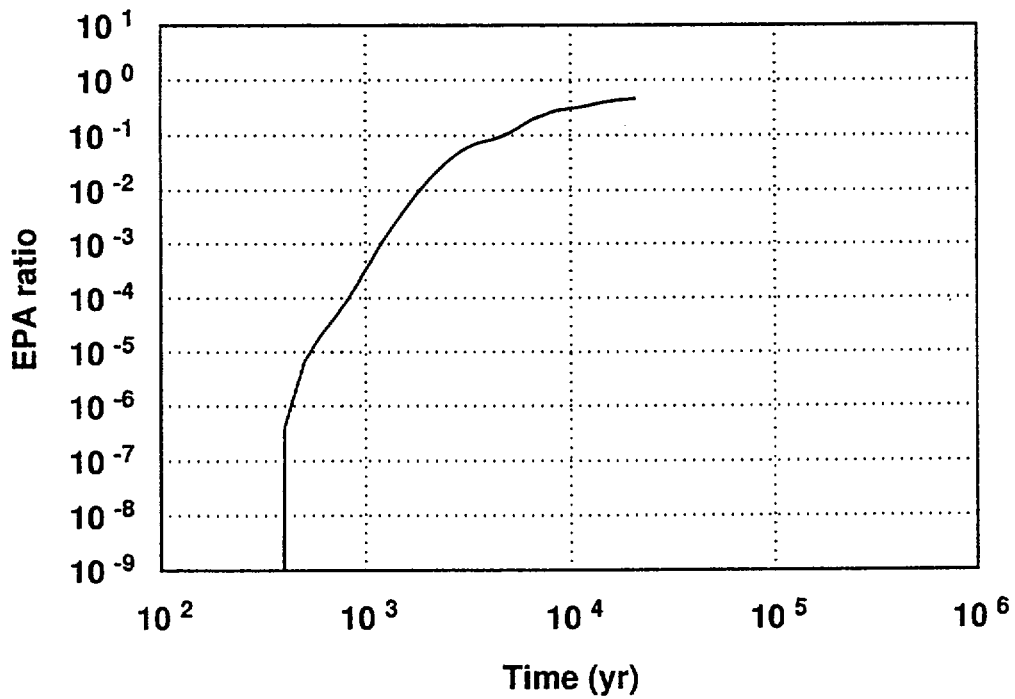


Figure 5-20. ^{14}C EPA ratio as a function of time for the composite-porosity model, using mean values for all parameters.

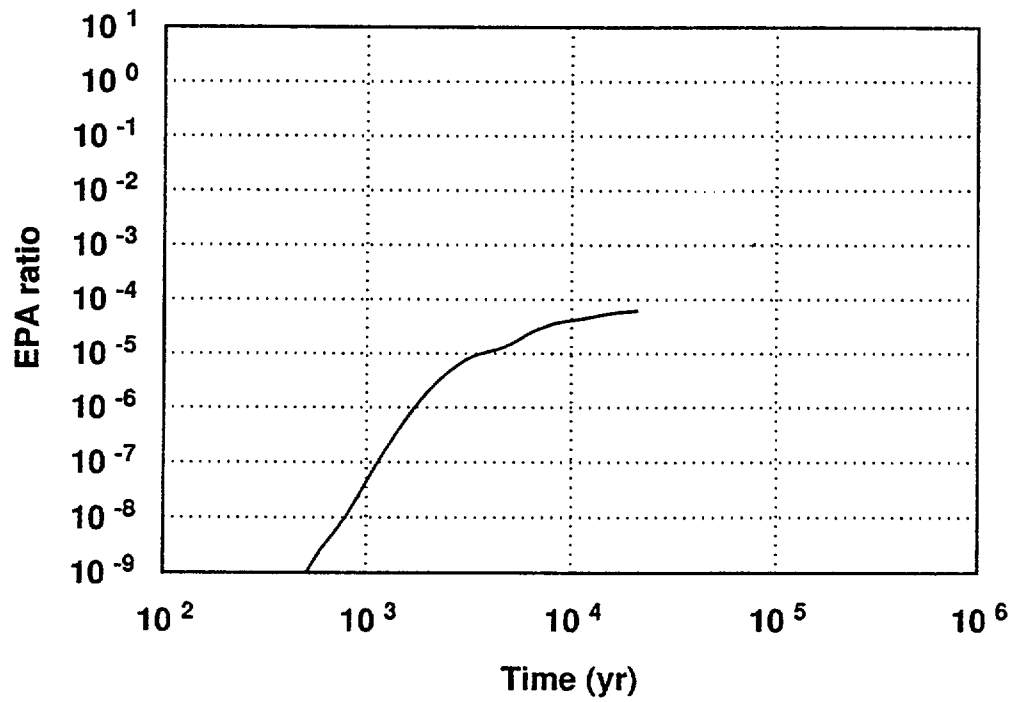


Figure 5-21. ^{14}C EPA ratio as a function of time for the weeps model, using mean values for all parameters.

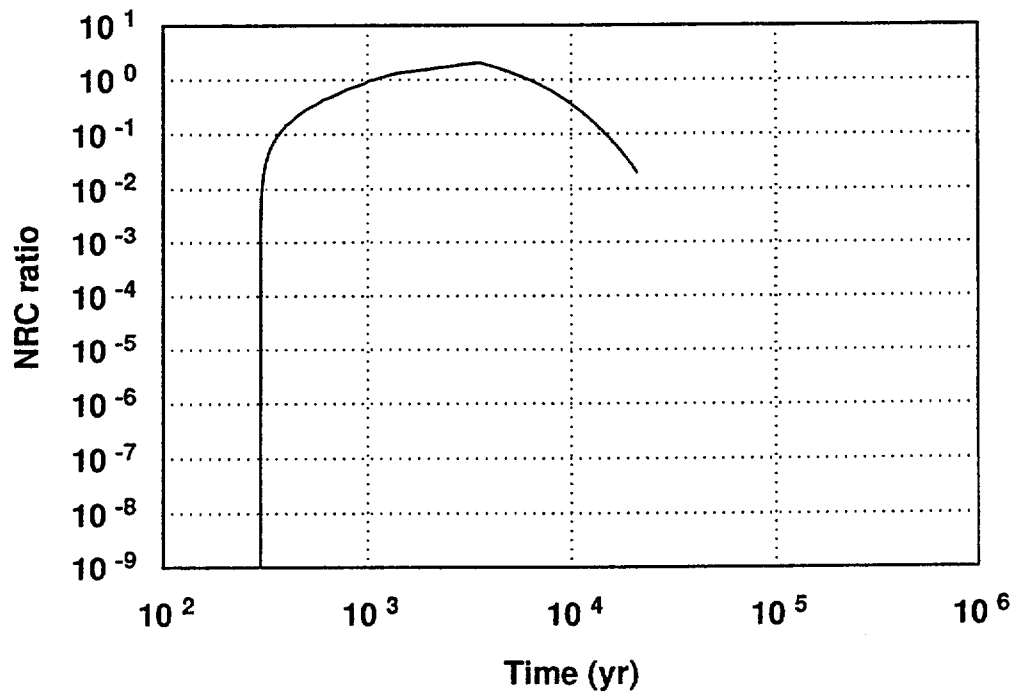


Figure 5-22. ^{14}C NRC ratio as a function of time for the composite-porosity model, using mean values for all parameters.

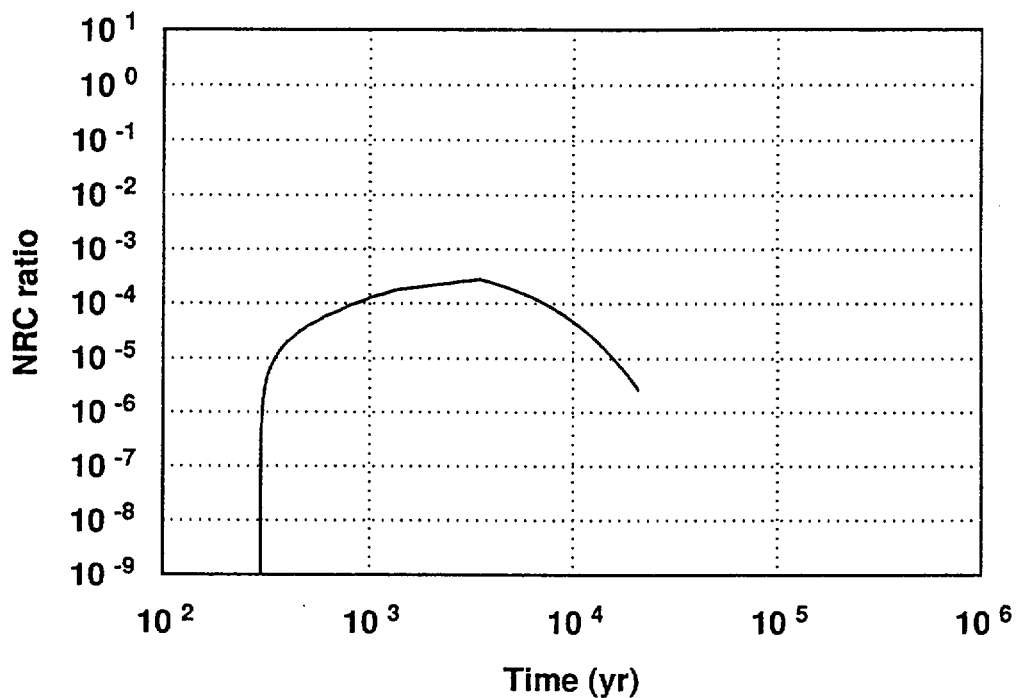


Figure 5-23. ¹⁴C NRC ratio as a function of time for the weeps model, using mean values for all parameters.

release rate to the accessible environment peaks at approximately 0.4 Ci/yr at 6000 yr. The EPA ratio (at 10,000 yr) is about 0.3. Also, for the composite-porosity model the NRC release-rate limit is exceeded, with the peak release rate reached at about 3000 yr. The peak release rate for the weeps model occurs at about the same time, but is four orders of magnitude lower. The reason for this, as has been stated before, is that only a small fraction of the waste containers release their radionuclides in the weeps calculation. For the weeps model, the EPA ratio is only 4×10^{-5} and the peak release-rate to the accessible environment is 6×10^{-5} Ci/yr at 6000 yr.